

# **Synthesis and characterisation of sulfonated Starbons<sup>®</sup>, bio-based catalysts**

**Cinthia Janet Mena Durán**

PhD

University of York  
Chemistry

August 2014



## Abstract

The overall objective of this thesis was to develop an enhanced understanding of the sulfonation of Starbons<sup>®</sup> and the properties of the sulfonated materials, using conventional and microwave heating. Starbons<sup>®</sup> are materials prepared from expanded starch. Due to their renewable nature, these materials are great candidates to be explored in our search for sustainable development. The sulfonated Starbons<sup>®</sup> (S-Starbons<sup>®</sup>) were tested as solid-acid catalysts in esterification reactions using microwave irradiation.

A green chemistry analysis of some current routes to sulfonated carbonaceous materials is presented in **Chapter 1**. Here, an in-depth description of Starbons<sup>®</sup> is also given, as a brief review of some techniques used in their characterisation. Synthesis and characterisation of S-Starbons<sup>®</sup> by conventional heating and microwave irradiation are presented in **Chapter 2** and **Chapter 3**, respectively. Elemental composition of Starbons<sup>®</sup> depends on carbonization temperature, changing from high-oxygenated (300 °C) to more carbon-like (800 °C) materials. After sulfonation, the sulfur content varies with carbonization temperature, being particular high for the most-oxygenated samples. All S-Starbons<sup>®</sup> present a characteristic IR band ca. 1030 cm<sup>-1</sup> independently of sulfonation method. <sup>13</sup>C solid-state NMR gives structural information from S-Starbons<sup>®</sup>, however, due to overlapping resonances it was difficult to identify the C–S resonance. XPS showed that sulfur (VI) is the only one observed in S-Starbons<sup>®</sup> 300, but sulfur (II) appears in higher temperature carbonized Starbons<sup>®</sup>. The main difference between microwave and conventional sulfonated Starbons<sup>®</sup> 300, was the appearance of another sulfur (VI) species in the microwaved samples. **Chapter 4** relates to the stability of the sulfur-bonding in S-Starbons<sup>®</sup>, through TG-FTIR analysis. This study suggests that stability of the sulfur bonding is higher in S-Starbon<sup>®</sup> 300 than in S-Starbon<sup>®</sup> 800. This observation was correlated with the catalytic performance of these materials (**Chapter 5**), where S-Starbon<sup>®</sup> 800 loses its activity more rapidly than S-Starbon<sup>®</sup> 300.



## Table of contents

Abstract	3
List of figures	11
List of tables	19
Acknowledgements	21
Dedication	22
Declaration	23
<b>Chapter 1. Introduction</b>	
1.1. Green chemistry, the approach to achieve sustainability	27
1.1.1. The green chemistry side of this project	29
1.2. Heterogeneous catalysis, as a green chemistry operational tool	30
1.2.1. Solid-acid catalysts	31
1.3. Carbon-based acid catalysts	
1.3.1. The “sugar catalyst”	32
1.3.2. Porous catalysts	35
1.3.3. Sulfonated Starbons <sup>®</sup> , a mesoporous bio-based alternative	37
1.4. Microwave chemistry	
1.4.1. What are microwaves?	40
1.4.2. Microwave heating	41
1.4.3. Microwave irradiation vs conventional heating	42
1.4.4. “Microwave activation”, “hot spots” and “super-heating effect”	44
1.5. Analytical techniques	
1.5.1. Infrared spectroscopy, attenuated total reflectance (ATR-FTIR)	44
1.5.2. Porosimetry characterisation	
1.5.2.1. Type of isotherms	46
1.5.2.2. Type of hysteresis	47
1.5.2.3. Surface area determination, BET calculation	48
1.5.2.4. Pore size distribution, BJH method	50
1.5.3. X-ray photoelectron spectroscopy (XPS)	51
1.5.4. Nuclear Magnetic Resonance	51

1.5.4.1. Solid-state NMR, Cross-Polarization (CP)/Magic Angle Spinning (MAS)	52
1.5.5. Thermogravimetric analysis coupled to infrared spectroscopy (TG-FTIR)	55
1.5.6. Gas Chromatography Analysis	56
1.6. Project scope and objectives	57

## **Chapter 2. Synthesis and characterisation of sulfonated Starbons<sup>®</sup> by conventional heating**

2.1. Introduction	61
2.2. Preparation of sulfonated Starbons <sup>®</sup>	61
2.3. Leaching of sulfuric acid from sulfonated Starbons <sup>®</sup> : washing with methanol	64
2.4. Characterisation of Starbons and Sulfonated Starbons <sup>®</sup>	
2.4.1. Elemental composition in Starbons <sup>®</sup> and sulfonated Starbons <sup>®</sup>	67
2.4.2. Approximation of an empirical formula for Sulfonated Starbons <sup>®</sup>	72
2.4.3. Surface and bulk compositions of sulfonated Starbons <sup>®</sup>	75
2.4.4. Characterisation of sulfonated Starbons <sup>®</sup> by FTIR	76
2.4.5. <sup>13</sup> C CP/MAS NMR studies on Sulfonated Starbons <sup>®</sup>	80
2.4.5.1. Structural changes in Starbon <sup>®</sup> 300	81
2.4.5.2. Identifying main functional groups in Sulfonated Starbons <sup>®</sup> in <sup>13</sup> C NMR spectra	83
2.4.5.3. Increasing temperature of carbonization of Starbons <sup>®</sup>	84
2.4.6. X-ray photoelectron spectroscopy studies on sulfonated Starbons <sup>®</sup>	
2.4.6.1. Before starting: data handling	86
2.4.6.2. Starbons <sup>®</sup> 300 and 800	87
2.4.6.3. Analysis of carbon bonding	89
2.4.6.4. The sulfur components in sulfonated Starbons <sup>®</sup>	95
2.4.7. Sulfur (VI) and acidity	100
2.4.8. Morphology and porosity of sulfonated Starbons <sup>®</sup>	
2.4.8.1. SEM images	102
2.4.8.2. Surface area and porosimetry	103
2.5. Conclusions	106

### **Chapter 3. Synthesis and characterisation of microwave sulfonated Starbons®**

3.1. Introduction	111
3.2. Bulk elemental composition	112
3.3. XPS analysis of microwave sulfonated Starbons®	115
3.3.1. Elemental composition	115
3.3.2. Carbon analysis	116
3.3.2.1. General overview	116
3.3.2.2. Quantification of components	121
3.3.3. High-resolution sulfur S2p spectra	123
3.4. Structural changes studied by <sup>13</sup> C solid-state NMR spectroscopy	127
3.5. FTIR characterisation	131
3.6. Acidity of microwave sulfonated Starbons®	133
3.7. Morphology and textural characterisation	135
3.8. Conventional versus microwave sulfonation at 90 °C	
3.8.1. Elemental composition	139
3.8.2. Chemical environments observed through XPS analysis	
3.8.2.1. Sulfonated Starbons® 300 at 90 °C	140
3.8.2.2. Sulfonated Starbons® 450 at 90 °C	141
3.8.2.3. Sulfonated Starbons® 800 at 90 °C	142
3.8.3. Structural composition by <sup>13</sup> C solid-state NMR	142
3.9. Conclusions	142

### **Chapter 4. Sulfonation of Starbons® and their thermal stability**

4.1. Introduction	147
4.2. Sulfur dioxide released during sulfonation of Starbons®	148
4.3. Thermal stability of sulfonated Starbons® prepared by conventional heating	151
4.4. Thermal stability of microwave sulfonated Starbons®	156
4.5. Sulfur dioxide released during decomposition of Starbon® 300 sulfonated at different temperatures using microwaves	160
4.6. Sulfur dioxide released in the decomposition of sulfonated Starbons® 800	161
4.7. The effect of methanol washing	162
4.8. Physisorbed sulfuric acid?	165

4.9. FTIR spectra of sulfonated Starbons <sup>®</sup> : looking at washing effect	167
4.10. Conclusions	168

## **Chapter 5. Uses of sulfonated Starbons<sup>®</sup> in esterifications**

5.1. Introduction	173
5.2. Esterification of lauric acid	
5.2.1. Microwave irradiation or conventional heating?	175
5.2.2. Microwave irradiation: time effect	177
5.2.3. Evaluation of Sulfonated Starbons <sup>®</sup>	178
5.2.4. Reusability of S-Starbons <sup>®</sup>	181
5.3. Esterification of levulinic acid	183
5.3.1. The Shu-Lawrence approach	186
5.3.2. Identification of the 'intermediate'	188
5.3.3. Performance of sulfonated Starbons <sup>®</sup> in the esterification of levulinic acid	193
5.4. Test in esterification of 4-phenyl butyric acid and benzoic acid with methanol	195
5.5. Test of microwave sulfonated Starbons <sup>®</sup>	197
5.6. Deactivation of sulfonated Starbons <sup>®</sup>	202
5.7. Conclusions	205

## **Chapter 6. Experimental**

6.1. Chemical reagents	209
6.1.1. Chemicals used for synthesis and characterisation of sulfonated Starbons <sup>®</sup>	209
6.1.2. Chemicals used in reactions	209
6.2. Carbonization treatment	209
6.3. Sulfonation process	210
6.3.1. Conventional sulfonation	211
6.3.2. Methanol washing	211
6.3.3. Microwave sulfonation	212
6.3.4. Quantification of sulfur dioxide (SO <sub>2</sub> ) released during sulfonation	213
6.4. Materials characterisation	
6.4.1. Elemental analysis	214

6.4.2. Infrared spectroscopy	215
6.4.3. X-Ray photoelectron spectroscopy (XPS)	215
6.4.4. Solid-state <sup>13</sup> C CP/MAS Nuclear Magnetic Resonance	215
6.4.5. Surface area and porosity	216
6.4.6. Scanning Electron Microscopy (SEM) analysis	216
6.4.7. Thermal gravimetric analysis coupled to infrared spectroscopy (TG-FTIR)	216
6.4.8. Acidity determination	217
6.5. Catalytic testing	217
6.5.1. Sample preparation	217
6.5.2. Catalyst recycling	218
6.5.3. Gas Chromatography and Mass Spectra analysis	218
6.5.4. NMR spectroscopy	220
6.5.5. XRF analysis	220
<b>Chapter 7. Thesis conclusion and further work</b>	
7.1. Conclusion and further work	223
7.1.1. New synthesis approaches	223
7.1.2. Characterisation outcomes	
7.1.2.1. Sulfonated Starbons <sup>®</sup> by conventional heating	224
7.1.2.2. Microwave sulfonated Starbons <sup>®</sup>	225
7.1.3. Catalyst performance overview	225
7.2. Further work	227
<b>Chapter 8. Abbreviations</b>	
8.1. List of abbreviations	231
<b>Chapter 9. References</b>	
9.1. References	234



## List of figures

### Chapter 1. Introduction

Figure 1.1. The twelve principles of green chemistry (paraphrased)	28
Figure 1.2. Research progress in green chemistry	28
Figure 1.3. Easy recovery of a solid catalyst	31
Figure 1.4. Schematic representation of preparation of sugar catalyst	33
Figure 1.5. Two typical methods for the preparation of ordered mesoporous carbons	36
Figure 1.6. Schematic representation of Starbons <sup>®</sup> preparation	38
Figure 1.7. New range of carbonized Starbons <sup>®</sup>	39
Figure 1.8. Electromagnetic spectrum	41
Figure 1.9. Microwave dielectric heating: dipolar polarization and ionic conduction mechanisms	42
Figure 1.10. Schematic representation of sample heating by conventional heating and using microwaves	43
Figure 1.11. Schematic diagram of multiple reflection in an ATR system	46
Figure 1.12. Adsorption isotherms commonly found in catalysts	46
Figure 1.13. Classification of adsorption-desorption hysteresis loops and its association with pores shapes	48
Figure 1.14. Schematic representation of the adsorption-desorption process in mesopores	50
Figure 1.15. Diagram of photoelectrons production in the XPS analysis	51
Figure 1.16. Spinning charge on nuclei generates magnetic dipole	52
Figure 1.17. Magic angle spinning (MAS) diagram	53
Figure 1.18. Cross-polarization pulse sequence sketch	55
Figure 1.19. Schematic representation of TG-FTIR analysis	56

### Chapter 2. Synthesis and characterisation of sulfonated Starbons<sup>®</sup> by conventional heating

Figure 2.1. pH changes during washing of sulfonated Starbon <sup>®</sup> 300	63
Figure 2.2. Qualitative scale for sulfates concentration (A) and washings of sulfonated Starbon <sup>®</sup> 800 (B)	64

Figure 2.3. Leaching of sulfonated Starbons <sup>®</sup> analysed by XRF	65
Figure 2.4. Sulfur content (%) for sulfonated Starbons <sup>®</sup> after washing with methanol	66
Figure 2.5. FT-IR spectra for sulfonated Starbon <sup>®</sup> 350 after methanol washes	67
Figure 2.6. C:O atomic ratio of Starbons <sup>®</sup> before sulfonation	68
Figure 2.7. Van Krevelen diagram for starting Starbons <sup>®</sup>	69
Figure 2.8. Chemical composition of Starbons <sup>®</sup> before and after sulfonation	70
Figure 2.9. Van Krevelen diagram for Starbons <sup>®</sup> sulfonated at 90 °C for 6 h and washed with MeOH (3 times). Inset figure showing the changes of oxygen (O) atoms per 100 carbon (C) atoms before and after sulfonation.	71
Figure 2.10. Chemical composition of Starbons <sup>®</sup> sulfonated at 90 °C for 6 h and treated with MeOH (W3)	72
Figure 2.11. Variation in chemical composition of Starbons <sup>®</sup> before and after sulfonation (Ca and Cb arbitrarily set to 10 for all samples)	73
Figure 2.12. Variation in chemical composition of Starbons <sup>®</sup> before and after sulfonation	76
Figure 2.13. FTIR spectra of original and sulfonated Starbon <sup>®</sup> 300	77
Figure 2.14. FTIR spectra sulfonated Starbons <sup>®</sup> carbonized at several temperatures	79
Figure 2.15. FTIR spectra showing p-TSA residues in Starbons <sup>®</sup> 300 and 350	80
Figure 2.16. NMR spectra for Starbons <sup>®</sup> 300 before and after sulfonation	82
Figure 2.17. Functional groups identified for sulfonated Starbon <sup>®</sup> 350	84
Figure 2.18. <sup>13</sup> C NMR spectra for sulfonated Starbons carbonized at several temperatures	85
Figure 2.19. Proposed “structures” for Starbon <sup>®</sup> 300 (a) and Starbon <sup>®</sup> (600)	86
Figure 2.20. Elemental ratio (from XPS analysis) for Starbons 300 and 800 before and after sulfonation.	89
Figure 2.21. XPS spectra for C1s of Starbon <sup>®</sup> 300 prior (left) and after sulfonation (right).	90
Figure 2.22. XPS spectra for C1s of Starbon <sup>®</sup> 800 prior (left) and after (right) sulfonation	91
Figure 2.23. XPS spectra for C1s for conventional sulfonated	93

Starbons <sup>®</sup> (a) 350 (b) 450 (c) 550 (d) 600 and (e) 700	
Figure 2.24. XPS spectra comparison for C1s for conventional sulfonated Starbons <sup>®</sup>	94
Figure 2.25. XPS S2p spectra for conventionally sulfonated Starbons <sup>®</sup>	96
Figure 2.26. High-resolution S2p spectra for sulfonated Starbons <sup>®</sup> sulfonated Starbons <sup>®</sup> (a) 300 (b) 350 (c) 450 (d) 550	97
Figure 2.26I. High-resolution S2p spectra for sulfonated Starbons <sup>®</sup> sulfonated Starbons <sup>®</sup> (e) 600 (f) 700 (g) 800	98
Figure 2.27. Proposed “structures” for sulfonated Starbon <sup>®</sup> 300 (a) and sulfonated Starbon <sup>®</sup> (600)	100
Figure 2.28. Sulfur content for sulfonated Starbons <sup>®</sup> at 90°C for 6h	101
Figure 2.29. SEM images of Starbon <sup>®</sup> 300 (a) sulfonated Starbon <sup>®</sup> 300 (b); sulfonated Starbon <sup>®</sup> 450 (c) Sulfonated Starbon <sup>®</sup> 550 (d)	103
Figure 2.30. (a) Nitrogen adsorption isotherms and (b) pore size distribution for sulfonated and non-sulfonated Starbon <sup>®</sup> 300	104
Figure 2.31. (a) Nitrogen adsorption isotherm and (b) pore size distribution for sulfonated Starbon <sup>®</sup> 550	105
Figure 2.32. Nitrogen adsorption isotherm (a) and pore size distribution (b) for Starbon <sup>®</sup> 800; nitrogen adsorption isotherm (c) and pore size distribution (d) for sulfonated Starbon <sup>®</sup> 800 (c)	106
<b>Chapter 3. Synthesis and characterisation of microwave sulfonated Starbons<sup>®</sup></b>	
Figure 3.1. Scheme of microwave sulfonation of Starbons <sup>®</sup>	112
Figure 3.2. Elemental composition of microwave sulfonated Starbons <sup>®</sup> (a) 300, (b) 450 and (c) 800	114
Figure 3.3. Atomic composition of microwave sulfonated Starbons <sup>®</sup> for C (a), O (b) and S (c)	116
Figure 3.4. High-resolution C 1s spectra of microwave sulfonated of Starbon <sup>®</sup> 300 at 90°C (a), 120 °C (b) and 150 °C(c)	117
Figure 3.5. High-resolution C 1s spectra of microwave (MW) sulfonated of Starbon <sup>®</sup> 450 at 90°C (a), 120 °C (b) and 150 °C(c). Van Krevelen diagram of MW sulfonated Starbons <sup>®</sup> 450 (d)	120
Figure 3.6. High-resolution C 1s spectra of microwave (MW) sulfonated of Starbon <sup>®</sup> 800 at 90°C (a), 120 °C (b) and 150 °C(c).	121
Figure 3.7. Deconvolution of high-resolution S2p spectra for microwave sulfonated Starbons <sup>®</sup> 300 (a), 450 (b) and 800 (c) at 90 °C	124
Figure 3.8. Comparison of high-resolution S2p spectra for	126

microwave sulfonated Starbons 300 (a), 450 (b) and 800 (c) at 90, 120 and 150 °C	
Figure 3.9. Identification of functional groups in <sup>13</sup> C solid-state CP/MAS NMR spectra for Starbon 300 before sulfonation	128
Figure 3.10. Curve-fitting of <sup>13</sup> C solid-state CP/MAS NMR spectrum of Starbon <sup>®</sup> 300 microwave sulfonated at 90°C	128
Figure 3.11. <sup>13</sup> C solid-state NMR spectra for microwave sulfonated Starbons 300 at 90°C (a), 120 °C (b) and 150°C (c)	130
Figure 3.12. <sup>13</sup> C Solid-state NMR spectra for microwave sulfonated Starbons <sup>®</sup> 450	131
Figure 3.13. FTIR spectra for microwave sulfonated Starbons <sup>®</sup> 300	132
Figure 3.14. FTIR spectra of Starbon <sup>®</sup> 450 before and after microwave sulfonation at 90°C and 120 °C.	133
Figure 3.15. Titration curve for microwave sulfonated Starbon <sup>®</sup> 300 at 90 °C	134
Figure 3.16. Acidity determined by titration with NaOH (a) Comparison between obtained and expected sulfonic groups (b) for sulfonated Starbons <sup>®</sup> 300	135
Figure 3.17. SEM limages for microwave sulfonated Starbons <sup>®</sup> at 90 °C (a) S-Starbon <sup>®</sup> 300 MW 90 (b) S-Starbon <sup>®</sup> 450 MW 90 (c) S-Starbon <sup>®</sup> 800 MW 90	136
Figure 3.18. Textural properties for microwave sulfonated Starbons <sup>®</sup> (a) S-Starbon <sup>®</sup> 300 MW 90 (b) S-Starbon <sup>®</sup> 450 MW 90 (c) S-Starbon <sup>®</sup> 800 MW 90	137
Figure 3.19. Surface area for microwave sulfonated Starbons <sup>®</sup> (a) 300 (b) 450 (c)800 (d) summary of pore volume	139
Figure 3.20. van Krevelen diagram (left) and sulfur content (right) for sulfonated Starbons <sup>®</sup> using conventional heating and microwaves	140
Figure 3.21. XPS spectra for sulfonated Starbons <sup>®</sup> 300 by conventional and microwave heating	141

#### **Chapter 4. Sulfonation of Starbons<sup>®</sup> and their thermal stability**

Figure 4.1. Sulfonation of Starbon <sup>®</sup> by conventional heating (a) and FTIR spectra of gases released during process of sulfonation (b)	148
Figure 4.2. Diagram of suggested methodology for quantification of SO <sub>2</sub> released during sulfonation	149
Figure 4.3. Quantified sulfur dioxide released during sulfonation of Starbons <sup>®</sup> 300 (a) and 800 (b) using microwaves.	150
Figure 4.4. TGA thermograms for conventional sulfonated Starbon <sup>®</sup>	152

300 (a) and Starbon® 800 (b)	
Figure 4.5. FTIR spectra of gases evolved from sulfonated Starbon® 800 at 290 °C	153
Figure 4.6. TGA thermograms and IR absorbance of SO <sub>2</sub> gas versus temperature for (a) sulfonated Starbon® 300 and (b) sulfonated Starbon® 800	154
Figure 4.7. Comparison in the re-usability of sulfonated Starbons® 300 and 800	155
Figure 4.8. TGA thermogram for microwave sulfonated Starbon® 300 at 90°C-30 min	157
Figure 4.9. TGA thermogram for microwave sulfonated Starbon® 800 at 90°C-30 min	158
Figure 4.10. TGA thermograms and IR absorbance of SO <sub>2</sub> gas versus temperature for microwave sulfonated Starbon® 300 (a) and sulfonated Starbon® 800 (b)	159
Figure 4.11. TGA thermograms (a) and IR absorbance of SO <sub>2</sub> gas versus temperature (b) for microwave sulfonated Starbon® 300 at 90, 120 and 150 °C	160
Figure 4.12. IR absorbances for evolving SO <sub>2</sub> as function of temperature for sulfonated Starbons® 800	161
Figure 4.13. IR absorbances for evolving SO <sub>2</sub> from sulfonated Starbon 300 before (left) and after (right) methanol washing	162
Figure 4.14. Schematic representation of likely sulfur groups present on surface of sulfonated Starbon® 300	163
Figure 4.15. IR absorbances for evolving SO <sub>2</sub> versus temperature for microwave sulfonated Starbon® 300 before and after methanol washing	164
Figure 4.16. Schematic representation of sulfonated sample at the first wash	166
Figure 4.17. IR absorbances for evolving SO <sub>2</sub> versus temperature for microwave sulfonated Starbon® 300 at 150 °C after first wash (a) and after 14 washes (b)	166
Figure 4.18. Infrared spectra of microwave sulfonated Starbon® 300 prepared at 150 °C, after first and fourteenth washes.	167
Figure 4.19. IR spectra of sulfonated Starbons® 300 conventional (left) and microwave sulfonated (b) at 90 °C, before and after methanol washes.	168
<b>Chapter 5. Uses of sulfonated Starbons® in esterifications</b>	
Figure 5.1. Mechanistic route of acid catalysed esterification	173

Figure 5.2. Comparison of the esterification of lauric acid by methanol using microwave irradiation and conventional heating	176
Figure 5.3. Esterification of lauric acid by MeOH at different times (MW fixed power 200 W)	178
Figure 5.4. Conversion in the esterification of lauric acid by MeOH using S-Starbons® (30 min, 200W)	179
Figure 5.5. Comparison of the esterification of lauric acid using MeOH and EtOH (30 min, 200 W)	180
Figure 5.6. Esterification of lauric acid by EtOH, using 40 mg S-Starbons® (30 min, 200 W)	181
Figure 5.7. Diagram of recovery and reuse of catalyst	182
Figure 5.8. Reusability of S-Starbons® 300 and 800 in esterification of lauric acid with methanol	183
Figure 5.9. Molecular structure of 4-oxo-pentanoic acid/levulinic acid	183
Figure 5.10. GC -FID chromatogram of mixture of levulinic acid and methanol (1:15, day 4)	184
Figure 5.11. Reaction of levulinic acid with refluxing methanol (15 mmol acid, 10 mL alcohol, at 75 °C) (a) Conversion to ester (b) Conversion to intermediate	185
Figure 5.12. Molecular structure of 4-alkoxy-g-valerolactone proposed by Shu and Lawrence (1995)	186
Figure 5.13. Change in conversion of ester and intermediate in a solution of levulinic acid and methanol (a) molar ratio 1:30 and (b) molar ratio 1:15	187
Figure 5.14. Change in conversion of ester and intermediate in a solution of levulinic acid and methanol (a) molar ratio 1:20 and (b) molar ratio 1:10	188
Figure 5.15. Proposed structure formed during methanol storage of levulinic acid	188
Figure 5.16. Levulinic acid and relationship to its derivatives	189
Figure 5.17. <sup>13</sup> C NMR spectra for mixture of levulinic acid-MeOH 48 h	190
Figure 5.18. Mass spectra of intermediate identified in levulinic acid and methanol (1:30) solution	191
Figure 5.19. Mass spectra of intermediate identified in levulinic acid and methanol-d <sub>4</sub> (1:30) solution	191
Figure 5.20. GC -FID chromatogram of mixture of levulinic acid and ethanol (1:15, day 5)	192
Figure 5.21. Comparison of the esterification of lauric acid by	193

methanol using microwave irradiation and conventional heating	
Figure 5.22. Esterification of levulinic acid by MeOH, using 20 and 40 mg of sulfonated Starbons <sup>®</sup> (30 min, 200 W)	194
Figure 5.23. Reusability of sulfonated Starbons <sup>®</sup> in esterification of levulinic acid with methanol (catalyst 400 mg; MW 200 W, 30 min)	194
Figure 5.24. Esterification of 4-phenyl-butyric acid (a) and benzoic acid (b) with methanol (MW 200 W, 30 min)	197
Figure 5.25. Esterification of lauric acid by methanol using microwave sulfonated Starbons <sup>®</sup> 300	199
Figure 5.26. Esterification of lauric acid by methanol using microwave sulfonated Starbons <sup>®</sup> 450	200
Figure 5.27. Esterification of lauric acid by methanol using microwave sulfonated Starbons <sup>®</sup> 800	200
Figure 5.28. Esterification of lauric acid by methanol using microwave sulfonated Starbons <sup>®</sup> 300 90, conventional and recycled sulfuric acid	201
Figure 5.29. Reusability of sulfonated Starbons <sup>®</sup> 300 in the esterification of lauric acid by methanol	202
Figure 5.30. Comparison in sulfur content left after three runs in sulfonated Starbons 300 and 800	203
Figure 5.31. Studies on leaching of sulfonated Starbons <sup>®</sup> 300	205
Scheme 5.1. Esterification of lauric acid by methanol	175
Scheme 5.2. Esterification of 4-phenyl butyric acid by methanol	195
Scheme 5.3. Esterification of benzoic acid by methanol	196
<b>Chapter 6. Experimental</b>	
Figure 6.1. Carbonization procedure for Starbons <sup>®</sup>	210
Figure 6.2. Schematic representation of the sulfonation of Starbons <sup>®</sup> by conventional heating	211
Figure 6.3. Experimental set up used during sulfonation of Starbons <sup>®</sup> by microwave irradiation. Collection of gases using H <sub>2</sub> O <sub>2</sub> solution (30% v/v)	212
Figure 6.4. Schematic representation of the quantification of sulfur dioxide through potentiometric titration	214
Figure 6.5. Reproducibility of results obtained in esterification of lauric acid with methanol (MW, 200W, 30 min) and associated errors	219



## List of tables

### Chapter 1. Introduction

Table 1.1. IUPAC pore size classification	35
---	----

### Chapter 2. Synthesis and characterisation of sulfonated Starbons<sup>®</sup> by conventional heating

Table 2.1. New range of carbonized Starbons <sup>®</sup>	62
Table 2.2. XRF analysis results	65
Table 2.3. Variations in atomic content of H, O and SO <sub>3</sub> before and after sulfonation on Starbons <sup>®</sup>	74
Table 2.4. Comparison between sugar catalyst and S-Starbons <sup>®</sup> formulas	74
Table 2.5. Percentage atomic content in sulfonated Starbons <sup>®</sup>	75
Table 2.6. Observed FTIR bands and their assignments	78
Table 2.7. Elemental composition ( atomic %) for Starbons <sup>®</sup> 300 and 800	88
Table 2.8. Bonds assignments for components of C (1s)	90
Table 2.9. Chemical states of C and their relative concentration for Starbons <sup>®</sup> 300 and 800 before and after sulfonation. (Binding energies presented in parenthesis)	92
Table 2.10. Chemical states of C and their relative concentration for Starbons <sup>®</sup> 350 to 700 after sulfonation conventionally. (Binding energies presented in parenthesis)	95
Table 2.11. Relative concentration of chemical states of sulfur and their binding energy (in parenthesis, eV)	99
Table 2.12. Surface characteristics of sulfonated Starbons <sup>®</sup>	105

### Chapter 3. Synthesis and characterisation of microwave sulfonated Starbons<sup>®</sup>

Table 3.1. Sulfur content in sulfonated samples prepared at 150 °C	115
Table 3.2. Relative concentrations of carbon functionalities in microwave sulfonated Starbons <sup>®</sup>	123
Table 3.3. Relative concentration of sulfur functionalities in microwave sulfonated Starbons <sup>®</sup> 300, 450 and 800	126

### Chapter 4. Sulfonation of Starbons<sup>®</sup> and their thermal stability

Table 4.1. Comparison of sulfonation methods	147
--	-----

Table 4.2. Sulfur content ( $\text{mmol g}^{-1}$ ) for sulfonated Starbons <sup>®</sup> 300	164
---	-----

### **Chapter 5. Uses of sulfonated Starbons<sup>®</sup> in esterifications**

Table 5.1. Molar ratios of the mixtures of levulinic acid in alcohols	186
---	-----

Table 5.2. Molecular masses for levulinic acid and derivatives	190
--	-----

Table 5.3. C:O atomic ratio and sulfur loading from some sulfonated Starbons <sup>®</sup>	195
---	-----

Table 5.4. Description of microwave sulfonated Starbons <sup>®</sup>	198
--	-----

## ***Acknowledgements***

I would like to thank all the people who contributed in the making of this PhD thesis. Firstly I want to thank to my super-supervisor, Dr. Duncan J. Macquarrie for all your time, knowledge and experience shared during these years. Thanks for your insightful questions, for your great advice, for signing my reports, for our research update/chat meetings, for your patience, for your support in my low moods and for giving me hugs when I need them. Gracias, Duncan.

I also express my gratitude to Professor James H. Clark, for giving me the opportunity to join this excellent Green Chemistry group.

I extend my gratitude to Dr. Vitaliy Budarin, Dr. Mario De bruyn, Dr. Thomas Farmer and Dr. Simon Breeden, for sharing your experience and knowledge while I carried out this research. Special thanks to the technical staff, Paul Elliot, Hannah Briers and Charlotte Brannigan, who make sure our labs keep running. Thanks, Alison Edmonds, Christine Vis and Rachel Crooks for your administrative assistance.

I am very grateful to Consejo Nacional de Ciencia y Tecnología, CONACyT-México for the financial support received through the scholarship Reg. 183392 and to Secretaría de Educación Pública (SEP) for complementary funding.

I would like to thank past and present members of the Green Chemistry group, in particular to Helen Parker, for all your support and advice since my arrival at York. I also thank Sasha, Rob, Lucie, Hemin, Abdul, Cheng, Maggie, Roy, Emma Coops, Andy Marriott, Gareth, Peter, Jimbo, Nonti, Keisuke and Tabitha, for all the good-bad-funny-stressful-happy times shared in labs, offices and abroad during this time.

Thanks to all my friends, for giving a special touch to my life. I especially thank my best friend, Martha, for the many adventures we have shared during our PhD time at York. Thanks to Manolo, Bere, Sam, Irma, Bárbara, Ana, Wera and Radek, for always having time for me to chat and laugh; a special “thank you” goes to Daniel, Gabo, don Gus, Andrés, Diana, Marcel, Nancy, Vicente, Alonso, Chukis and doña Soco for cheering me up via internet. Thanks to my little ones, Greg, Lucas, Marianita, Cannelle and Greyson and their respective parents for giving me a “break from chemistry” to experience my maternal love.

A huge “thank you” to my Abuelito Mágico, don Alfredo Buenfil, and his family, for all your love and support during all these years; thanks for going that 4<sup>th</sup> of August 2000 to find me at Pebá, offering me the opportunity to keep growing; who would say we’d be at this stage? Thanks to my family, especially to my parents, Aurora and Julio, for encouraging me to follow my ideas and dreams; to my loves Bere and Zoe, who fill my heart and make me very happy. Finally, thanks to Enrique, for being my companion through the distance and the years.

## **Dedication**

*To all the honest hard-working Mexicans, whose families live in social and economic inequality. Although the way to succeed is tough, it is also possible.*

## **Declaration**

I hereby declare that the work presented in this thesis is my own, except where otherwise acknowledged, and has not previously been submitted for a degree at this or any other university.



# **Chapter 1**

## ***Introduction***



## 1.1. Green chemistry, the approach to achieve sustainability

In recent times, a high concern has arisen into the concept of sustainability, becoming the centre of attention for all the actors in society: industry, research, education, government and public in general.<sup>1</sup> It was in the report “Our common future”<sup>2</sup> prepared by the United Nations where the term *sustainable development* was first defined as: “*Meeting the needs of the present generation without compromising the ability of future generations to meet their own needs.*” Since then, a combination of endeavours from scientists, industrialists and governments have been channelled to make sustainability an achievable goal.

In the early 1990s, Paul Anastas throughout his work in the US Environmental Protection Agency (EPA) created the concept of *green chemistry*, defined as the “design of chemical products and processes to reduce or eliminate the use and generation of hazardous substances”.<sup>3,4</sup> As Sheldon<sup>5</sup> remarks that does not mean that research on green chemistry did not exist before the early 1990s, solely that it did not have the name.

Green chemistry contains in its definition the word “design” and how its inventor has alluded through several of his publications on the topic,<sup>4,6,7</sup> it necessitates “the conscious and deliberative use of a set of criteria, principles, and methodologies”. This guide is provided in the Twelve Principles of Green Chemistry (**Figure 1.1.**).

These principles sort the fundamental approaches taken to achieve the green chemistry goals of benign products and processes, and have been used as guidelines and design criteria by molecular scientists.<sup>6</sup>

1. Waste prevention instead of remediation
2. Atom efficiency
3. Less hazardous/toxic chemicals
4. Safer products by design
5. Innocuous solvents and auxiliaries
6. Energy efficient by design
7. Preferably renewable raw materials
8. Shorter syntheses (avoid derivatization)
9. Catalytic rather than stoichiometric reagents
10. Design products for degradation
11. Analytical methodologies for pollution prevention
12. Inherently safer processes

**Figure 1.1.** The twelve principles of green chemistry (paraphrased)<sup>5</sup>

Since the appearance of the green chemistry principles, there has been a significant growth in the volume and scope of green chemistry related research. In his review in 2005, Clark<sup>8</sup> already remarks the rising of local and international initiatives to fund the area; as well the increasing appreciation of the value of green chemistry at all stages in the lifecycle from “cradle to grave” (**Figure 1.2.**). Although most of the research effort had been centred in the manufacturing area, at the time some other stages were becoming more thoroughly explored, creating optimism in the development of this emerging discipline.

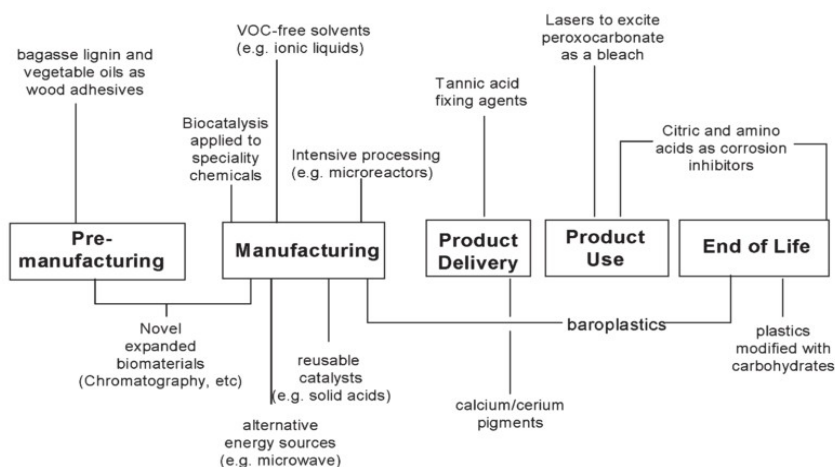


**Figure 1.2.** Research progress in green chemistry (taken from Clark, 2006<sup>8</sup>)

The green chemistry strategy aims to achieve sustainability at the molecular level<sup>4</sup> and the twelve principles of green chemistry constitute a guiding framework<sup>7</sup> to make it possible. Then, through the application of the green chemistry concept, the design of new chemical products and processes can be accomplished, which maintain and improve our quality of life but with few/no environmental impacts. However, we need to bear in mind, that a large impact would be got when all aspects of the process life-cycle are embedded in the green chemistry concept: from the raw materials used to the efficiency and safety of the transformation, the toxicity and biodegradability of products and reagents used.

### 1.1.1. The green chemistry side of this project

The overall aim of this work is to apply the green chemistry concept to develop strong solid-acid catalysts (Principle 9), based on renewable materials (Principle 7), using a type of modified starch through controlled carbonization, denominated Starbons<sup>®</sup> and described as “mesoporous materials”.<sup>9</sup> This project also involves the use of microwave chemistry like an alternative to conventional heating as an approach to improve energy efficiency (Principle 6). One of the important aspects of this research was not only the synthesis but also the characterisation of the sulfonated Starbons<sup>®</sup>, prepared by conventional heating and at big scale (**Chapter 2**) and using microwave irradiation (**Chapter 3**), providing an in-depth knowledge of the properties of these novel materials. Further characterisation related to the thermal stability of sulfonated Starbons<sup>®</sup> is presented in **Chapter 4**, to get a better understanding of its intrinsic properties. Finally, **Chapter 5**, deals with the evaluation of these materials in esterification reactions using both conventional and microwave heating, and including pretreatment, reuse and leaching trials. As presented in **Figure 1.2.**, this project falls into the manufacturing research progress carried out in green chemistry, according to Clark,<sup>8</sup> as it combines the use of recyclable catalysts and microwaves in the production of chemicals from platform molecules, like levulinic acid.

**Maybe not completely green?** It is worth mentioning at this stage, that sulfuric acid was used for sulfonation of materials, despite the fact of its hazards, although it should also be borne in mind that is cheap, readily available<sup>10</sup> and sulfur reservoirs are not at risk of depletion.<sup>11</sup> In addition sulfuric acid possesses a high ability to create efficient active solids.<sup>12</sup> However, proposals to move toward a greener process include the change of origins and quantities of sulfuric acid. Then, in this new approach, the sulfuric acid used was a commercial one with 95 % purity against 99.999 % used in previous synthesis;<sup>13,14</sup> as well, the ratio of material used is 1 g of solid to 7 mL of sulfuric acid (1:7), decreased compared with previous syntheses in which the ratio used was 1:10.<sup>13,14</sup> These attempts were also combined with the successful demonstration that recovery and reuse the sulfuric acid in the preparation of more sulfonated Starbons® is possible and leads to active catalysts.

## **1.2. Heterogeneous catalysis, as a green chemistry operational tool**

In fact, as far as chemistry is concerned, catalysis is the key to sustainability, it has been regarded as the “pillar of green chemistry”<sup>15</sup> because its potential to achieve both economical and environmental goals.<sup>16</sup> Heterogeneous catalysis covers all the cases where the catalyst and the substrate are in different phases. However, when chemists refer to heterogeneous catalysis, they usually describe a system where the catalyst is a solid and the reactants are (most often) gases or liquids.<sup>17</sup> It has been already mentioned that green chemistry attempts to get optimized processes, this could be accomplished through the replacement of stoichiometric methodologies with green catalytic alternatives,<sup>5</sup> as pointed out in the twelve principles guidelines. Among the desirable characteristics of a catalyst we can enumerate its activity, stability, insolubility and ease to be recovered.<sup>10,16</sup> Then, in a solid-liquid interaction, the catalyst (solid) could be easily removed from mixture and reused over and over (**Figure 1.3.**).

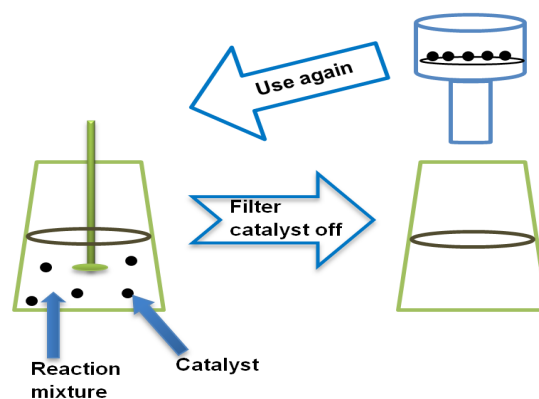


**Figure 1.3.** Easy recovery of a solid catalyst (adaptation from Clark, 2002<sup>10</sup>)

### 1.2.1. Solid-acid catalysts

Use of acid catalysts is widespread, as it can be applied in all sectors of the chemical, pharmaceutical and associated industries, as well the largest scale use is in the petrochemical industries where the processes are largely quite efficient and the use of solid-acid catalysts, mainly zeolites is well established.<sup>10,12</sup> Among the solid acids, we can find mixed oxides such as silica–alumina and sulfated zirconia, acidic clays, zeolites, supported heteropolyacids, organic ion exchange resins and hybrid organic–inorganic materials such as mesoporous oxides containing pendant organic sulfonic acid moieties.<sup>18</sup> Thus, sulfonated Starbons® will fall in the latter category. The conversion reagent–products over solid acids used as catalysts represents a convenient choice to replace conventional processes carried out in concentrated aqueous acid solutions, as they are considered not to be environmentally friendly; they are difficult to separate from the organic products and their use leads to large volumes of hazardous waste.<sup>10</sup> In addition, an aqueous work-up for esterification can lead to hydrolysis of the product, then a dry agent is needed; increasing the steps and materials for purification. Also, the recovery of catalyst requires purification or concentration, which often is difficult and wasteful.

Then recyclable solid-acid catalysts can eliminate hazardous waste associated with conventional acids, giving the opportunity to achieve sustainability through the green chemistry principles. Just as it was mentioned above, there are several types of known solid inorganic acids amongst which we find sulfated

zirconia, which is very widely applied and has been extensively studied due to its acid strength, in spite of the microporosity characteristic of the material;<sup>19–21</sup> as well, the use of sulfonic silicas in catalysis have emerged like a way to develop efficient and recyclable solid catalysts,<sup>20,22</sup> although their preparation could be very costly.<sup>23</sup> However, the present study focuses more on carbon-base acid catalysts which is presented next.

### 1.3. Carbon-based acid catalysts

#### 1.3.1. The “sugar catalyst”

In this section, a short review about some carbonaceous solid-acid catalysts developed recently is presented. In 2004, *Hara et al*<sup>24</sup> reported the preparation of a strong solid acid obtained through the incomplete carbonization of sulfoaromatic hydrocarbons, resulting in small polycyclic aromatic carbon sheets, with attached sulfonic groups ( $\sim\text{SO}_3\text{H}$ ). This carbon-base catalyst exhibited a remarkably high-content of acid sites and high activity, comparable to sulfuric acid, although very low surface area. In spite of its high catalytic activity, it is worth mentioning some drawbacks from this approach, as the use of petroleum-based materials such as naphthalene; as well the high temperature of sulfonation (200 to 300 °C), compared with our approach, in which we use bio-based starting materials, commercial  $\text{H}_2\text{SO}_4$  acid (95 % purity) and lower temperatures in the sulfonation process.

In 2005, the sugar catalyst made its first appearance,<sup>25</sup> in this work the preparation of a carbon-based solid acid was carried out using D-glucose as precursor, again the approach consisted in the partial carbonization of the precursor followed by its sulfonation with sulfuric acid at 150 °C (**Figure 1.4**).

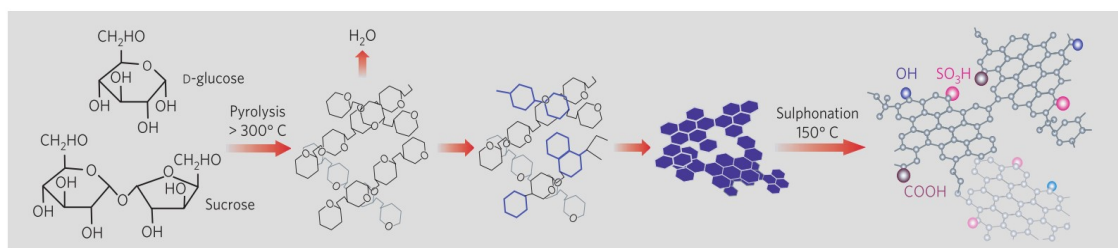


**Figure 1.4.** Schematic representation of preparation of sugar catalyst (from Toda *et al*<sup>25</sup>)

The surface area obtained for this material was even lower ( $<2\text{m}^2\text{g}^{-1}$ ) than that reported for the past carbonized materials ( $<24\text{m}^2\text{g}^{-1}$ ).<sup>24</sup> This time, the authors of the sugar catalyst, claimed to have obtained very stable and high activity catalyst, as well as high recyclability. We are going to see further, that other researchers attributed this high activity to the leaching of sulfonic-aromatic groups from the materials.<sup>26</sup> In the subsequent years of its appearance, the sugar catalyst has undergone some modifications like the temperature of carbonization of the D-glucose precursor or the sulfonation process;<sup>27,28</sup> further developments include the switch to cellulose as starting material;<sup>29</sup> and subsequently, the use of wood powder with other materials as  $\text{ZnCl}_2$ , to prepare another kind of carbon material. This new material was shown to be highly porous, representing an improvement in the synthesis<sup>30</sup> of the sulfonated material, in which fuming sulfuric acid (15 %  $\text{SO}_3$ ) was used. Although this methodology could be very effective to bond sulfonic groups to the materials, it is worth pointing out the hazard of its manipulation. Another approach proposed by Hara's group to create very efficient solid-acid carbon catalysts consisted in using as precursors resorcinol and a formaldehyde solution to form an aerogel.<sup>31</sup> This method improved the porosity of the obtained material, but it is worth mentioning that this design uses benzene derivatives and formaldehyde, a carcinogenic compound; in addition, the quantity of sulfuric acid used was astonishingly high: 4.0 g of solid and 200 mL of fuming  $\text{H}_2\text{SO}_4$  (15 %  $\text{SO}_3$ ), making this process a bit far from the green chemistry concept. At this point, it is worth asking how much can we sacrifice to get “very efficient” materials in exchange for not providing environmentally friendly initiatives? We should bring back the twelve principles of green chemistry to re-evaluate whether our strategies to achieve sustainability are consistent.

The use of D-glucose as starting material for the creation of solid acids based on the sulfonation of amorphous polycyclic carbons, caused great interest to scientific community that some other investigations were carried out afterwards. For example, the preparation of a “very strong” sugar catalyst carbonized at 400 °C, which after sulfonation with sulfuric acid, showed that can be used up to 50 cycles in the esterification of oleic acid.<sup>32</sup>

Another study suggested the use of other sulfonating agents such as p-Toluenesulfonic acid (p-TSA),<sup>33</sup> although the material seems to be very efficient catalytically, its activity looks to be more related to the residues of p-TSA on the material than to sulfonic groups attached, because the analysis of the sample in the infrared spectra showed bands associated specifically to p-TSA.<sup>34–36</sup> Another draw back from this proposal is related to the fact of preparing p-TSA, as precursors involved will be toluene (petroleum based material) and sulfuric acid.

One more methodology recommended consisted of using a mixture of D-glucose and starch in aqueous solution,<sup>37</sup> which was carbonized at 400 °C after 24 h of repose. Afterwards, the resulting black solid was sulfonated with sulfuric acid (>98 %) at 150–160 °C for 5 hours. Although the materials presented modest catalytic activity and it was noticed that deactivation when increasing the cycles of the esterification of oleic acid with methanol, it is worth pointing out that these authors suggested to reactivate their catalysts using more sulfuric acid solutions (5 % and 98 %). This methodology invites to bring up our 12 principles of green chemistry, is it a good idea to use more and more sulfuric acid?

Other types of sulfonated carbons have been also proposed as potential materials to replace traditional liquid acids. These materials include sulfonated activated carbon,<sup>38</sup> this research proposed another way to carry out sulfonation, through a reduction process with 4-benzene-diazonium sulfonate salts and hypophosphorous acid (H<sub>3</sub>PO<sub>2</sub>). Although the materials showed high activities during first runs, the authors suggests to reactivate the materials with sulfuric acid, just like previous case.<sup>37</sup> Another synthesis, which use this sulfonating agent, 4-benzene-diazonium sulfonate salts, was the preparation of sulfonated

graphene,<sup>39</sup> in this investigation, the materials obtained seem to be very active to hydrolysis reactions and keep their activity through several cycles (>5). In contrast to the previous methodologies, the reactivation with sulfuric acid was not needed. Finally, another interesting approach to create a carbonaceous solid acid catalyst was using lignosulfonate, waste of paper-making industry, in a reaction with sulfuric acid.<sup>40</sup> This new catalyst tested in esterification reactions, presented activities comparable to the resin Amberlyst-15, a well-known acid catalyst.

### **1.3.2. Porous catalysts**

A porous material is a solid matrix composed of an interconnected network of pores (voids), filled with a fluid (liquid or gas). These kind of materials provide higher surface areas within pores, allowing high interaction between the solid and its surroundings. Another intrinsic characteristic is their volume ratio, which is related to the diffusion process that takes in place into the materials, this is driven by the pore size.

According to the International Union of Pure and Applied Chemistry (IUPAC), porous materials are divided into three classes<sup>41</sup> which are summarized in **Table 1.1**.

<b>Pore type</b>	<b>Size (nm)</b>
Micropores	< 2
Mesopores	2 – 50
Macropores	> 50

As mentioned previously, heterogeneous catalysis can play a key role in the development of environmentally benign processes; so, the search for efficient solid catalysts is fundamental. Although, zeolites are very popular due to their highly ordered structure and excellent thermal stability, some of their applications are limited because of their microporosity; as presents high surface

area but diffusion into the small pores makes harder the interaction of the molecules. Then, in this respect, ordered mesoporous catalysts could open the door for new catalytic processes.<sup>42</sup> As mesoporous materials, are more suitable for liquid-phase applications, because their pore size allow access to specific active sites and provide efficient diffusion/mass transfer of liquid phase analyte and substrate.<sup>43</sup>

One example of these materials are the ordered mesoporous carbons, in which there is an increasing interest because of their potential applications. Several strategies have been proposed for preparation of these ordered mesoporous carbons prepared by controlling carbonization<sup>44,45</sup> materials which could be modified to solid acids later. Two typical methods for the preparation of ordered mesoporous carbon materials are presented below in **Figure 1.5**. showing the silica hard templates and the use of copolymers.

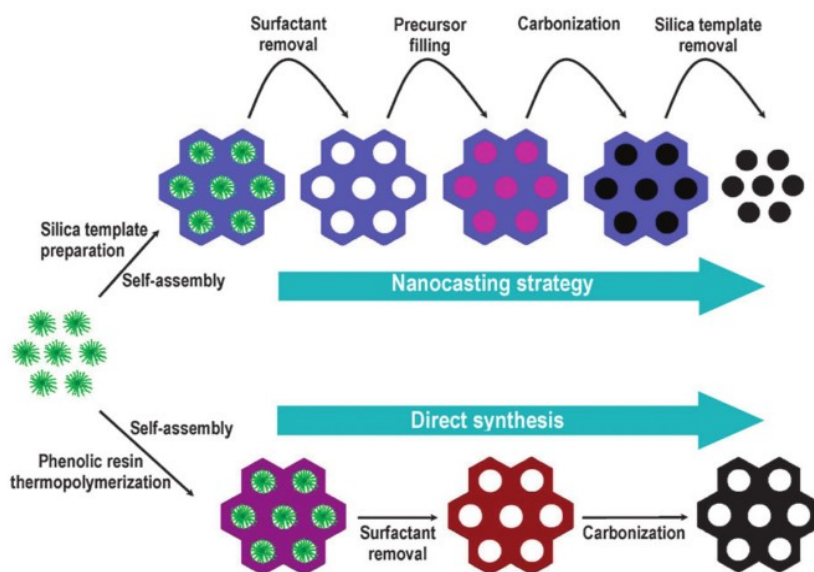


**Figure 1.5.** Two typical methods for the preparation of ordered mesoporous carbons<sup>44</sup>

Although these methodologies give some advantages like tunable porosity, uniform pores and high surface they also present some disadvantages as the use of expensive silica sources<sup>23</sup> or the use of hydrofluoric acid to remove silica<sup>45</sup> and in general, the use of several steps and reagents to prepare the material.

Research associated with the use of silica supports in the preparation of solid acids was applied to the synthesis of sulfonated carbon nanocages,<sup>46</sup> materials which possess high surface area and highly ordered mesopores. Despite the fact that sulfonated carbon nanocages present relatively high catalytic activity and reusability, their preparation including several steps and sulfonation was carried out using benzene-sulfonic reagents, materials coming from petroleum sources. Active solid acid catalysts using ordered mesoporous carbons as precursor has been also proposed by Xing *et al.* In this approach the sulfonation was carried out through vapour-phase transfer using sulfur trioxide. These materials presented high catalytic activity and reusability in the condensation of bulky molecules such as benzaldehyde and ethylene glycol.<sup>23</sup>

As it is presented above, ordered mesoporosity on carbons is a desirable characteristic, which could be achieved through the use of silica supports or templates,<sup>44</sup> however, most of these methodologies require of several steps in the preparation, energy consumption to remove templates, generating unnecessary waste,<sup>47</sup> getting us away from the green chemistry concept.

### 1.3.3. Sulfonated Starbons<sup>®</sup>, a mesoporous biobased alternative

In 2006, Budarin *et al* reported a novel approach for the generation of a new family of mesoporous carbonaceous materials with surfaces ranging from hydrophilic to hydrophobic, which is controlled by the degree of carbonization<sup>9</sup>. The strategy consisted in synthesizing mesoporous carbonaceous materials, called “**Starbons<sup>®</sup>**”, using mesoporous expanded starch as the precursor without the need for a templating agent.<sup>48</sup> A schematic representation of the methodology is presented in **Figure 1.6**. First, a simple process of gelatinization in water opens up and disorders the dense biopolymer network, after which it partially recrystallizes during a process of retrogradation. Exchanging water with ethanol prevents collapse of the network structure during the drying process. After drying, the expanded mesoporous starch is obtained. In the final stage of the process, mesoporous starch is doped with a catalytic amount of p-toluenesulfonic acid and heated under vacuum. This enables fast carbonization and fixing of the mesoporous structure. Heating at different temperatures,

ranging from 150 to 800 °C produces a variety of mesoporous materials from amorphous carbons to graphite-like activated carbons.

Since their discovery, the method for preparing Starbons<sup>®</sup> has been very well explored and the resulting materials characterised. Through this way, the elemental composition dependency from the carbonization temperature was found, the starch-like material at low temperatures switches to graphitic-like at high temperature of carbonization.<sup>9</sup> It is worth mentioning that at the beginning, these procedures were carried out at scale of some grams and using a kind of starch identified as *Hylon starch*.

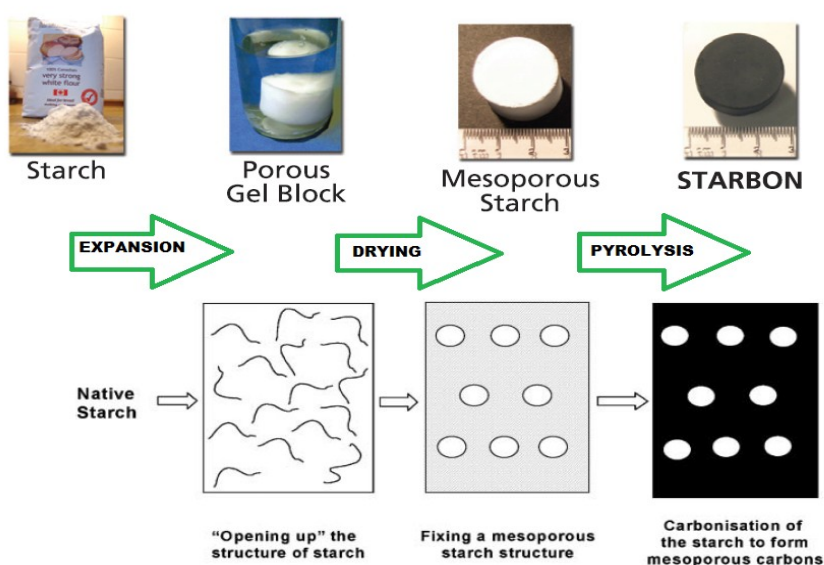


**Figure 1.6.** Schematic representation of Starbons<sup>®</sup> preparation

Growing interest in moving the preparation of Starbons<sup>®</sup> from lab-bench scale to industrial scale, motivated the synthesis of the materials used and characterised in this project. How will our Starbons<sup>®</sup> change?

Then, it is important to mention that the main variations from previous Starbons<sup>®</sup> include the use of a different starting material: *Cleargum starch*. According to Shuttleworth,<sup>49</sup> *Cleargum* starch differs from *Hylon* starch in the percentage of amylose; as the later contains 70 % of amylose and the former, contains, 27 %. *Cleargum* starch, this material also received an acidic treatment before

gelatinisation. The preparation of the mesoporous starch carried out at Contract Chemicals Ltd., Knowsley (>100 kg) and the large scale carbonization (over 10 Kg) at 300°C, 400°C and 800 °C done at Nabertherm, Germany. The 300, 400 and 800 materials were examined “as received” and the other Starbons® were prepared from these by lab-scale carbonization of the 300 to produce 350 and 400 for further temperatures (**Figure 1.7.**). This carbonization was done under nitrogen flow (100 mLmin<sup>-1</sup>), using over 50 g of starting material, this approach is also significantly different from previous synthesis, where carbonization was done in the scale of few grams.

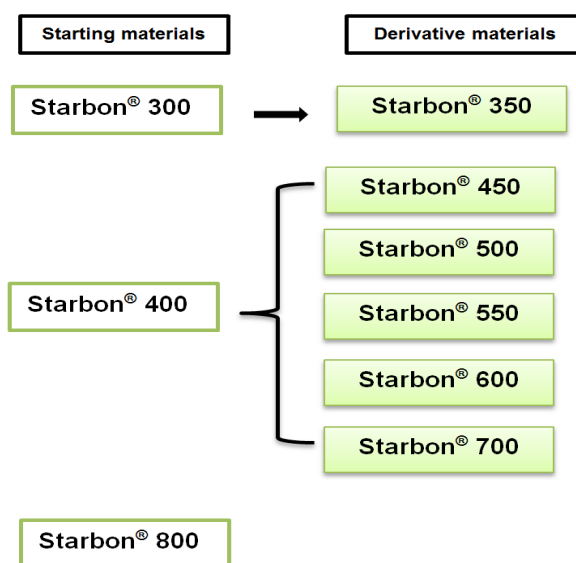


**Figure 1.7.** New range of carbonized Starbons®

To keep the scale-up approach, sulfonation of Starbons® was carried out at higher proportions using over 80 g of these carbonaceous materials, compared with small quantities prepared previously.<sup>13,14</sup> Other modifications in the preparation of sulfonated Starbons® were the suppression of “conditioning steps” with toluene after sulfonation, trying to get a greener method, bearing in mind the green chemistry concept, so it was intended to decrease the number of reagents and steps in preparation and to eliminate some toxic components. As mentioned initially, our sulfonation was carried out using a higher ratio of Starbon® to acid, so the proposed proportion was 1 g Starbon®: 7 mL H<sub>2</sub>SO<sub>4</sub> (95 %), using less pure sulfuric acid than before (99.999 %),<sup>13</sup> it is important to point out that further reduction in acid content led to mixtures which were very difficult

to stir.

With this switch to a scale-up approach and the above mentioned changes, we intended with the realization of this work to carry out a re-discovery of Starbons<sup>®</sup> and sulfonated Starbons<sup>®</sup>, through their characterisation and tests on catalysis applications. This was done, keeping in mind that, because of their nature, Starbons<sup>®</sup> have shown to be versatile materials, with tuneable surface properties, not only related to porosity characteristics related, but also to the several functional groups present on the materials.

The move towards more environmentally sustainable approaches in chemical processes, have stimulated the use of recyclable solid acids,<sup>50</sup> in this approach sulfonated Starbons<sup>®</sup> emerge as good candidates to be used.

#### **1.4. Microwave chemistry**

The use of microwaves as an energy source for chemical reactions and processes has been extensively investigated during recent years,<sup>51</sup> indeed, the technique was nominated as the “Bunsen Burner of the 21<sup>st</sup> century”.<sup>52</sup> Among the most common benefits claimed due to the use of microwaves in assisted synthesis we find: very rapid reactions, in many cases during just a few minutes, because of high and heterogeneous temperatures and possibly combined with pressure effects (if reaction occurs in closed vessels); higher degree of purity achieved due to short residence time at high temperatures; yields often better, obtained within shorter times and with purer products.<sup>53</sup> Microwave irradiation was used for the synthesis of sulfonated Starbons<sup>®</sup> (**Chapter 3**) as well as for the evaluation of the sulfonated Starbons<sup>®</sup> in esterification reactions (**Chapter 5**).

##### **1.4.1. What are microwaves?**

Microwaves are a form of electromagnetic radiation that belongs to the lower frequency end of the electromagnetic spectrum, the frequency range of which is defined from 300 to about 300 000 megahertz (MHz)<sup>54,55</sup> (**Figure 1.8**). The most

usual frequency used in industrial, medicinal, domestic or scientific applications has been prescribed by international legislation<sup>51,53,56</sup> and corresponds to the value of 2450 MHz (or 2.45 GHz), with a wavelength of 12.2 cm.

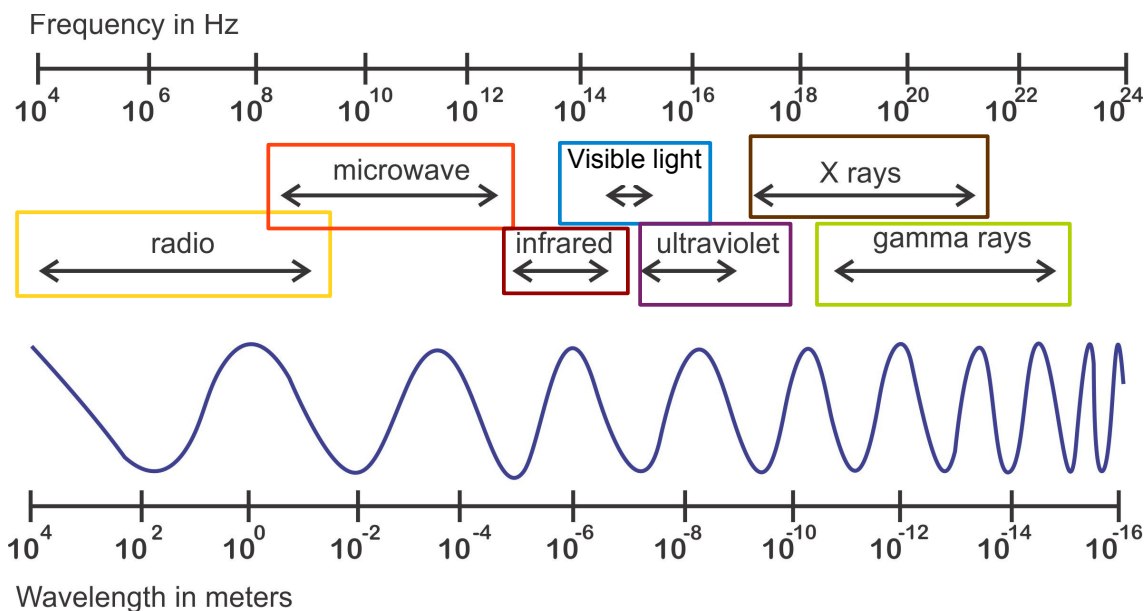


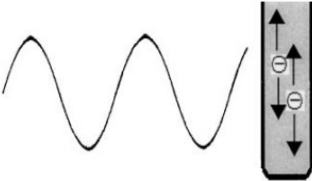
**Figure 1.8.** Electromagnetic spectrum

### 1.4.2. Microwave heating

Heating of materials exposed to microwave irradiation results from the material-wave interaction, as well as the capacity of some materials (liquids and solids) to transform electromagnetic energy into heat.<sup>53,57</sup> Transformation into heat of a part of the energy contained in the microwaves is called dielectric heating.<sup>51,55</sup> According to Loupy, the physical origin of this heating conversion is related to the ability of the electric wave component to induce polarization of charges within the heated product.<sup>58</sup> As the reversals of the electric field are faster than the polarization of the molecules, this process induces stirring and friction on molecules, promoting heating of the irradiated media.<sup>53,58</sup>

There are two principal mechanisms through which microwave dielectric heating is generated: the dipolar polarization and the ionic conduction.<sup>55,59</sup> These two mechanisms are presented in **Figure 1.9**. In the dipolar polarization

mechanism, the heat is generated through the interaction of the waves with the substance which must have a dipole moment. Polar molecules placed in an electric field, become aligned to the field; when the electric field starts oscillating, the molecules begin to align and realign, creating an internal friction and then internal heat.<sup>55,58</sup> The ionic conduction mechanism, requires the presence of free ions or ionic substances, the heat is generated by the motion of the ions in the material as they try to orient themselves to the oscillating applied field.<sup>55</sup> From this information it is inferred that non-polar molecules such as toluene, carbon tetrachloride, diethyl ether and benzene are microwave-inactive, while polar molecules such as H<sub>2</sub>O, methanol, ethanol acetonitrile and CH<sub>2</sub>Cl<sub>2</sub>, are microwave-active, remembering that polar molecules can align themselves with the electric field.<sup>56</sup>

Dipolar polarization mechanism	Ionic conduction mechanism
	
Heat generated by the rotational movements of molecules during matter-wave interaction	Heat generated by the motion of ions/ionic material during matter-wave interaction

**Figure 1.9.** Microwave dielectric heating: dipolar polarization and ionic conduction mechanisms<sup>55</sup>

### 1.4.3. Microwave irradiation vs conventional heating

In general, chemical synthesis has been done through conductive heating using an external heat source. However, this approach has shown to be slow and sometimes has been considered inefficient. Microwave heating is different from conventional heating,<sup>60</sup> as was mentioned above, the interaction between the electromagnetic wave and the irradiated medium produces the heat in medium. So, a fundamental difference between microwave and conventional heating could be pointed out: in conventional heating heat energy is transferred to the

material through convection, conduction and radiation of heat from the surfaces of the vessel, in other words, heat transfers take place from the heating device to the medium; while in microwave heating, heat is spread inside of the irradiated medium, through molecular interaction with the electromagnetic field (**Figure 1.10**). Then, in conventional heating heat transfers depend on thermal conductivity, on the temperature difference from the heating medium to the vessel walls and finally to the solution being heated, as well as on convection currents, this causes that temperature increment to often be slow. In microwave heating, the conversion of electromagnetic energy to thermal energy is through direct interaction of the incident radiation with the molecules of the material, it is a mass heating, then heat goes from the medium to the outside. In this approach the important parameters are the microwave power used and the dipolar characteristics of the irradiated material, then much faster temperature increases can be obtained.<sup>60,61</sup>

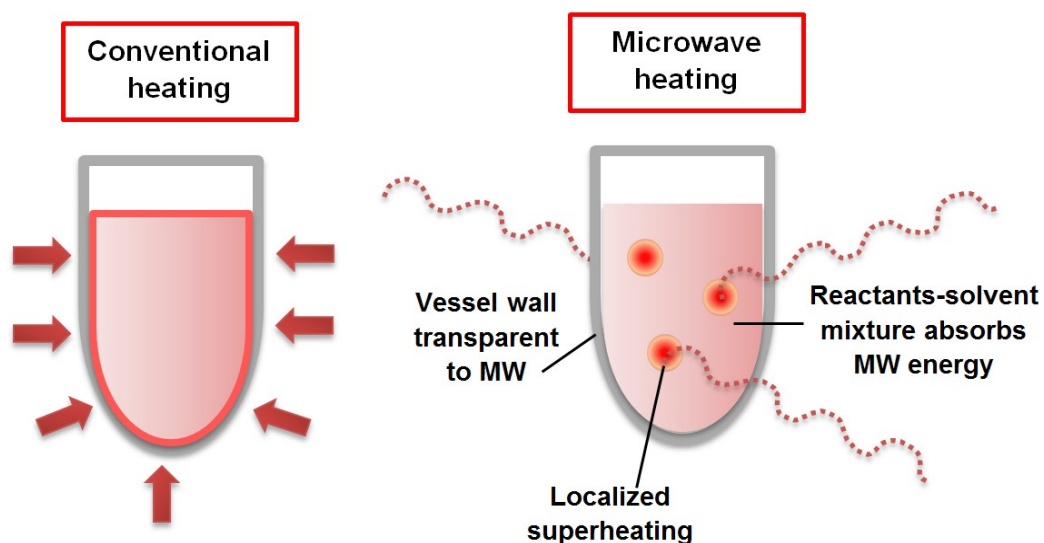


**Figure 1.10.** Schematic representation of sample heating by conventional heating and using microwaves (adaptation from Hayes, 2002<sup>54</sup>)

#### **1.4.4. “Microwave activation”, “hot spots” and “super-heating effect”**

At this stage it is worth referring to terms associated with microwaves. One of them is the term “microwave activation”, which does not refer to a “direct molecular activation”, because of the microwave irradiation.<sup>60</sup> Here it is important to mention the corresponding energy for the microwaves with frequencies 300 MHz and 300 GHz which result in  $1.24 \times 10^{-6}$  and  $1.24 \times 10^{-3}$  eV, respectively. These energies are much lower than typical ionization energies of biological compounds (5 eV), of bond energies (5 eV), and even lower than hydrogen bonds (2.10 eV), van der Waals intermolecular interactions (2 eV); so molecular transformations because of the microwave interactions should be discarded.<sup>58,60</sup>

As microwave heating does not depend on thermal conductivity of the vessel materials, the distribution of the heat is heterogeneous and the creation of local “hot spots” may occur if the heat generation is faster than heat distribution.<sup>58,60</sup> The hot spots then can become the “super-heating effect”, describe as local overheating.<sup>51</sup> This difference in the way how energy is delivered in microwave heating, makes microwaves attractive to explore in the processing of materials and synthetic transformations.

### **1.5. Analytical techniques**

A brief review is given for some of the analytical techniques employed in characterisation of the materials synthesized as well in the analysis of the products obtained in reactions carried out in this work. Specific details of the measurements are presented in the Experimental section in **Chapter 6**.

#### **1.5.1. Infrared spectroscopy, attenuated total reflectance (ATR-FTIR)**

In the infrared spectroscopy technique, samples are exposed to infrared (IR) radiation. Molecules with covalent bonds may absorb IR radiation. This absorption is quantized, then only certain frequencies of IR radiation are absorbed; when radiation is absorbed, the molecule moves to a higher energy

state. The energy associated with IR radiation is sufficient to cause molecules to rotate (if possible) and to vibrate. The energy required for causing a change in the rotation level is smaller than the one required for causing a change in the vibration level, then each vibrational change has multiple rotational changes associated with it. Therefore, gas phase IR spectra consists of a series of discrete lines; as free rotation does not occur in condensed phases, the IR absorption spectrum for a solid or liquid is composed of broad vibrational absorption bands. In this project, both gases and solids are analysed by IR spectroscopy, in a wavenumber range which corresponds to the mid-region from 4000–400  $\text{cm}^{-1}$ . Molecules absorb radiation when a bond in the molecule vibrates at the same frequency as the incident energy; once the molecules have absorbed the energy, they have more energy and vibrate at higher amplitudes. The frequency absorbed depends on the masses of the atoms in the bond, the geometry of the molecule, the strength of the bond, and several other factors. Not all molecules can absorb IR radiation. The molecule must have a change in dipole moment during vibration in order to absorb IR radiation. Then, different functional groups absorb characteristic frequencies of IR radiation, this will allow the structural elucidation and the possible compound identification.<sup>34,62,63</sup>

In the attenuated total reflectance (ATR) approach, the IR travels throughout an optical element of high refractive index, called ATR crystal until it reaches the sample (of low refractive index). From this interaction two phenomena can be distinguished: a complete reflection of radiation (1), that means sample does not absorb any of the input radiation; alternatively, if the sample absorbs part of the radiation, then IR is attenuated at the frequency where the sample absorbs (2). These processes are related to the angle of incidence between the interaction of the beam and sample.<sup>62,63</sup> Schematically ATR analysis is presented in **Figure 1.11**.

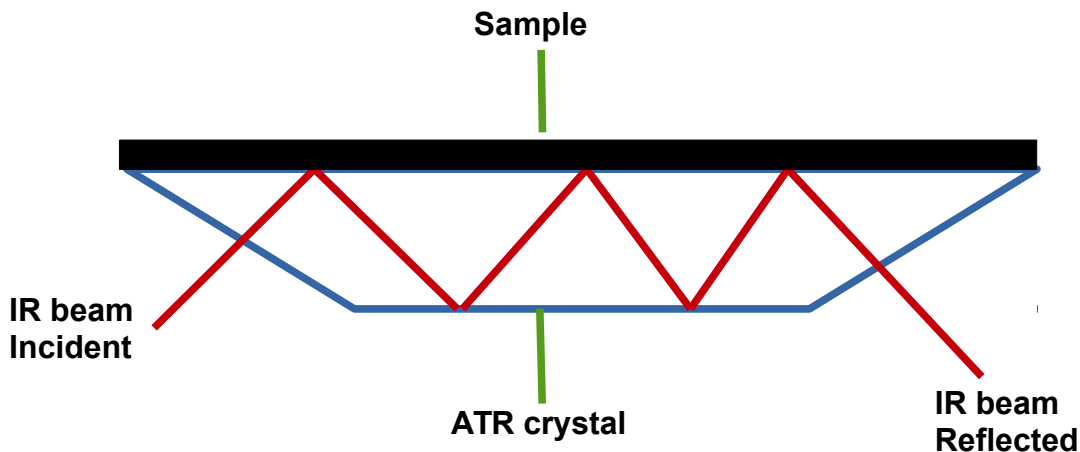


**Figure 1.11.** Schematic diagram of multiple reflection in an ATR system

## 1.5.2. Porosimetry characterisation

### 1.5.2.1. Type of isotherms

Porosimetry analysis is an important technique which provides information related to surface properties of solid materials, such as surface area, pore size and pore volume. This analysis was done for the prepared sulfonated Starbons®. The most common approach utilizes nitrogen adsorption at boiling temperature (77 K) to determine surface area and textural properties. The first approximation in the identification of the “type” of material is given by its isotherm. According to the IUPAC<sup>41</sup> there are six types of isotherms, but the mostly common found in catalysts are four,<sup>64</sup> presented below in **Figure 1.12**.

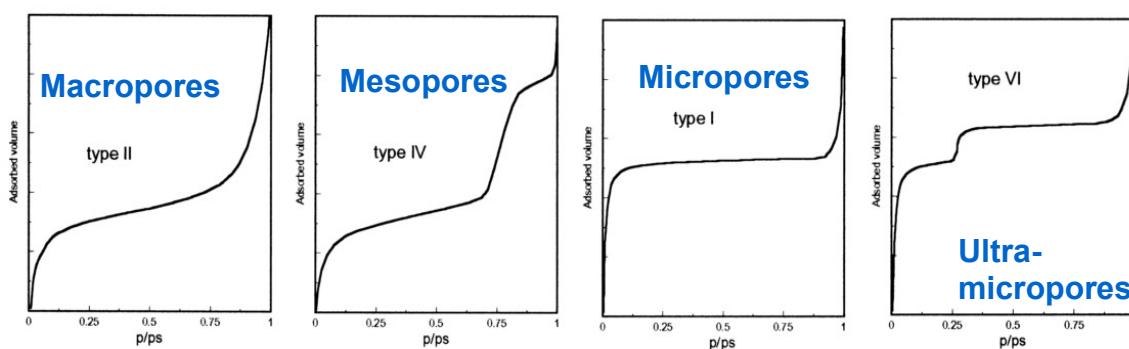


**Figure 1.12.** Adsorption isotherms commonly found in catalysts

As shown in **Table 1.1**, there are different pore sizes, then the shape of the isotherm obtained during adsorption of nitrogen by the material will indicate what kind of pores are present on the sample. *Type II* isotherm corresponds to macroporous solids, in which it is observed that at low relative pressure, the formation of a monolayer of adsorbed molecules is the prevailing process; while at high relative pressure a multilayer adsorption takes place, the amount adsorbed increases gradually as the relative pressure increases, although the multilayer buildup close to the saturation vapor pressure may be quite abrupt. In this case, the adsorption and desorption branches of the isotherm coincide, there is no hysteresis. In isotherm *type IV*, the adsorption proceeds via multilayer adsorption followed by capillary condensation; the adsorption process is initially similar to that on macroporous solids, but at higher pressures the amount adsorbed rises very steeply due to capillary condensation in mesopores. After these pores are filled, the adsorption isotherm levels off. Capillary condensation and capillary evaporation often do not take place at the same pressure, which allows the appearance of hysteresis loops. Isotherm *type I*, corresponds to microporous solids; in these materials, the adsorption takes place also at very low relative pressures because of the strong interaction between pore walls and adsorbate. Pore filling takes place without capillary condensation in the low relative pressure region ( $<0.3$ ), then the monolayer formation is not distinguishable. The *type VI* isotherm represents stepwise multilayer adsorption on a uniform non-porous surface or it has been suggested, corresponds to materials which contain ultramicropores (pore size  $<0.7$  nm).<sup>64</sup> The step-height represents the monolayer capacity for each adsorbed layer and, in the simplest case, remains nearly constant for two or three adsorbed layers.<sup>41,64,65</sup> Then for mesoporous materials, as our Starbons<sup>®</sup>, the expected isotherm corresponds to the *type IV*.

#### 1.5.2.2. *Type of hysteresis*

Adsorption on mesoporous materials occurs via multilayer adsorption followed by capillary condensation.<sup>65</sup> Ideally a reversible process will be expected in the adsorption–desorption process, but in mesoporous materials there are delays in the processes causing the formation of hysteresis. This characteristic could be

related to the shape of pores or the porous network present in the materials (**Figure 1.13**). Types H1 and H2 hystereses are characteristic of solids with aggregates or agglomerates of spheroidal particles. These hysteresis are as well assigned to cylindrical or ink-bottle shaped pores. If the pores have uniform size and shapes corresponds to type H1; if there are non-uniform then corresponds to H2.<sup>41,65</sup> Most mesoporous carriers and catalysts present these types of hystereses.<sup>64</sup> While hystereses Type H3 and H4 are associated with agglomerates or aggregates of particles forming slit shaped pores (plates or edged particles like cubes). If size and shape are uniform we have type H4 if they are not uniform, hysteresis corresponds to type H3.<sup>41,65</sup> Common materials with these characteristics are active carbons and zeolites.<sup>64</sup>

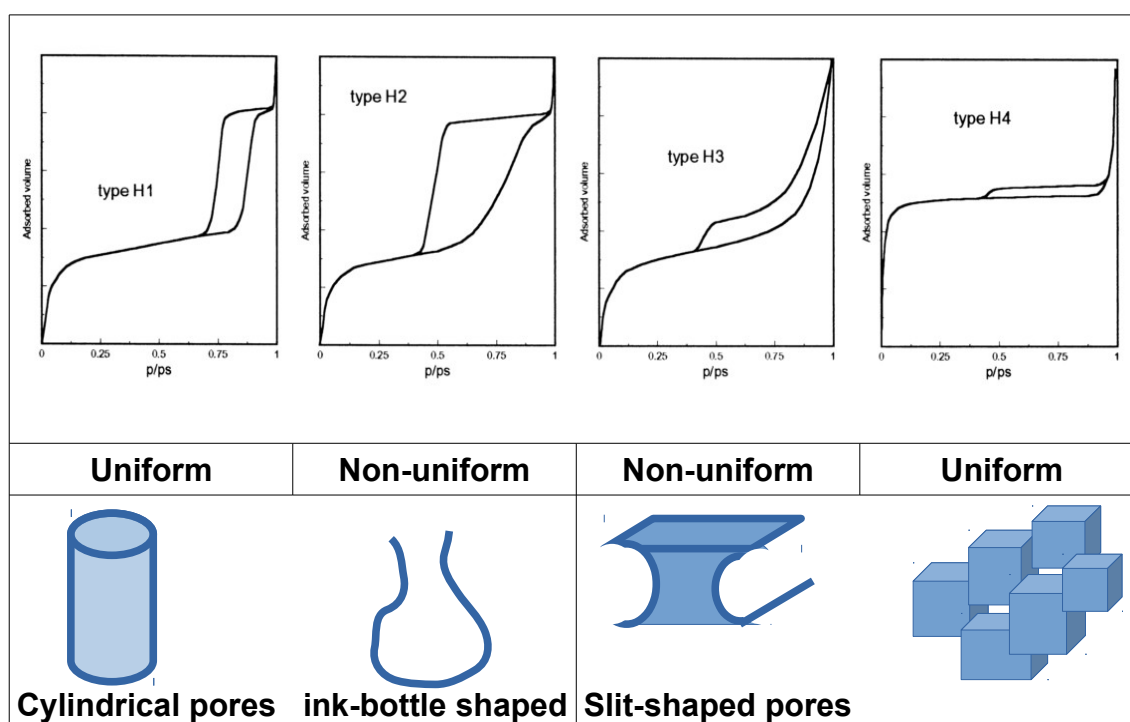


**Figure 1.13.** Classification of adsorption-desorption hysteresis loops and its association with pores shapes

### 1.5.2.3. Surface area determination, BET calculation

The Brunauer-Emmet-Teller (BET) method is a widely employed procedure used to evaluate specific surface area of a solid material. It is based on the evaluation of the monolayer capacity ( $n_m$ ), which is the number of adsorbed molecules in the monolayer on the surface material. This approach utilizes gas

adsorption experimental data and fitting these values into the BET equation (**Equation 1.1.**). The plot of relative pressure ( $p/p_0$ ) against the quantity of molecules adsorbed at certain relative pressures gives a straight line with slope,  $m$  and intercept,  $b$ . From these values, the monolayer capacity could be obtained as well, the constant  $C$ , related to enthalpy energy of the adsorbate on the solid.<sup>66</sup>

$$\frac{p/p_0}{n(1-p/p_0)} = \frac{C-1}{n_m C} \frac{p}{p_0} + \frac{1}{n_m C}$$

$$\mathbf{y} = \mathbf{m} \mathbf{x} + \mathbf{b}$$

**Equation 1.1.** BET equation and its linear approach;  $n$ , amount of gas adsorbed at relative pressure,  $p/p_0$ ;  $n_m$  is the monolayer capacity and  $C$  is dimensionless constant<sup>66</sup>

Thus, specific surface area,  $S$  can be calculated (**Equation 1.2.**) once the monolayer capacity is obtained, this is multiplied by the cross-sectional area ( $a$ ) of the adsorbed molecule in the monolayer on a given surface . In the case of nitrogen ( $N_2$ ), the accepted cross-sectional area<sup>64,66</sup> is  $0.162 \text{ nm}^2$ .

$$S = \frac{n_m N a}{m \times 22400}$$

**Equation 1.2.** Determination of specific surface area BET equation; where  $n_m$  is the monolayer capacity;  $N$ , Avogadro number,  $a$ , is the cross-sectional area of the adsorbed molecule;  $m$ , mass of sample; 22400 is the volume (mL) of occupied by a gas at STP.

It is worth mentioning that BET calculation was used to determine the surface area of the materials presented in this thesis.

#### 1.5.2.4. Pore size distribution, BJH method

The method of Barrett-Joyner-Halenda (BJH) was used in the characterization of the materials analyzed by porosimetry in this work. This method is widely used in calculation of pore size distribution on mesoporous materials. The model is based on the Kelvin equation (that relates vapour pressure depression to capillary radius); the BJH method proposes that adsorption in mesopores of a given size occurs as multilayer adsorption, followed by capillary condensation at a specific relative pressure. Capillary condensation is a process seen as filling a *pore core*, that is, space which is not occupied by the multilayer film on the pore walls. The desorption is illustrated as capillary evaporation at a relative pressure. The capillary evaporation consists in emptying of the *pore core* but maintaining the multilayer film, followed by thinning of the multilayer.<sup>65</sup> (**Figure 1.14.**) It is worth mentioning that this approach assumes a geometric model cylindrical or slit pores.<sup>64</sup>

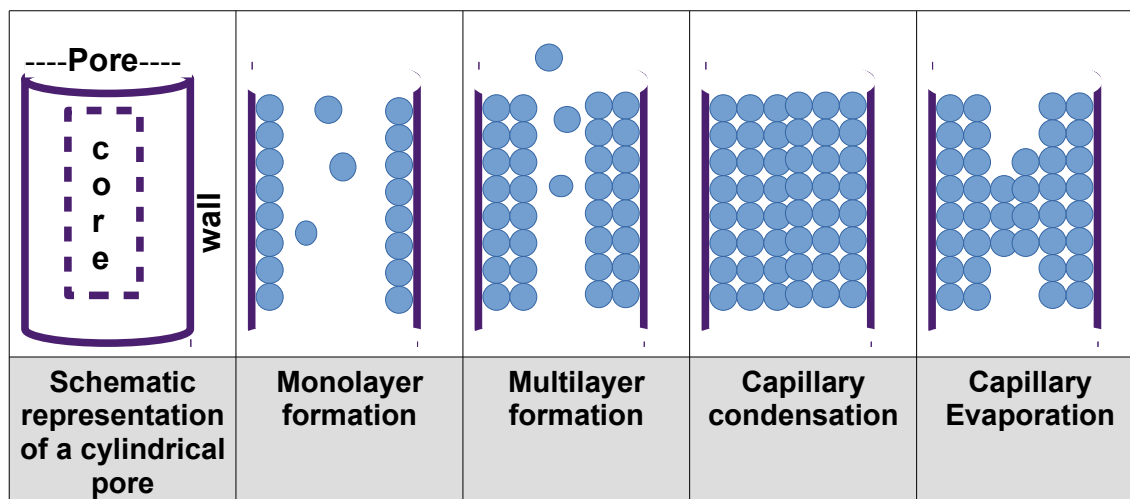


**Figure 1.14.** Schematic representation of the adsorption-desorption process in mesopores<sup>67,68</sup>

To obtain the pore size distribution using BJH method, a graphical plot of  $dV/d\log(r)$  versus pore diameter ( $r$ ) is used, where  $dV/d\log(r)$  represents the differential of the volume adsorbed as function of pore size ( $r$ ). The semi-logarithmic approximation is often used when the pores have wide distribution (e.g. from 2 to 100 nm).

### 1.5.3. X-ray photoelectron spectroscopy (XPS)

XPS also known as ESCA (Electron Spectroscopy for Chemical Analysis) is a technique used to characterize material surfaces. The method consists in the bombardment of the surface with X-rays resulting in the ejection of electrons from the atoms located on the surface (**Figure 1.15**). These emitted electrons are subsequently separated according to their energy and counted. The energy of photoelectrons is related to their atomic and molecular environment, providing information about the oxidation state of the atom where it is originated; as well as details about the bonded atoms. The quantity of electrons emitted is related to the concentration of the emitting atom. The XPS spectrum is a plot of the number of emitted electrons per energy interval versus their binding energy, this allows the identification of the elements present on the surfaces.<sup>62,63,69</sup>

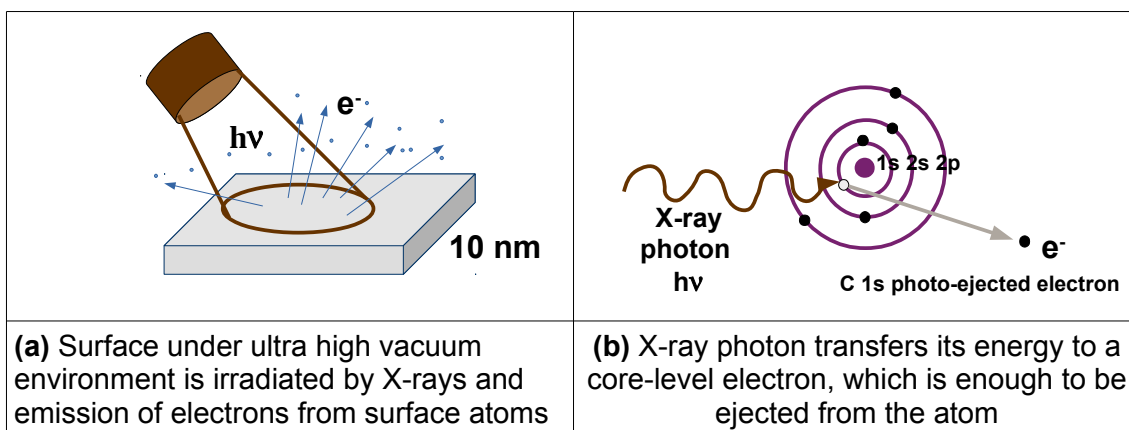


**Figure 1.15.** Diagram of photoelectrons production in the XPS analysis

Then, the basic XPS analysis of a surface can provide both qualitative and quantitative information of the elements which compose the material. This technique was used to characterise the surface of Starbons<sup>®</sup> and sulfonated Starbons<sup>®</sup> prepared during the development of this project.

### 1.5.4. Nuclear Magnetic Resonance

Nuclear magnetic resonance (NMR) spectroscopy is a technique that allows identification of the different chemical environments of the NMR-active nuclei

present in a molecule, providing information about the shape and structure of molecules. This technique is classified as an absorption method, this means a sample can absorb electromagnetic radiation under appropriate conditions in a magnetic field. Absorption is a function of certain nuclei in the molecule. These nuclei rotate about an axis (**Figure 1.16.**) and therefore have a nuclear spin, represented as  $I$ , the spin quantum number. In addition, nuclei are charged. The spinning of a charged body produces a magnetic moment along the axis of rotation. For a nucleus to give a signal in an NMR experiment, it must have a non-zero spin quantum number and must have a magnetic dipole moment. Among the common nuclei analysed we find  $^1\text{H}$  and  $^{13}\text{C}$ . The NMR spectrum is formed by a plot of the frequencies of the absorption versus peak intensities. Because the spread of frequencies is caused by the different chemical environments, the signals are described as having a chemical shift from some standard frequency.<sup>34,62,70</sup>

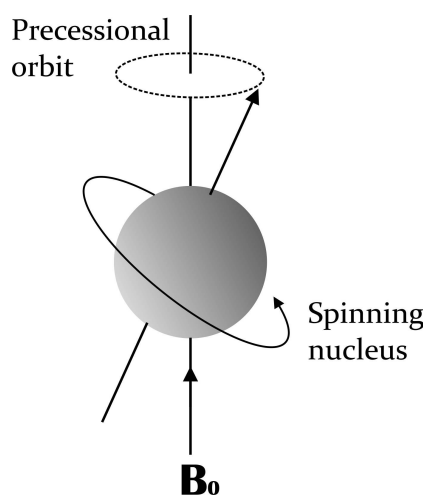


**Figure 1.16.** Spinning charge on nuclei generates magnetic dipole

#### 1.5.4.1. Solid-state NMR, Cross-Polarization (CP)/Magic Angle Spinning(MAS)

Broad lines are observed in the NMR spectra of solid samples, this phenomenon can be attributed to two principal factors: chemical shift anisotropy and dipolar couplings. The first one is related to the spatial orientation of the molecule, which in a powder or non-crystalline material occurs in all the directions possible, affecting the observed chemical shift. The second factor refers to the inter- and intra-molecular spatial interaction between two nuclei.

These broad lines can be narrowed with the use of high-resolution techniques as Magic Angle Spinning (MAS) and Cross-polarization (CP). In general, NMR properties of a molecule are tensor properties. That means, their value depends upon the spatial relationship of the molecule to the applied magnetic field. As such, each property can be described using three principal components, plus three angles to specify the orientation of the molecule within the applied magnetic field. For all such interactions, the magnitude of the interaction depends upon  $(3\cos^2 \theta - 1)$ , where  $\theta$  is the angle between the magnetic field and a significant molecular direction. In the liquid state, fast isotropic molecular tumbling causes  $(3\cos^2 \theta - 1)$  to go to zero, so that no anisotropic interactions are present. In the solid state, these interactions can dominate the observed spectrum. Then MAS approach, involves spinning the sample about a particular axis at very fast speeds. Taking into account that anisotropic interactions depend upon the term  $(3\cos^2 \theta - 1)$ , these interactions can go away, simply set this mathematical expression equal to zero, and solve for the angle  $\theta$ . The result is  $54.74^\circ$ , which is called the “magic angle” (**Figure 1.17.**). Effectively the fast, random tumbling of molecules present in solution is artificially reintroduced for solids using this technique. In practice, the spinning rate of the sample about the magic angle needs to be fast relative to the observed static line width of the sample, then, if the observed anisotropic line width is 20 kHz, then the sample must spin faster than 20 kHz.<sup>71</sup>

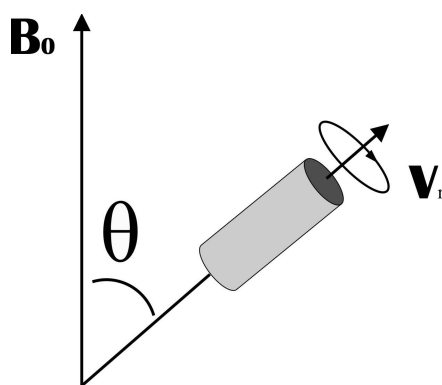


**Figure 1.17.** Magic angle spinning (MAS) diagram.  $B_0$  represents the direction of the magnetic field. The sample rotor is rotated rapidly at a velocity,  $v_r$ , and an angle,  $\theta$ , relative to the magnetic field. The angle is set to  $54.74^\circ$

The strong dipolar coupling between protons and carbons could be overcome using cross-polarization. The fundamental strategy behind CP is to create a

very large amount of magnetization by irradiating a group of high abundance nuclei, typically protons, and transferring this magnetization to a group of low abundance nuclei, typically carbon in order to increase the magnetization and thus the observed signal intensity of the low abundance nuclei.<sup>62,71,72</sup> In practice CP is achieved using a pulse sequence (**Figure 1.18.**). This shows the case for protons as the high abundance nuclei and carbon as the low abundance nuclei. First a standard 90° pulse is applied to the protons to create the initial magnetization. Then a pair of special spin-locking pulses is applied. This pair of pulses must meet the requirements of the “Hartmann-Hahn” match condition:

$$\gamma_H B_H = \gamma_C B_C$$

**Equation 1.3.** The Hartmann-Hahn condition

In this equation,  $\gamma_H$  is the gyromagnetic ratio of the high abundance nucleus;  $B_H$  is the applied field for the high abundance nucleus;  $\gamma_C$  is the gyromagnetic ratio for the low abundance nucleus; and  $B_C$  is the applied field for the low abundance nucleus. This spin-locking pulse pair is followed by a decoupling scheme to decouple the protons from carbon during the acquisition of the carbon signal. The duration of the spin-locking pair of pulses is known as the “contact time” and is typically set for between 1 and 10 ms. The overall sensitivity gain achievable is equal to the ratio of the gyromagnetic ratios, from protons and carbons this ratio  $\gamma_H / \gamma_C$  is equal to 4, so there is a four-fold potential gain in the signal-to-noise ratio.<sup>62,71</sup>

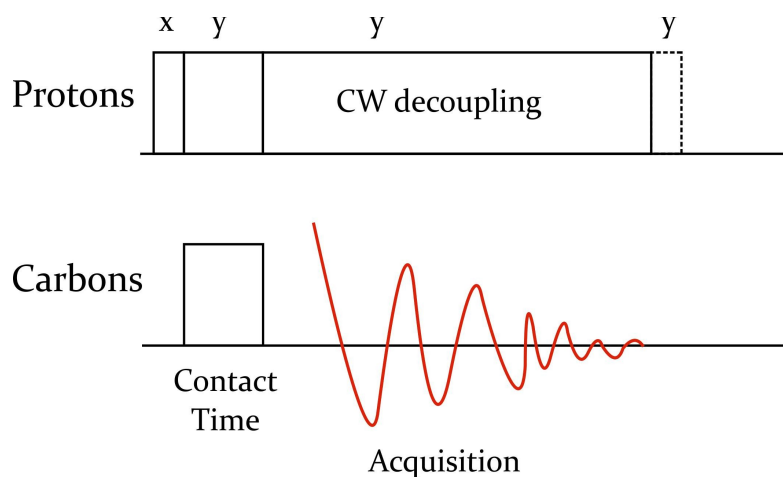


**Figure 1.18.** Cross-polarization pulse sequence sketch. The high abundance nuclei, such as protons, are first irradiated with a standard  $90^\circ$  pulse to create the initial magnetization. A special pair of spin-locking pulses is applied during a period called the contact time in order to transfer the magnetization from the protons to the low abundance nuclei, such as carbons. Protons are then decoupled from carbons during the acquisition of the carbon signal<sup>71</sup>

Solid-state  $^{13}\text{C}$  CP/MAS NMR spectroscopy has been used to study the structure of the Starbonds<sup>®</sup> and sulfonated Starbonds<sup>®</sup> prepared in this work.

### 1.5.5. Thermogravimetric analysis coupled to infrared spectroscopy (TG-FTIR)

Thermal analysis experiments permit the evaluation of the physical and chemical changes that a sample may suffer during exposition to thermal induced conditions. Thermogravimetric analysis (TGA) is used to monitor the change in mass (weight) of a sample as it is heated or held isothermally at specific temperature. During the analysis an inert gas is passed through the system to provide an appropriate atmosphere for the analysis as well as a carrier of the decomposed materials or gases formed during heating.<sup>62,63</sup>

Identification of the volatile products formed during the heating process can be carried out using coupled techniques like TG-MS (Thermogravimetry–Mass Spectrometry) or TG–FTIR (Thermogravimetry–FT infrared). TG-FTIR analyses the gases evolved from thermal analysis taking the advantage that FTIR

spectrometer counts with an interferometer, which allows fast analysis in the complete IR spectra range (4000–400  $\text{cm}^{-1}$ ). The technical requirements for this methodology include a heated transfer line (minimum at 200 °C) to prevent condensation of travelling gases; a heated gas cell with appropriate windows (ZnSe) and also a fast detector like a liquid nitrogen cooled MCT detector.<sup>73</sup> It is worth mentioning that these characteristics were covered in the equipment Brüker Equinox 55 used during the thermal decomposition of sulfonated Starbons®. The analysis (TG-FTIR) is schematically depicted in **Figure 1.19**.

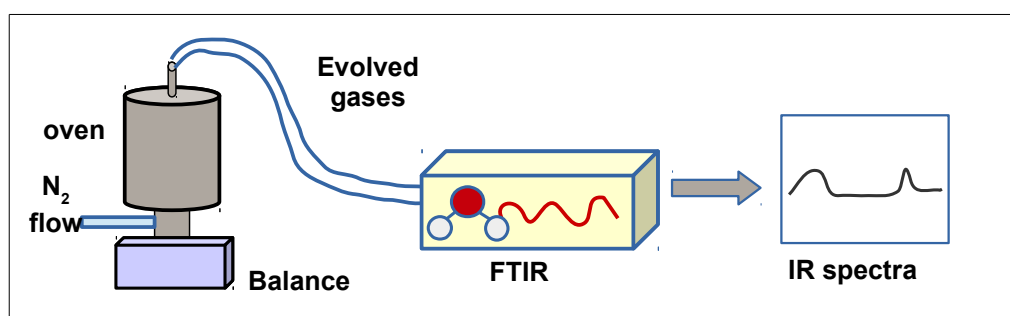


**Figure 1.19.** Schematic representation of TG-FTIR analysis

### 1.5.6. Gas Chromatography Analysis

Gas chromatography (GC) was used for the analysis of reaction mixtures during the study of sulfonated Starbons® as catalysts (**Chapter 5**). GC enables the dynamic separation and identification of volatile components in a mixture. Its use can be qualitative and quantitative. Among the components of this technique<sup>62,74</sup> we find:

- ◆ A carrier gas, which carries the sample through the system. Helium is the most common gas used.
- ◆ A GC injector, which allows the introduction of the sample through the system and to the gas stream.
- ◆ A column, which is in charge of separation of the components of the mixture. Selection of column is related to the characteristics of samples like polarity and volatility.
- ◆ A detector, responsible for the identification of components. The most popular is the flame ionization detector (FID). This detector is very

sensitive for any type of hydrocarbon component. Organic components burn in a flame.

- ◆ Data acquisition, this component converts the electrical signals generated by the detector to a chromatogram peak. The peak area is representative of the concentration of the component in the mixture. As each component has a different susceptibility to the detector, a calibration curve is needed. A chromatogram plots the retention time (distance in minutes from the point of injection to the peak maximum) *versus* signal intensity.

## 1.6. Project scope and objectives

The aim of this project was to apply the green chemistry concept to prepare strong solid-acid catalysts from a bio-based material, Starbon<sup>®</sup> (carbonized expanded starch). The development of the project originated a “rediscovery” of these *Cleargum* based Starbons<sup>®</sup>; as well it creates helpful and interesting information from the sulfonated Starbons<sup>®</sup>. Then, the particular objectives of the thesis are enumerated below:

- Synthesis of a range of carbonized Starbons<sup>®</sup> (350–700°C) from precursor scale-up Starbons<sup>®</sup> prepared at 300, 400 and 800 °C.
- Synthesis and characterisation of sulfonated Starbons<sup>®</sup> via conventional heating. Creation of a range of sulfonated Starbons<sup>®</sup> from 300 to 800 °C.
- Synthesis and characterisation of sulfonated Starbons<sup>®</sup> using microwave irradiation using Starbons<sup>®</sup> 300, 450 and 800.
- Test of sulfonated Starbons<sup>®</sup> as solid acid catalysts in esterification reactions
- Study of reactions using microwave and conventional heating, including reuse and leaching studies.
- Development of an understanding of the effects of the sulfonation process on the materials themselves and on their effectiveness as catalysts.



## ***Chapter 2***

### ***Synthesis and characterisation of sulfonated Starbons<sup>®</sup> by conventional heating***

Some of the results present in this  
section have been published in  
Res.J.Chem. Environ 18 (8) 2014



## 2.1. Introduction

This chapter deals with the preparation and sulfonation of Starbons<sup>®</sup> done by conventional heating. During this process, modifications to previous methodologies were promoted, such as the decrease of sulfuric acid used and elimination of some conditioning steps. This sulfonation approach is the first reported to be carried out at large scale (over 80 g of material). The crucial component of this research consisted in the study of the characteristics and properties evolved from the synthesis of these new materials. Characterisation of materials consisted in determination of elemental composition by CHN analysis; as well, the structural changes suffered by the materials and studied by FT-IR spectroscopy and <sup>13</sup>C CP/MAS NMR spectroscopy; in addition, the identification of the chemical species formed after sulfonation, analysed by X-ray photoelectron spectroscopy (XPS).

## 2.2. Preparation of sulfonated Starbons<sup>®</sup>

Starbons<sup>®</sup> are carbonaceous materials discovered in Green Chemistry Centre of Excellence at the University of York. Among their interesting characteristics are their mesoporosity and functionality dependence on the degree of carbonization. During the first synthesis of these materials many attempts at changing the methodology and the starting material were carried out, studies that are out of the scope of the present thesis. As mentioned in **Chapter 1**, these Starbons<sup>®</sup> were prepared from expanded *Cleargum* starch by Contract Chemicals Inc., this being the first trial to prepare Starbons<sup>®</sup> at very large scale (over 100 kg).

Another important procedure in preparation of these Starbons<sup>®</sup> is the carbonization, which was carried out for Starbons<sup>®</sup> 300, 400 and 800 (°C), on a large scale at Nabertherm, in Germany. These three pyrolysed Starbons<sup>®</sup> were the starting materials for a range of new carbonized Starbons<sup>®</sup> presented already in **Figure 1.7.** and summarized below in **Table 2.1.**

Table 2.1. New range of carbonized Starbons®					
Starting material	Temperature/ °C				
Starbon® 300	350				
Starbon® 400	450	500	550	600	700
Starbon® 800	No treatment required				

Sulfonation was carried out using commercial sulfuric acid (95%) in a ratio 1 g of Starbon® to 7 mL of acid, with constant stirring at 90 °C for 6 h as described in the experimental section in **Chapter 6**. Afterwards, materials were washed repeatedly with hot distilled water; this was done at constant stirring at temperatures over 80 °C for 20 minutes with the aim to remove the excess of sulfuric acid. This sulfonation approach is a modification of previous sulfonation procedure carried out on Starbons® and tested in different reactions.<sup>13,75,76</sup> In the previous procedure a ratio of 1 g of Starbon® to 10 mL of sulfuric acid (99.999 %) is used; the washes are carried out using room temperature water, without stirring. As well, in the new approach the ratio of acid:Starbon® has decreased and “conditioning steps” with toluene and boiling water used in the previous synthesis have been eliminated, looking for a more sustainable way to prepare sulfonated Starbons®.

pH of solutions was monitored after every wash; **Figure 2.1** shows pH increments as the number of washes increases, suggesting that most of sulfuric acid in excess is removed during the first five washes. In the subsequent washes, pH remains steady, and does not rise to neutral pH as other authors have mentioned during preparation of acid catalysts using sulfuric acid.<sup>75</sup> Thus, another way to determine the end of hot water washings was performed.

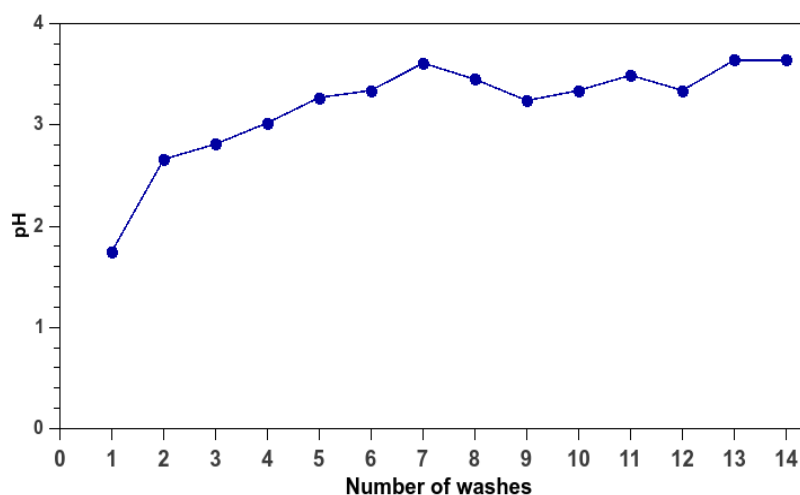
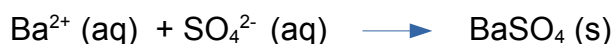


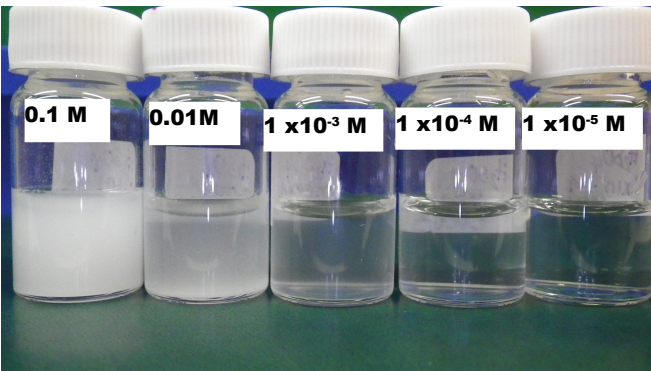
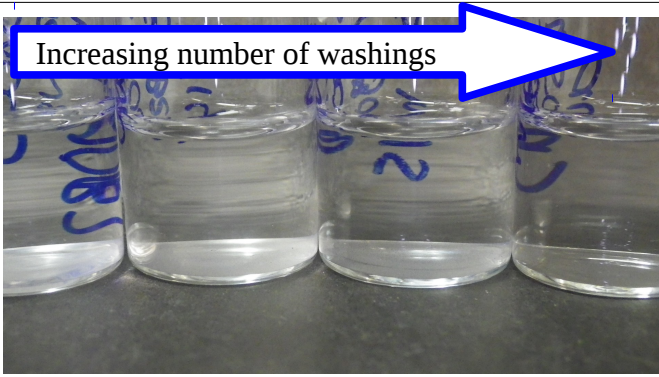
**Figure 2.1.** pH changes during washing of sulfonated Starbon® 300

Then, sulfonated Starbons® were washed until sulfates were not longer detected in the washing water through a test with a barium chloride ( $\text{BaCl}_2$ ) solution; this approach has been followed by other authors during the preparation of sulfonated materials.<sup>30,77</sup> The test consisted in the reaction of an acidic solution of  $\text{BaCl}_2$  (0.1M in HCl 0.1M) with sulfates remaining in washings of sulfonated Starbon®, this forms a white precipitate of barium sulfate according to the equation below (**Equation 2.1.**)



**Equation 2.1.** Precipitation reaction of barium ions and sulfates

A qualitative scale of standard solutions containing barium chloride and sulfuric acid at different concentrations was created like a visual reference to determine the end of material washing (**Figure 2.2**). The top of the figure (A) shows that higher concentration of sulfates (0.1 M) gives a very distinguishable white precipitate, while at concentrations lower than 0.001 M the solution is much clearer. The bottom of the figure (B) corresponds to actual washes of sulfonated Starbon® 800, in which the last two samples display a clearer solution, which indicate the end of hot water washings of the sulfonated Starbon®.

<p><u>Qualitative scale</u></p> <p>Colour changes due to different concentration of sulfuric acid. 3 mL of solution with 300 mg of BaCl<sub>2</sub> 0.1M (in HCl 0.1M)</p>	<p><b>A</b></p> 
<p><u>Samples</u></p> <p>Water washes of sulfonated Starbon<sup>®</sup> 800. 13 – 16</p>	<p><b>B</b></p> 

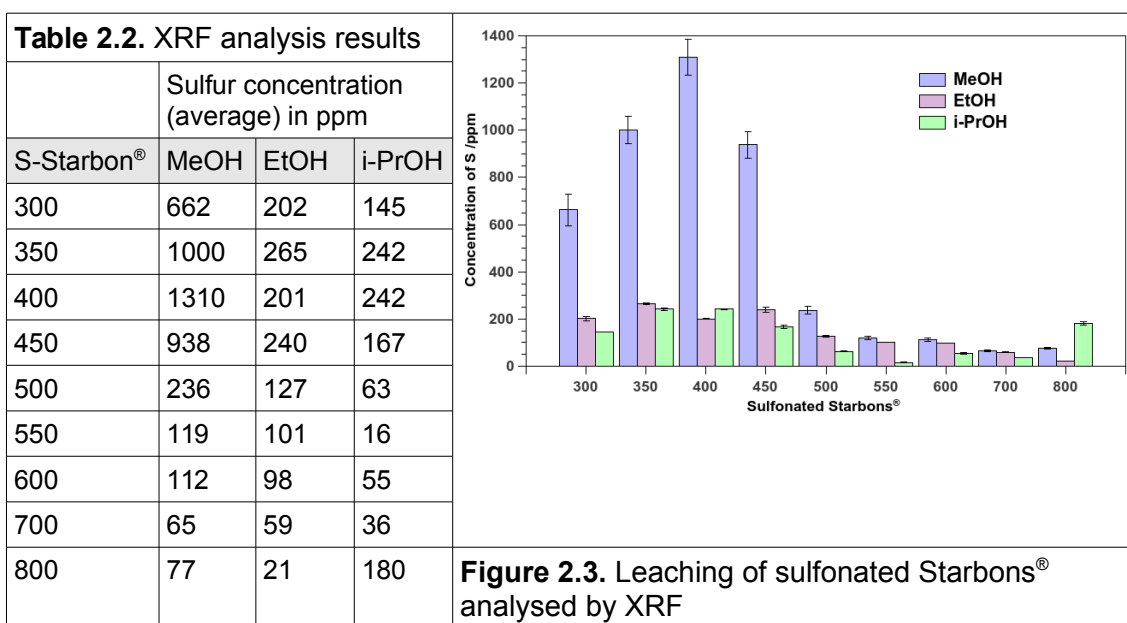
**Figure 2.2.** Qualitative scale for sulfates concentration (A) and washings of sulfonated Starbon<sup>®</sup> 800 (B)

### 2.3. Leaching of sulfuric acid from sulfonated Starbons<sup>®</sup>: washing with methanol

Leaching of sulfur from sulfonated Starbons<sup>®</sup> was observed during preliminary studies on the application of these materials as catalysts in esterifications of some organic acids with methanol, ethanol and 2-propanol, these observations suggest that homogeneous catalysis was responsible of high conversions obtained. As reactions aforementioned were carried out using microwave irradiation, thus a similar procedure using alike conditions was followed for washing the sulfonated Starbons<sup>®</sup>.

Thus, determination of sulfur released from sulfonated Starbons<sup>®</sup> was done through the analysis of reaction mixtures prepared using 3 mL of alcohol and 20 mg of catalyst; mixtures were heated in a CEM Discover reactor under the following microwave conditions: fixed power 200 W, at constant stirring for 5

minutes. After reaction finished, the catalyst was filtered off and the liquid fraction was analysed by X-ray fluorescence (XRF) spectroscopy. Results presented in **Table 2.2** and **Figure 2.3** show that high concentration of sulfur (as ppm) is observed for all the range of sulfonated materials washed with methanol, except for Starbon® 800. The concentration of sulfur was significantly greater for low-temperature carbonized Starbons® ( $T < 500\text{ }^{\circ}\text{C}$ ), being the highest for sulfonated Starbon® 400, with a sulfur concentration of 1300 ppm determined in the methanol wash. The sulfur content determined through this analysis was also higher for the first four samples of the series in the ethanol and 2-propanol washes, but sulfur concentration in these two solvents was much lower than that found in methanol washes. These observations are quite similar to the results obtained by Mo *et al*, who found that deactivation of sulfonated carbon catalysts is higher using methanol as washing solvent<sup>26</sup>. From these results, it was also noticed that the sulfur content found in the range of alcohol washes is lower for high-temperature Starbons® ( $T > 500\text{ }^{\circ}\text{C}$ ) than that obtained for low-temperature materials, which would indicate less leaching of sulfur compounds.



After these findings, an extra treatment of washing the sulfonated Starbons® with methanol was carried out. The procedure is described in the Experimental section in **Chapter 6** and consisted in using microwave irradiation, as this technique would be used for carrying reactions out. It was found that sulfur

content decreased for the materials after methanol treatment (**Figure 2.4**), suggesting that physisorbed sulfuric acid was removed.

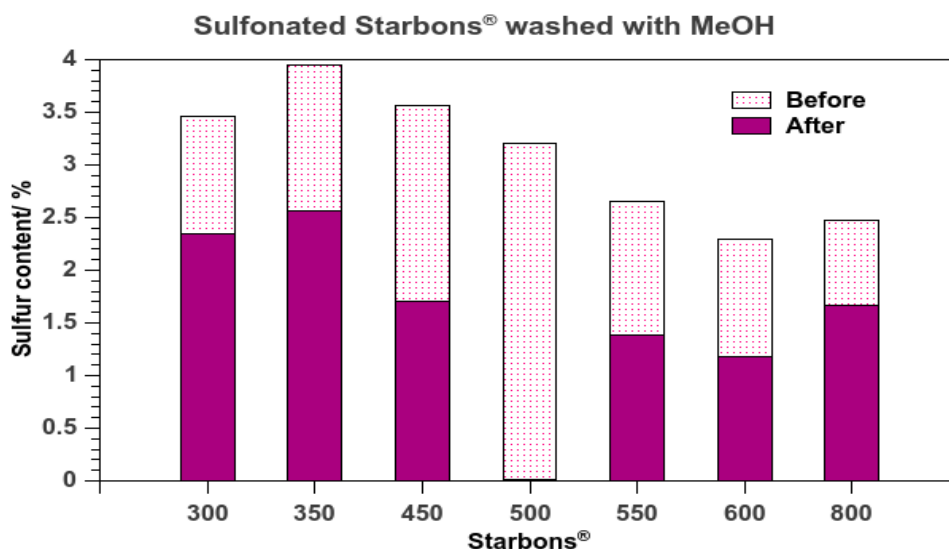


**Figure 2.4.** Sulfur content (%) for sulfonated Starbons® after washing with methanol

This perceptible removal of excess of sulfuric acid and/or physisorbed sulfates was examined in the infrared spectra of sulfonated Starbon® 350. FT-IR spectra (**Figure 2.5**) shows that after increasing the number of washes, the region  $1450\text{--}1350\text{ cm}^{-1}$  related to covalent sulfates<sup>34</sup> decreases. The absorbance identified for S=O stretching at  $1040\text{ cm}^{-1}$  did not change in a perceptible trend with increasing the number of methanol washes, as the band seems much broader for sulfonated Starbon® 350 after second wash than for the first wash. Looking at the spectra at lower wavenumbers ( $900\text{--}750\text{ cm}^{-1}$ ), it is found a flattening of the absorbance at  $830\text{ cm}^{-1}$  assigned to sulfate ester SOR,<sup>78</sup> suggesting that this type of sulfur bond is broken during the methanol treatment using microwave irradiation. Therefore it seems that methanol washing removes physisorbed sulfuric acid and some covalently bonded sulfates. After this procedure of washing the initial sulfonated Starbons® with methanol by triplicate, the new sulfonated Starbons® washed three times were bor®n, “S-Starbons® W3”. Thus, from now on, “**sulfonated Starbons®**” or “**S-Starbons®**” refer to these Starbons® sulfonated by conventional heating and washed with methanol three times.

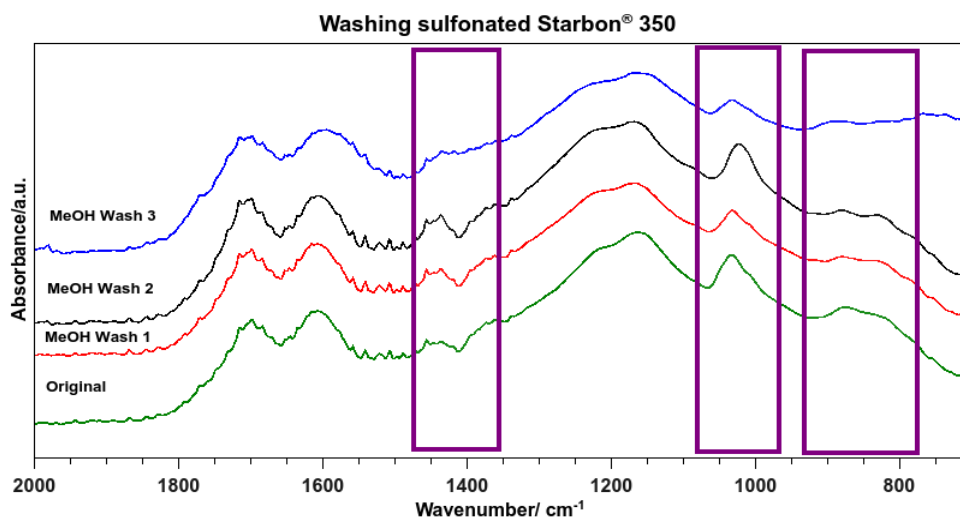


**Figure 2.5.** FT-IR spectra of sulfonated Starbon® 350 after methanol washes

## 2.4. Characterisation of Starbons® and Sulfonated Starbons®

### 2.4.1. Elemental composition in Starbons® and sulfonated Starbons®

Starbons® are carbonaceous materials whose properties depend on the degree of carbonization.<sup>9</sup> A study of the composition in Starbons® before and after sulfonation was carried out by elemental analysis. **Figure 2.6** shows the carbon-oxygen ratio, C:O atomic ratio for original Starbons® as function of temperature of carbonization. Composition found in these materials, prepared from *Cleargum* starch, differs from the composition observed in earlier synthesized Starbons®, as in those materials the maximum C:O atomic ratio observed was 8 for Starbon® 700;<sup>9</sup> whilst in this new generation of Starbons®, the C:O ratio observed is 18 for 700 and over 30 for Starbon® 800, which could be due to different starch precursor or some differences in the preparation methodology, as these materials were prepared at large scale by *Contract Chemicals*, as has been already said. However, that study is not comprised in this work.

Taking as starting point that unmodified starch has a C:O ratio equal to one, for these new expanded starch-based materials the C:O ratio obtained from elemental analysis is over two; this change in C:O ratio was already observed in previous Starbons®: C:O ratio increases as temperature does.<sup>43</sup> Then, Starbon®

300 presents the lowest C:O ratio, suggesting to contain more oxygen groups than other Starbons<sup>®</sup>. Increasing in the C:O ratio is steep, having a value lower than 6 for the low temperature Starbons<sup>®</sup>, up to 450; and higher than 10 for high-temperature Starbons<sup>®</sup>. As it was shown previously in Budarin *et al* work<sup>9</sup>, as temperature of carbonization increases, the structure of Starbons<sup>®</sup> become more graphitic-like. These changes in composition of the Starbons<sup>®</sup> due to carbonization could be mainly attributed to dehydration and decarboxylation processes.<sup>79,80</sup> It is worth mentioning that preparation of Starbon<sup>®</sup> 350 came from Starbon<sup>®</sup> 300 and Starbons<sup>®</sup> 450–700 were prepared from Starbon<sup>®</sup> 400. This description was presented in **Table 2.1**.

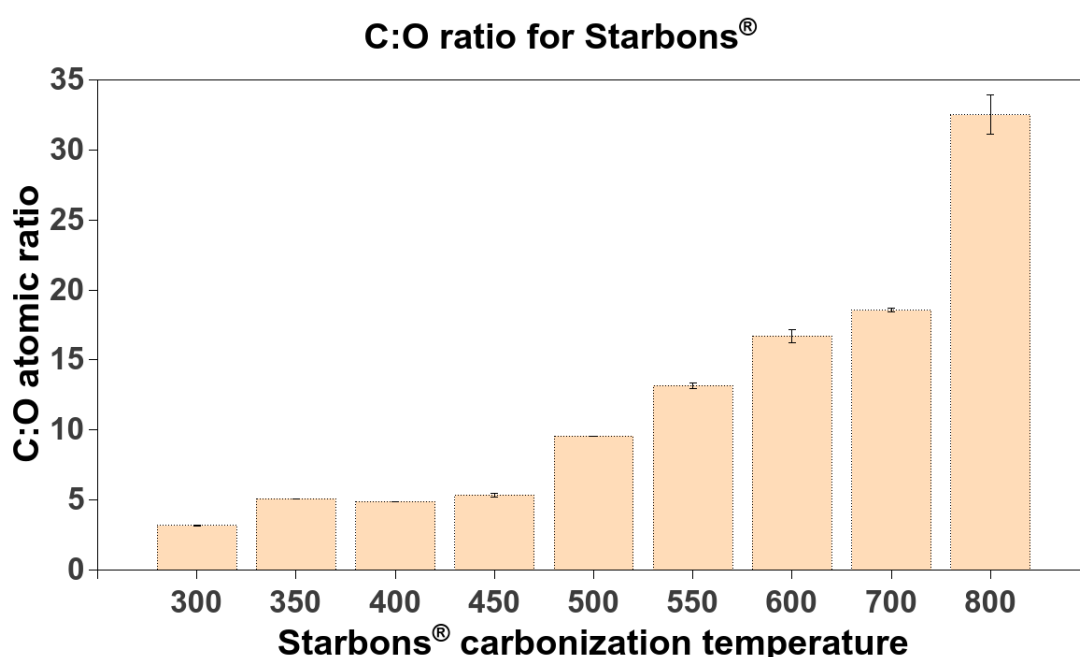


**Figure 2.6.** C:O atomic ratio of Starbons<sup>®</sup> before sulfonation

Another way to evaluate the carbonization process qualitatively is through the van Krevelen diagram which uses the O:C ratio as the abscissa and the H:C ratio as the ordinate in a plot.<sup>81</sup> This diagram provides information about the changes in chemical structure after carbonization. **Figure 2.7** shows the atomic ratios of H/C and O/C for the starting Starbons<sup>®</sup> in which it could be observed the most oxygenated sample corresponds to Starbon<sup>®</sup> 300, as it has 35 oxygen (O) atoms per 100 carbon (C) atoms. This sample seems also to be the most

saturated one, as it contains 71 hydrogen (H) atoms per 100 of C atoms. It can be noticed that composition for these two low-temperature carbonized Starbons<sup>®</sup> showed a significant decrease in the number of oxygens (65) and hydrogens (129) per 100 carbon atoms, from the C:O ratio of original starch. Starbons<sup>®</sup> 350 and 400 have similar O:C and H:C ratios: 20 O atoms per 100 C and 60 H atoms per 100 C atoms, suggesting that contains less oxygenated groups than Starbon<sup>®</sup> 300, but they have quite significant saturated groups. After carbonization at 450 °C, decrease in the O:C ratio is very significant as Starbons<sup>®</sup> carbonized at 500, 600, 700 and 800 present less than 10 atoms of O for 100 of carbon. Starbon<sup>®</sup> 800 shows the lowest atomic ratio, just 4 oxygen atoms per 100 of carbon, suggesting the formation of polycyclic aromatic structures<sup>9</sup> during carbonization at higher temperatures. Both Starbons<sup>®</sup> 450 and 550 did not follow the trend, as the content of oxygenated groups is higher than expected and it is not quite different from the content found in parent Starbon<sup>®</sup> 400. This abnormality from the trend is observed in Starbon<sup>®</sup> 450, as it contains fewer saturated groups than would be expected.

**van Krevelen diagram for Starbons<sup>®</sup>**

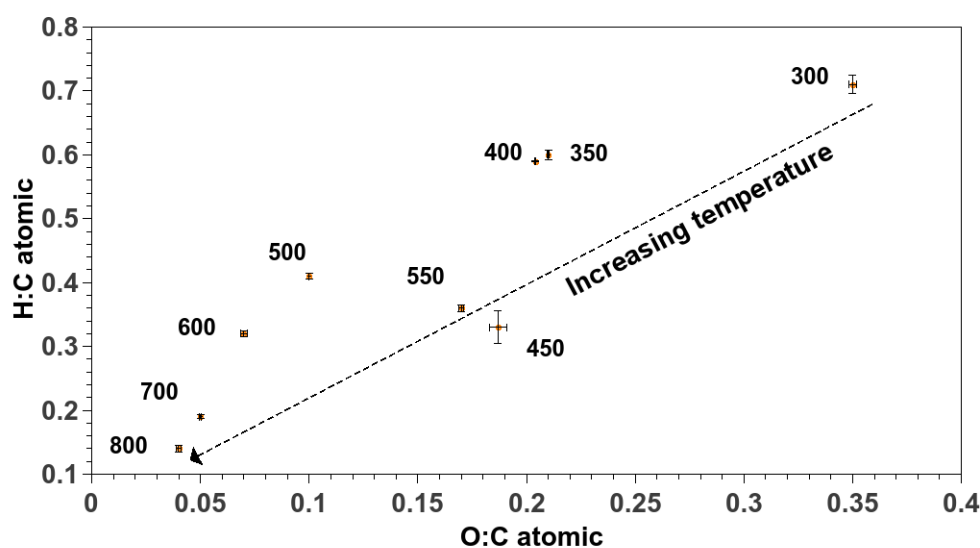


**Figure 2.7.** Van Krevelen diagram for starting Starbons<sup>®</sup>

When chemical compositions of Starbons<sup>®</sup> are compared before and after conventional sulfonation, it is found a small variation in the C:O atomic ratio for the low temperature Starbons<sup>®</sup> ( $T < 500$  °C); the ratio drops, suggesting an increase in the oxygenated groups in these materials. As temperature of

carbonization increases, the change in oxygen composition after sulfonation is very significant (**Figure 2.8**). A general trend in decreasing the C:O atomic ratio is followed, and for Starbon<sup>®</sup> 800 is very noticeable, as the C:O ratio drops from 32 to 6, and it is also slightly lower than the one obtained for Starbon<sup>®</sup> 700. The increase of oxygen in Starbons<sup>®</sup> after sulfonation would suggest that this oxygen would come from sulfonic groups (~SO<sub>3</sub>H) attached to the material or oxidation of functional groups as alcohols or aldehydes to carboxylic acids.

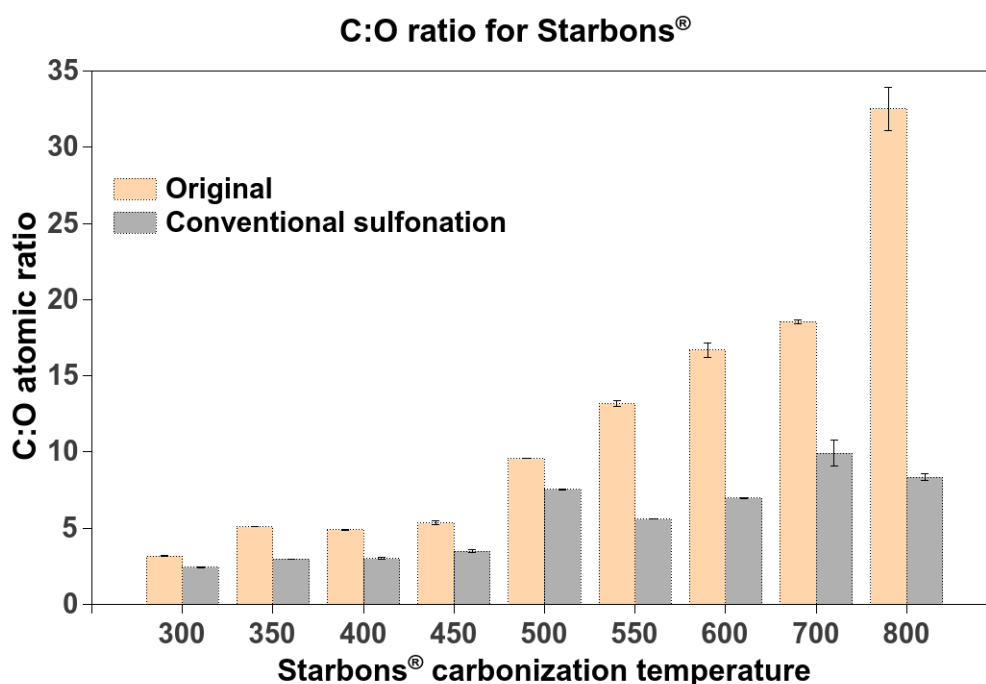


**Figure 2.8.** Chemical composition of Starbons<sup>®</sup> before and after sulfonation

Van Krevelen diagram for Starbons<sup>®</sup> after sulfonation (**Figure 2.9**), provides useful information about their atomic composition to monitor changes suffered by the materials. Then, it could be seen that S-Starbon<sup>®</sup> 300 presents the highest content in oxygenated and saturated groups. Although the increase in oxygen-carbon ratio is less significant than for other sulfonated Starbons<sup>®</sup>; as this was from 35 to 41 O atoms per 100 of C atoms; meanwhile Starbons<sup>®</sup> 350 and 400 rose from 20 to 34 oxygen atoms per 100 carbon atoms (inset **Figure 2.9**). This increment in oxygen atoms is also significant for Starbon<sup>®</sup> 800, which parent sample presented just 4 O atoms per 100 of C atoms; and after sulfonation there are 12 oxygen atoms per 100 of carbon. The trend for original Starbons<sup>®</sup> is followed: as temperature of carbonization increases there is a

decrease in the O:C and H:C atomic ratios. The variations in oxygen-carbon ratios after sulfonation are more notable for low temperature Starbons<sup>®</sup> (<450) than the middle-chart ones: 500 and 550. In this case there is a general trend similar to the original Starbons<sup>®</sup>, however sulfonated Starbon<sup>®</sup> 400, presents less hydrogen than expected; and sulfonated Starbon<sup>®</sup> 500 presents less oxygenated groups than anticipated, maybe because there were not found sulfur groups attached.

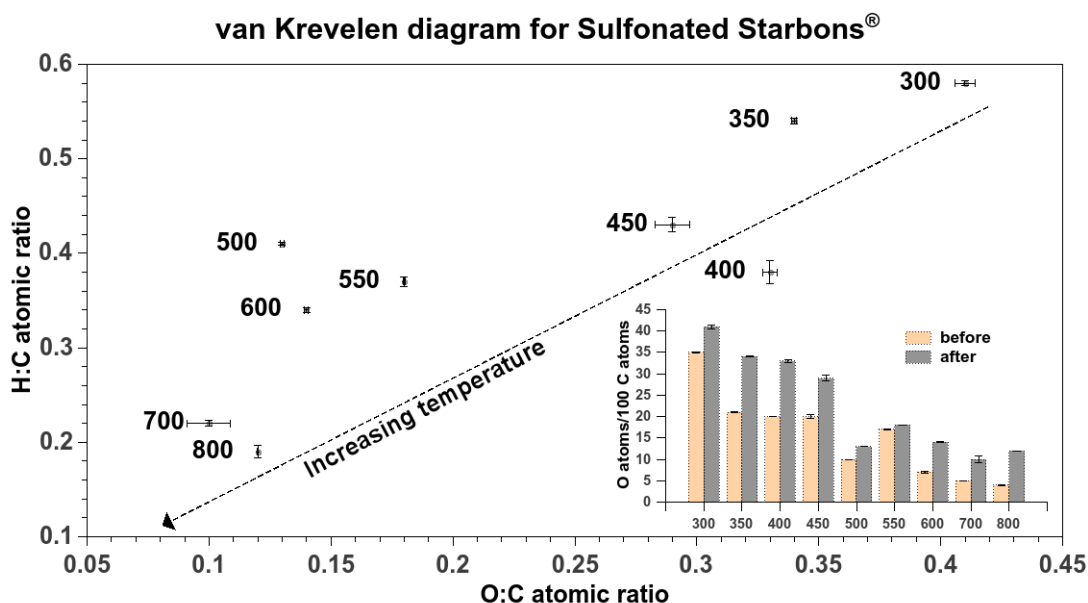


**Figure 2.9.** Van Krevelen diagram for Starbons<sup>®</sup> sulfonated at 90 °C for 6 h and washed with MeOH (3 times). Inset figure showing the changes of oxygen (O) atoms per 100 carbon (C) atoms before and after sulfonation.

A study between elemental composition and sulfur content was also done for conventionally sulfonated Starbons<sup>®</sup>. **Figure 2.10** shows the content of sulfur (mmol per gram) is higher for low temperature Starbons<sup>®</sup> 300–450, than for high-temperature carbonized Starbons<sup>®</sup>. Similar sulfur contents are observed for Starbons<sup>®</sup> 550–800 (less than 0.6 mmol g<sup>-1</sup>), but an anomalous observation is found in Starbon<sup>®</sup> 500, in which the content observed was negligible. It is worth remembering these sulfonated Starbons<sup>®</sup> were treated with methanol after leaching observed during test reactions. This fact may imply for this particular Starbon<sup>®</sup>, strong attachment of sulfur groups during sulfonation was unsuccessful.

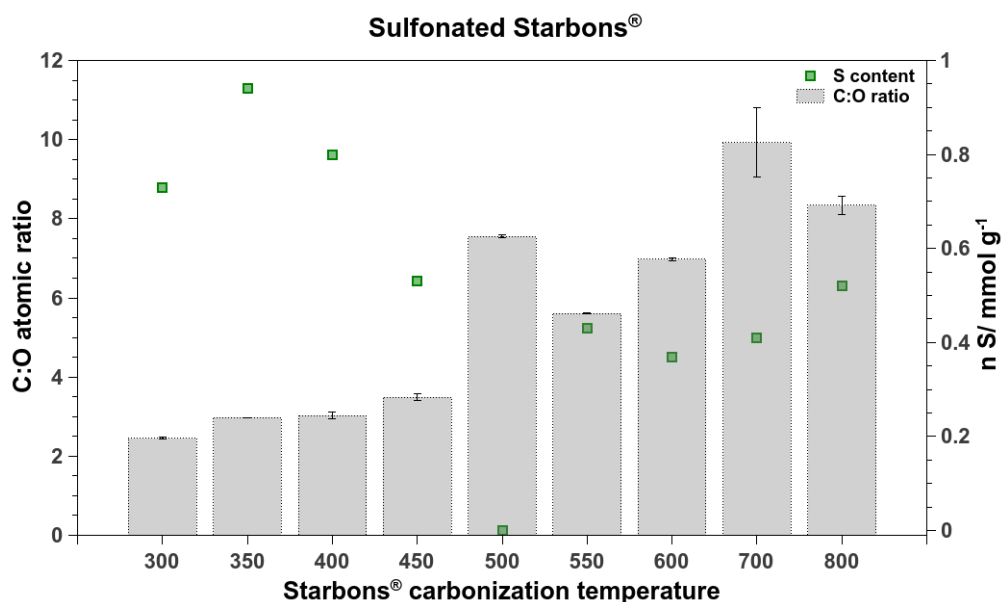


**Figure 2.10.** Chemical composition of Starbons® sulfonated at 90 °C for 6 h and treated with MeOH (W3)

#### 2.4.2. Approximation of an empirical formula for Sulfonated Starbons®

An attempt to find an empirical molecular formula for Starbons® after sulfonation was made, once the elemental composition has been found for these materials and assuming that all the sulfur is present in samples as sulfonic groups. In **Figure 2.11** is shown the trend in composition changes before (b) and after (a) sulfonation. A general trend is found: the content of oxygen in sample increases after sulfonation for all the samples. The hydrogen content decreases after sulfonation for low temperature Starbons® ( $T < 450^{\circ}\text{C}$ ), just Starbon® 450 presents an increment in the hydrogen content in sample. For high-temperature Starbons®, the variation shows a very small increase after treatment. When sulfonic groups present on samples are analysed before and after sulfonation, it could be observed an increment in these groups in the materials. However, Starbon® 300 showed the other way round, as the presence of sulfonic groups due to p-TSA added during the synthesis<sup>9</sup> and before sulfonation is higher than for the sulfonated Starbon® 300. Starbons® 350, 400, 450 and 800 also presented sulfur in the starting material; for the low temperature ones, residues of p-TSA were identified in the FTIR spectra. However, for Starbon® 800 is difficult to say that remaining p-TSA is still in the sample, as high temperature carbonization would decompose the p-toluenesulfonic acid, which could still

react with material to form other sulfur groups. This would explain the presence of sulfur in sample before sulfonation and the absence of bands in the IR spectrum corresponding to p-TSA.

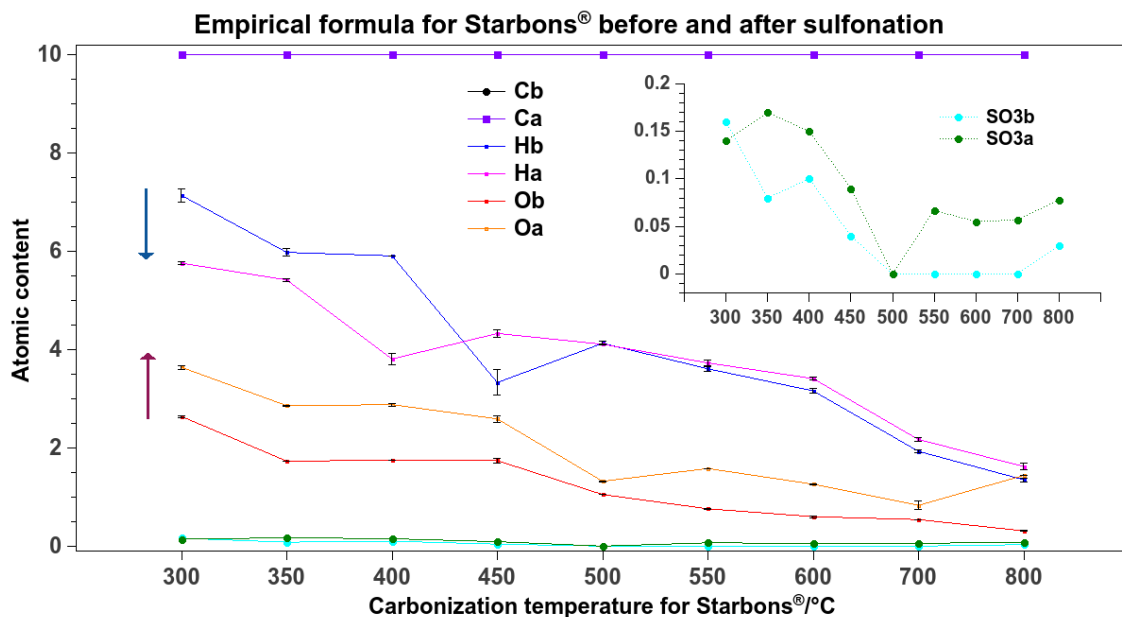


**Figure 2.11.** Variation in chemical composition of Starbons® before (b) and after (a) sulfonation (Ca and Cb arbitrarily set to 10 for all samples)

The trend observed in **Figure 2.11** could be also summarized in **Table 2.3**, in which the oxygen content before (b) and after (a) sulfonation is presented, considering the formula  $C_{10}H_xO_y(SO_3)_z$ . The quantity shown is considering the oxygen left after the formation of sulfonic groups. Then, it could be observed that there is an increase in the oxygen content after treatment with sulfuric acid, implying that sulfonation process sulfonates and oxidizes the materials. As far is known, in previous works with acid Starbons®<sup>13,75,76</sup> this characteristic has not been reported.

**Table 2.3.** Variations in atomic content of H, O and SO<sub>3</sub> before and after sulfonation on Starbons®

Starbons®	H <sub>b</sub>	O <sub>b</sub>	(SO <sub>3</sub> ) <sub>b</sub>	H <sub>a</sub>	O <sub>a</sub>	(SO <sub>3</sub> ) <sub>a</sub>
300	7.14	<b>2.64</b>	0.165	5.76	<b>3.64</b>	0.143
350	5.99	<b>1.73</b>	0.076	5.42	<b>2.86</b>	0.174
400	5.91	<b>1.74</b>	0.099	3.81	<b>2.88</b>	0.146
450	3.33	<b>1.73</b>	0.044	4.33	<b>2.59</b>	0.092
500	4.13	<b>1.05</b>		4.11	<b>1.32</b>	
550	3.61	<b>0.759</b>		3.73	<b>1.58</b>	0.067
600	3.16	<b>0.599</b>		3.41	<b>1.26</b>	0.055
700	1.93	<b>0.539</b>		2.17	<b>0.83</b>	0.057
800	1.35	<b>0.232</b>	0.025	1.62	<b>1.44</b>	0.078

A comparison between the composition determined in sulfonated Starbons® and other sulfonated sugar-based catalysts was made. The comparison is presented in **Table 2.4**, considering previous formula  $C_{10}H_xO_y(SO_3)_z$ . In this matter, sulfonated Starbons® presented a slightly higher sulfur content than the one prepared by Okamura et al;<sup>28</sup> although same trend was found in both sulfonated materials: increasing the temperature of carbonization of sugar, decreases the content of sulfur in samples. Other differences found between sulfonated Starbons® and sulfonated sugars are related to the hydrogen and oxygen contents, which are significant higher for sugars carbonized at 300 and 400, suggesting that they contain more oxygenated groups than sulfonated Starbons®, as sulfur content is similar for these two samples. It is worth mentioning at this stage, that for these “sugar catalysts”, it was found an excess of sulfuric acid coming from the samples when they were tested in catalysis.<sup>26</sup>

**Table 2.4.** Comparison between sugar catalyst and S-Starbons® formulas

Temperature	Sugar catalyst			S-Starbons®		
	x	y	z	x	y	z
<b>300</b>	7.1	5.5	0.11	5.76	3.6	0.14
<b>400</b>	4.5	3.5	0.14	3.81	2.9	0.15
<b>500</b>	5.0	2.6	0.14	4.11	1.4	0
<b>600</b>	3.7	0.35	0.05	3.41	1.3	0.06

### 2.4.3. Surface and bulk compositions of sulfonated Starbons®

X-ray photoelectron spectroscopy (XPS) analysis was carried out during the characterisation of sulfonated Starbons®. In this section the results in the atomic concentration are presented to compare with the bulk composition. **Table 2.5** presents the results obtained for the percentage atomic content of C, O, S, for sulfonated Starbons® at their different carbonization temperatures. From these values it can be seen that concentration of oxygen drops as temperature rises; the other way round is for carbon concentration, which increases as temperature does. As the concentration of sulfur is very heterogeneous for the range of sulfonated Starbons®, a notable trend was not found. The highest concentration is found for S-Starbon® 300 and the lowest for S-Starbon® 400. Although, percentages lower than 1.0% were also found for high-temperature Starbons® 700 and 800.

Starbon®	% at. C	% at. O	% at. S	Starbon®	% at. C	% at. O	% at. S
<b>300</b>	78.0	19.87	2.13	<b>550</b>	87.23	11.28	1.49
<b>350</b>	79.02	19.38	1.60	<b>600</b>	89.26	9.66	1.08
<b>400</b>	82.39	16.98	0.64	<b>700</b>	92.35	6.78	0.87
<b>450</b>	83.63	15.10	1.27	<b>800</b>	93.14	6.03	0.83

A comparison between the C:O atomic ratio determined for bulk analysis and surface analysis was made (**Figure 2.12**). From this comparison it was found that C:O ratios are higher on the surfaces of the materials than in the bulk of samples; as well, the content of sulfur for most of the materials. Although, sulfonated Starbon® 400 presents an abnormality because it displayed lower S concentration on the surface than in the bulk material. It seems that most of the functional groups are well exposed at low depth analysis (~10 nm). The trend of increasing C:O atomic ratio as temperature raises, is very similar to that observed in the bulk composition; however, in the surface analysis, concentration S-Starbon® 800 presents the highest C:O atomic ratio; meanwhile, in the bulk composition, this atomic ratio was a bit lower than

Starbon® 700, which presented the highest atomic ratio for bulk analysis of S-Starbons®. The differences between bulk and surface compositions were also observed during the preparation of previous Starbons®, this observation was attributed to the carbonization mechanism which goes from external surface into the interior bulk of the materials.<sup>9</sup>

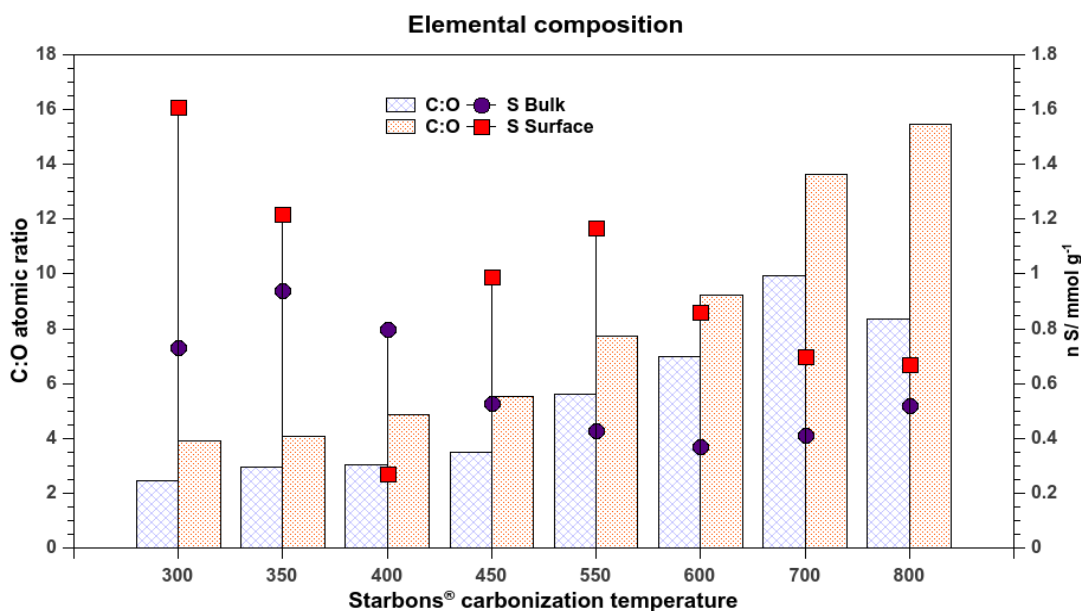


**Figure 2.12.** Variation in chemical composition of Starbons® before and after sulfonation

#### 2.4.4. Characterisation of sulfonated Starbons® by FTIR

Fourier transform infrared (FTIR) spectroscopy is a traditional technique applied in structural analysis and it was used to characterise chemical structures of sulfonated Starbons®. All the FTIR spectra were obtained in a Bruker Vertex 70 (ATR), in the frequency range from 4000 to 600  $\text{cm}^{-1}$  with a resolution of 4  $\text{cm}^{-1}$  and 64 scans. Due to these equipment characteristics, peaks appearing in the region 2300–2000  $\text{cm}^{-1}$  could be difficult to analyse. The spectrum for Starbon® 300 before and after sulfonation is shown in **Figure 2.13**. Although the spectrum of original Starbon® 300 looks a bit noisy due to the strongly absorbing nature of carbonaceous materials, it can be seen the existent similarities with the sulfonated Starbon®. A broad band rises from 3800-2600  $\text{cm}^{-1}$ , in this region ca. 3400 $\text{cm}^{-1}$ , could be identified O-H vibration,<sup>34</sup> corresponding to OH groups from carboxylic acids and alcoholic groups from sugars present in the starch-based material, as well any phenolic groups<sup>37</sup> which have been formed during the

carbonization of the starch precursor. There is also a small peak at  $2900\text{ cm}^{-1}$  could be assigned to  $\text{CH}_x$  stretching vibrations.<sup>82</sup> Vibrational bands corresponding to carbonyl  $\text{C}=\text{O}$  and  $\text{C}=\text{C}$  stretchings are observed in both materials and were assigned to  $1705\text{ cm}^{-1}$  and at  $1600\text{ cm}^{-1}$  vibrations, respectively.<sup>34</sup> The latter band designated to alkenes could be associated with furan moieties present in degraded sugars. This absorption could be related as well to presence of aromatic groups in Starbon<sup>®</sup> 300, although another characteristic band for aromatic groups ca.  $1500\text{ cm}^{-1}$ , is hardly distinguishable in the spectra because of the broad bands in that region, however as it will be seen afterwards,  $^{13}\text{C}$  solid-state NMR studies confirm the presence of aromatic groups in the materials. In the spectra is also noticed a band around  $1430\text{ cm}^{-1}$  which could correspond to the vibration of  $\text{C}-\text{O}$  stretching and  $\text{OH}$  bending of carboxylic acids.<sup>82,83</sup> As well for original and sulfonated Starbon<sup>®</sup> 300, a broad band around  $1200\text{ cm}^{-1}$  is observed; in this broad region, a band centered at  $1160\text{ cm}^{-1}$  is distinguished, which could be assigned to antisymmetrical  $\text{C}-\text{O}-\text{C}$  stretching of sugars and furans and a shoulder at  $1220\text{ cm}^{-1}$  is also observed, this suggests the presence of  $\text{Ar}-\text{OH}$  groups.<sup>84</sup> Bands in low region at  $893\text{ cm}^{-1}$  observed for both original and sulfonated Starbon<sup>®</sup> 300 could be related to symmetrical  $\text{C}-\text{O}-\text{C}$  stretching<sup>85</sup>; and the absorption appearing at  $767\text{ cm}^{-1}$  can be assigned to the presence of aromatic  $\text{C}-\text{H}$  out of plane deformations.<sup>34,83,86</sup>

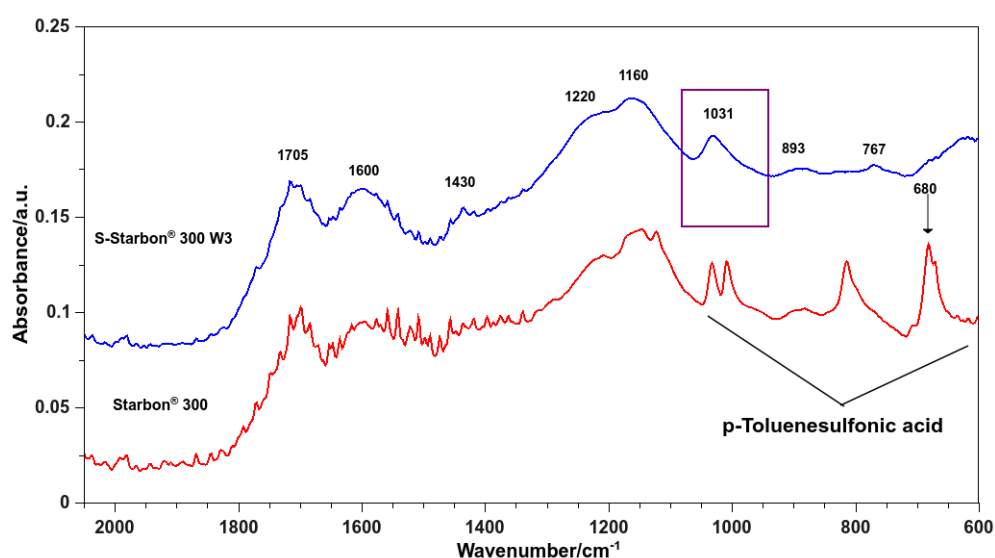


**Figure 2.13.** FTIR spectra of original and sulfonated Starbon<sup>®</sup> 300

Compared with Starbon® 300, S-Starbon® 300 W3 spectra exhibits a noticeable peak at 1031 cm<sup>-1</sup>, which is assigned to symmetric S=O stretching of sulfonic groups<sup>37,84-87</sup> attached to the material. The asymmetric mode is expected to appear at 1184 cm<sup>-1</sup>,<sup>46,86-88</sup> however, it is difficult to distinguish because of the broad band of the furan C-O linkages of Starbons® in the region 1400-1100 cm<sup>-1</sup>. It is worth mentioning that there is a shift of the S=O vibration, as it would be expected at 1050 cm<sup>-1</sup>; this displacement to lower frequency vibrations has been associated with bulky/cyclic substituents attached to the sulfur, which affects the bond order and tends to lower the frequency vibration.<sup>89</sup>

The absorption observed at 680 cm<sup>-1</sup> has been assigned to S=O bending mode of -SO<sub>3</sub>H.<sup>90</sup> Parent Starbon® 300 spectra shows bands at 680 (just mentioned previously), 812, 1001, 1028 and 1120 cm<sup>-1</sup>, which have been identified as correspondent to residues of p-toluenesulfonic acid (p-TSA). Bands appearing at 812, 1001 and 1120 cm<sup>-1</sup> correspond to bending (C-H) of benzene ring and the one at 1028 cm<sup>-1</sup> is assigned to C-S stretching.<sup>36</sup> This compound was used during the preparation of Starbon® 300 as previously reported by Budarin *et al*<sup>9</sup> and traces of it was found in the material. These bands are not present in the sulfonated Starbons®, suggesting that treatment with sulfuric acid removed the surface p-TSA. Then, after this analysis, a summary of the vibrational bands assignments observed in sulfonated Starbon® 300 is presented in **Table 2.6**.

Wavenumber cm <sup>-1</sup>	IR band assignment	Wavenumber cm <sup>-1</sup>	IR band assignment
3400	O-H stretching	1220	Ar-OH groups
2900	CH <sub>x</sub> stretching	1160	asymmetrical C-O-C stretching
1705	C=O stretching	1031	S=O symmetric stretching of ~SO <sub>3</sub> H
1600	C=C stretching	893	symmetrical C-O-C stretching
1430	C(=O)-O stretching	680	S=O bending

**Figure 2.14.** shows the IR spectra for sulfonated Starbons<sup>®</sup>, carbonized at different temperatures. In all of them, a band observed at 1031 cm<sup>-1</sup> is preserved, indicating the presence of sulfonic groups, through the symmetric S=O stretching, although elemental composition showed that sulfur content varies with temperature, in the spectra there is not a notable difference in the intensity of the band at 1031 cm<sup>-1</sup>. One of the most important differences observed among the spectra are the changes in the band at 1705 cm<sup>-1</sup> corresponding to C=O and the one, C=C at 1600 cm<sup>-1</sup> carbonization temperatures increment. The first band decreases when temperatures are higher, while the C=C increases with temperature; suggesting the disappearance of carboxylic groups and the transformation of the Starbon<sup>®</sup> to more graphitic-like structure.<sup>9</sup> These changes agreed with the elemental composition shown previously, in which there is an increase in the C:O ratio with raising the carbonization temperature. This also could be supported by the appearance of peaks at 1445, 875 and 830 cm<sup>-1</sup> related to aromatic groups.<sup>34</sup> This structural information is further supported by the analysis using <sup>13</sup>C CP/MAS NMR spectroscopy. Unfortunately, it was not possible to obtain adequate FTIR spectra of higher temperature materials, due to the increased broad band absorption which occurs in very dark materials, observed in the past by Budarin *et al.*<sup>9</sup>

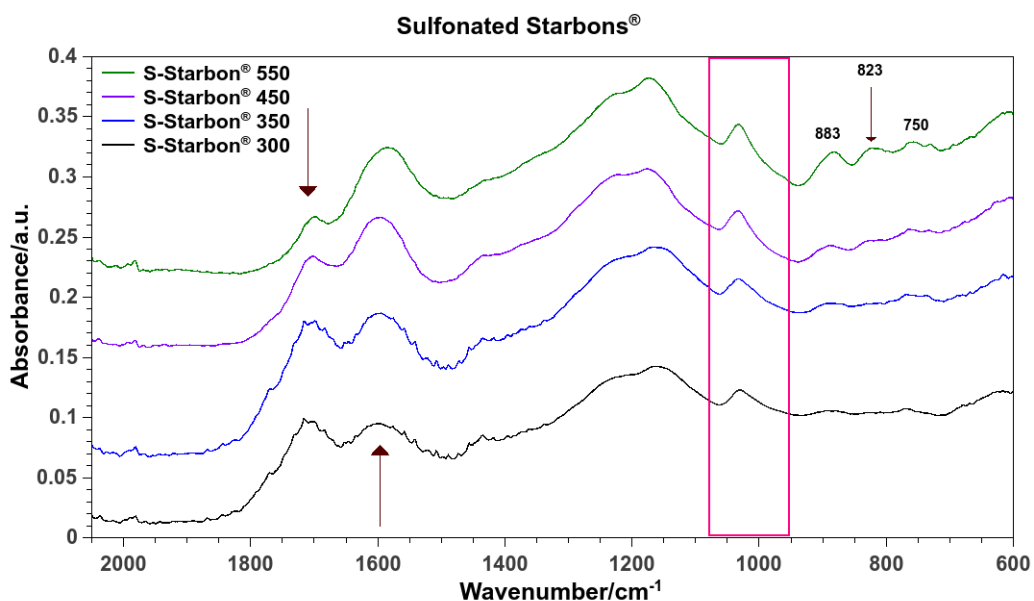


**Figure 2.14.** FTIR spectra sulfonated Starbons<sup>®</sup> carbonized at several temperatures

#### 2.4.4.1. Residues of *p*-Toluenesulfonic acid

In previous section, it was mentioned that remaining *p*-toluenesulfonic acid (*p*-TSA) was observed in the original Starbon® 300, and some traces of this compound were also observed in Starbons® 350 before sulfonation, due to the fact that Starbon® 300 was the precursor of Starbon® 350. Complementary information is obtained from the elemental composition, in which is determined that there is less than half of sulfur content (%weight) in Starbon® 350 that the one observed in Starbon® 300. This lower concentration was also observed in the FTIR spectra presented in **Figure 2.15**, where the peaks corresponding to *p*-TSA have decreased significantly, suggesting that further thermal treatment (350 °C) could also remove unbounded *p*-TSA.

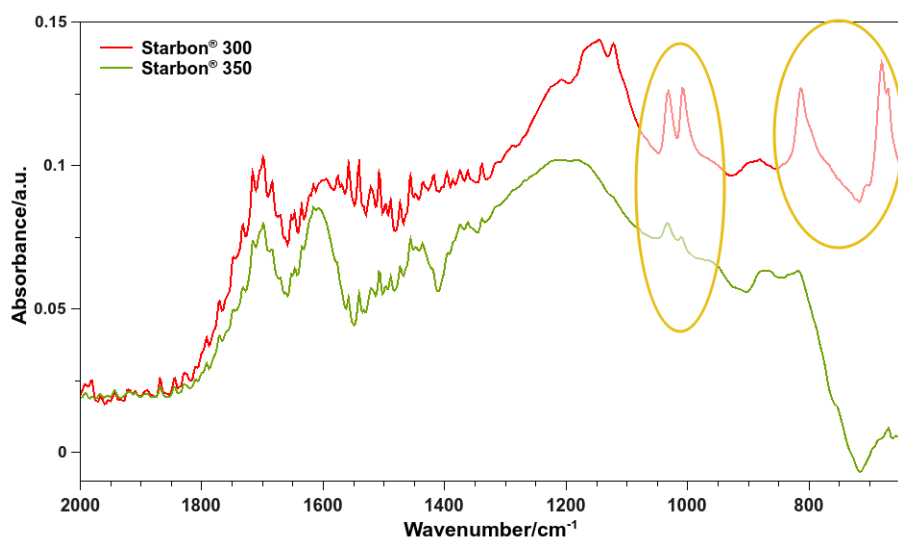


**Figure 2.15.** FTIR spectra showing *p*-TSA residues in Starbons® 300 and 350

#### 2.4.5. <sup>13</sup>C CP/MAS NMR studies on sulfonated Starbons®

The use of high-resolution techniques as Magic Angle Spinning (MAS) and Cross-Polarization (CP) has allowed the achievement of well-resolved <sup>13</sup>C NMR spectra for solid carbonaceous samples. This technique was used to obtain information about different structural types present in Starbons® and sulfonated Starbons®.

#### 2.4.5.1. Structural changes in Starbon® 300

Solid-state  $^{13}\text{C}$  NMR spectra obtained for Starbon® 300 before and after sulfonation are displayed in **Figure 2.16**. There are distinguishable differences between two spectra prior and after sulfonation. The main difference is the decrease of the broad band around 30–40 ppm, which is attributed to methylene and methine linkages.<sup>91–93</sup> As well, the broadness of the peak centred at ca. 130 ppm, which is characteristic of saturated systems C=C or aromatic rings,<sup>91,93,94</sup> which also contains the bands at 108 and 140 ppm of furan carbons<sup>91</sup>, The band which appears at ca.150 ppm, correspondent to phenolic groups<sup>91,93,95</sup> is preserved after sulfonation and seems broader than original one. It is interesting to notice the appearance of a small peak at ca. 165 ppm, which could be attributed to carbon in ester/lactones environment;<sup>93</sup> the peak corresponding to the carboxylic acids at 175 ppm<sup>34,93</sup> is embedded in the broad band in sulfonated Starbon® 300. The resonance observed at high downfield at ca. 205 ppm for the Starbon® 300, could be assigned to aldehyde groups,<sup>96</sup> groups which disappeared after sulfonation. Instead of these hydrogenated carbonyls, the appearance of the resonance at 190 ppm suggests the formation of ketones.<sup>96</sup> As shown previously through the elemental composition, sulfonation increments the oxygen content in Starbons®, this would promote appearance of more oxidized components; thus, lactones, esters and carboxylic acids could be related to the oxidation of aldehyde groups; or the ketone groups derived from oxidation of alcohol groups.

In both spectra, a small resonance ca. 70 ppm is observed, this band is assigned to ether structures<sup>95</sup> which is more apparent in sulfonated Starbon® 300 than in starting material. It is interesting to notice that sulfonated Starbon® 300 presents a noticeable peak centred at 53 ppm, this peak is assigned to methoxy groups,<sup>92</sup> which would suggest that it is formed after methanol washing, because the sulfonated Starbon® 300 prior methanol treatment did not present this band. As mentioned in section 2.3., the sulfonated Starbons® studied here correspond to sulfonated Starbons® (W3) “washed” with methanol.

Although elemental analysis showed high sulfur content on sulfonated Starbon® 300, the C–S bond, expected at around 140 ppm,<sup>28</sup> was not distinguished in its NMR spectra because of the broadness from the overlapping bands corresponding to aromatic (130 ppm) and phenolic groups (150 ppm). However, Starbon® 300, the starting material, presents a well defined peak around 140 ppm, which could be assigned either to the S–C aromatic bond, of p-TSA residues, or to the furan carbons. These broadening in resonances could be associated as well to the amorphous structure of materials.<sup>93</sup>

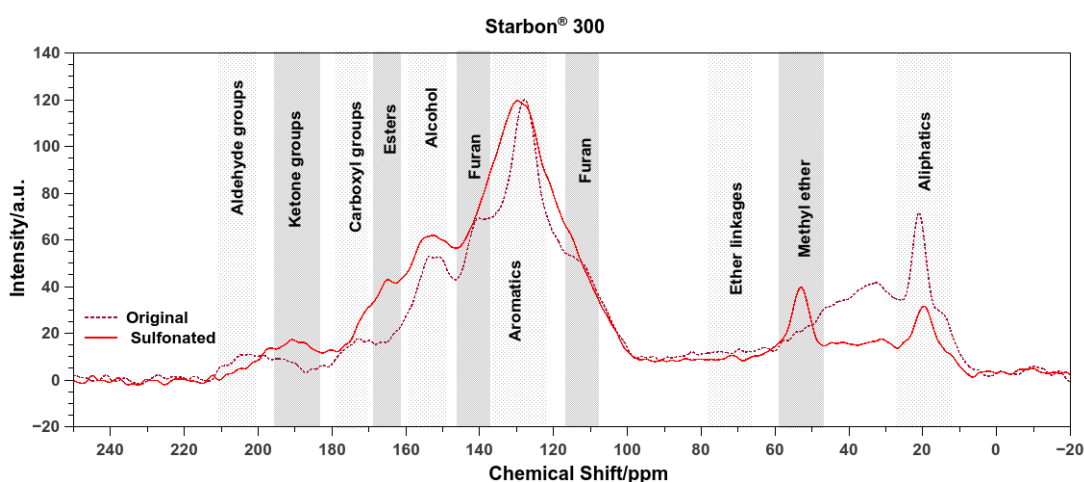


**Figure 2.16.** <sup>13</sup>C Solid-state NMR spectra for Starbons® 300 before and after sulfonation

The structural changes observed by solid-state <sup>13</sup>C NMR could be correlated with the variations in atomic ratios determined in the materials. Then, the drop in the C:O atomic ratio for sulfonated Starbons® 300, could be attributed to oxidation of some components of starting Starbons® (formation of lactones, esters, carboxylic acids, ketones) as well to attachment of sulfonic groups to the structure. This decrease was from 3.18 to 2.45 and has been showed before in **Figure 2.8**. Another observation concerning the atomic composition changes in these materials refers to the increment of C:H atomic ratio, presented in the approximation of the Empirical Formula, in **Figure 2.11**. This would suggest the appearance of conjugated and aromatic systems in the material after sulfonation, which would be associated with the broadening of band at ca. 130 ppm observed in the solid-state <sup>13</sup>C NMR spectra.

#### 2.4.5.2. Identifying main functional groups in Sulfonated Starbons® in <sup>13</sup>C NMR spectra

A reference <sup>13</sup>C NMR spectra was created to identify the main components in sulfonated Starbons®, after the previous review during working through the structural differences found by <sup>13</sup>C solid-state NMR between Starbons® 300 prior and post sulfonation. This reference spectra is displayed **Figure 2.17.** and shows the different carbon resonances regions identified on sulfonated Starbon® 350 and their corresponding assignment. In the upfield region around 20–30 ppm, the resonances are assigned to aliphatic carbons, suggesting the presence of methylene and methyl end groups derived of the starch decomposition.<sup>91</sup> The resonance located at 52 ppm corresponds to methoxy groups,<sup>92</sup> CH<sub>3</sub>-O-, which could be formed during the treatment of the sulfonated Starbons® with methanol. It is worth mentioning that this resonance does not appear in the spectrum of sulfonated materials before methanol washing, which would suggest that methanol may react with alcohol groups or carboxylic acids, present on the structure of the material, forming these methoxy species. The resonance ca. 65 ppm corresponds to ether structures,<sup>91,93</sup> which were also observed in Starbon® 300, before sulfonation. Presence of these ether linkages could be due to the remaining glycosidic bonds of component sugars of starch or cross-linking of starch chains.<sup>96</sup> At this point it is worth referring to the structural changes promoted by thermal treatment of polysaccharides, the approach considers the breakdown of components, internal reactions and rearrangement.<sup>80,96,97</sup> Thus, in the case of starch, the breakdown would lead first to formation of oligosaccharides and then to respective monosaccharides, these then suffer dehydration and fragmentation.<sup>80</sup> It has been suggested that first product from dehydration of hexoses and pentoses are hydroxy methyl furfural (HMF) and furfural, respectively; products identified as reactive to carbonaceous materials.<sup>98</sup> Then it has been suggested that furfuryl alcohol and furfural are the predominant pyrolysis products in starch carbonized at 350 °C.<sup>96</sup> This would explain the presence of furan moieties in the structure of sulfonated Starbon® 350, with corresponding resonances at ca. 113 ppm and ca.142 ppm.<sup>91,98,99</sup> Identification of furan moieties was already observed during synthesis of original Starbons®.<sup>9</sup> The band centred at 128 ppm has been

identified as conjugated and aromatic systems found in pyrolysed carbonaceous materials.<sup>28,91,93</sup> These aromatic clusters would be formed by condensation via intermolecular dehydration of aromatic molecules derived from decomposition/dehydration of the monosaccharides components of starch<sup>80</sup>.

The band which appears at ca. 150 ppm has been identified as OH-substituted carbons of phenols,<sup>28,91,93</sup> components present in Starbon<sup>®</sup> 300 before and after sulfonation. Beside the phenolic groups, a small band appears at ca. 165 ppm, which has been assigned to C in esters environment.<sup>93</sup> It is worth mentioning this band seems to appear after sulfonation of Starbons<sup>®</sup>, as shown in Starbon<sup>®</sup> 300. Between 175 and 180 ppm the resonance observed is assigned to carboxylic acids.<sup>93,96,100</sup> At very high downfield, around 195–205 ppm the resonance is assigned to ketone or aldehyde groups,<sup>95,96</sup> which also are related with the increasing O:C ratio for sulfonated Starbons<sup>®</sup>, presented previously.

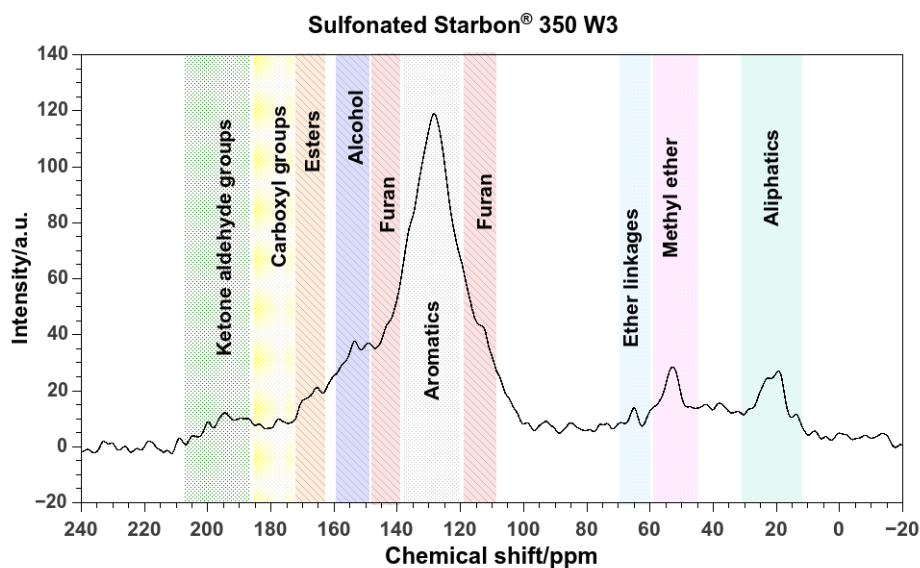


**Figure 2.17.** Functional groups identified for sulfonated Starbon<sup>®</sup> 350

#### 2.4.5.3. Increasing temperature of carbonization of Starbons<sup>®</sup>

<sup>13</sup>C solid-state NMR spectra (**Figure 2.18**), shows that there are significant structural changes in the materials when carbonization temperature of Starbons<sup>®</sup> increases. From the broadness and several functionalities identified

in Starbon® 300 to a narrow band centred at ca. 130 ppm for Starbon® 600, the changes suggest the transformation of the furan rings observed in low-temperature Starbons® to polycyclic aromatic system in the high-temperature ones; this has already been observed for thermal treatment of starch<sup>96</sup> or cellulose.<sup>93</sup>

Another observation as carbonization temperature increases in Starbons®, is the dropping in the aliphatic resonances at upfield regions, being less noticeable at Starbons® treated above 500 °C. The methoxy group identified at 53 ppm also decreases in intensity as temperature rises. Other obvious changes are the decrease in phenolic (150 ppm) and carboxylic groups (195 ppm), as the materials are carbonized. These structural changes could also be correlated with the increase in the C:O ratio for high-temperature Starbons® and found previously in the transition from starch-like to graphitic-like materials.<sup>9</sup>

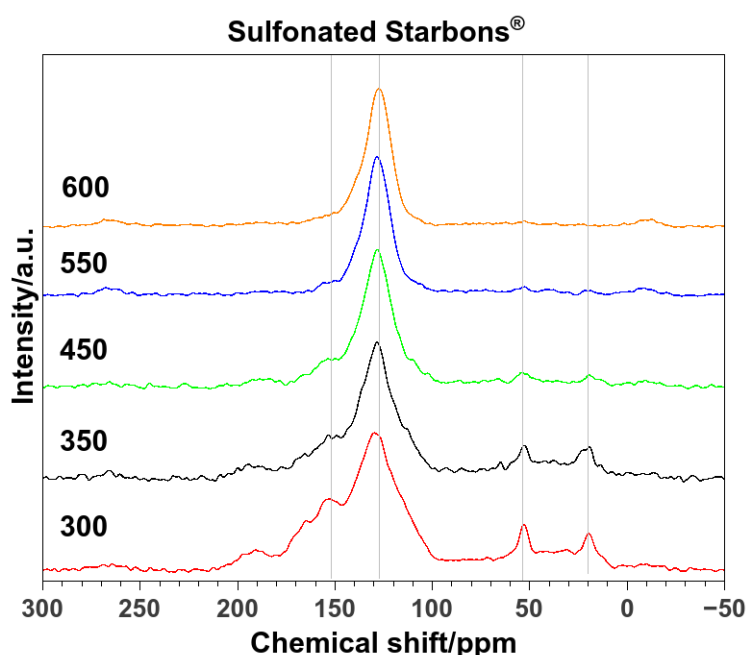


**Figure 2.18.** <sup>13</sup>C NMR spectra for sulfonated Starbons® carbonized at several temperatures

<sup>13</sup>C solid-state NMR spectra showed there are significant structural changes from low-temperature sulfonated Starbons® to high-temperature ones; changing from a polyfunctional material to an aromatic-predominant material. Through the spectra it was not possible to identify the C–S bond corresponding to sulfonic groups attached to the structure, because of overlapping of resonances with the

furan moieties at 140 ppm. The methoxy resonance observed at ca. ~50 ppm is suggested to appear because of the methanol treatment carried out on materials, as mentioned earlier.

**Figure 2.19.** shows suggesting structures for starting materials Starbons<sup>®</sup> 300 and 600, based on the information obtained by <sup>13</sup>C solid-state NMR about carbon functional groups present on their respective sulfonated Starbons<sup>®</sup>.

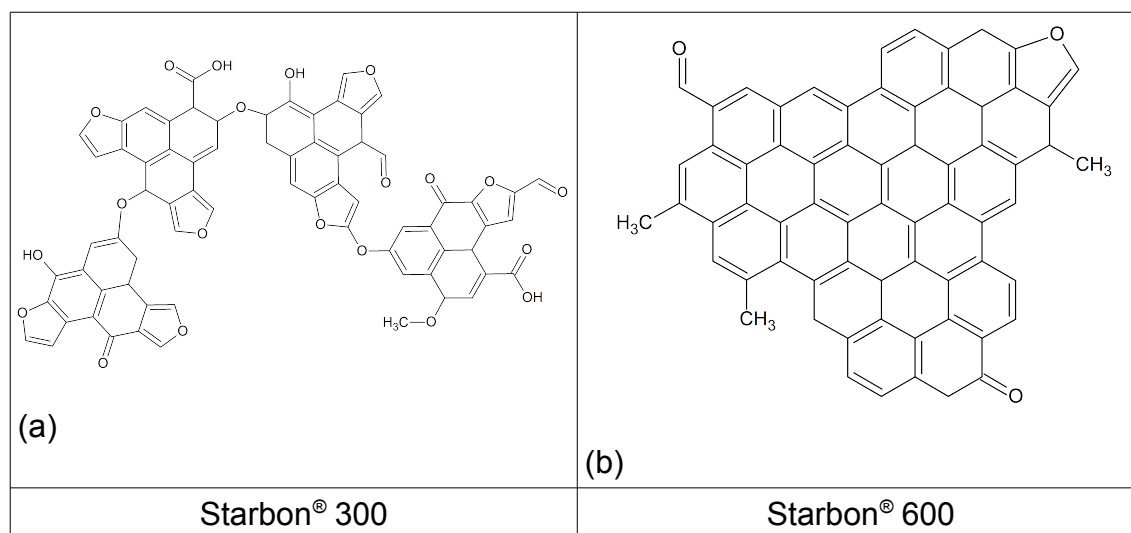


**Figure 2.19.** Proposed “structures” for Starbon<sup>®</sup> 300 (a) and Starbon<sup>®</sup> (600)

#### 2.4.6. X-ray photoelectron spectroscopy studies on sulfonated Starbons<sup>®</sup>

X-ray photoelectron spectroscopy (XPS) technique is widely applied to study the surface compositions of materials as metals, polymers, semiconductors, etc. This method could also be applied to determine the chemical or electronic states of the elements present on the material's surface providing useful information for characterisation. With this aim, parent Starbons<sup>®</sup> and sulfonated Starbons<sup>®</sup> were analysed.

##### 2.4.6.1. Before starting: data handling

Analysis of results was carried out as follows: the data obtained from the spectrometer were converted into the VAMAS file format (\*.vms) and imported into the CasaXPS software package for manipulation and curve-fitting. All C1s

peaks were recalibrated so that the peak maximum appeared at a binding energy of 284.5 eV and all binding energies (BEs) are measured relative to this C 1s (hydrocarbon) reference. The elemental composition data are derived from the survey scans via the instrument quantification software.

Carbon analysis: The C1s core level peak positions of the carbon atoms were centered at 284.5 eV. The deconvolutions were done considering Gaussian fitting. The full width at half-maximum (FWHM) was considered equal for all the carbon components.

Sulfur analysis: the S 2p peaks were fitted using a Gaussian function with provision for the 1.2 eV spin-orbit splitting for  $2p_{1/2}$  and  $2p_{3/2}$ ; the 1:2 intensity ratio of this splitting was maintained in the fitting.

Plots: dots correspond to the actual measurements and the yellow line corresponds to the spectra fitting.

#### 2.4.6.2. Starbons<sup>®</sup> 300 and 800

These two materials represent the extremes of the range of Starbons<sup>®</sup> studied. The low temperature one presents more starch-like characteristics and the high-temperature one, is more graphitic-like as reported by *Budarin et al.*<sup>9</sup>. And from previous section of <sup>13</sup>C NMR these characteristics are reconfirmed, as Starbon 300 presents a wide range of functional groups, hydroxy groups, carbonyls and carboxyl groups; while Starbon<sup>®</sup> 800 is more related to polycyclic aromatic carbons. Then, parent and sulfonated Starbons<sup>®</sup> 300 and 800 were analysed by XPS to determine their compositions. As it has been noted before p-toluensulfonic acid (p-TSA) is used catalytically during preparation of parent Starbons<sup>®</sup> 300 and 800. Then, the presence of sulfur in the original materials is related to this compound; which presence was observed by FTIR in Starbon<sup>®</sup> 300, while for Starbon<sup>®</sup> 800, the presence of the compound p-TSA is not confirmed by FTIR, however, elemental analysis showed that Starbon<sup>®</sup> 800 contains sulfur, which would be derived from p-TSA. **Table 2.7** shows the atomic percentage composition found for these materials. As expected, higher percentage of carbon is observed for Starbon<sup>®</sup> 800 than 300; the other way round is found for the content of oxygen, which is higher for Starbon<sup>®</sup> 300 than 800. The sulfur content on surface, is close to double for both Starbons<sup>®</sup> after

sulfonation, but a better analysis could be made, when comparing the elemental ratios, presented in **Figure 2.20**.

	Parent			Sulfonated		
	<b>C</b>	<b>O</b>	<b>S</b>	<b>C</b>	<b>O</b>	<b>S</b>
Starbon <sup>®</sup> 300	84.61	14.26	1.14	78	19.87	2.13
Starbon <sup>®</sup> 800	97.14	2.44	0.41	93.14	6.03	0.83

A massive drop in the C:O ratio is observed from original material to the sulfonated Starbon<sup>®</sup> 800, indicating the increase of oxygen content in the sample, due to the attachment of sulfonic groups or the oxidation of the sample.<sup>101</sup> This decrease in C:O ratio is less obvious for Starbon<sup>®</sup> 300, mainly because original material already contains oxygenated groups in the structure. The sulfur-carbon ratio observed on the surfaces of Starbons<sup>®</sup> 300 and 800 increased by double after sulfonation. It is important to point out that initial content of sulfur in parent Starbons<sup>®</sup> can be related to p-TSA remaining in the structure. As has been mentioned, p-TSA was used during the synthesis of Starbons<sup>®</sup> 300 and 800. The presence of p-TSA in parent Starbon<sup>®</sup> 300 was confirmed in previous studies by FTIR; however, in the case of parent Starbon<sup>®</sup> 800, there is no IR information. In this case, it is difficult to discern whether the sulfur observed corresponds just to physisorbed p-TSA on the material instead of bounded to the structure of Starbons<sup>®</sup>, as high-temperature treatment can promote the decomposition of p-TSA and subsequent sulfonation of the material. Both Starbons were treated in a similar way for the sulfonation (H<sub>2</sub>SO<sub>4</sub> 95% in a ratio 1: 7 mL; at 90°C for 6 h), however, the concentration of sulfur is higher for the Starbon<sup>®</sup> 300 than Starbon<sup>®</sup> 800, suggesting that sulfuric acid reacts in higher proportion with the functionalities found in Starbon<sup>®</sup> 300 than for the high-temperature carbonized Starbon<sup>®</sup>.

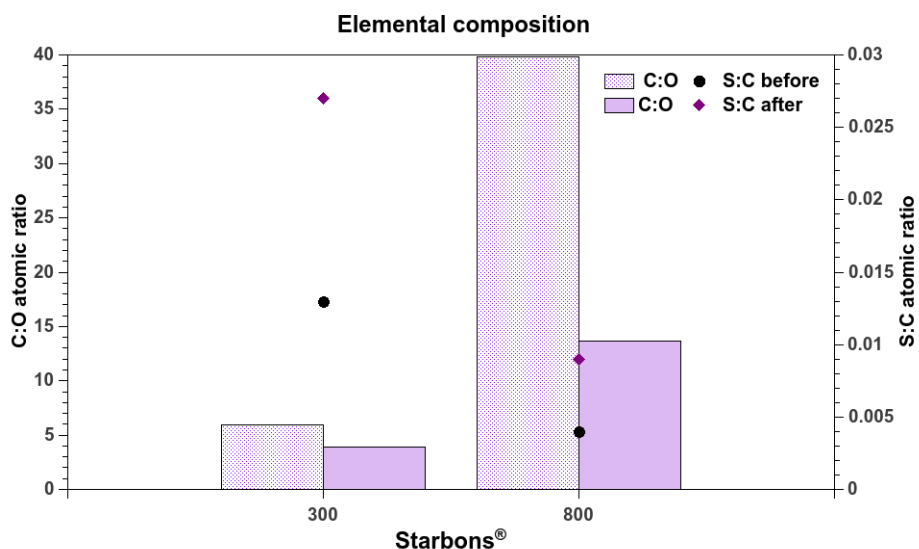


**Figure 2.20.** Elemental ratio (from XPS analysis) for Starbons® 300 and 800 before and after sulfonation.

#### 2.4.6.3. Analysis of carbon bonding

The analysis of the high-resolution C1s peak shape with peak fitting is a powerful tool to identify the functionalities present on the sample. Depending on the chemical environment of the carbon atom, the C1s peak can present high-chemical shifts making it relatively easy to identify its main components. This process was carried out using CasaXPS software, as mentioned previously. In this respect, a chart based on literature review was created as a reference for the assignments made for each component. However, it is not always as straightforward, because some species could present very similar chemical shifts. **Table 2.8** presents the assignments considered in this study for the different carbon environments found in Starbons® and sulfonated Starbons®.

Table 2.8. Bonds assignments for components of C1s		
Binding Energy/eV	Bond	References
284.3 – 284.8	C = C (sp <sup>2</sup> )	102,107 106
285.1 – 285.5	C – C (sp <sup>3</sup> )	102,107
285.3	<u>C</u> – COO	108
285.7	C – S	109
286.0 – 287.0	C – O (alcohol/phenol)	92,107,110 106
287.2 – 288.0	C = O or O – C – O	92,102,103,107 106
289.0 – 290.2	O – C = O	92,103,107,111 106
290.2 – 292.1	$\pi - \pi^*$ transitions	102,103 104 105

**Figure 2.21.** shows a comparison between Starbon<sup>®</sup> 300 and sulfonated Starbon<sup>®</sup> 300, prepared by conventional sulfonation. Broadening of the C 1s peak could be observed after treatment; as well, increasing of oxidized states, components observed at 287.6 eV and 289.9 eV, corresponding to C=O and O-C=O, respectively. These results agreed with the increasing of oxygen content observed by elemental analysis, suggesting that sulfonation of Starbons<sup>®</sup> promotes the oxidation of the components.

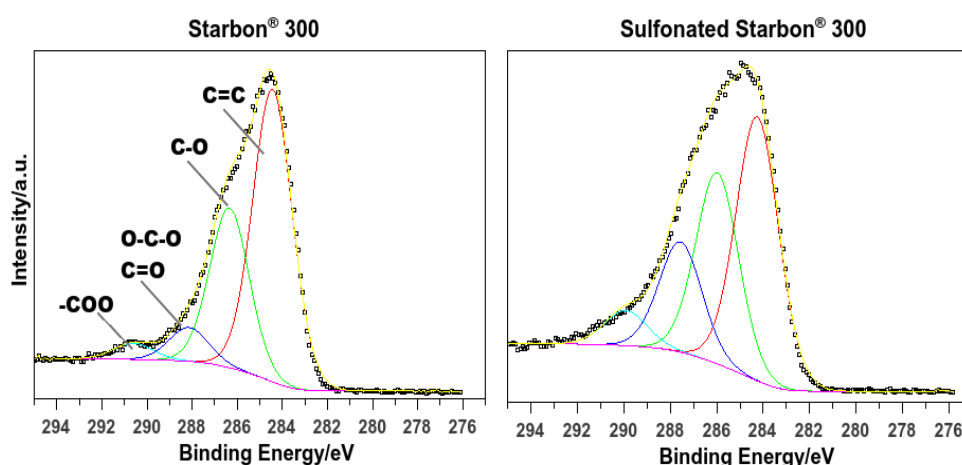


**Figure 2.21.** XPS spectra for C1s of Starbon<sup>®</sup> 300 prior (left) and after sulfonation (right).

A comparison between Starbon<sup>®</sup> 800 before and after sulfonation is shown in **Figure 2.22**. The spectra shows that Starbon<sup>®</sup> 800 is very different from Starbon<sup>®</sup> 300, as there is a noticeable decrease in the oxygenated carbon and the presence of aromatic carbon has increased substantially. A long tailing above 290 eV is observed, attributed to  $\pi - \pi^*$  transitions of the aromatic groups present in the material.<sup>106</sup> Another characteristic observed in these high-temperature Starbons<sup>®</sup>, is the presence of a peak around 285.5 eV in both sulfonated and non-sulfonated Starbons<sup>®</sup> 800; according to the references presented in **Table 2.8.**, this peak could be assigned either to  $sp^3$  carbon-carbon bonds or to C-S bonds, the later is considered an option because, as seen by elemental composition, both materials contain sulfur in the structure. After conventional sulfonation of Starbon<sup>®</sup> 800 there are slight changes in the carbon components, as the decrease of carbon-carbon bonds and the small increase in oxidized forms of carbon as alcohols, carbonyls and carboxyl groups; suggesting the reaction of C=C bonds with sulfuric acid.<sup>101,107</sup> **Table 2.9** summarizes the relative concentration of each component determined for Starbons<sup>®</sup> 300 and 800 before and after sulfonation.

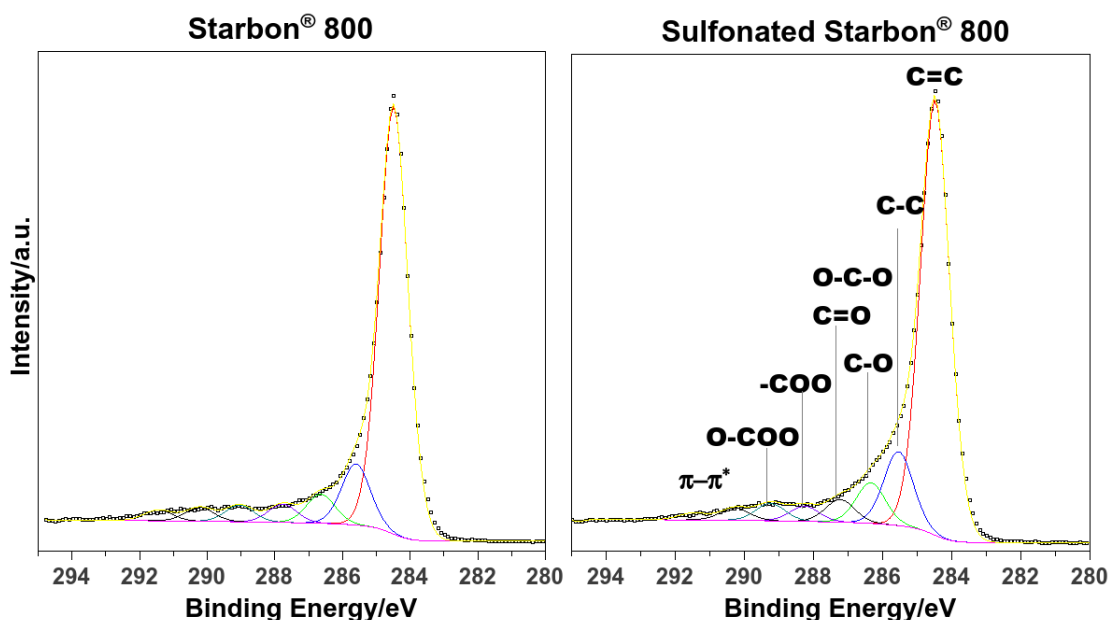
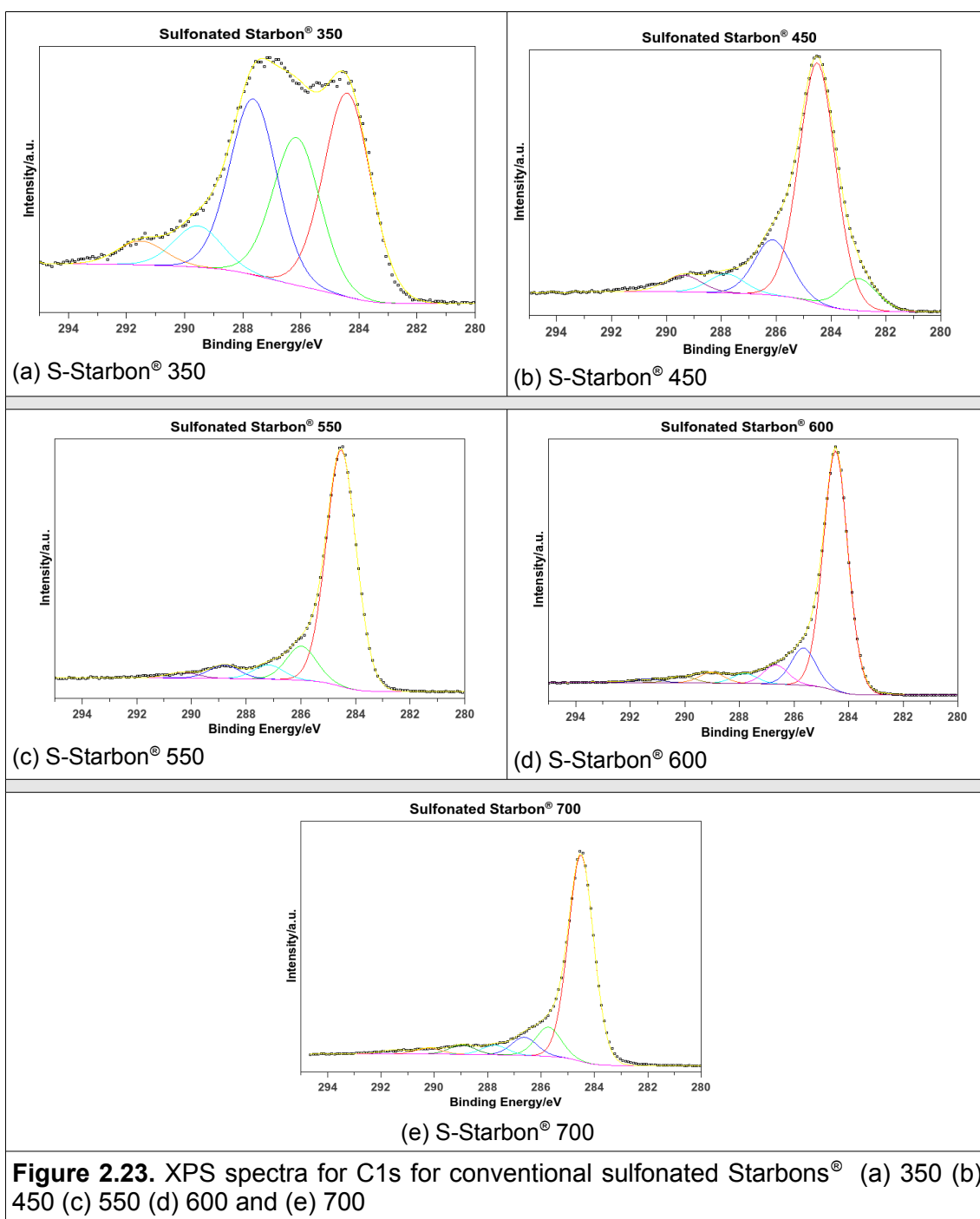


**Figure 2.22.** XPS spectra for C1s of Starbon<sup>®</sup> 800 prior (left) and after (right) sulfonation

**Table 2.9.** Chemical states of C and their relative concentration (%) for Starbons<sup>®</sup> 300 and 800 before and after sulfonation. (Binding energies presented in parenthesis)

	C = C	C - C / C - S	C - O	C = O, O - C - O	O - C = O	$\pi - \pi^*$
<b>Starbon<sup>®</sup> 300</b>	58.2 (284.5)	-	31.8 (286.3)	6.8 (288.2)	3.2 (290.6)	
<b>S-Starbon<sup>®</sup> 300 W3</b>	44 (284.5)	-	31.9 286.0	18.3 (288.5)	5.8 (289.9)	
<b>Starbon<sup>®</sup> 800</b>	74 (284.5)	10.6 (285.6)	5.1 (286.6)	3.2 (287.7)	2.9 (289.0)	4.2 (290.2-292)
<b>S-Starbon<sup>®</sup> 800 W3</b>	69.7 (284.5)	11.9 (285.5)	6.5 (286.3)	3.7 (287.9)	3.2 (289.0)	5 (290.2-292)

A similar analysis in spectra of C1s is carried out for subsequent sulfonated Starbons<sup>®</sup>, presented in **Figure 2.23**. Sulfonated Starbon<sup>®</sup> 350 still presents broad bands similar to Starbon<sup>®</sup> 300, which is the starting material from carbonization. However, as temperature of carbonization increases, the peaks get narrow, indicating a shift from oxidized carbon to more graphitic-like. Sulfonated Starbon<sup>®</sup> 450 presents an abnormality as one of its components appears at lower BE's, 283 eV. According to the references in XPS Handbook<sup>106</sup> low BE's in carbon indicates carbides, however in this material is very unlikely to contain them; so another assignment needs to be made. Some authors assigned the appearance of amorphous carbon, during modification of polymers with plasma.<sup>104</sup>



Another way to present this transition from starch-like to graphitic-like for sulfonated Starbons® as temperature increases is displayed through the comparison of the high-resolution C1s spectra of each sample (**Figure 2.24.**). It can be observed the narrowing of the peaks after 450 °C and the appearance of tailing after BE at 290 eV, indicating the presence of shake up electrons attributed to aromatic systems.<sup>106</sup> Although sulfonation of Starbon® 500 was carried out, the spectra is not presented because the elemental analysis did not

show sulfur at all, suggesting an unsuccessful sulfonation.

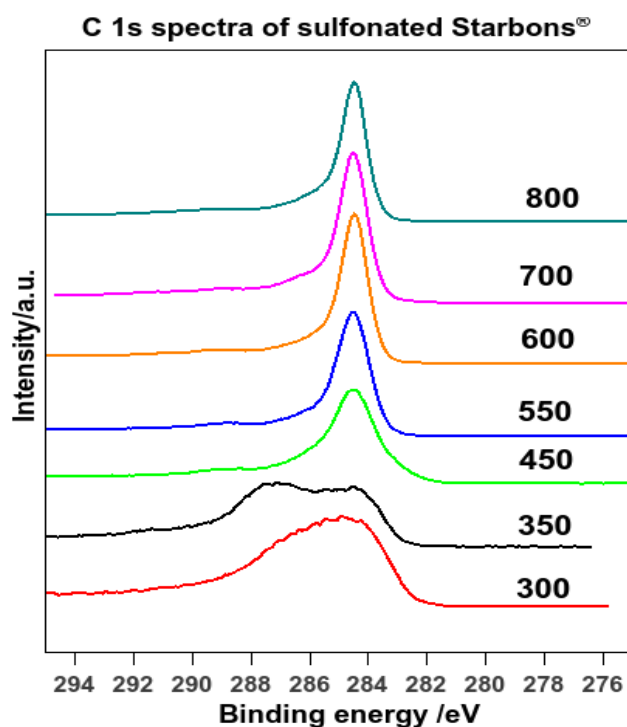


**Figure 2.24.** XPS spectra comparison for C1s for conventional sulfonated Starbons®

Relative concentrations of carbon components found in sulfonated Starbons® are presented in **Table 2.10**. As **Figure 2.24** suggests there is an increase in  $sp^2$  carbon bond and a general decrease of oxygenated carbon as temperature increases. The appearance of a band around 285.6–285.9 eV is observed for sulfonated Starbons® 600 and 700, as found in sulfonated Starbon 800, previously. The assignment of the peak at ~285.6 eV to C–C or C–S is still difficult to be made, because there is not spectra for Starbons® 600 and 700 before sulfonation; however, the analysis of sulfur by XPS would complement the information needed to make the corresponding designation. The decrease in the component C–O is noticeable from sulfonated Starbon® 350 to 450, as it changes from 28 % to 15 %. A drastic drop of this component is found for sulfonated Starbons® 600 and 700, in which this component represents less than 6%. Higher concentration (26 %) for carbon double bond oxygen (C=O or O–C–O) is observed in sulfonated Starbon® 350, even higher than sulfonated Starbon® 300 (18%); however, in higher temperature carbonized Starbons®, 450

and onwards, this component appears in very low concentration, less than 6 %. The carboxylic component is observed in all the sulfonated Starbons<sup>®</sup>, its concentration is usually lower than other oxygenated components and did not follow a clear trend as carbonization temperature increases.

**Table 2.10.** Chemical states of C and their relative concentration (%) for Starbons<sup>®</sup> 350 to 700 after sulfonation. (Binding energies presented in parenthesis)

	<b>C = C</b>	<b>C – C C – S</b>	<b>C – O</b>	<b>C = O, O – C – O</b>	<b>O – C = O</b>	<b><math>\pi - \pi^*</math></b>
<b>S-Starbon<sup>®</sup> 350 W3</b>	38.6 (284.5)	-	28.5 (286.3)	25.9 (287.9)	7 (290.6)	
<b>S-Starbon<sup>®</sup> 450 W3</b>	66.1 (284.6)	<b>Amorphous C</b> 8.9 (283.0)	15.2 (286.1)	5.2 (287.8)	4.6 (289.4)	
<b>S-Starbon<sup>®</sup> 550 W3</b>	77.7 (284.5)		11.2 (286.0)	4.7 (287.2)	4.5 (288.8)	1.9 (290.3)
<b>S-Starbon<sup>®</sup> 600 W3</b>	78.8 (284.5)	8.8 (285.9)	4.7 (286.3)	3.5 (288.3)	2.6 (289.4)	1.6 (290.8)
<b>S-Starbon<sup>®</sup> 700 W3</b>	73.3 (284.5)	11.4 (285.6)	5.8 (286.6)	3.1 (287.8)	3.3 (289)	3.1 (290- 291.3)

#### 2.4.6.4. The sulfur components in sulfonated Starbons<sup>®</sup>

X-ray photoelectron spectroscopy was also used to identify the sulfur species present in sulfonated Starbons<sup>®</sup>. **Figure 2.25** shows the S2p core level spectra for a range of sulfonated Starbons<sup>®</sup> prepared by conventional heating (90 °C and 6 h). In the figure, two main bands could be distinguished: one centred above 167 eV and another ca. 163.5 eV. The high binding energy is attributed to oxidized states of sulfur: sulfones, sulfonic acids and sulfates (referred as S-ox subsequently) and the low binding energy represents sulfur in “reduced” systems, with R–S configuration (labelled as S-red).<sup>105,106,112–114</sup>

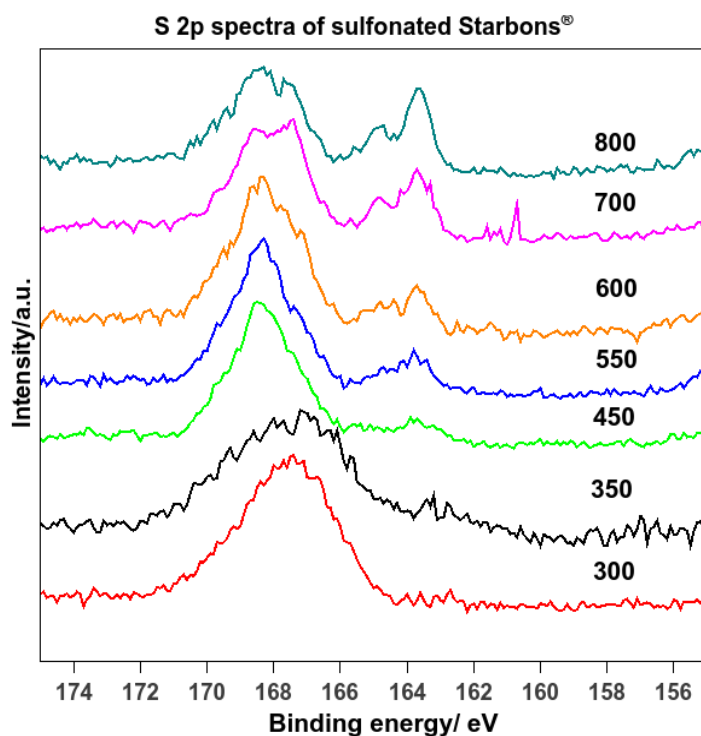


**Figure 2.25.** XPS S2p spectra for conventionally sulfonated Starbons®

High-resolution S2p core level spectra for sulfonated Starbons® are presented in **Figure 2.26**. The S2p peaks were fitted using Gaussian function through CasaXPS software. In this process, the spin-orbit splitting  $2p_{1/2}$  and  $2p_{3/2}$  was considered with a binding energy of 1.2 eV and the 1:2 intensity ratio of this splitting was maintained in the fitting.<sup>115,116</sup>

Sulfonated Starbons® 300 and 350 (**Figure 2.26. (a)** and **(b)**) present similar spectra, with just one band centred at 167 eV, identified as S(VI) which is attributed to the presence of sulfonic acids on the materials.<sup>112,114</sup> Looking at all the spectra presented in **Figure 2.26.**, it is noticed that reduced sulfur assigned to S(II)<sup>112</sup> band ca. ~163.5 eV is only observed for high temperature Starbons®, (450 onwards). When comparing our sulfonated Starbons® with other sulfonated carbons, it is interesting to find that materials with similar structure to our graphitic-like Starbons® do not present reduced sulfur S(II) in their structure and just S (VI), attributed to sulfonic acid.<sup>27,28</sup> This difference could be attributed either to the distinct nature of the material or the sulfonation approach.

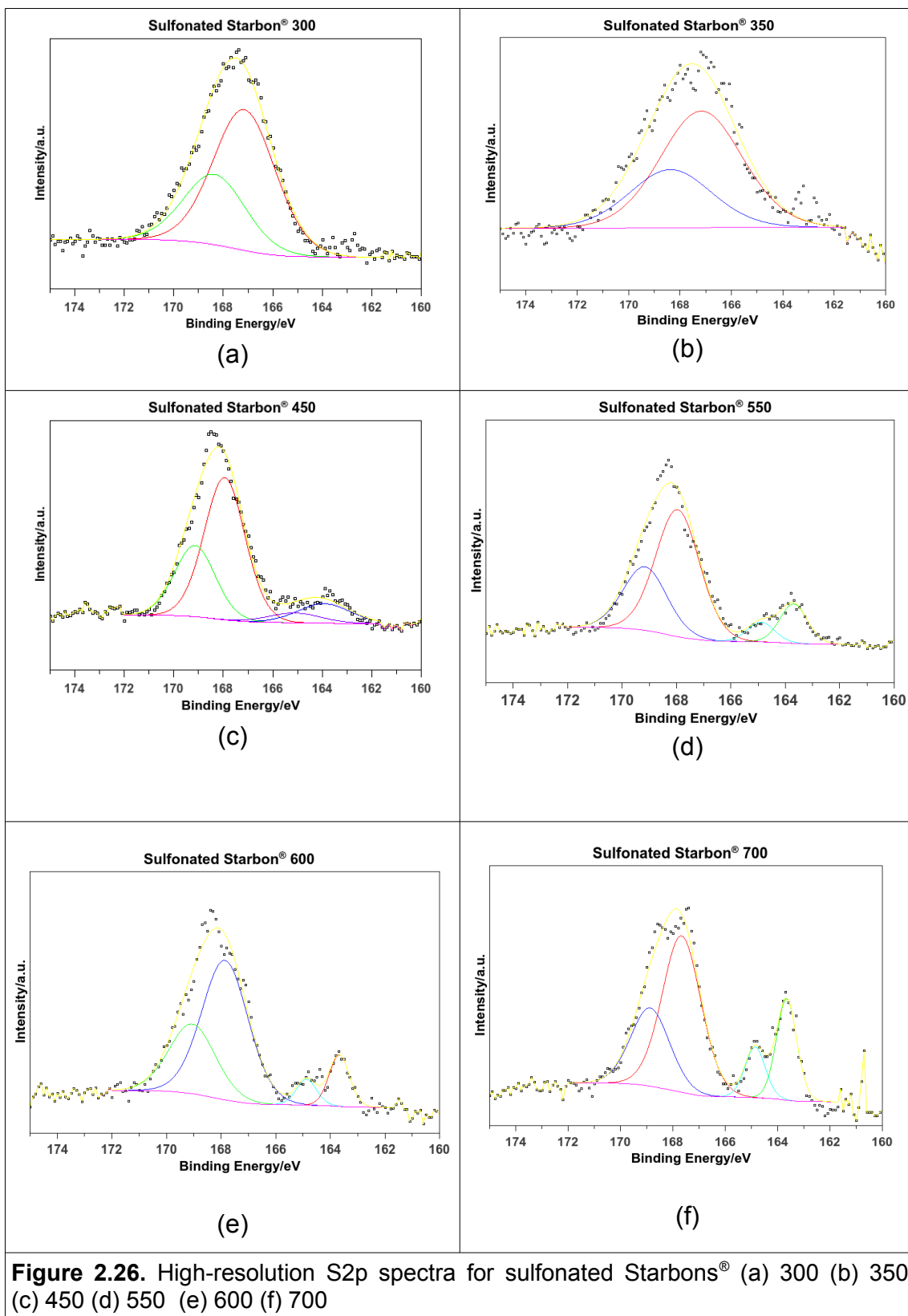


**Figure 2.26.** High-resolution S<sub>2p</sub> spectra for sulfonated Starbons® (a) 300 (b) 350 (c) 450 (d) 550 (e) 600 (f) 700

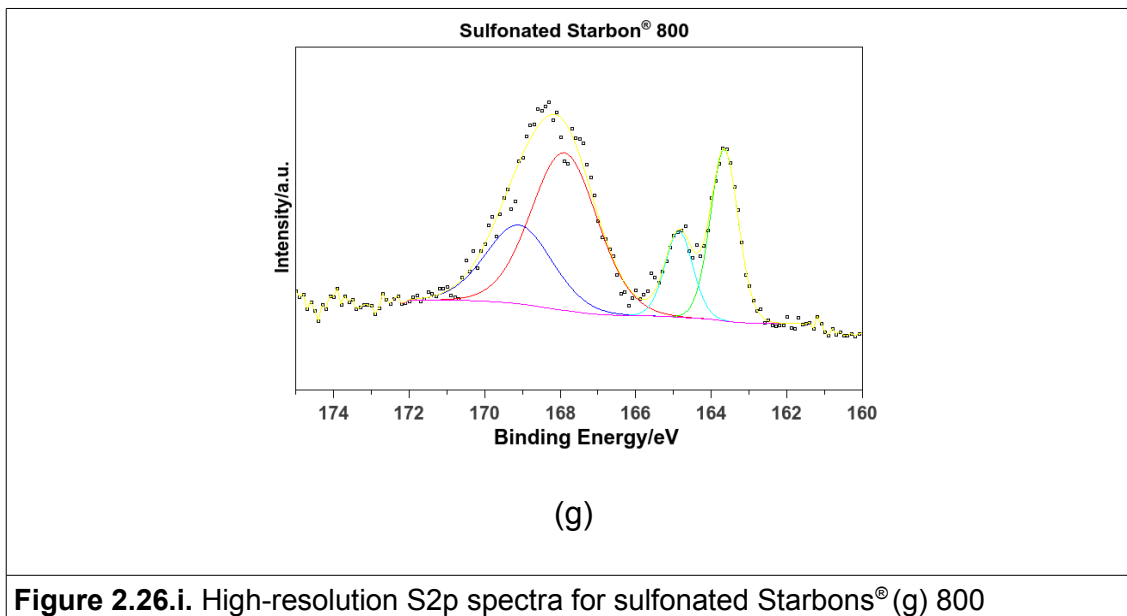


**Figure 2.26.i.** High-resolution S2p spectra for sulfonated Starbons® (g) 800

A rough quantification of the sulfur components is presented in **Table 2.11.**, composition is based on the areas of each component. Similar concentration of reduced sulfur is observed for Starbons® 450, 550 and 600 (15 %). For Starbons® 700 and 800, there is an increase in the quantity of reduced sulfur, as it was observed 25 % and 31 % respectively, suggesting that more graphitic-like Starbons® possess more reduced sulfur. At this point, it is worth mentioning that during sulfonation of Starbons®, gases were released; sulfur dioxide was identified among those gases. In the following chapter, of microwave sulfonated Starbons® is presented an attempt to quantify it using a hydrogen peroxide solution. However, results were erratic and difficult to correlate.

<b>Table 2.11.</b> Relative concentration (%) of chemical states of sulfur and their binding energy (in parenthesis, eV)		
<b>Starbon<sup>®</sup> Carbonization Temperature/°C</b>	<b>S2p3/2 Ox</b>	<b>S2p3/2 Red</b>
300	100 (167.2)	
350	100 (167.2)	
450	85 (167.9)	15 (163.8)
550	85 (167.9)	15 (163.7)
600	85 (167.9)	15 (163.7)
700	75 (167.7)	25 (163.7)
800	69 (167.9)	31 (163.6)

XPS analysis showed that there are significant differences in the nature of carbon and sulfur present in the range of sulfonated Starbons<sup>®</sup> prepared. Results suggest that sulfonation promotes the oxidation of components of original Starbons<sup>®</sup>, these results are in agreement with the increasing in oxygen content observed by elemental analysis; in addition with the appearance of more oxygenated carbon compounds as carboxylic acid and ketones in sulfonated Starbons<sup>®</sup>. The analysis of S2p spectra showed there are two different sulfur species: oxidized S(VI) and reduced S(II). The former appears above 167 eV and the latter, ca. 163.5 eV. Low temperature Starbons 300 and 350 presents only the oxidized form of sulfur S(VI); while high-temperature Starbons<sup>®</sup>, present the two species, oxidized S(VI) and reduced S(II). It is assumed that all S(VI) present corresponds to sulfonic acid groups, meanwhile S(II) is thought to be attached as C–S–C bonds. Although this assignation would need to be more supported by other analysis, the C1s spectra for sulfonated Starbons 600, 700 and 800 showed a band at 285.6 eV, which corresponds to C–S bonds; thus, is very tentative to accept the formation of the C–S–C.

The suggested structures for Starbon<sup>®</sup> 300 and Starbon<sup>®</sup> 600 (**Figure 2.19.**) were modified to integrate the sulfur groups identified on their respective sulfonated Starbons<sup>®</sup>, according with the information obtained for their S2p spectra by XPS analysis (**Figure 2.27.**). The main difference between

sulfonated Starbon<sup>®</sup> 300 and sulfonated Starbon<sup>®</sup> 600 is the presence of reduced sulfur S(II) in S-Starbon<sup>®</sup> 600. It is important to point out that both structures are proposed with the aim to schematically represent the functional groups present on the materials.

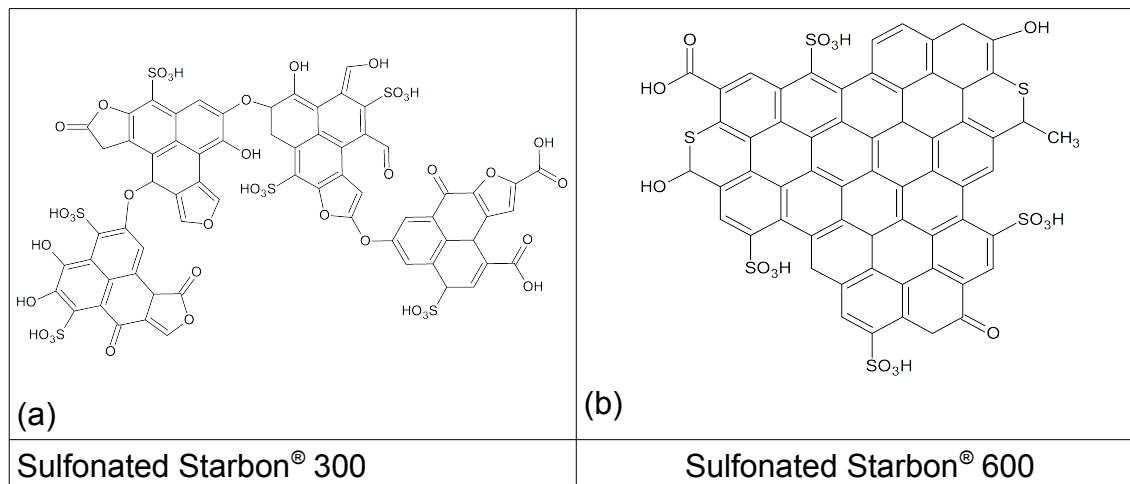


**Figure 2.27.** Proposed “structures” for sulfonated Starbon<sup>®</sup> 300 (a) and sulfonated Starbon<sup>®</sup> (600)

#### 2.4.7. Sulfur (VI) and acidity

Quantity of sulfonic groups ( $\sim\text{SO}_3\text{H}$ ) attached to sulfonated Starbons<sup>®</sup> was estimated by titration using an aqueous solution of NaOH. The procedure used for sulfonated Starbons<sup>®</sup> is a modification of the method proposed by P. Lin *et al*<sup>46</sup> for sulfonated carbon nanocage materials. In our work, 20 mg of sample was dispersed in 15 g of methanol-aqueous (1:1) solution of NaCl (2 M); sample was stirred overnight at room temperature. Afterwards, the dispersion was filtered to remove the solid sulfonated Starbon<sup>®</sup> and then, filtrate was titrated potentiometrically using NaOH 0.005 M. It is worth mentioning that this approach consider that all the ( $\text{H}^+$ ) coming from the interchange with ( $\text{Na}^+$ ) come from sulfonic acid groups. Thus, a comparison between sulfur (VI) determined by XPS and acidity was intended to find possible correlations (**Figure 2.28**). The acidity (quantity of  $\sim\text{SO}_3\text{H}$  groups  $\text{mmol g}^{-1}$ ) determined using this methodology gives lower values than S(VI) determined by XPS. However, there is a trend between S(VI) and acidity, both decrease with increment of temperature of carbonization of sulfonated Starbon<sup>®</sup>. The acidity obtained for

sulfonated Starbon<sup>®</sup> 300 was 0.82 mmol g<sup>-1</sup> almost half of the value of S(VI) content obtained by XPS. Sulfonated Starbons<sup>®</sup> 350 and 450 present 0.57 and 0.40 mmol g<sup>-1</sup>, respectively. Again, values above the half of S(VI) determined by XPS. This observation would indicate that S(VI) does not only corresponds to sulfonic acids, but to other S(VI) species as sulfates or sulfones; as well, it could be considered that sodium chloride solution possibly does not interact with all the sulfonic acid groups present on sulfonated materials. Lower acidity density respect to their S(VI) content was also observed in other sulfonated carbons.<sup>27</sup> This observation can explain why some authors when refer to “acidity density”, make the assumption that sulfur content determined by elemental analysis or by XPS corresponds only to sulfonic acid groups (~SO<sub>3</sub>H).<sup>28,31</sup>

Sulfonated Starbons<sup>®</sup> 550, 600, 700 and 800 present very low values in their acidity; values are too low in comparison with the quantity of sulfur (VI) obtained by XPS. This lack of correlation could be associated with the increasing hydrophobicity of samples, making more difficult the interaction of the sodium chloride solution (H<sub>2</sub>O-MeOH,1:1). It is worth mentioning, that this solution was prepared with methanol trying to improve the interaction with hydrophobic materials. Then, this observation for hydrophobic sulfonated Starbons<sup>®</sup>, may apply for sulfonated Starbons<sup>®</sup> 300 and 350, as they also present some hydrophobic carbons in their structure, as it has been demonstrated by FTIR and <sup>13</sup>C solid-state NMR.

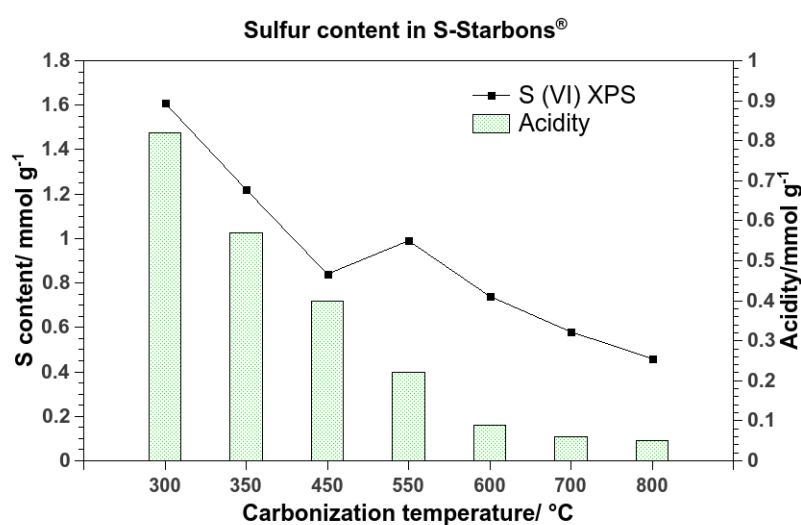


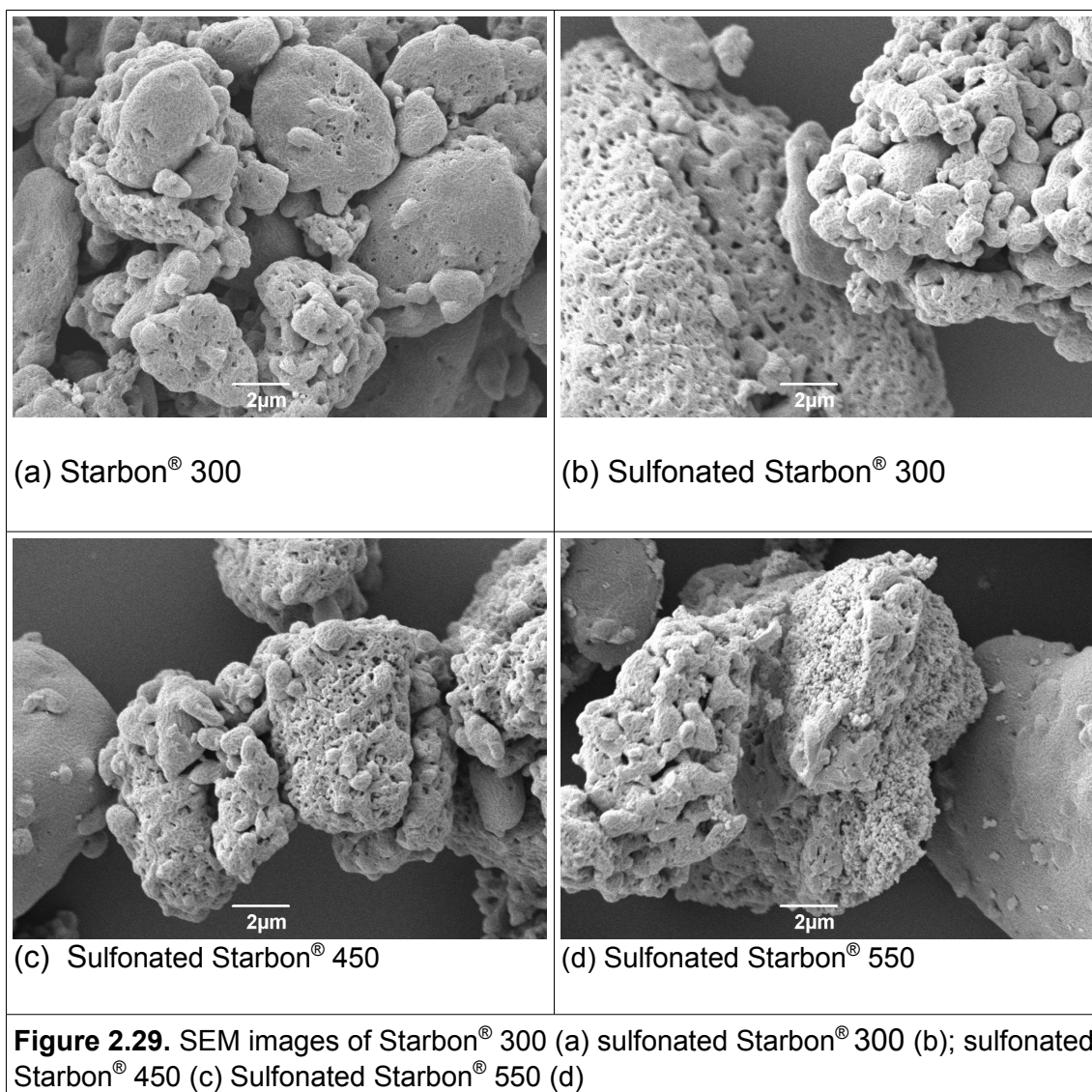
**Figure 2.28.** Sulfur content for sulfonated Starbons<sup>®</sup> at 90°C for 6h

The acidity obtained for sulfonated Starbon<sup>®</sup> 300 is lower than the one obtained in sulfonated nanocages<sup>46</sup> (1.53 mmol/g<sup>-1</sup>) following similar procedures in the quantification of sulfonic acid groups. In general, the acidities (~SO<sub>3</sub>H density) determined for sulfonated Starbons<sup>®</sup> have lower values in comparison with other sulfonated carbonaceous materials.<sup>30,31</sup> This could be attributed not just to the difference of starting materials, but as well the methodologies used in their synthesis. Sulfonation of those materials is done using fuming sulfuric acid (15% SO<sub>3</sub>), in solid (g) – acid (mL) ratios which go from 1:30 to 1:50, while our synthesis is carried out in ratios 1 g : 7 mL of sulfuric acid, in our approach of sustainable development of solid acid catalysts.

## **2.4.8. Morphology and porosity of sulfonated Starbons<sup>®</sup>**

### *2.4.8.1. SEM images*

The morphology of the materials was observed by Scanning Electron Microscopy (SEM). In **Figure 2.29**, parent and sulfonated Starbons<sup>®</sup> 300 are shown (a) and (b); the analysis suggests there are not severe physical changes in the materials after sulfonation carried out at 90°C for 6h. Porous structure of the original material is preserved. This characteristic is also observed in sulfonated Starbons<sup>®</sup> 450 and 550, in which porosity is preserved. From these SEM images, it is discerned Starbons<sup>®</sup> and sulfonated Starbons<sup>®</sup> are formed as porous agglomerates.<sup>64</sup> This observation is further supported with the results obtained by N<sub>2</sub> adsorption-desorption isotherms and pore size distribution shown afterwards.



#### 2.4.8.2. Surface area and porosimetry

Following the previous comparison approach between parent and sulfonated Starbon® 300, porosimetry measurements shown that both materials have very similar nitrogen adsorption isotherms in which the condensation step starts at higher relative pressure  $P/P_0 \approx 0.8$  (**Figure 2.30.a**). According to the IUPAC classification, the isotherms observed in these materials are type IV, corresponding to mesoporous materials;<sup>41,64</sup> this means, materials with pore size between 2 to 50 nm, as presented in **Table 1.1**. The pore size distribution observed for non and sulfonated Starbons® are quite similar, showing mesopores with pore diameters in the range of 30 nm. However, both materials,

parent and sulfonated Starbons<sup>®</sup> 300, presented very low surface area 16 and 32 m<sup>2</sup>g<sup>-1</sup>, respectively. These values are significant lower to the ones expected. This observation was attributed to the fact that starting materials (scale up carbonized materials) were left several weeks in sealed containers, this suggests that some of the volatiles, which were known to have recondensed in the mesopores, have slowly polymerised, blocking the pores.<sup>117</sup>

The pore size distribution (PSD) shows a slight increase in the pore volume in the materials after sulfonation, it seems that pores were opened during the process (**Figure 2.30b**). This observation differs to the one reported for the sulfonation of activated carbon by Liu *et al*, as they found a decrease in pore volume due to the sulfonic groups SO<sub>3</sub>H grafted into the material.<sup>38</sup> However, their material had much smaller pore diameters, making it potentially more prone to pore blocking.

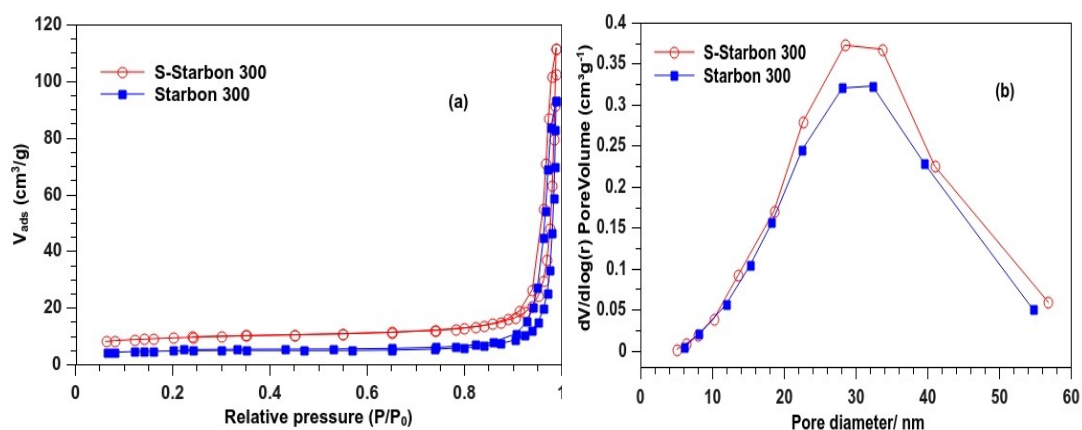


**Figure 2.30.** (a) Nitrogen adsorption isotherms and (b) pore size distribution for sulfonated and non-sulfonated Starbon<sup>®</sup> 300

As reported in previous works related to preparation of Starbons<sup>®</sup>, microporosity of materials increases as carbonization temperature increments<sup>9</sup>. This could be observed in the isotherm and pore size distribution of sulfonated Starbon<sup>®</sup> 550 shown in **Figure 2.31.**, there is a significant contribution of micropores to the surface area and their presence is noticeable in the PSD plot.

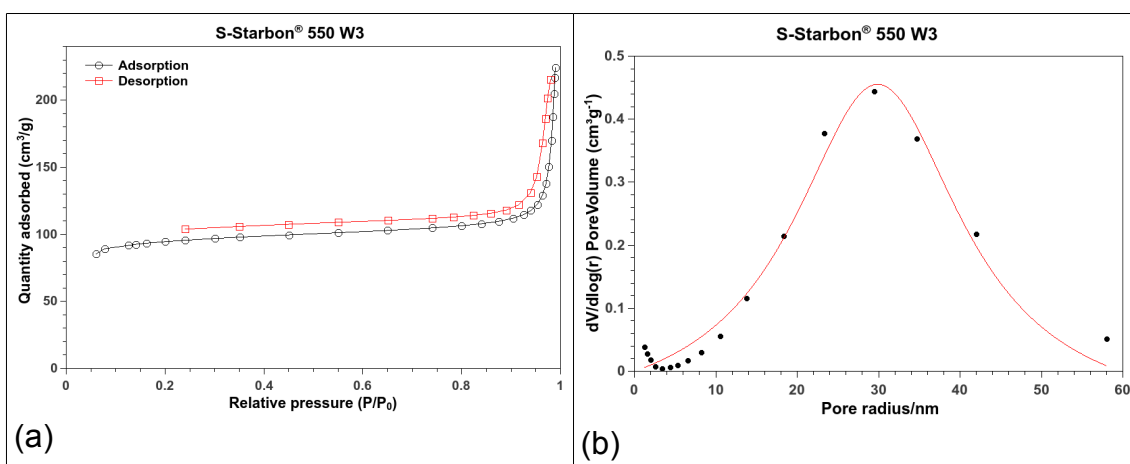


**Figure 2.31.** (a) Nitrogen adsorption isotherm and (b) pore size distribution for sulfonated Starbon® 550

**Table 2.12.** summarizes the surface areas, pore diameter and pore volume obtained for the range of prepared sulfonated Starbons®. As mentioned earlier, low surface area obtained in S-Starbon® 300 might be related to the problems found in the starting material (“pore blocking”). Thus, a general trend of increasing surface area with carbonization temperature is observed, just it has been observed in previous synthesis.

S-Starbon®	Surface area m <sup>2</sup> g <sup>-1</sup>	Pore volume cm <sup>3</sup> g <sup>-1</sup>	Pore diameter nm
300	32	0.16	30
350	285	0.13	26
450	308	0.20	30
550	324	0.20	28
600	379	0.15	28
700	344	0.20	29
800	97	0.20	29

However, sulfonated Starbon® 800 falls out of the trend. It is important to point out that starting material Starbon® 800, possesses a surface area of 387 m<sup>2</sup>g<sup>-1</sup>, then reduction of surface area is significant. **Figure 2.31.** displays the N<sub>2</sub> adsorption-desorption isotherm of parent (a) and sulfonated (c) Starbons® 800.

The isotherm shows a decrease in the total volume adsorbed for sulfonated material, suggesting a minor micropores contribution to surface area. This observation can be correlated with the PSD plot **Figure 2.32.**, in which micropores are hardly distinguished on sulfonated Starbon® 800 (d). Then, it seems the micropores present in the starting Starbon® 800 are blocked during sulfonation with sulfuric acid at 90 °C for 6 hours; but the mesopore volume does not change significantly.

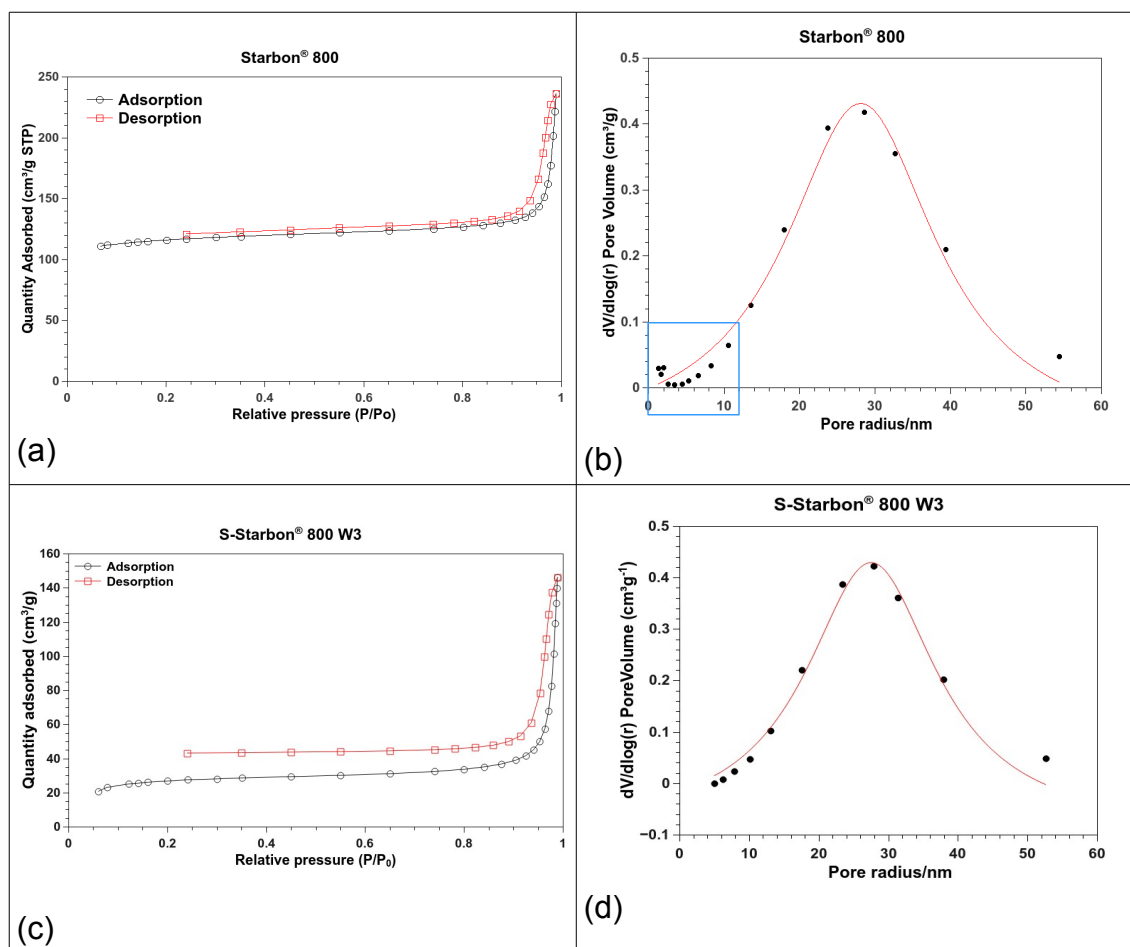


**Figure 2.32.** Nitrogen adsorption isotherm (a) and pore size distribution (b) for Starbon® 800; nitrogen adsorption isotherm (c) and pore size distribution (d) for sulfonated Starbon® 800 (c)

## 2.5. Conclusions

Synthesis of a range of sulfonated Starbons® was carried out following a new sulfonation approach. This methodology proposes the use of commercial sulfuric acid (95%) and a lower ratio of Starbon®–sulfuric acid (1 g: 7 mL). Sulfonation was performed in a range of carbonized Starbons® prepared from

the first scale-up Starbons<sup>®</sup> 300, 400 and 800 °C, synthesized at Green Chemistry Centre of Excellence, University of York.

Elemental analysis of the new carbonized Starbons<sup>®</sup> showed an increasing C:O ratio as temperature of carbonization increments suggesting the formation of aromatic polycyclic materials. This observation is further supported by FTIR, <sup>13</sup>C solid-state NMR and C1s XPS analysis.

Sulfonation of Starbons<sup>®</sup> promotes the appearance of an absorbance at ca.~1030cm<sup>-1</sup>, observed in the FTIR spectra of sulfonated Starbons. This band is identified as the symmetric S=O stretching related to sulfonic acids attached to samples. However, the band assigned to C–S bond is not observed neither in the IR spectra nor <sup>13</sup>C solid-state NMR spectra because of overlapping and broadening of the bands located at around 140 ppm. However, XPS analysis C1s for high-temperature Starbons 600, 700 and 800 shows a peak at ~285.6 eV attributed to this bond. It is interesting to notice, that other sulfonated Starbons like 300 or 350, do not show this peak; this could be due to the high concentration of the other oxygenated components compared with the carbon-sulfur groups.

Studies by elemental analysis showed that sulfur content is higher for low-temperature Starbons<sup>®</sup> (300 and 350 °C) than for higher temperature carbonized samples. This trend is also observed by the surface elemental composition done by XPS. Changes in C:O atomic ratio of Starbons<sup>®</sup> after were related to the inclusion of sulfonic acids to the structures and to the oxidation of the components present in the starting materials. Oxidation of functional groups is further confirmed by <sup>13</sup>C solid-state NMR and C1s XPS, which shows the appearance of more oxygenated functional groups as ketone, aldehydes, esters and carboxylic acids. The analysis of high-resolution S2p spectra showed that S(VI) assigned to sulfonic acids appears in all the sulfonated Starbons studied. However, for Starbons<sup>®</sup> carbonized at temperatures of 450 °C and onwards, the presence of reduced sulfur S(II) is identified.

Density of sulfonic acid groups, referred as “acidity” was determined using a NaCl ionic interchange solution; however, the values obtained are lower than the ones expected from the estimation of S(VI) determined by XPS. This observation, can be associated to the presence of other S(VI) species in the materials apart from sulfonic acids; however, it can be considered the fact of weak interaction between the NaCl solution with the materials because of sample's hydrophobicity.

Sulfonation of Starbons® do not seem to affect the mesoporosity of samples, but it possible affect the micropores present in samples, decreasing the surface area from starting material to the sulfonated one, as was observed for sulfonated Starbon® 800.

## **Chapter 3**

### ***Synthesis and characterisation of microwave sulfonated Starbons®***



### 3.1. Introduction

Microwave irradiation is a well-known method for heating and drying materials, the use of which has been widespread in recent years as a “green approach” in organic synthesis, because of its easy manipulation and instantaneous, rapid and specific heating.<sup>118–120</sup> Microwave-assisted sulfonation using sulfuric acid as sulfonating agent has already been tested with naphthalene and naphthol, results showed high conversions and selectivity under non-severe reaction conditions.<sup>57,121</sup> These observations motivated us to use microwave irradiation and commercial sulfuric acid as an alternative route for synthesis of sulfonated Starbons<sup>®</sup>. This chapter deals with the preparation and characterisation of the resulting microwave sulfonated Starbons<sup>®</sup>. The synthetic approach involves the use of three different starting materials Starbons<sup>®</sup> 300, 450 and 800, (same carbonized Starbons<sup>®</sup> used in conventional sulfonation) and exploring three temperatures (90, 120, 150 °C) taking advantage of the controlled microwave assistance. Sulfonation was carried out using the “open vessel” method in a microwave reactor CEM Discover.

In this new process (**Figure 3.1.**), there were some changes compared with the Starbons<sup>®</sup> sulfonation by conventional heating; among them, the suppression of methanol washes, trying to reduce the number of steps in the production of the solid acid catalyst; another change involves the use of microwave irradiation for the washes with hot water, which were carried out in shorter times (10 min) than conventional washes (20 min); sample was extensively washed until no sulfates were detected when tested with a BaCl<sub>2</sub> solution (0.1 M). Microwave sulfonated Starbons<sup>®</sup> were prepared using 2.0 g of material and 14 mL of sulfuric acid (95%); keeping the same ratio as for the materials prepared by conventional heating.

As mentioned in **Chapter 2**, sulfur dioxide (SO<sub>2</sub>) is released during sulfonation of Starbons<sup>®</sup>; which was also observed during microwave sulfonation. Then, a suitable set up was used during the preparation of microwave sulfonated Starbons<sup>®</sup> to collect the released SO<sub>2</sub> in a hydrogen peroxide solution H<sub>2</sub>O<sub>2</sub> (30

% v/v) forming sulfuric acid which can be quantified. However, the main findings from this approach are presented in **Chapter 4**.

Characterisation of these novel sulfonated Starbons<sup>®</sup> is presented throughout this chapter. The first section presents the characterisation by elemental analysis to determine the composition of materials. In the following section, X-ray photoelectron spectroscopy (XPS) is used to identify the chemical states of carbon and sulfur that constitute these microwave sulfonated Starbons<sup>®</sup>. The chemical environment for carbons found by XPS is further supported by <sup>13</sup>C solid-state NMR and FTIR. Subsequently, acidity quantification for microwave sulfonated Starbons<sup>®</sup> 300 is presented followed by morphology and surface studies. Finally, a small comparison between samples prepared conventionally and using microwaves at 90 °C is made to find out similarities and differences.

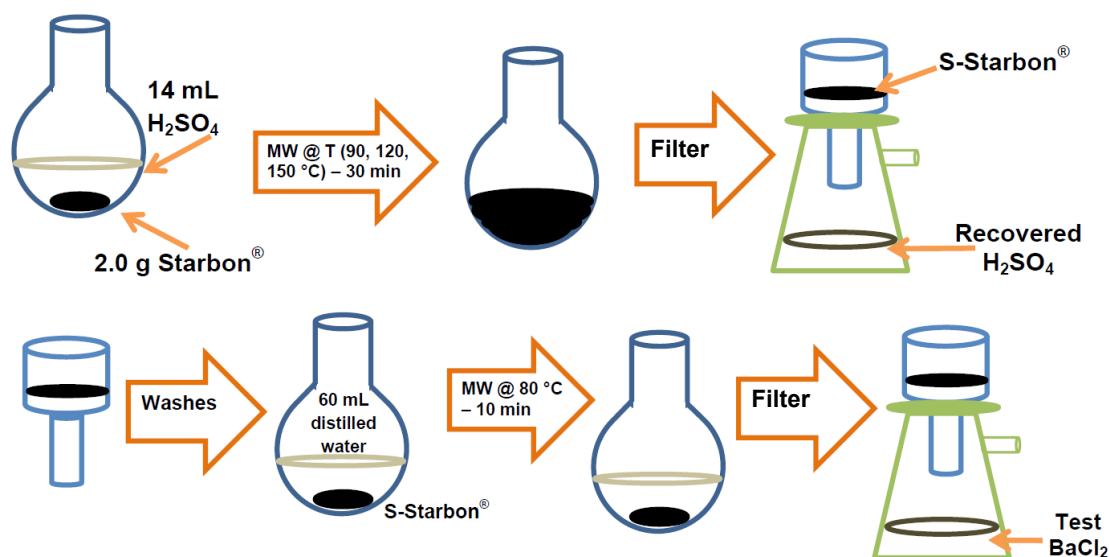


**Figure 3.1.** Scheme of microwave sulfonation of Starbons<sup>®</sup>

### 3.2. Bulk elemental composition

Determination of elemental composition of bulk materials was carried out. **Figure 3.2.** shows the C:O molar ratio and sulfur content (mmol/g) obtained for the three selected materials at different microwave sulfonation temperatures. A general trend was found, as temperature of sulfonation increases, C:O ratio

decreases for all materials, suggesting the formation of more oxygenated materials after treatment. This is more noticeable for Starbon<sup>®</sup> 800, the C:O ratio of which drops from 30 for original Starbon<sup>®</sup> 800 (**Figure 2.6**) to 10 for sulfonated sample at 90°C; being even lower for sample prepared at 150 °C, in which the C:O ratio is around 6 (**Figure 3.2.c**). Meanwhile for Starbon<sup>®</sup> 300, the changes in C:O ratio are less obvious as temperature of sulfonation increases (**Figure 3.2.a**); very similar ratios were found for sample prepared at 120 and 150 °C. For Starbon<sup>®</sup> 450, there is a continuous decrease as temperature of sulfonation gets higher, changing from 4.5 for sample prepared at 90°C to 3.0 for the one prepared at 150 °C (**Figure 3.2.b**).

Examination of sulfur content on samples shows that, in general, this increases with microwave sulfonation temperature. Starbon<sup>®</sup> 300 presents the highest sulfur contents among the materials, 450 and 800; it was determined up to 1.3 mmol/g for sample prepared at 150 °C (**Figure 3.2.a**). Although for samples prepared at 90 and 120 °C, there is not a significant difference (0.95 mmolg<sup>-1</sup>). This behaviour was also observed for Starbon<sup>®</sup> 450 samples prepared at 90 and 120 °C, as both of them present similar sulfur content (**Figure 3.2.b**). When sulfonation is carried out at 150 °C, the content reached over 0.64 mmolg<sup>-1</sup>. Starbon<sup>®</sup> 800 shows an increment in sulfur content as sulfonation temperature increases, changing from 0.48 mmolg<sup>-1</sup> for sample sulfonated at 90 °C to 0.88 mmolg<sup>-1</sup> for sample sulfonated at 150 °C (**Figure 3.2.c**). Sulfonation temperature seems to have a greater impact on the sulfur content in Starbons<sup>®</sup> 800, because high temperature promoted higher sulfur contents on these materials.

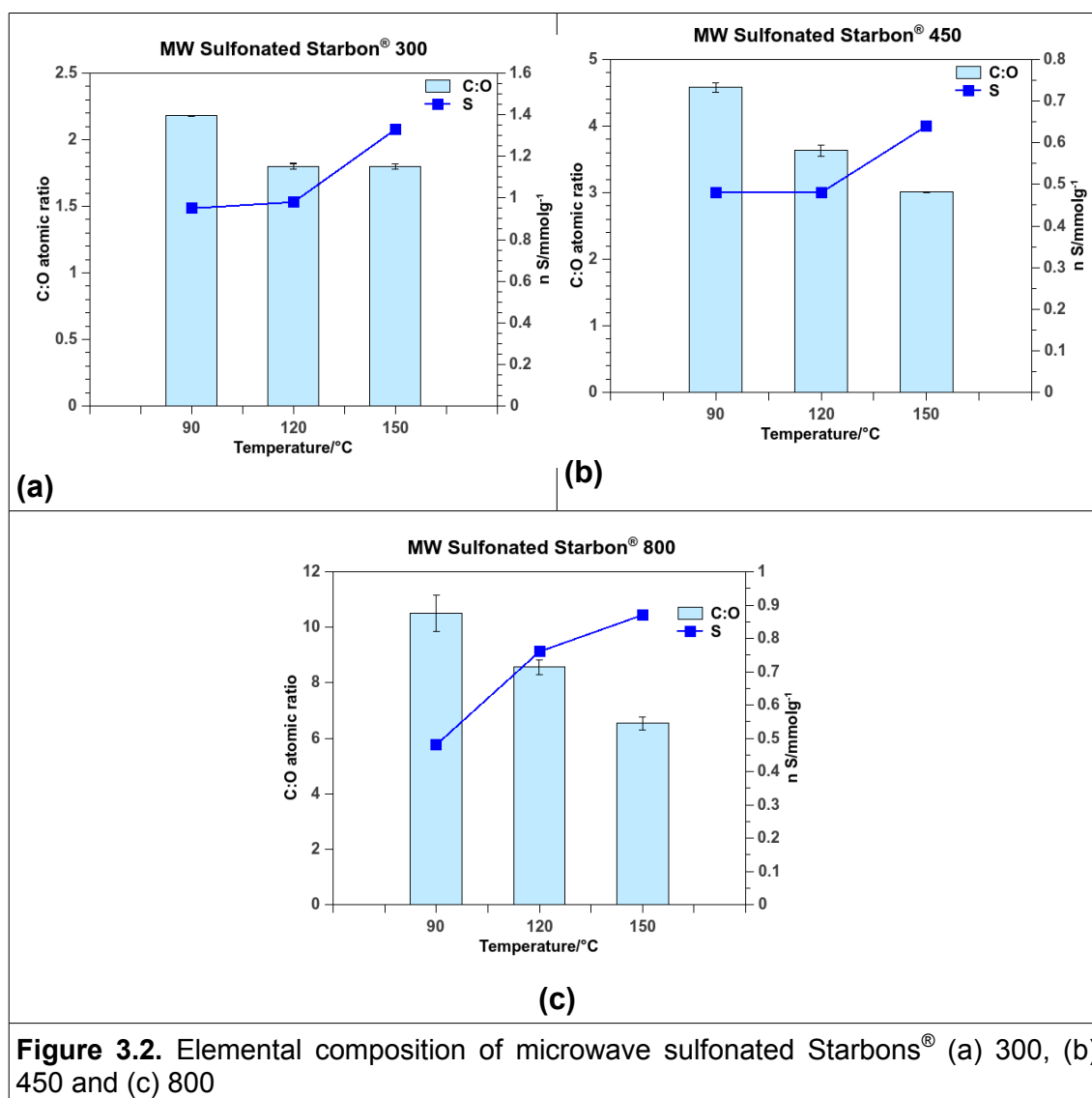


**Figure 3.2.** Elemental composition of microwave sulfonated Starbons® (a) 300, (b) 450 and (c) 800

The microwave sulfonated Starbons® prepared at 150°C were compared with other sulfonated carbons. With this aim a brief review on the methodology used for sulfonation of sugars<sup>27,28</sup> proposed by Hara *et al*, was done. The main findings are presented in **Table 3.1**. It is worth mentioning that Hara's approach used higher acid:solid ratio, of 10 mL acid for 1 g of solid; and longer reaction times, which is over 15 hours. The comparison of sulfur content between sulfonated sugars carbonized at 300°C and 600°C and sulfonated Starbons® 300 and 800, shows the former materials contain less sulfur than sulfonated Starbons® prepared using microwave irradiation. These results would suggest that microwave sulfonation would be a more effective method to carry out sulfonations at this temperature of 150°C and it could be achieved in shorter times.

<b>Table 3.1.</b> Sulfur content in sulfonated samples prepared at 150 °C			
	<b>Hara's methodology 150 °C – 15 h</b>		<b>MW sulfonation 150 °C – 30 min</b>
<b>Carbonization Temperature/°C</b>	<b>mmol S g<sup>-1</sup></b>	<b>Carbonization Temperature/°C</b>	<b>mmol S g<sup>-1</sup></b>
300	0.49	300	1.33
600	0.37	800	0.87

### 3.3. XPS analysis of microwave sulfonated Starbons®

#### 3.3.1. Elemental composition

Core-level X-ray photoelectron spectroscopy (XPS or ESCA) is an important technique for characterisation of carbonaceous materials, as it allows for the determination of chemical composition and nature of chemical bonds on surfaces and interfaces.<sup>122</sup> The elements C, S and O were observed in the full-scan XPS spectrum; this survey allowed the determination of elemental composition of microwave sulfonated Starbons® 300, 450 and 800 prepared at 90°C, 120 °C and 150 °C to find out main differences (**Figure 3.3**). This analysis helped to complement the information obtained previously by the elemental analysis of bulk samples. As expected, carbon composition is higher for Starbon® 800 at over 93 % (**Figure 3.3.a.**), meanwhile for Starbon® 300, it is around 76 %; although significant differences were not found among the sulfonation temperatures. However, oxygen content in samples changes dramatically as it drops from 20 % to 6 % from 300 to 800, respectively (**Figure 3.3.b.**). This trend was already mentioned in **section 2.4.6** and previously reported as increasing C:O ratio with increasing carbonization temperature.<sup>9,13</sup> Although, the oxygen content in samples seems to be affected by the temperature of sulfonation, these changes are not regular among them. The sulfur content determined by XPS was shown to be significantly higher for sulfonated Starbon® 300 than for sulfonated Starbons® 450 and 800 (**Figure 3.3.c.**); showing the highest percentage of sulfur (%S) in Starbon® 300 microwave sulfonated at 150 °C. In spite of the composition differences between Starbon® 450 and Starbon® 800, both materials present similar quantities of sulfur, with a concentration less than 1.5 % ( $\pm 0.1$  %).

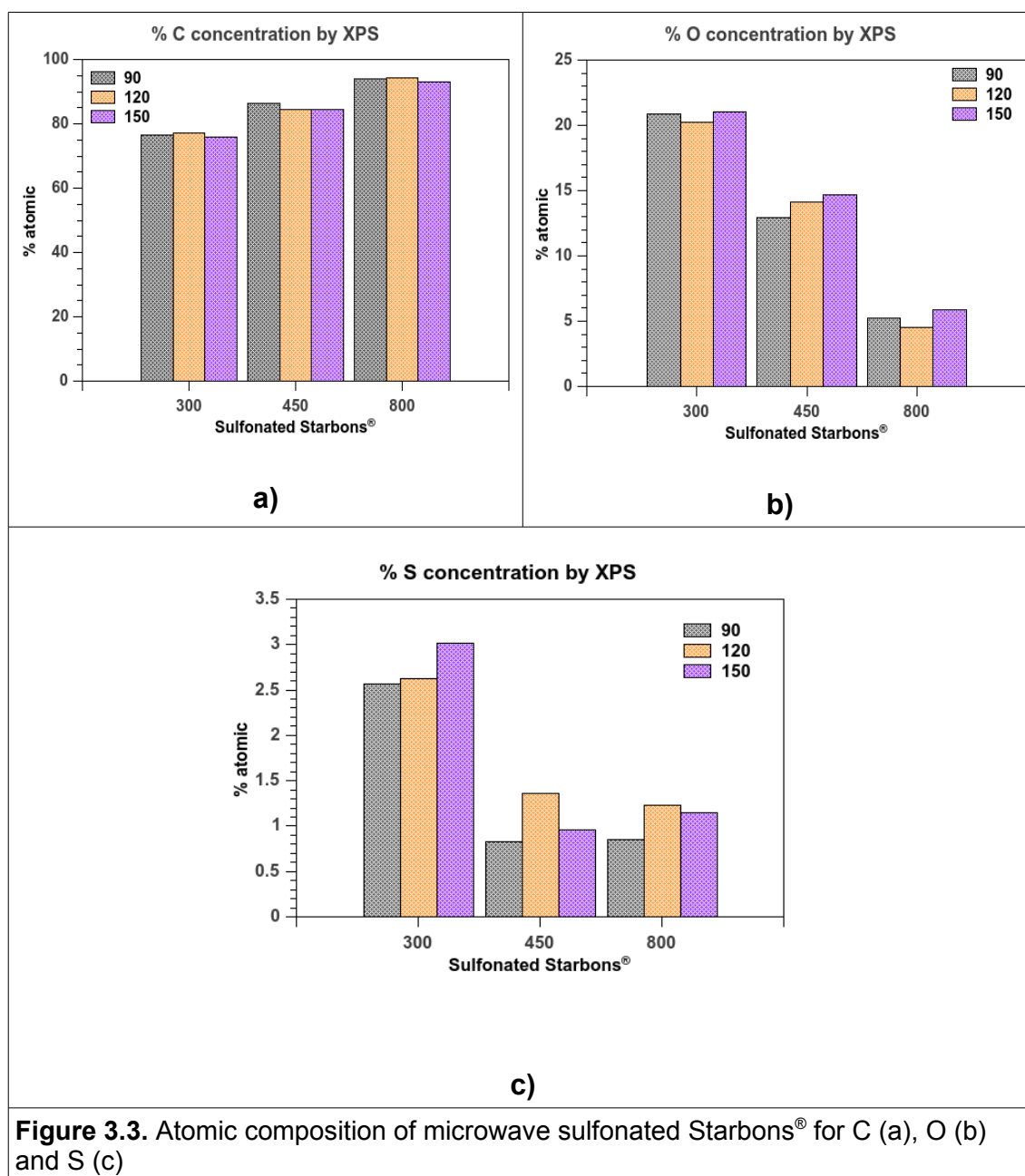


**Figure 3.3.** Atomic composition of microwave sulfonated Starbons® for C (a), O (b) and S (c)

### 3.3.2. Carbon analysis

#### 3.3.2.1. General overview

High-resolution C1s curve analysis was carried out for microwave sulfonated Starbons® similar to the approach presented previously for conventional sulfonated Starbons® in **Chapter 2**. This analysis was done using CasaXPS software package. **Figure 3.4**, presents the high-resolution C1s spectra obtained for Starbon® 300 microwave sulfonated at 90°C (a), 120°C (b) and 150°C (c). As can be seen, the shape of each C1s curve is quite different

among the samples; the different carbon functionalities could be identified through a peak fitting analysis. The assignment of the carbon bonds found in microwave sulfonated Starbons<sup>®</sup> are based on the ones reported in **Table 2.8**.

Five components can be identified in all sulfonated Starbon<sup>®</sup> 300 samples. The concentration of each component varies with temperature of sulfonation. These five components identified are the  $sp^2$ -hybridized C=C centred at ca. 284.5 eV;<sup>102,103</sup> a carbon oxygen (C–O) bond at 286.2–286.4 eV; double bond to oxygen (C=O, O–C–O) at 287.6–287.8 eV, the bond O–C=O appearing at 289.3–289.6 eV and the long tailing with a maximum at 291.2 eV, is attributed to  $\pi-\pi^*$  “shake up”.<sup>107,123</sup> The relative concentration of each component was calculated considering their peak areas ratio; the findings are presented in **Table 3.2**.

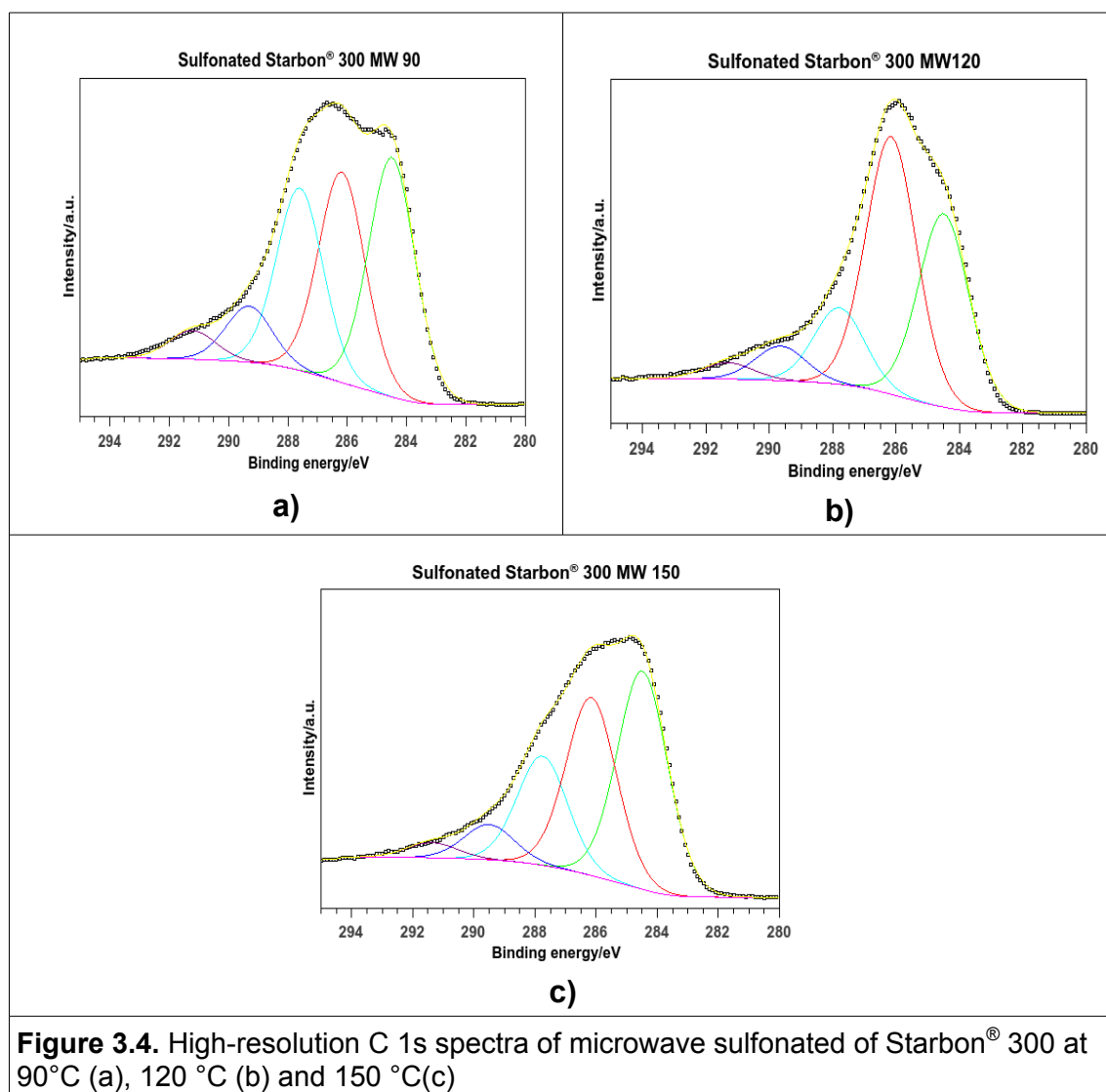


**Figure 3.4.** High-resolution C 1s spectra of microwave sulfonated of Starbon<sup>®</sup> 300 at 90 °C (a), 120 °C (b) and 150 °C (c)

The carbon components present in microwave sulfonated Starbons<sup>®</sup> 450 prepared at 90 °C, 120 °C and 150 °C were determined following a similar analysis to previous sample. Thus, deconvolution of the high-resolution C1s spectra was done and presented in **Figure 3.5**. The shape of every C1s envelope for each sample looks very different among them; changing from a narrow band of Starbon<sup>®</sup> 450 sulfonated at 90 °C to a broad band for sample sulfonated at 150 °C. Starbon<sup>®</sup> 450 microwave sulfonated at 90 °C presents a particular shape after deconvolution of the curve, because the maximum is centred at 285.6 eV, and presents a small band at 284.5 eV, this one has been assigned to sp<sup>2</sup> C=C bond.<sup>102,103</sup> Meanwhile for Starbons<sup>®</sup> 450 microwave sulfonated at 120 °C and 150 °C, the band attributed to C=C is more prominent than the peak observed at 285.6 eV, differing from the observation in sample prepared at 90 °C. This peak observed at 285.6 eV was also observed in conventional sulfonated Starbons<sup>®</sup> 600, 700 and 800; as discussed in **Chapter 2**, this peak could be attributed to aliphatic carbons with sp<sup>3</sup> hybridization C–C<sup>102,107</sup> or to C–S bonds, observed in sulfonated graphene;<sup>109</sup> although some other authors have reported that the appearance of C–S bond from sulfonic acids attached to carbons, appears at higher binding energies, at 288.7-288.8 eV,<sup>90,124</sup> however this latter value differs from the “expected range” for C–S bonds published by Briggs in the XPS and Auger Database and the Polymer Database.<sup>106</sup>

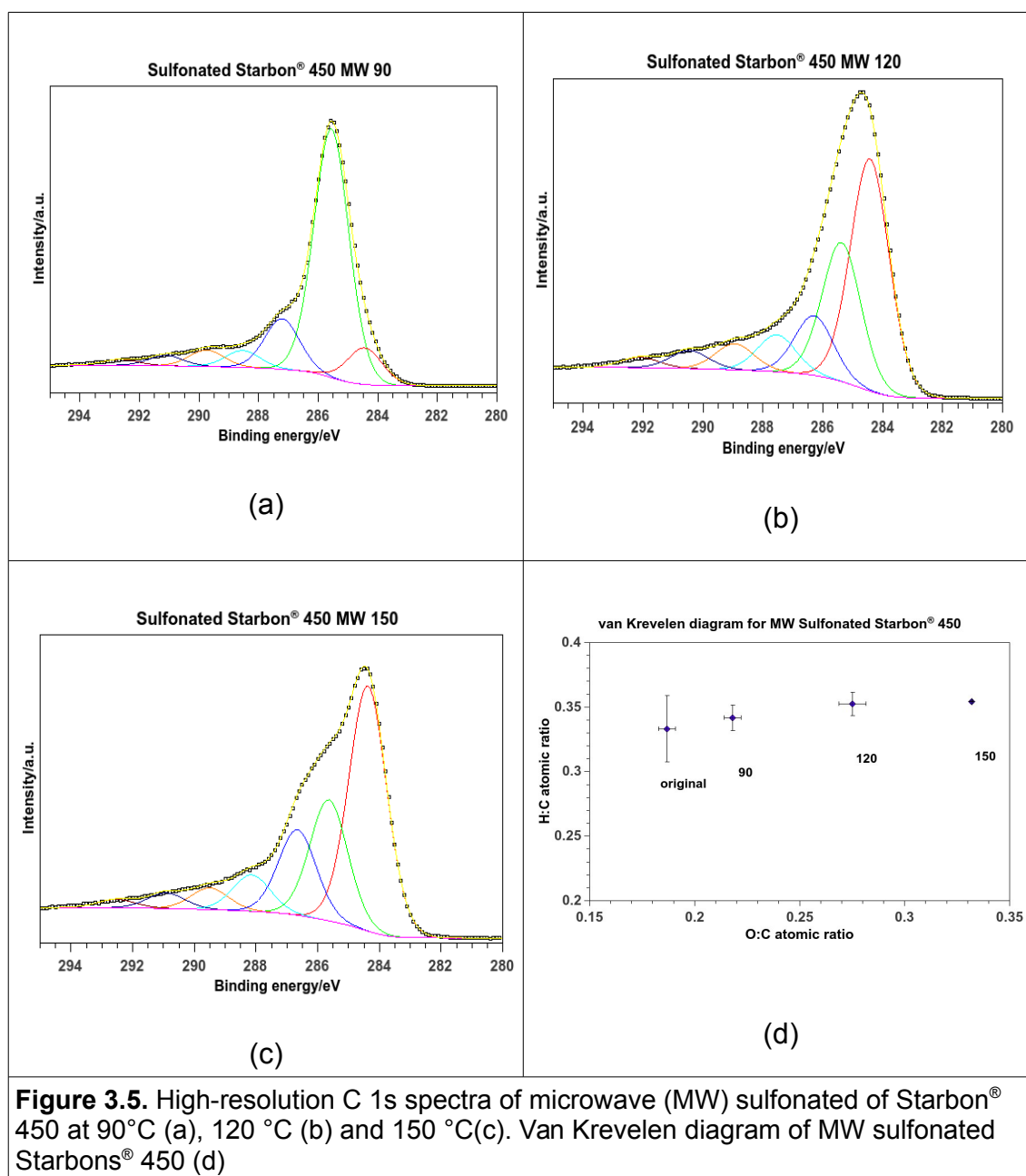
The high concentration of the carbon species observed at 285.6 eV in MW sulfonated Starbon<sup>®</sup> 450 at 90 °C, makes it difficult to “accept” that most of the carbon present in the material is solely related to C–S bonds, as the quantity of sulfur determined is less than 1%, which makes it unlikely that 64% of the carbon can be attributed to the C–S bonds. Thus, another approximation was used to find the nature of the carbon at that binding energy 285.6 eV. During the search, it was found that some authors have also referred to this signal as a β-carbon, C–COOR found in different XPS studies on other carbon derivatives.<sup>92,108</sup> Other researchers have assigned this signal to “amorphous carbon”, implying the breaking of a rigid structure to give sp<sup>3</sup> carbon bonds,<sup>125</sup> which was suggested to have arisen due to the strong oxidation of sulfuric acid;<sup>90</sup> this observation at 285.6 eV is similar to the above related to

aliphatic carbons with  $sp^3$  hybridization.

Analysis carried to determine if this peak was due to  $\beta$ -carbons, shows that all three microwave sulfonated Starbons<sup>®</sup> 450 samples have similar concentration of carboxylates, and therefore it is unlikely that the peak is due to  $\beta$ -carbons. The reasonable assignment for this high-intensity band in sulfonated Starbons<sup>®</sup> 450 prepared at 90 °C would be related to  $sp^3$  C–C bonds. Unfortunately, as will be seen in the <sup>13</sup>C solid-state NMR section, the spectra obtained for Starbon<sup>®</sup>450 microwave sulfonated at 90 °C has poor quality and it does not provide enough information to confirm the massive increase in aliphatic carbons.

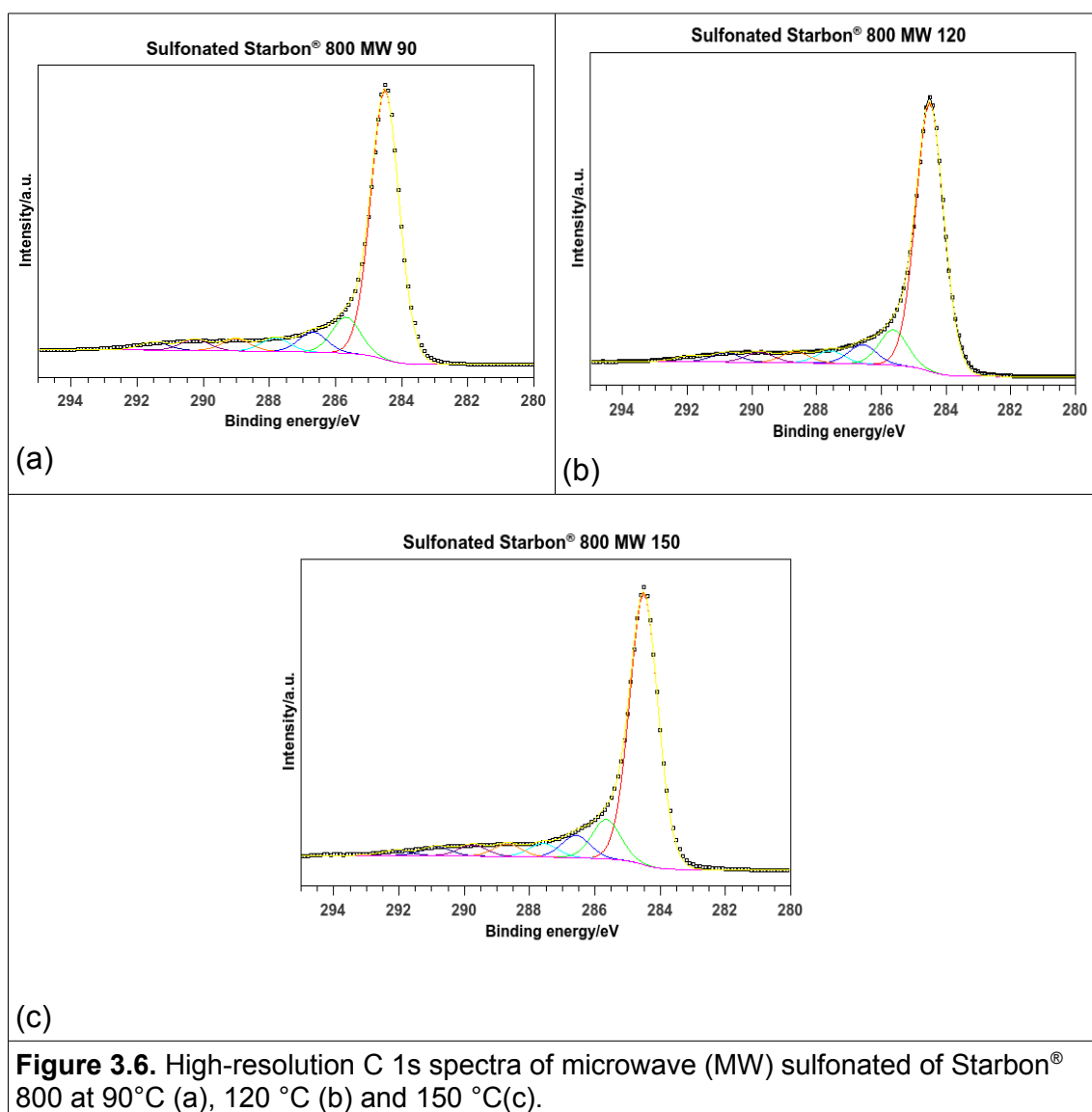
An analysis of the bulk elemental composition (**Figure 3.5d**) shows that Starbon<sup>®</sup> 450 sulfonated at 90°C presents the lowest O/C ratio, which could explain the low quantity of oxygenated moieties observed on the surface of the sample, although when the H/C ratio is examined, the ratio is very similar among the three samples, approximately 35 H atoms per 100 of C atoms.

Continuing with the analysis of the components observed in microwave sulfonated Starbon<sup>®</sup> 450 at 90, 120 and 150 °C, the peak fitting also distinguished bands centred in the ranges 286.2–287.2, 287.6–288.4 and 289.0–289.6 eV which have been assigned to single C–O bond ethers or hydroxyl groups, double oxygen bond O–C–O, carbonyl or quinone groups (C=O) and carboxylic groups, esters or lactones (-COOR) respectively.<sup>102,103,107,126</sup> At higher binding energies, there were two bands identified, one ca. 290.5–290.8 eV and another ca. 291.4–292.0 eV; some authors refer to the first signal as carbonates (O–COO–), found in oxidation of carbon nanotubes<sup>107,125</sup> or acid treated carbon-fibres<sup>102</sup> and the last one assigned to  $\pi$ – $\pi^*$  transitions in aromatic rings.<sup>103,125,127</sup>



The deconvolution of high-resolution C1s spectra for microwave sulfonated Starbon® 800 are presented in **Figure 3.6**. There are not significant differences among the three spectra, as they presented a maximum band at ca. 284.5 eV corresponding to C=C bonds; in all spectra, a signal at 285.6 eV is observed, similar to microwave sulfonated Starbons® 450; which could be assigned to  $sp^3$  C–C bonds.<sup>102,107</sup> However, the oxygenated carbon moieties appeared in lower concentration than for Starbons® 450, which could also be related with the lower oxygen atomic percentage present in the sample, determined in the XPS survey. These findings would suggest that sulfonation at different temperatures

did not promote drastic changes on these materials.



### 3.3.2.2. Quantification of components

When analysing the concentration of the components (**Table 3.2**) of microwave sulfonated Starbon® 300 at different temperatures, it is found that sample sulfonated at 150 °C presents the highest concentration of C=C bonds, close to 40 %. The concentration obtained for the signal corresponding to carbon single bound to oxygen are similar among them, being just slightly higher for 120 and 150 than for sample prepared at 90 °C. The concentration found for carbon double bound to oxygen decreases from 25 % to 20 % from samples prepared

at 90 °C and 150 °C, respectively. Meanwhile, the signal assigned to ester type compounds varies without a noticeable trend, being higher for microwave sulfonated sample at 120 °C. In these samples, the carbonate O-COO- component was not observed.

As mentioned previously, Starbon® 450 microwave sulfonated at 90 °C presents a maximum ca. 285.6 eV, then compositional analysis for this sample differs considerably from other two samples prepared at 120 and 150 °C. This signal at 285.6 eV represents 64 % of total carbon moieties found on surface of Starbon 450 sulfonated at 90 °C, meanwhile both Starbons® 450 prepared at 120 and 150 °C have higher concentration of C=C bonds (over 40 %) and over 20 % of the band ca. 285.6 eV. The concentration of oxygenated moieties for single and double carbon-bond oxygen, seems to be slightly higher for sulfonated sample at 150. The remaining components are very similar among them.

The analysis of the concentration of moieties observed in Starbons® 800 microwave sulfonated at 90, 120 and 150 °C, presents a maximum of sp<sup>2</sup> C=C bonds over 70%, this concentration is higher for Starbon® 800 than for Starbons® 300 and 450 with respect to the other components, these did not differ greatly within the three distinct temperatures of sulfonation, suggesting that modification of 800 would need more effort.

**Table 3.2.** Relative concentrations (%) of carbon functionalities in microwave sulfonated Starbons®

	C = C	C – C	C – O	C=O, O-C-O	-COO	O-COO	$\pi-\pi^*$
<b>300-MW90</b>	33.4		29.4	25.4	7.8		4
<b>300-MW120</b>	28.7		32.8	21.6	9.6		7.3
<b>300-MW150</b>	39.3		32	19.6	6.3		2.7
<b>450-MW90</b>	9.7	64	12.9	4.1	4.1	2.6	2.5
<b>450-MW120</b>	42.5	26.7	12.5	6.8	4.8	3.3	3.1
<b>450-MW150</b>	46	22.7	16	7	4.1	2.9	1.6
<b>800-MW90</b>	72	9.6	5.3	3	2.7	2.4	1.5
<b>800-MW120</b>	72.2	9.5	5.2	3	2.7	2.5	1.6
<b>800-MW150</b>	70.7	10.2	3.5	3.2	2.9	2.4	1.4

### 3.3.3. High-resolution sulfur S2p spectra

Further analysis on the chemical bonding formed in Starbons® after microwave sulfonation was carried out. High-resolution XPS measurements on sulfur were performed; a strong S2p signal was detected for microwave sulfonated samples 300, 450 and 800 at the three temperatures 90°C, 120°C and 150°C. The spectrum of each sample was fitted by two components, considering that each component has a S2p<sub>3/2</sub> and S2p<sub>1/2</sub> doublet with a fixed intensity ratio of 2:1 and an energy of separation of 1.2 eV. The fitted spectra for samples sulfonated at 90°C are shown in **Figure 3.7**. It can be seen that sulfonated Starbons® 450 and 800 present a component at low binding energies, in which S2p<sub>3/2</sub>A is centred at 163.5 eV, which could be assigned to R–S thiophenic species, i.e. C–S bonds.<sup>109,114,128</sup> Whilst, microwave sulfonated Starbon® 300 did not present this component, instead it presented a very broad band which was fitted into two oxidized components, one with S 2p<sub>3/2</sub>A at 167.5 eV and another band S 2p<sub>3/2</sub>B appearing at 169.8 eV. The first peak is attributed to sulfonic acid<sup>112,114</sup> although some authors refer the appearance of this band at higher binding energies at 168–168.7 eV.<sup>37,90,129,130</sup> Although, the component appearing at 169.8 eV is very

tentatively assigned to sulfates, the data reported for sulfur in sulfates do not exceed 169 eV.<sup>112</sup> This peak has been assigned to “persulfates” (C-O-O-SO<sub>3</sub>) as in the work by Siow *et al*<sup>131</sup> on sulfonated surfaces of polymers prepared with SO<sub>2</sub> by plasma treatments. However, due to the differences between our method of synthesis and the plasma approach that assignment was discarded. Bands at higher binding energies, over 169 eV, have been also reported in sulfur compounds of this type ROSO<sub>2</sub>OR,<sup>112</sup> identified as organo sulfate esters. These compounds would be more reasonable to be attributed to our materials. It is worth mentioning that appearance of this component at higher binding energy was not observed during the conventional sulfonation of Starbon® 300, suggesting that microwave sulfonation promotes the formation of this sulfur species.

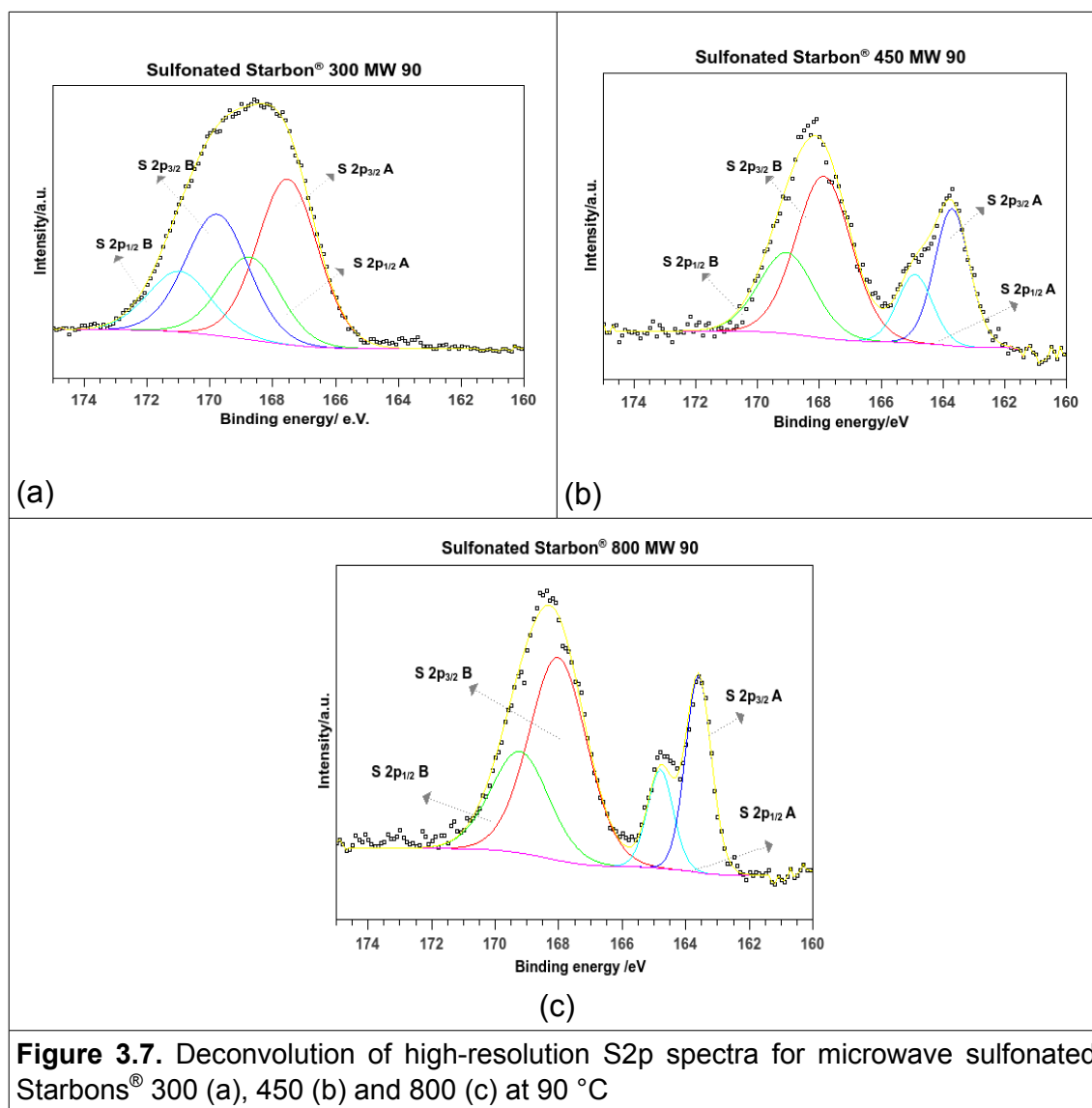


**Figure 3.7.** Deconvolution of high-resolution S<sub>2p</sub> spectra for microwave sulfonated Starbons® 300 (a), 450 (b) and 800 (c) at 90 °C

**Figure 3.8** presents the high resolution S2p spectra of the microwave sulfonated Starbons<sup>®</sup> 300, 450 and 800 at different temperatures. It can be seen that spectra are very similar among them; for Starbon<sup>®</sup> 300, the two oxidized components are observed in all the temperatures. For Starbons<sup>®</sup> 450 and 800, spectra are also similar, presenting the reduced and oxidized components along the treatment temperatures. A quantification of the concentration of each component was carried out in every sample through the fitting analysis as presented in **Figure 3.7**. A summary of these findings is presented in **Table 3.3**. For the microwave sulfonated Starbon<sup>®</sup> 300, the concentration of the component appearing at 169.8 eV, is higher for the sample sulfonated at 150 °C, being slightly higher than 50 %. In Starbon<sup>®</sup> 450, the oxidized component at 167.5 eV is found in less quantity for the treatment at 90°C, meanwhile treatments at 120 and 150 °C present similar quantities, approximately 80 %. For the spectra of Starbon<sup>®</sup> 800, similar concentrations are found in the component at 167.5 eV, around 70 %, being slightly lower for sample treated at 90°C. It is interesting to notice that Starbon<sup>®</sup> 800 presented higher concentration of reduced component, than Starbon<sup>®</sup> 450, which did not vary noticeable among the different treatment temperatures.

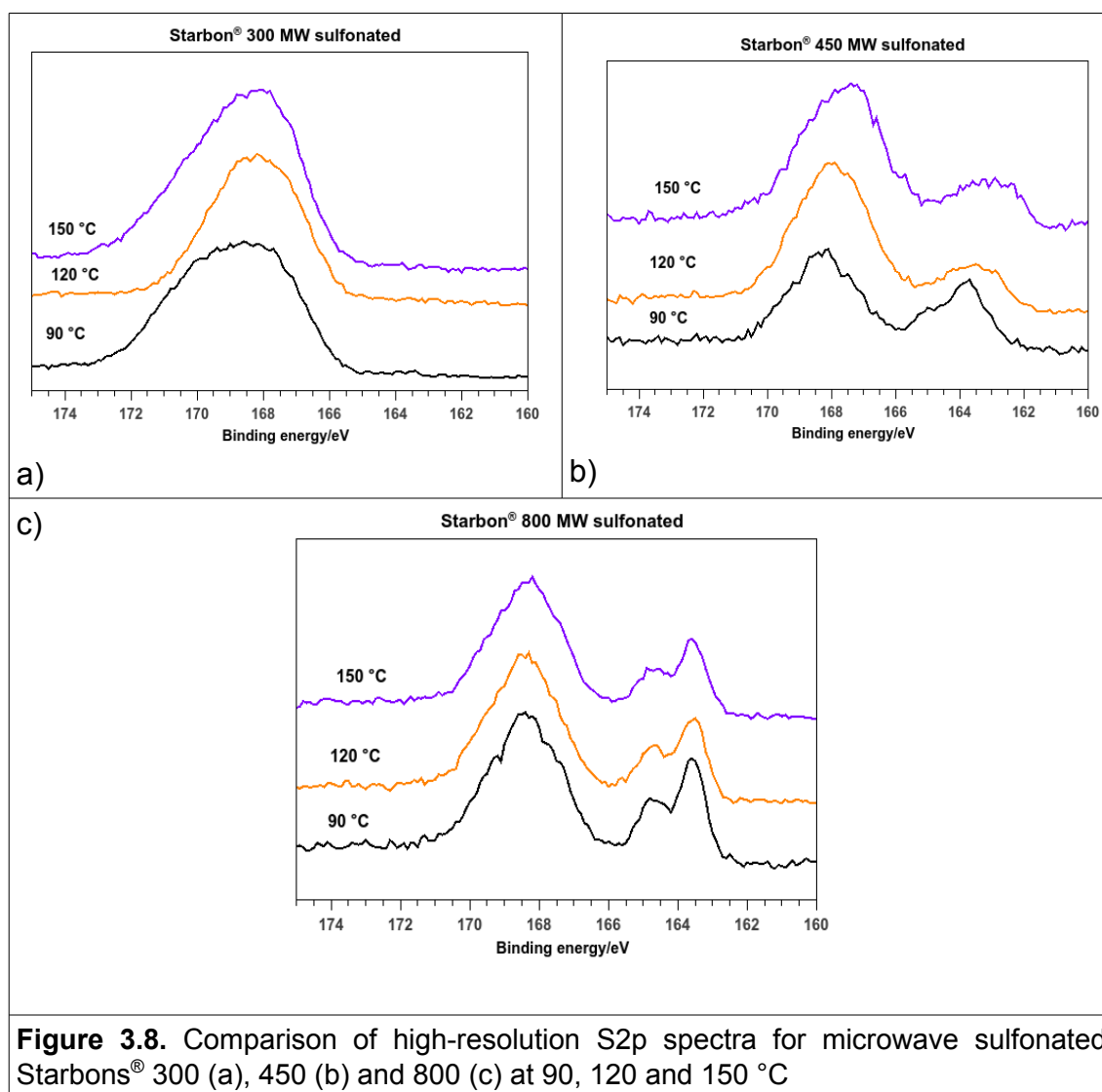


**Table 3.3.** Relative concentrations (%) of sulfur functionalities in microwave sulfonated Starbons® 300, 450 and 800

	<b>-SO<sub>3</sub>H</b> (167.5 eV)	<b>ROSO<sub>2</sub>OR</b> (169.8 eV)		<b>R-S-R</b> (163.5 eV)	<b>-SO<sub>3</sub>H</b> (167.5 eV)	
<b>300-MW90</b>	56.7	43.3		<b>450-MW90</b>	65.2	34.8
<b>300-MW120</b>	64.4	35.6		<b>450-MW120</b>	81.9	18.1
<b>300-MW150</b>	49.7	50.3		<b>450-MW150</b>	79.9	20.1
				<b>800-MW90</b>	69.8	30.2
				<b>800-MW120</b>	72.4	27.6
				<b>800-MW150</b>	72.9	26.1

### 3.4. Structural changes studied by $^{13}\text{C}$ solid-state NMR spectroscopy

XPS analysis has given a remarkable framework in the characterisation of microwave sulfonated Starbons<sup>®</sup> because of the useful information provided about composition of the materials. These studies could be complemented with  $^{13}\text{C}$  solid-state CP/MAS NMR spectroscopy, as this gives a powerful approach to molecular analysis of carbonaceous materials.<sup>132</sup> It is worth mentioning that sulfonated Starbon<sup>®</sup> 800 was not able to be analysed, because of its highly conductive characteristics.

An overview of the functionalities found in Starbon<sup>®</sup> 300 before sulfonation is presented in **Figure 3.9**. Some of these chemical groups have been already mentioned in the previous chapter. In the downfield region, mainly aliphatic groups are found; terminal methyl groups ca. 15 ppm and a noticeable resonance at 20 ppm assigned to the carbon of a methyl group attached to aromatic carbon.<sup>95</sup> A broad band arises from 30 to 50 ppm, which could be attributed to methylene or methine linkages.<sup>91</sup> A broad band with distinguishable peaks appears above 108 ppm; in this region, carbons belonging to furan moieties could be identified at 108 ppm and 138 ppm.<sup>91</sup> In the middle of this region, a sharp peak arises, which is assigned to aromatic components in the materials, specifically referred to as polycondensed aromatic rings.<sup>91–93,133,134</sup> A perceptible resonance is observed at 153 ppm, which has been attributed to carbon in phenolic functionalities.<sup>28,91–93</sup> Resonances at 175 ppm and 200 were assigned to carboxyl groups and ketone-aldehydes groups, respectively.<sup>93</sup>

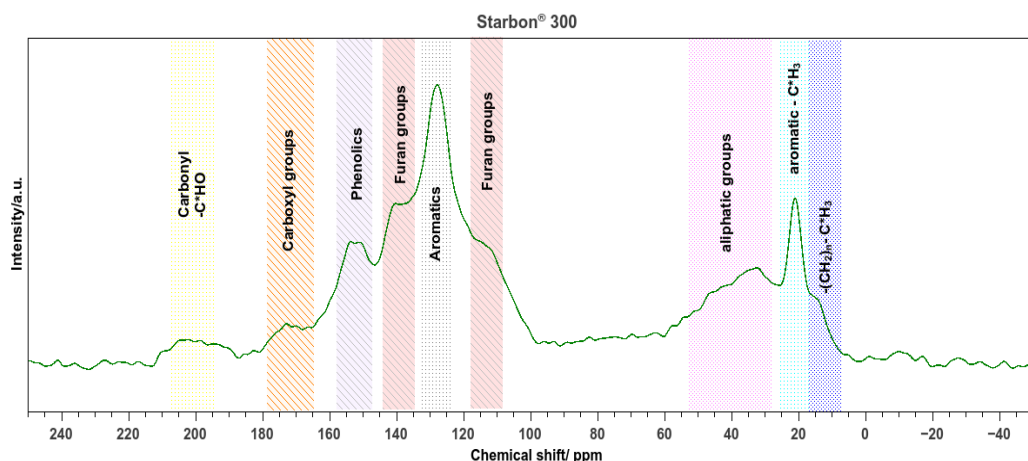


**Figure 3.9.** Identification of functional groups in  $^{13}\text{C}$  solid-state CP/MAS NMR spectra for Starbon<sup>®</sup> 300 before sulfonation

After sulfonation of Starbon<sup>®</sup> 300, the most remarkable change is the broadening of the NMR spectra, especially the band centered at 128 ppm. The identification of the resonances present in the sample was carried out through the deconvolution of the spectra using a Lorentzian multippeak fitting (**Figure 3.10**). Curves arisen during the fitting process were analysed and assigned to reasonable carbon functionalities. The analysis was more qualitative than quantitative, there is no attempt to determine the concentration of each resonance. It is interesting to notice in **Figure 3.10**, the contribution of different components to the width of spectra.

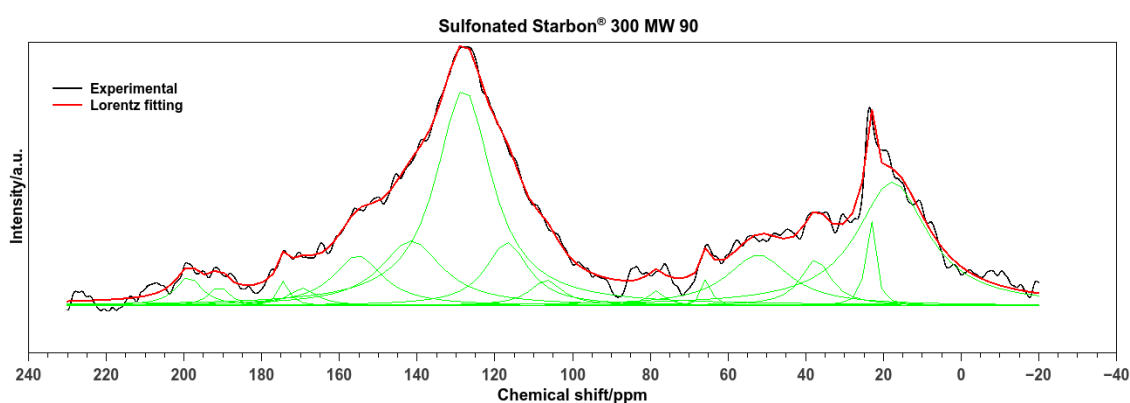


**Figure 3.10.** Curve-fitting of  $^{13}\text{C}$  solid-state CP/MAS NMR spectrum of Starbon<sup>®</sup> 300 microwave sulfonated at 90°C

After the identification of contribution of each component through curve fitting, a shading of the spectra was carried out to make recognition of the functionalities present in each sample easier (**Figure 3.11**). The analysis of the spectra in the upfield region, allows the identification of terminal methyl groups ca. 15 ppm; it is worth mentioning that resonances appearing at 24 ppm and 65 ppm have been identified as 2-propanol residues used for cleaning and maintenance of NMR equipment.

As found in Starbon<sup>®</sup> 300 original, the spectrum presents a broad band observed in the range 35–60 ppm, which is attributed to methylene groups. In the broad band ca. 128 ppm could be identified several components, this main peak at 128 ppm assigned to aromatic groups; the band at 108 ppm and 140 ppm could be attributed to furan rings, however at 140 ppm is also expected to see the bond between aromatic carbon and sulphur;<sup>28</sup> then this resonance could represent both moieties. Samples sulfonated at these different temperatures, present resonances at 155 ppm and 165 ppm. The first one is attributed to carbon in phenolic groups, which were also found in original Starbon<sup>®</sup> 300. The resonance at 165 ppm is assigned to ester groups, which could be promoted by the oxidation with sulfuric acid, as was observed in a similar treatment of starch with HNO<sub>3</sub><sup>93</sup> and previously in the sulfonation of Starbons<sup>®</sup> by conventional heating; the formation of more oxygenated functionalities is reflected with the increasing in oxygen, as shown by elemental composition. It is interesting to notice along the different sulfonation temperatures of Starbon<sup>®</sup> 300, the continuity of the aldehyde (190 ppm) and ketone (203 ppm) resonances,<sup>93</sup> suggesting that microwave treatment did not affect these functional groups during sulfonation.

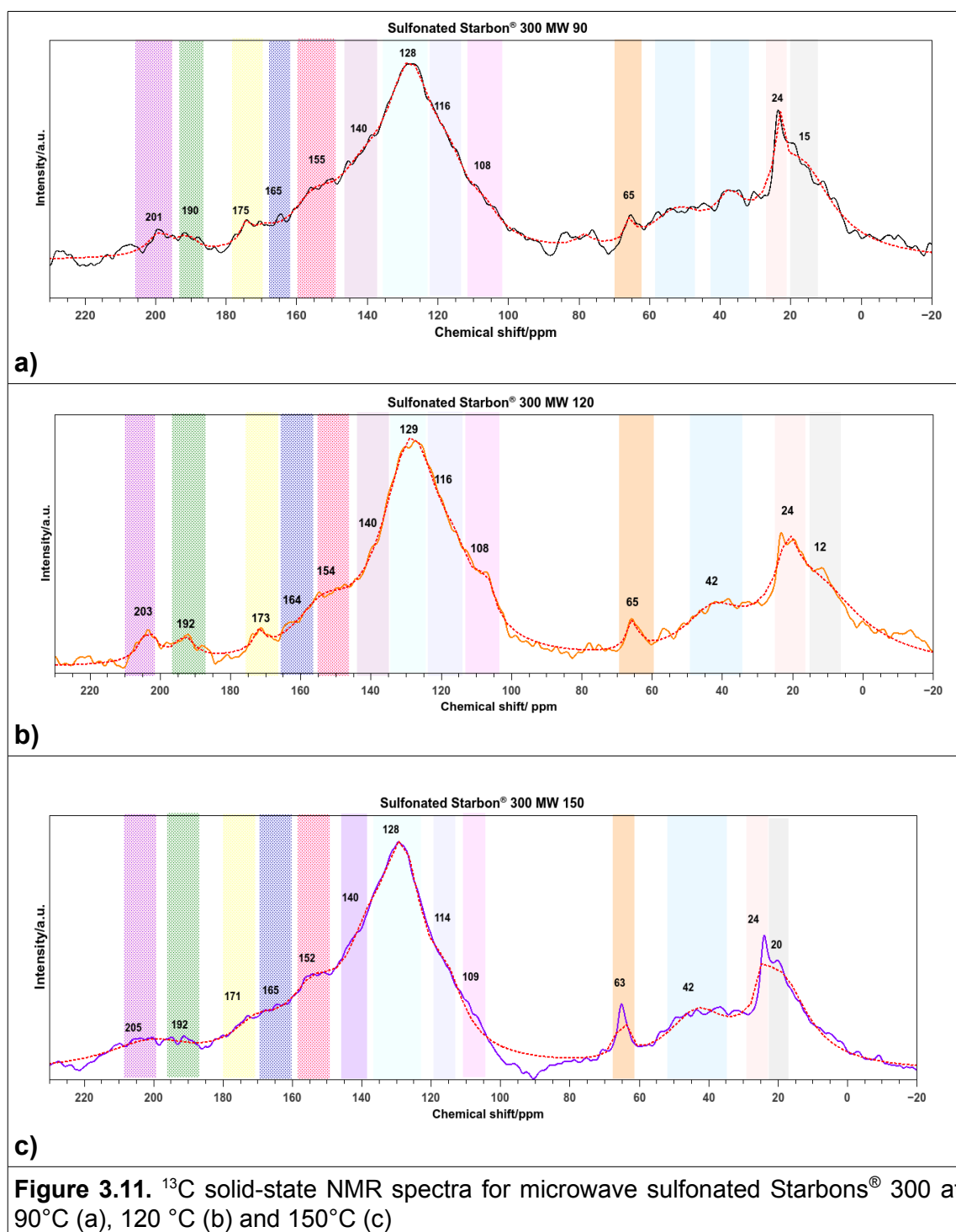


**Figure 3.11.**  $^{13}\text{C}$  solid-state NMR spectra for microwave sulfonated Starbons® 300 at 90°C (a), 120 °C (b) and 150°C (c)

The  $^{13}\text{C}$  solid-state NMR spectra for parent Starbon® 450 and microwave sulfonated Starbons® 450 are presented in **Figure 3.12**. Unfortunately some spectra are noisy and was harder in some cases to confirm the existence of resonances. The identification of main components on materials was achieved through a reasonable curve-fitting. As found previously, resonances at 24 and

65 ppm belong to 2-propanol contaminant. Spectra pre and post-sulfonation are very similar, they show a noticeable resonance at ~128 ppm, corresponding to aromatic carbons in polycondensed systems. The bands visible at 108 and 140 ppm could be attributed to furan rings present in Starbons® 450; although, the latter could also be due to aromatic carbon-sulfur bond in sulfonated Starbons®.

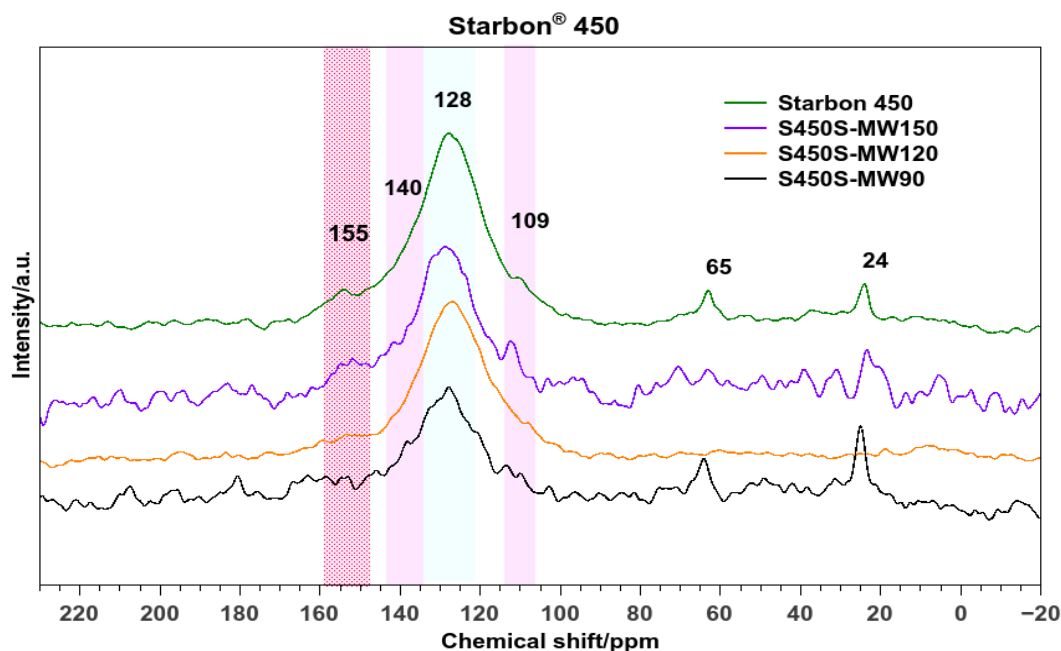


**Figure 3.12.**  $^{13}\text{C}$  Solid-state NMR spectra for microwave sulfonated Starbons® 450

### 3.5. FTIR characterisation

Infrared spectroscopy was applied in further evaluation of the chemical structure of the microwave sulfonated Starbons®. **Figure 3.13** shows the FTIR spectra for microwave sulfonated Starbons® 300 at 90, 120 and 150 °C, which present similarities with the conventional sulfonated Starbons® 300 displayed in **Chapter 2**. In all spectra, two main bands are distinguished at 1715  $\text{cm}^{-1}$  and 1600  $\text{cm}^{-1}$  which were assigned to C=O and C=C stretchings, respectively,<sup>34,37,80,90,129</sup> observation that agrees with the presence of carboxyl groups and saturated-aromatic carbons found through XPS and  $^{13}\text{C}$  solid-state NMR analysis. Looking at this region, a particularity is observed in Starbon® 300 microwave sulfonated at 150°C, as it shows a small shoulder at 1770  $\text{cm}^{-1}$ , this

vibration could be assigned to formation of lactones<sup>135</sup> during the process of sulfonation at higher temperatures, as samples prepared at 90°C and 120°C do not show this particular band. Moving to lower wavenumbers, a broad band is observed in the region 1350–1100 cm<sup>-1</sup>, in which two maxima could be distinguished: one ca. 1225 cm<sup>-1</sup> and another ca. 1160 cm<sup>-1</sup>, the first one is assigned to vibration of ether bridges C–O–C,<sup>34,129</sup> while the second band could be attributed to C–O stretching of alcohol groups.<sup>90,136</sup> The presence of sulfonic groups –SO<sub>3</sub>H can be identified by stretching vibrations at 1392 cm<sup>-1</sup> and 1183 cm<sup>-1</sup> (–SO<sub>2</sub>– asymmetric and symmetric, respectively), however when absorptive water combines with the sulfonic group, the asymmetric and symmetric modes shift to lower wavenumbers, 1150 and 1030 cm<sup>-1</sup>.<sup>46,90,137</sup> In this respect, the asymmetric vibration of sulfonic groups overlaps in the band observed at 1160 cm<sup>-1</sup>, described earlier; whereas, the symmetric mode is quite noticeable in all microwave sulfonated Starbons® 300; as in conventional sulfonated Starbons; with that band at 1030 cm<sup>-1</sup> attributed to symmetric S=O stretching. In the FTIR spectrum of Starbon® 300 microwave sulfonated at 150 °C two bands can be distinguished at 886 cm<sup>-1</sup> and 820 cm<sup>-1</sup>, which can be related to sulfate esters like in conventional sulfonated Starbons® before methanol treatment. It is worth remembering that microwave sulfonated Starbons® were not treated with methanol.

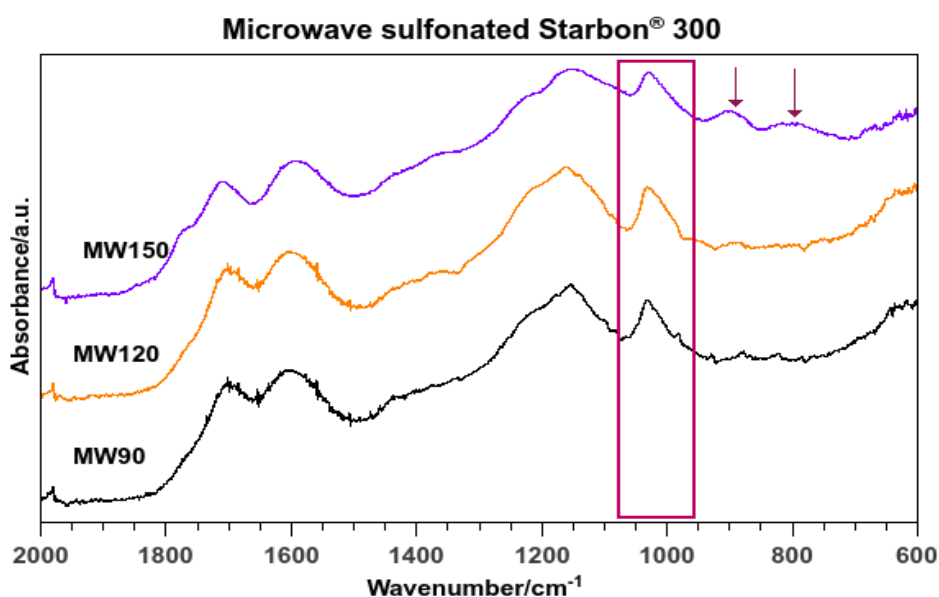


**Figure 3.13.** FTIR spectra for microwave sulfonated Starbons® 300

FTIR spectra for microwave sulfonated Starbon® 450 at 90 and 120 °C are compared with the Starbon® 450 before sulfonation and presented in **Figure 3.14**. The spectra looks very different to Starbon® 300, as the band corresponding to C=O stretching and located at 1705 cm<sup>-1</sup> has decreased significantly for these materials. Whereas, the vibration corresponding to C=C stretching ca. 1600 cm<sup>-1</sup> is more prominent than the one for Starbons® 300. In the original Starbon® 450, the broad band ca. 1200 cm<sup>-1</sup> seems to be less prominent than the ones in microwave sulfonated Starbon® 450; the peaks corresponding to ether bridges (1225 cm<sup>-1</sup>) and C-C or C-O stretching (1160 cm<sup>-1</sup>) are hardly discriminated in the original Starbon® 450, meanwhile are obvious in sulfonated ones. The symmetric stretching of sulfonic groups rises at 1030 cm<sup>-1</sup>,<sup>46,90,137</sup> as expected this band is not observed in the original material, confirming the functionalization of the materials through microwave sulfonation.

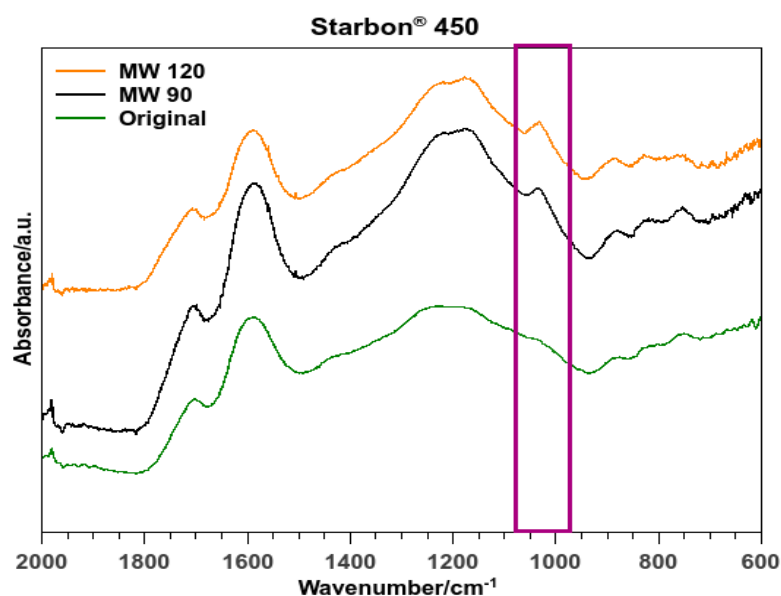


**Figure 3.14.** FTIR spectra of Starbon® 450 before and after microwave sulfonation at 90°C and 120 °C.

### 3.6. Acidity of microwave sulfonated Starbons®

Acidity of microwave sulfonated Starbons® 300 was determined using the NaCl solution, following the methodology presented in **Chapter 2**, the method used is a modification of the one proposed by Lin *et al*<sup>46</sup> as in this work the solution of sodium chloride is prepared using a mixture of methanol-water (1:1). After

stirring the mixture of sulfonated Starbons<sup>®</sup> and NaCl solution overnight, sample is filtered and the filtrate is titrated potentiometrically with a NaOH solution. **Figure 3.15.** corresponds to a titration curve for sulfonated Starbon<sup>®</sup> 300 prepared at 90°C using microwaves, in which the equivalence point is pointed out. Titrations were carried out in triplicate and an average of mmol of sulfonic groups (-SO<sub>3</sub>H) per gram was determined.

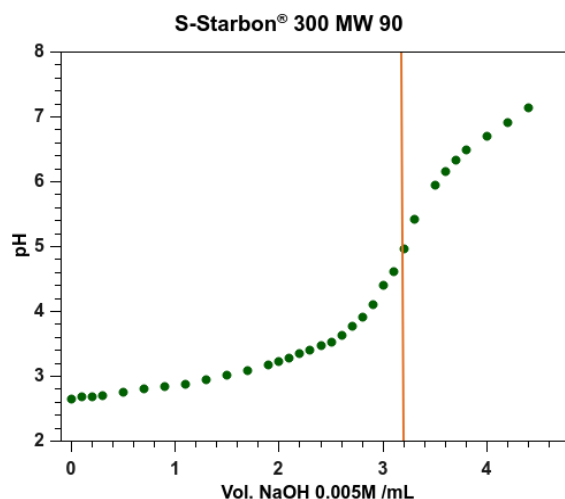
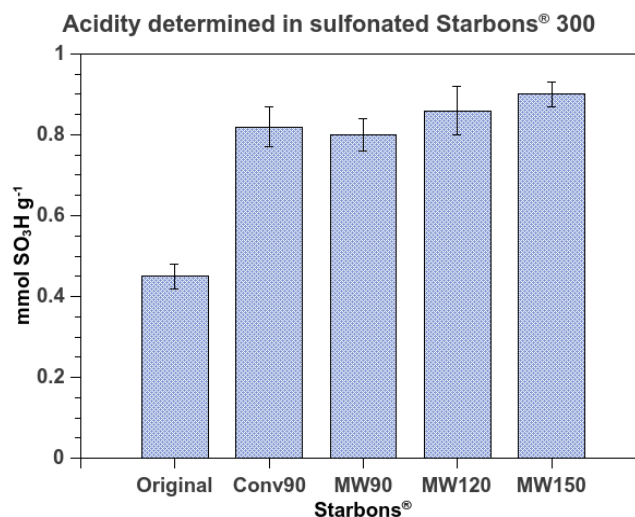


**Figure 3.15.** Titration curve for microwave sulfonated Starbon<sup>®</sup> 300 at 90 °C

**Figure 3.16.** shows a comparison of sulfonic groups determined in sulfonated Starbons<sup>®</sup> 300 through the titration with NaOH. It is interesting to notice that sulfonated Starbons<sup>®</sup> 300 either prepared by conventional heating or using microwave irradiation at different temperatures, present similar quantities of sulfonic groups determined by potentiometric titrations (**Figure 3.16.a**). However, the values obtained by titration related to sulfonic acids are lower than those expected from S (VI) quantified on the surface by XPS analysis (**Figure 3.16 b**). This difference between the “expected” quantity of S(VI) and the quantity “determined” by exchange using NaCl solutions has also been observed in **Chapter 2**, and in other materials, such as sulfonic silica materials.<sup>138,139</sup> As has already been mentioned, this fact would indicate that not all the S(VI) on samples are as sulfonic acids, but as well as sulfones or sulfates, as the case of microwave sulfonated Starbons 300, with the presence of organo sulfate esters, ROSO<sub>2</sub>OR.



(a)

	Quantity of SO <sub>3</sub> H/ mmol g <sup>-1</sup>		
	Titration*	S (E.A)**	S(XPS)***
<b>Original</b>	<b>0.45</b>	0.90	0.89
<b>Conv90</b>	<b>0.82</b>	0.73	1.61
<b>MW90</b>	<b>0.80</b>	0.95	1.09
<b>MW120</b>	<b>0.86</b>	0.98	1.26
<b>MW150</b>	<b>0.90</b>	1.33	1.12

\* determined by titration with NaOH

\*\* expected from sulfur determined by elemental analysis

\*\*\* expected from sulfur determined by XPS analysis

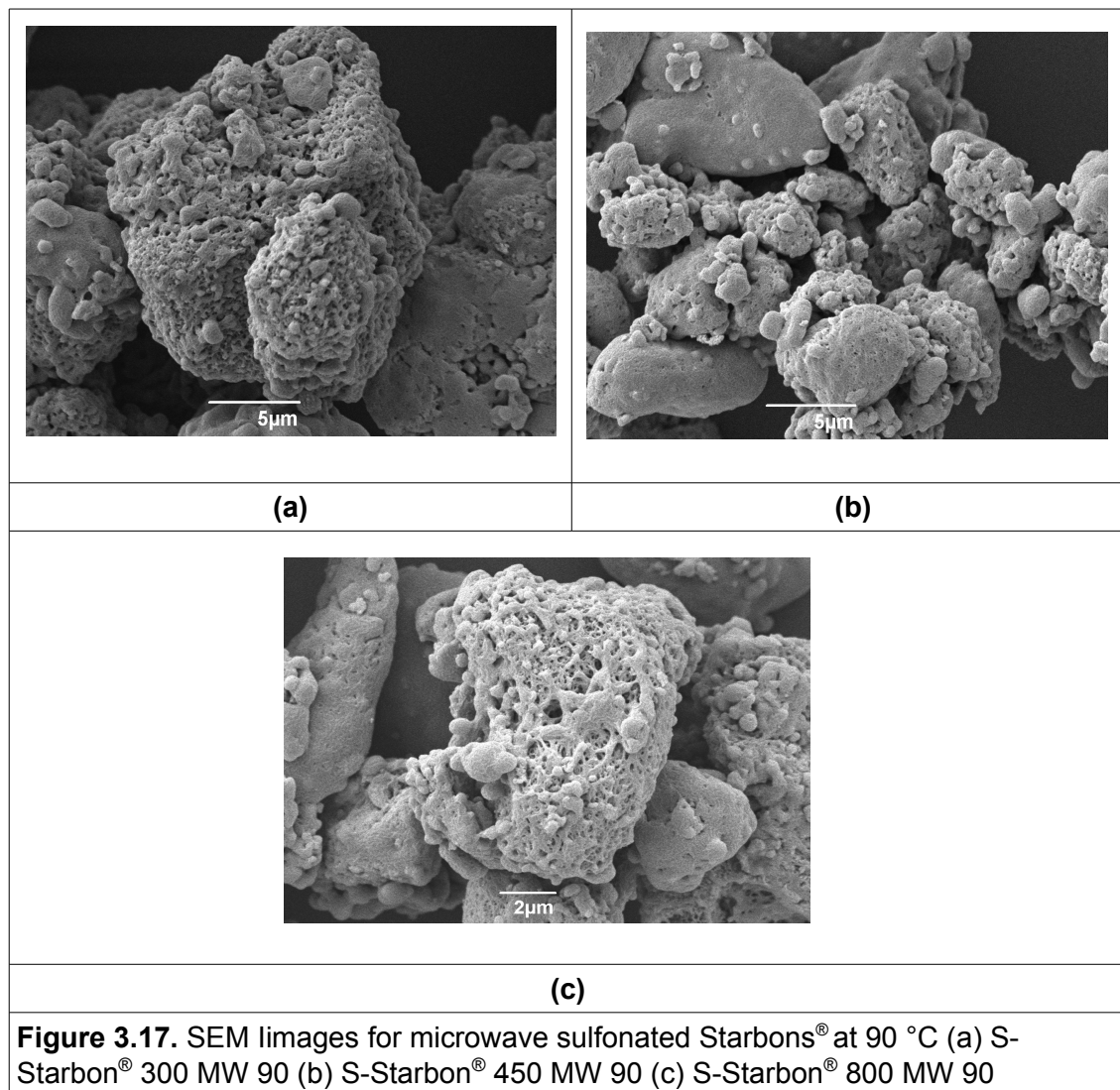
(b)

**Figure 3.16.** Acidity determined by titration with NaOH (a) Comparison between obtained and expected sulfonic groups (b) for sulfonated Starbons® 300

### 3.7. Morphology and textural characterisation

The morphology of the samples was observed by Scanning Electron Microscopy. The images (Figure 3.17 a-c) show that materials retain their porous structures after microwave sulfonation at 90 °C. Although, for samples

carbonized at high temperatures (450 and 800 °C) it was common to observe some condensed particles, it looks like materials were encapsulated. In the three Starbons<sup>®</sup>, particle sizes are not homogeneous and vary from 10 – 50 μm. In Starbon<sup>®</sup> 450, it can be observed agglomerates of small particles which form lumps.



The pore size distribution showed that microwave sulfonated Starbons<sup>®</sup> prepared at 90°C are mesoporous materials, they possess pores with an average diameter of 30 nm (**Figure 3.18 a-c**). From the surface area analysis was found that micropores ratio increases as temperature of carbonization does, as was mentioned in **Chapter 2**. For Starbon<sup>®</sup> 300, the ratio of micropores was 47 %; and for the Starbon<sup>®</sup> 450, the ratio increased to 75 % and for Starbon<sup>®</sup> 800 the contribution of micropores to the total surface area

was 87%. The increase of microporosity with increment of temperature has been observed during the synthesis of Starbons<sup>®</sup>, previously.<sup>9</sup>

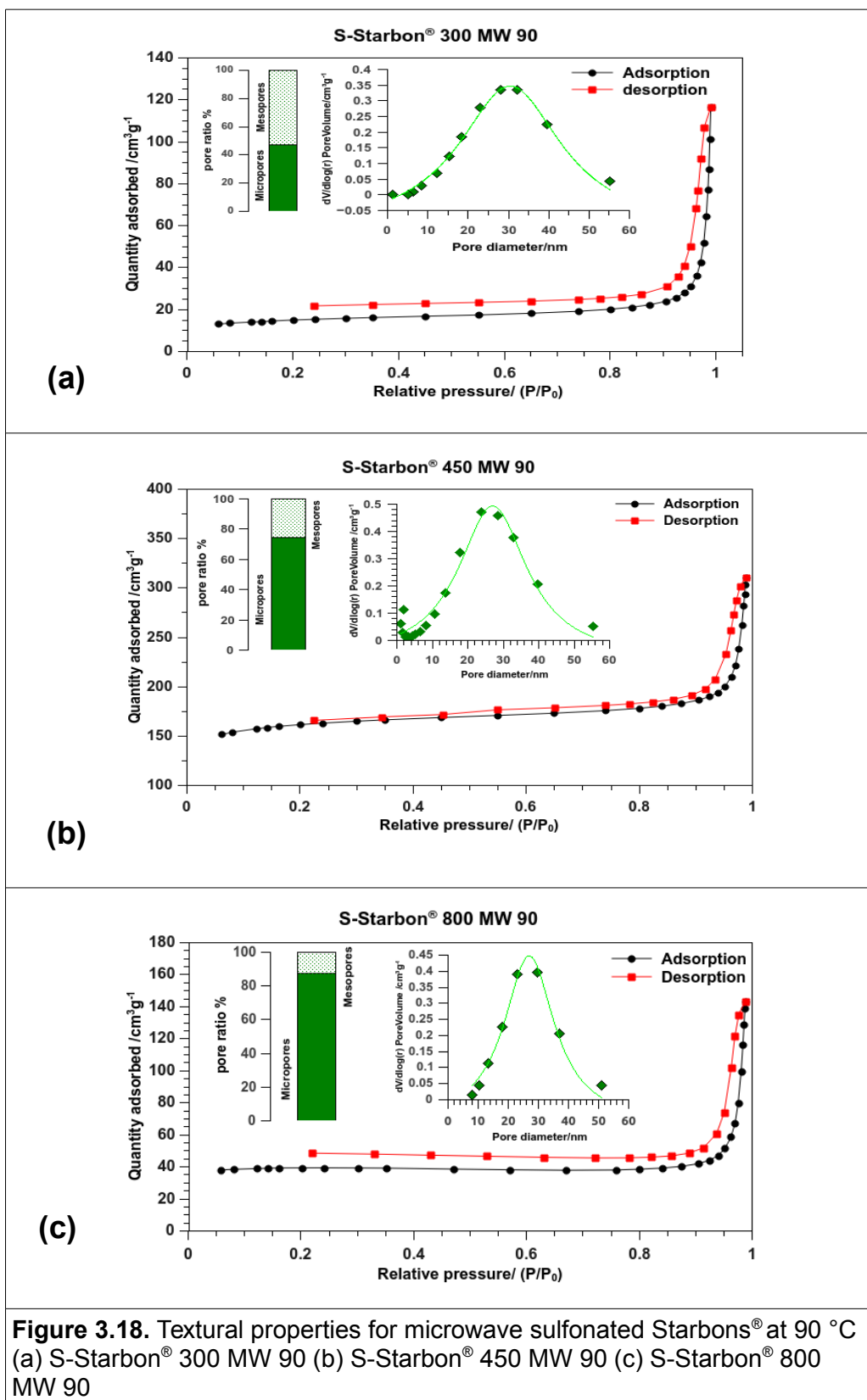


**Figure 3.18.** Textural properties for microwave sulfonated Starbons<sup>®</sup> at 90 °C (a) S-Starbon<sup>®</sup> 300 MW 90 (b) S-Starbon<sup>®</sup> 450 MW 90 (c) S-Starbon<sup>®</sup> 800 MW 90

Microwave sulfonation for Starbon<sup>®</sup> 300 showed interesting changes on surface area, as this increases noticeably with temperature of sulfonation. As mentioned previously, the starting material based on *Cleargum* starch, showed very low surface area, attributed to a pores blocking phenomenon during preparation. Results presented in **Figure 3.19a** suggest that sulfonation using microwaves would 'unblock' the pores, as the surface area changed from 16 m<sup>2</sup>g<sup>-1</sup> from starting material, Starbon<sup>®</sup> 300 to 240 m<sup>2</sup>g<sup>-1</sup> for sample microwave sulfonated at 150 °C. However, for Starbon<sup>®</sup> 450 (**Figure 3.19b**) the surface does not change significantly through the different temperatures of microwave sulfonation, then non-effect can be observed. While, for Starbon<sup>®</sup> 800, it seems that surface area changed in a different way, decreasing from the original material (390 m<sup>2</sup>g<sup>-1</sup>) through the different temperature treatment using microwave irradiation (**Figure 3.19c**). This phenomenon was observed in the conventional sulfonation of Starbon<sup>®</sup> 800 and it can be attributed to micropores blockage. It is interesting to notice that pore volume for original and microwave sulfonated Starbons<sup>®</sup> did not vary widely; when the three temperature Starbons<sup>®</sup> are compared, that Starbon<sup>®</sup> 450 has bigger pore volume than Starbons<sup>®</sup> 300 and 800 (**d**).

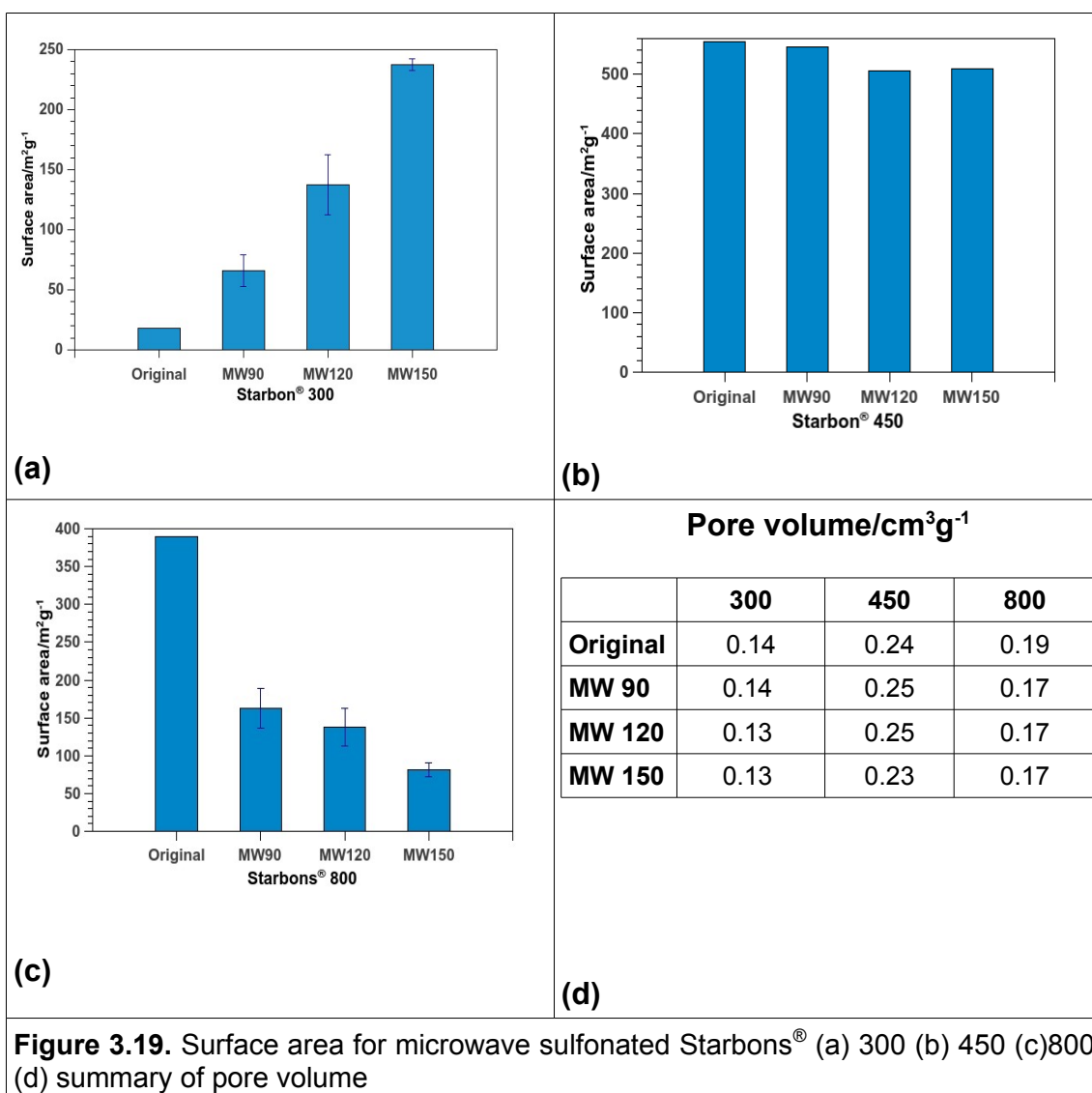


**Figure 3.19.** Surface area for microwave sulfonated Starbons<sup>®</sup> (a) 300 (b) 450 (c)800 (d) summary of pore volume

### 3.8. Conventional versus microwave sulfonation at 90 °C

#### 3.8.1. Elemental composition

The elemental composition of Starbons<sup>®</sup> after sulfonation showed an increase in the oxygenated groups (O:C ratio) either *via* conventional or using microwave irradiation (**Figure 3.20**); however, a specific trend was not observed with respect to the method of sulfonation. Values are too similar for both methodologies. With respect to the sulfur content, Starbon<sup>®</sup> 300 showed higher content when sulfonation was carried out using microwave irradiation than conventional heating. At this point, it is worth mentioning that sulfur quantification of all samples was determined just once, however an estimate of the sulfur variation among different samples is presented in **Figure 3.20**. For

Starbons<sup>®</sup> 450 and 800, the sulfur content does not differ significantly from both methods of sulfonation. However, it is important to point out that microwave sulfonated Starbons<sup>®</sup> were not treated with methanol as the conventional sulfonated ones were; as seen in **Chapter 2**, the treatment with methanol decreases the sulfur content from the original sulfonated samples. This suggests that overall quantity of sulfur attached to material could be lower than it appears.

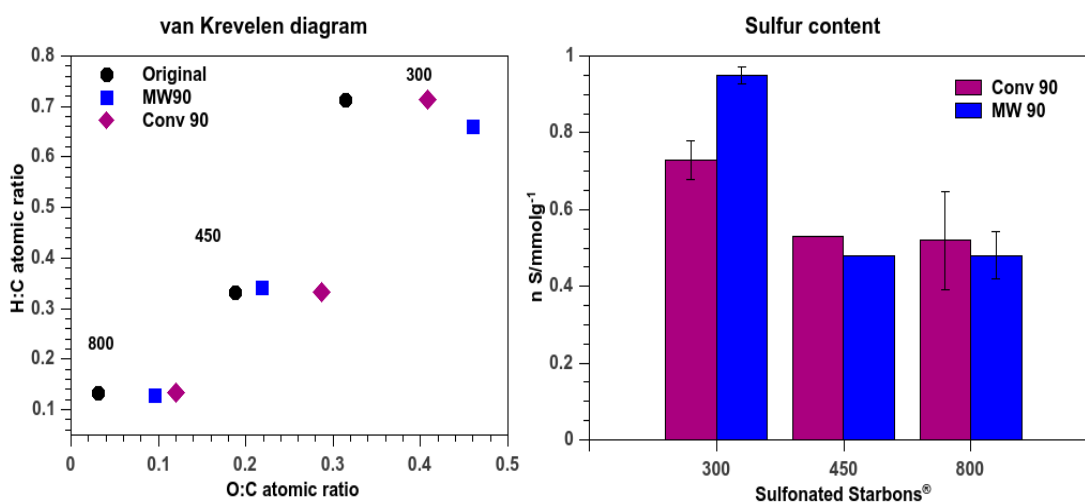


**Figure 3.20.** van Krevelen diagram (left) and sulfur content (right) for sulfonated Starbons<sup>®</sup> using conventional heating and microwaves

### 3.8.2. Chemical environments observed through XPS analysis

#### 3.8.2.1. Sulfonated Starbon<sup>®</sup> 300 at 90 °C

The number of carbon species identified by the analysis of high-resolution C1s spectra is different from microwave sulfonated Starbon<sup>®</sup> 300 (5) and conventional sulfonated Starbon<sup>®</sup> (4); a broader spectrum is obtained for the former, the components of which indicate there are more oxygenated carbons than in conventional sulfonated sample. Tailing of the spectra is observed in the microwave sulfonated Starbon<sup>®</sup>, but not in the conventional sulfonated system. Analysis of the S2p spectra showed that sulfonated Starbons<sup>®</sup> using microwaves present another S(VI) specie, identified as ROSO<sub>2</sub>OR which does not appear in the conventional sulfonated sample (**Figure 3.21.**)

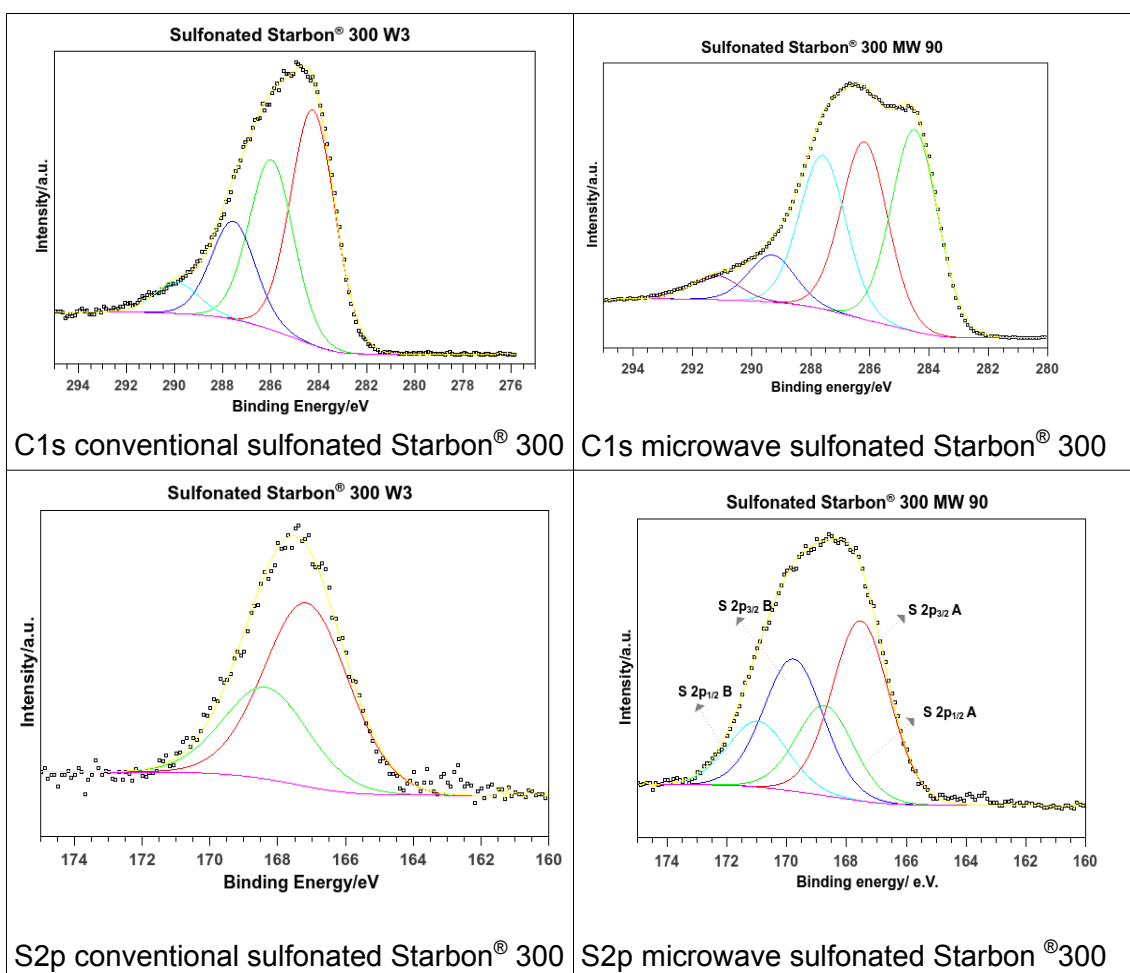


**Figure 3.21.** XPS spectra for sulfonated Starbons<sup>®</sup> 300 by conventional and microwave heating

### 3.8.2.2. Sulfonated Starbon<sup>®</sup> 450 at 90 °C

Analysis of the C1s spectra showed that microwave sulfonated Starbons<sup>®</sup> present a prominent peak at 285.6 eV, while samples prepared by conventional heating present a small band in the same binding energy. It seems that microwave sulfonation promotes the appearance of a more oxygenated carbon, identified as carbonate O-COO-, which is not observed in Starbon<sup>®</sup> 450 sulfonated by conventional heating. Another interesting finding is the ratio of sulfur (VI) and sulfur (II) found by analysis of the S2p spectra. It seems that microwave sulfonated Starbons has a lower ratio of S(VI), around 65 % compared with Starbon<sup>®</sup> 450 sulfonated conventional heating, which presents 85 %.

### 3.8.2.3. Sulfonated Starbon® 800 at 90 °C

According with the C1s spectra, the main difference between microwave and conventional sulfonated Starbons® 800 is the appearance of the oxygenated component, carbonate O-COO- in the sample prepared using microwaves. However, its relative concentration is significantly low, being around 2%. The S2p spectra shows that both samples present S(VI) and S(II) in the same proportion (70:30).

### 3.8.3. Structural composition by <sup>13</sup>C solid-state NMR

Unfortunately, no significant information were retrieved from the <sup>13</sup>C solid-state NMR spectra of microwave sulfonated Starbon® 450, due to its poor quality. However, a signal centred at 130 ppm is identified, as in conventional sulfonated Starbon® 450; this signal is associated to polycyclic aromatic groups.

The <sup>13</sup>C solid-state NMR spectrum for microwave sulfonated Starbon® 300 is broader than the one obtained for conventional sulfonated Starbon® 300. The spectra indicates the presence of oxygenated carbons in higher proportion than in conventional sulfonated one; which agrees with the XPS results present previously.

## 3.9. Conclusions

In this chapter the sulfonation of Starbons® 300, 450 and 800 using microwave irradiation has been described. The synthesis was done at three different temperatures 90, 120 and 150 °C. The resulting materials were then characterised. The analysis by elemental composition showed the sulfur content is higher for sulfonated Starbons® 300 independent of sulfonation temperature; however, in sulfonated Starbons® 800, the higher content was observed at the highest sulfonation temperature, 150 °C.

The analysis of the high-resolution C1s spectra of the samples showed that more oxygenated carbons are observed in microwave sulfonated Starbons® when temperature of sulfonation increases; this was more noticeable on

microwave sulfonated Starbons<sup>®</sup> 800. Analysis of the S2p spectra on microwave sulfonated Starbons<sup>®</sup> showed the appearance of another sulfur specie (VI), assigned to organo sulfate esters, ROSO<sub>2</sub>OR in Starbon<sup>®</sup> 300 together with the species assigned to sulfonic acids. For Starbons<sup>®</sup> 450 and Starbons<sup>®</sup> 800 both present sulfur (VI) and a reduced sulfur species (II); proportion of S(VI) to S(II) is slightly higher for Starbons<sup>®</sup> 800 than for 450.

Microwave sulfonated Starbons<sup>®</sup>, presented a band ca.~1030 cm<sup>-1</sup> assigned to S=O stretching, as was observed in conventional sulfonated Starbons<sup>®</sup> indicating the presence of sulfonic groups attached. The increasing surface area of the microwave sulfonated Starbons<sup>®</sup> 300 suggest that microwaves would unblock the porous of the materials, as the starting material presented a surface area of 16 m<sup>2</sup>g<sup>-1</sup>, and the sample sulfonated at 150 °C reaches over 200 m<sup>2</sup>g<sup>-1</sup>. The surface area of Starbons<sup>®</sup> 800 decreased after microwave sulfonation, this phenomenon was also observed in the conventional sulfonation of Starbon<sup>®</sup> 800 and it can be related with the blockage of micropores of the sample.

The results obtained in microwave sulfonated Starbons<sup>®</sup>, make it attractive to keep exploring this methodology, as it represents an opportunity to develop novel sulfonated materials, reducing the time for preparation.



# Chapter 4

## *Sulfonation of Starbons<sup>®</sup> and their thermal stability*



## 4.1. Introduction

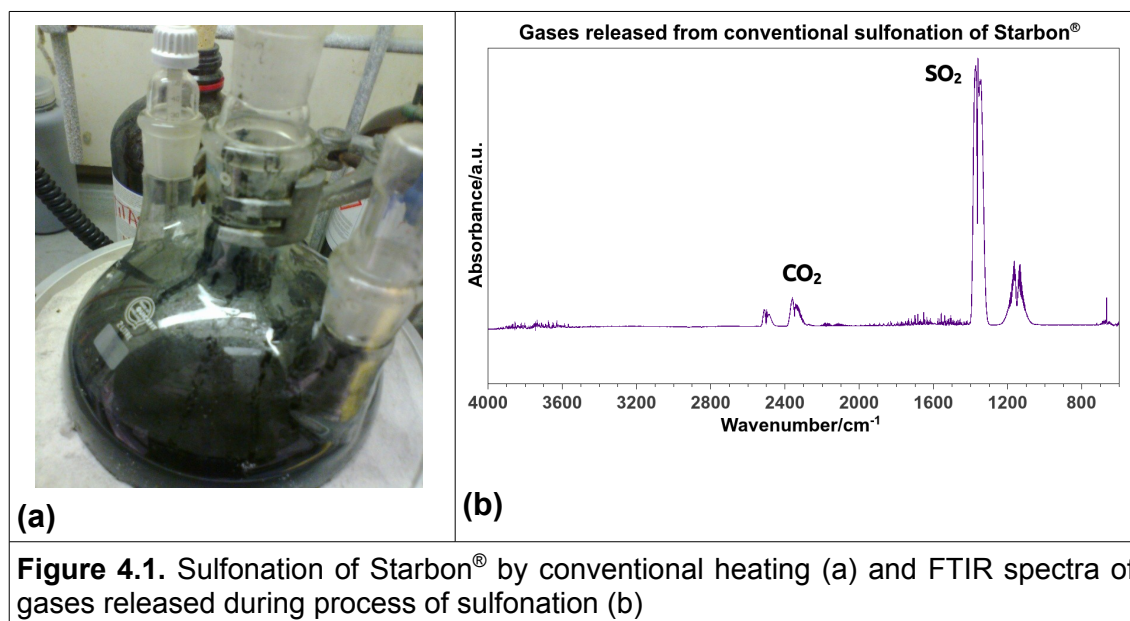
The preparation and characterisation of sulfonated Starbons<sup>®</sup> using conventional heating and microwave irradiation has already been discussed in **Chapters 2** and **3**, respectively. In the present chapter, attention is addressed to the sulfonation process and studies on the thermal stability of sulfonated Starbons<sup>®</sup>. This investigation was carried out using thermogravimetric analysis coupled to infrared spectroscopy (TG-FTIR), in which gases evolved from samples during heating treatment were analysed, providing useful information about the materials.

Sulfonation is a substitution reaction used to attach sulfonic groups ( $\sim\text{SO}_3\text{H}$ ) to organic compound through a carbon-sulfur bond. Some of the agents used for sulfonation of materials include, sulfuric acid, sulfur trioxide ( $\text{SO}_3$ ) or some derivatives such as chlorosulfonic acid.<sup>140</sup> As mentioned previously, in this study, sulfonation of materials was carried out using commercial sulfuric acid 95 %. **Table 4.1.** summarizes the conditions used for sulfonation of Starbons<sup>®</sup> *via* conventional and microwave treatments.

	CONVENTIONAL	MICROWAVE IRRADIATION
Mass of Starbon	~80 g of Starbon <sup>®</sup> prepared at temperatures from 300 – 800 °C	~ 2 g of Starbon <sup>®</sup> 300, 450 and 800
Ratio	1 g of solid: 7 mL acid	1 g of solid: 7 mL acid
Temperature and time	Constant stirring @ 90°C for 6 h	Constant stirring @ 90, 120 and 150 °C for 30 min (200 W)
Post-sulfonation treatment	Washed several times (t >20; time: 20–30 min) at constant stirring with hot water (~80°C). Methanol treatment using microwave irradiation (200 W, 10 min; 3 times)	Washed with hot water using microwave irradiation @ 80 °C (t > 12; time: 10 min)

## 4.2. Sulfur dioxide released during sulfonation of Starbons®

Formation of gases on the top of the reaction mixture was observed during sulfonation of Starbons® by conventional heating (**Figure 4.1.a**); these gases were collected using a syringe and subsequently the sample was analysed by FTIR-ATR to identify the components of the gaseous mixture. In the IR spectra obtained (**Figure 4.1.b**), the components identified were sulfur dioxide (SO<sub>2</sub>) observed at 1375 cm<sup>-1</sup> and 1160 cm<sup>-1</sup>; and carbon dioxide (CO<sub>2</sub>) between 2200-2400 cm<sup>-1</sup>.<sup>83</sup>



Release of SO<sub>2</sub> would imply a reduction of S(VI) present in sulfuric acid to S(IV) within sulfur dioxide, which has been associated with thermal decomposition of sulfur trioxide and/or sulfates, which has been observed during the oxidation of hydrocarbons, such as anthracene with sulfuric acid.<sup>141</sup> This process can be represented in **Equation 4.1**. It is worth mentioning that sulfur dioxide was also observed during the sulfonation of Starbons® by microwave irradiation. As it was seen in previous **Chapters 2** and **3**, the samples got more oxygenated groups after treatment with sulfuric acid, in agreement with this suggestion.



**Equation 4.1**

An attempt to quantify sulfur dioxide released during sulfonation from both methods, microwaves and conventional heating was made. The proposed methodology consisted in collecting the  $\text{SO}_2$  (g) in a solution of  $\text{H}_2\text{O}_2$  (30% v/v) giving sulfuric acid as product. The gases were collected using nitrogen as a carrier gas, with an aliquot from solution then titrated with NaOH solution (**Figure 4.2.**).

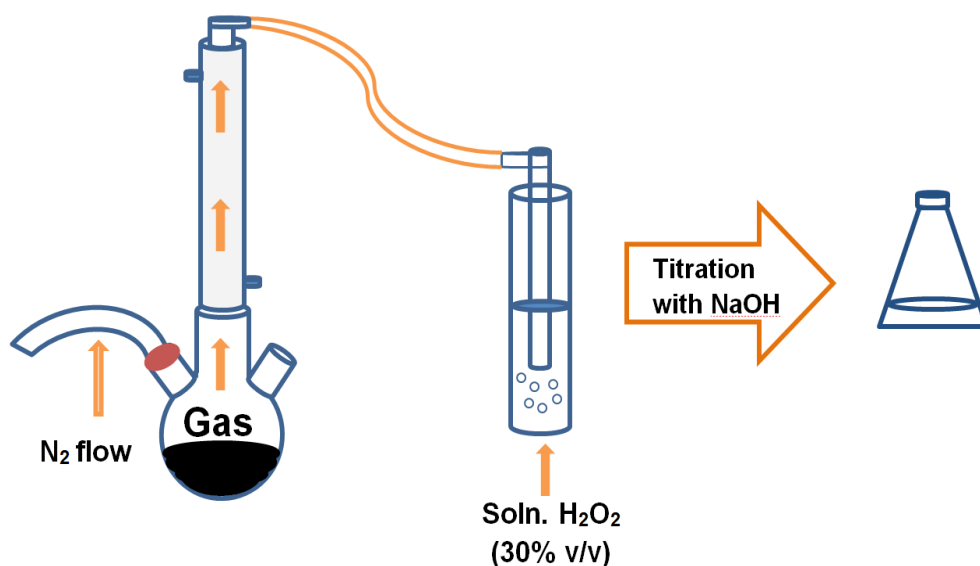
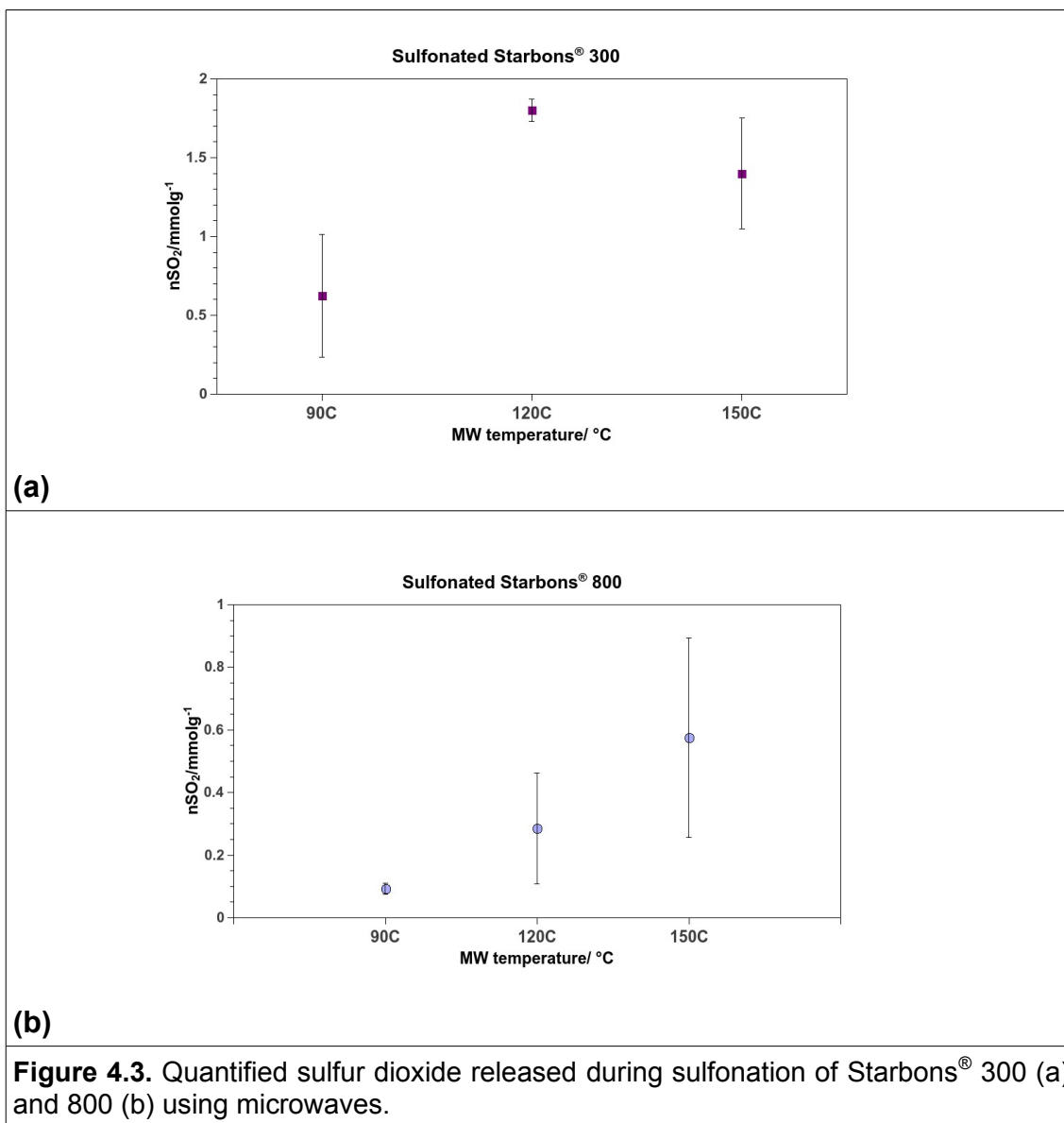


**Figure 4.2.** Diagram of suggested methodology for quantification of  $\text{SO}_2$  released during sulfonation

This methodology was tested in microwave sulfonated Starbons<sup>®</sup>, prepared at three different temperatures with the aim to find any correlation between  $\text{SO}_2$  released from samples and temperature of sulfonation. The trend is presented in **Figure 4.3**. The quantity of sulfur dioxide determined by titration of hydrogen peroxide solution, showed that Starbon<sup>®</sup> 300 (**a**) released greater quantities than Starbon<sup>®</sup> 800 (**b**). It also seems, that higher temperatures of sulfonation using microwaves give higher concentrations of sulfur dioxide, however, large variations in the values obtained were also observed. The fact that Starbon<sup>®</sup> 300 showed a greater release of  $\text{SO}_2$  during sulfonation could be correlated with the presence of several functionalities in Starbon<sup>®</sup> 300 (**Chapter 2**) which could experience oxidation, promoting at same time sulfuric acid reduction.<sup>141</sup>



Although, the proposed quantification of sulfur dioxide release using a solution hydrogen peroxide would be very useful in terms of correlation of sulfur used during sulfonation and sulfur attached to samples, this technique showed large deviations in the values and not a great correlation in some cases. These variations could be related to the heterogeneity of samples, as well as some details that could be improved in measurement, like the nitrogen flow, which was not controlled.

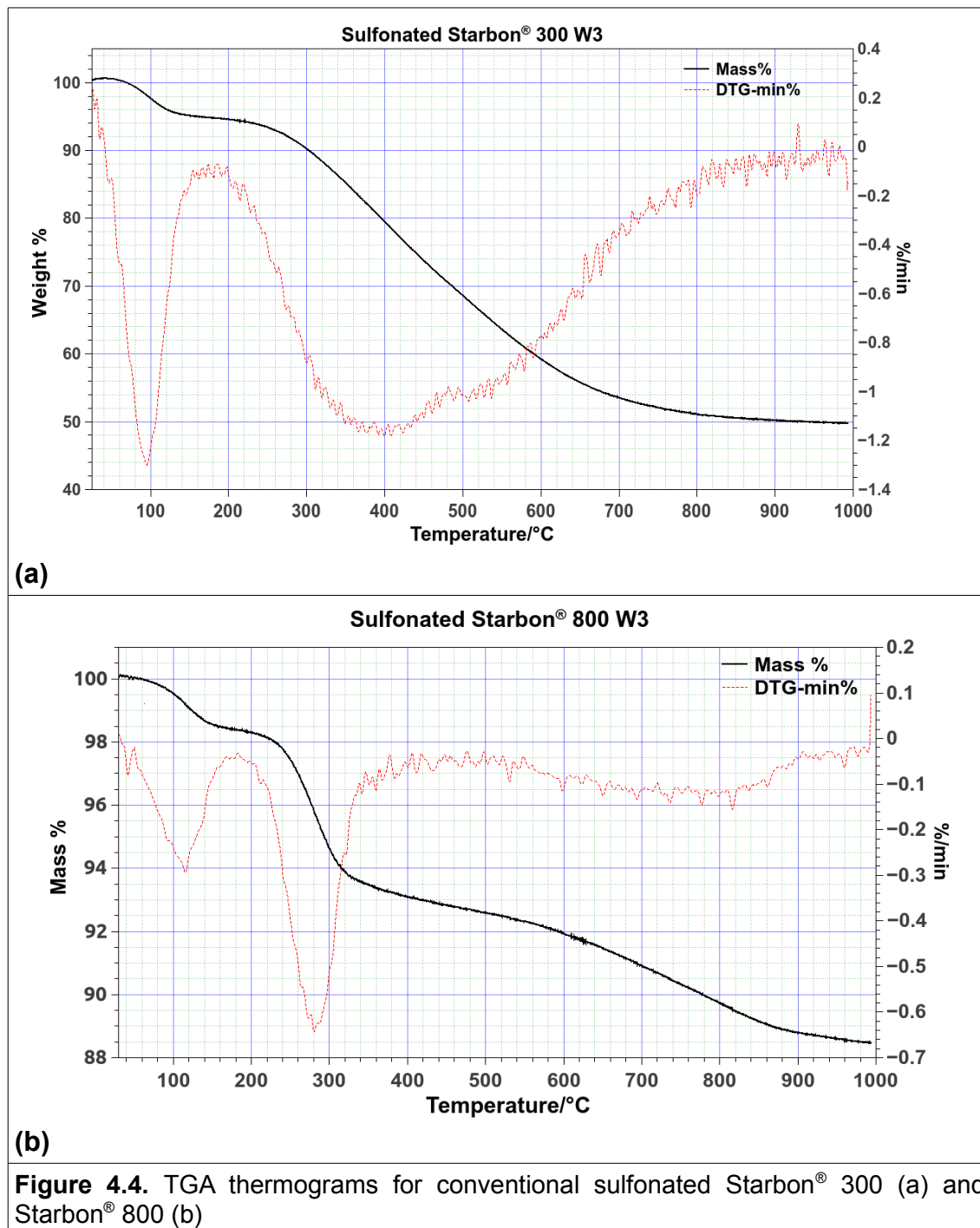
### 4.3. Thermal stability of sulfonated Starbons® prepared by conventional heating

Thermogravimetric analysis (TGA) has been the conventional and most popular technique used to study the thermal stability and decomposition of materials. This method measures the mass changes of the material as a function of temperature and time, providing information about the degradation of the material. When this technique is coupled to FTIR, the information obtained is even more useful, as it allows the analysis of gases evolved during thermal treatment, suggesting degradation pathways of the material.<sup>73,142</sup>

Thermal stability of sulfonated Starbons® was studied through the coupled technique of TG-FTIR. The measurements were carried out in a Netzch STA 490, using 50 mg of sample in an inert atmosphere with nitrogen flow at 100 mLmin<sup>-1</sup>. The temperature programme was set to increase at 10°C per minute from room temperature up to 1000 °C.

TGA thermograms for sulfonated Starbons® 300 (S300SW3) and 800 (S800SW3) are displayed in **Figure 4.4**. The decomposition profiles are different from each other; the weight loss for S300SW3 is approximately 50 % and for S800SW3, just 12 %. This big difference could be attributed to higher content of oxygenated groups of sulfonated Starbon® 300 compared to sulfonated Starbon® 800 (already shown in **Chapter 2**), which decompose during heating. Both thermograms showed weight losses below 150 °C which can be attributed to moisture loss from the samples.<sup>142,143</sup> In that first stage, sulfonated Starbon® 300 shows higher weight loss than sulfonated Starbon® 800, which some authors have related with high hydrophilicity in these lower temperature samples.<sup>144</sup> In the second stage, the mass dropped dramatically for S300SW3 (approximately 40 wt%) from 200 to 700 °C; this mass change is due to decarboxylation and dehydroxylation of the samples,<sup>142,145,146</sup> together with the release of sulfur dioxide coming from decomposition of sulfonic groups attached to sulfonated Starbons®.<sup>144,147,148</sup> For sulfonated Starbon® 800, the mass dropped only slightly by 5 wt%, from 200 to 400 °C which could be related to sulfonic groups splitting and CO<sub>2</sub> and H<sub>2</sub>O release<sup>144,147,148</sup> and a third stage is observed

from 500 °C to 1000 °C, in which sample lost 4 wt%.



Gases evolving from the materials were monitored by FTIR whilst the sample was heated within the TGA oven and analysed in a spectrometer Bruker Equinox 55. An important strength of the TGA-FTIR analysis is the ability to display gas component evolution profiles in real time on exactly the same line as the TGA weight loss profile. A series of spectra were collected over the time-

temperature range. **Figure 4.5.** shows the spectra of gases evolved at 290 °C from sulfonated Starbon® 800, S800SW3. The main compounds distinguished are water at 4000–3500  $\text{cm}^{-1}$  and 2000–1400  $\text{cm}^{-1}$  observed as well in starch decomposition;<sup>142</sup> carbon dioxide at ca. 2385, 2338  $\text{cm}^{-1}$  and absorbance due to sulfur dioxide identified at 1375–1324  $\text{cm}^{-1}$ .<sup>83</sup>

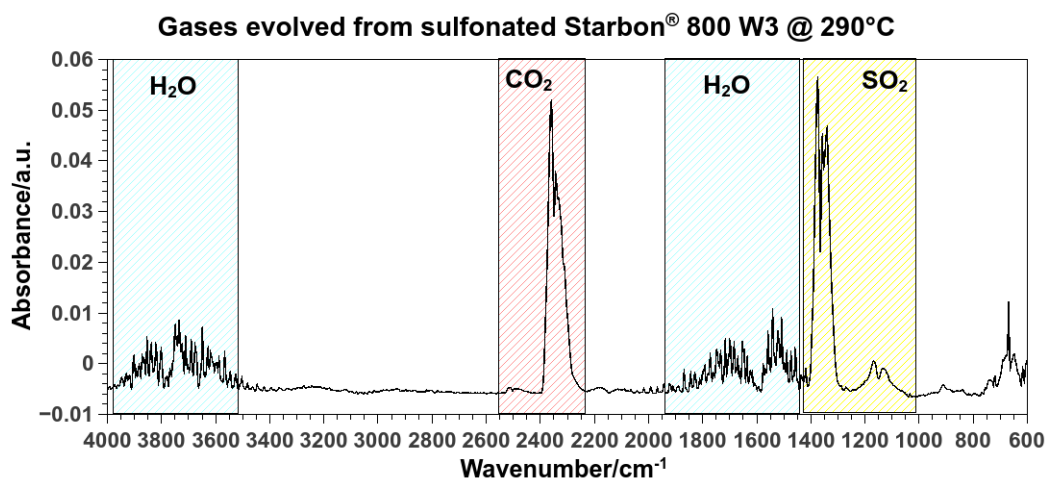
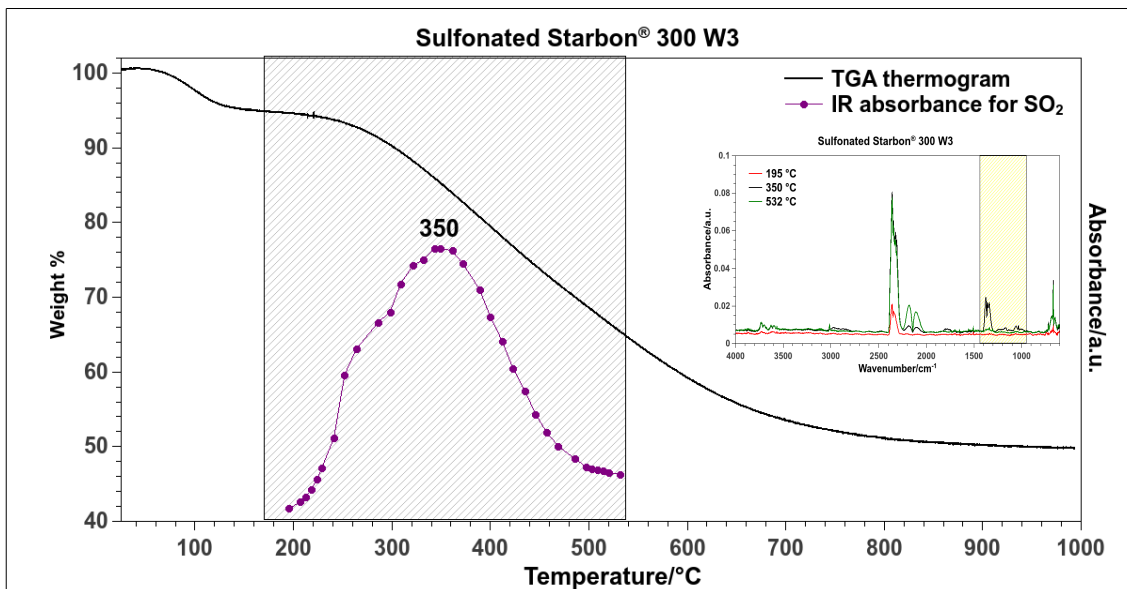
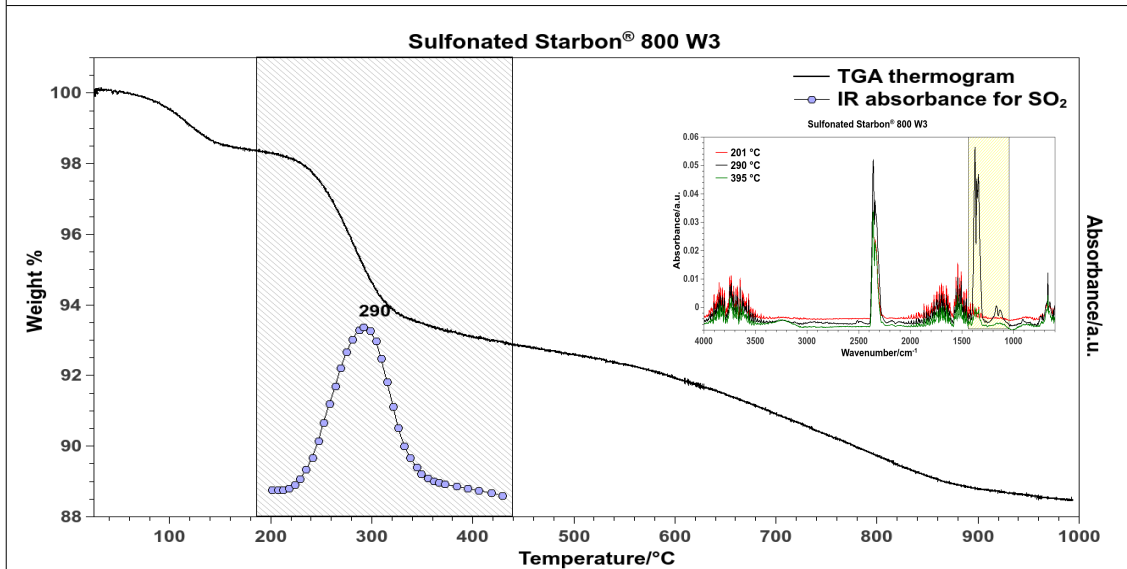


**Figure 4.5.** FTIR spectra of gases evolved from sulfonated Starbon® 800 at 290 °C

Sulfur dioxide ( $\text{SO}_2$ ) is produced by the degradation of the sulfonic groups from the materials. Sulfur dioxide released during heating of the material was measured by monitoring the absorbance band at at  $\sim 1375 \text{ cm}^{-1}$  as function of temperature. A correlation between the weight loss of sulfonated Starbons® 300 and 800 and  $\text{SO}_2$  gas phase absorbance as a function of temperature is presented in **Figure 4.6.**



(a)



(b)

**Figure 4.6.** TGA thermograms and IR absorbance of SO<sub>2</sub> gas *versus* temperature for (a) sulfonated Starbon® 300 and (b) sulfonated Starbon® 800

The diagram shows that the temperature range of SO<sub>2</sub> released from sulfonated Starbon® 300 is from 200 to 500 °C, which is wider than the one observed for sulfonated Starbon® 800, in which SO<sub>2</sub> is released between 200 to 400 °C. The maximum absorbance for sulfur dioxide was observed at 350 °C and 290°C for sulfonated Starbons® 300 and 800, respectively. This would suggest that sulfonic groups are more strongly attached to sulfonated Starbon® 300 than to sulfonated Starbon® 800.

As will be seen in **Chapter 5**, it is worth mentioning that deactivation of S800SW3 occurs more rapidly during use as a catalyst than for S300SW3 (**Figure 4.7.**), which is consistent with this suggestion. As was previously mentioned in **Chapter 2**, sulfonated Starbon® 300 present more sulfur groups attached to the material than sulfonated Starbon® 800, especially more sulfur (VI) groups, assigned to sulfonic groups.

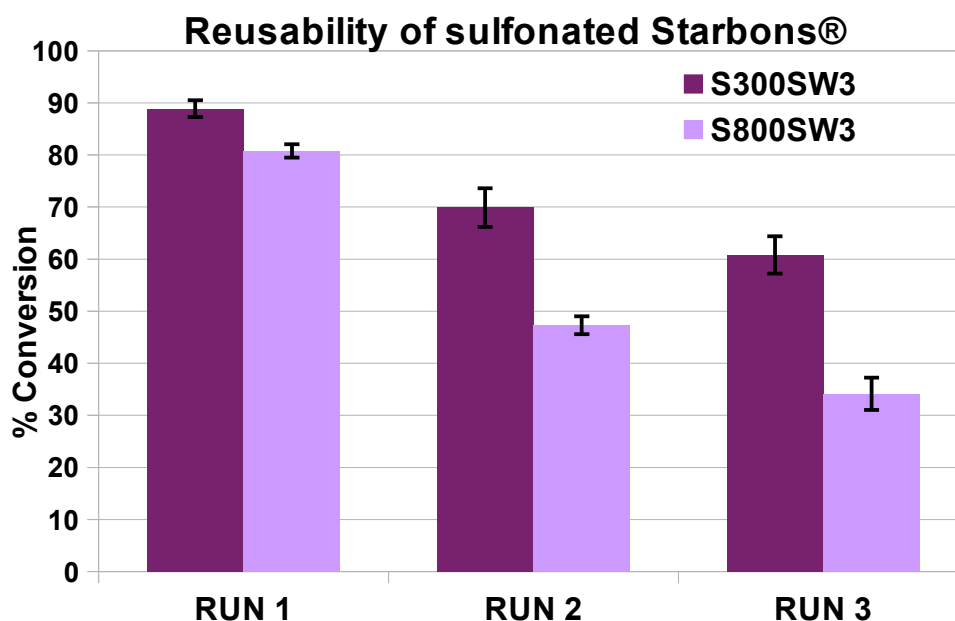


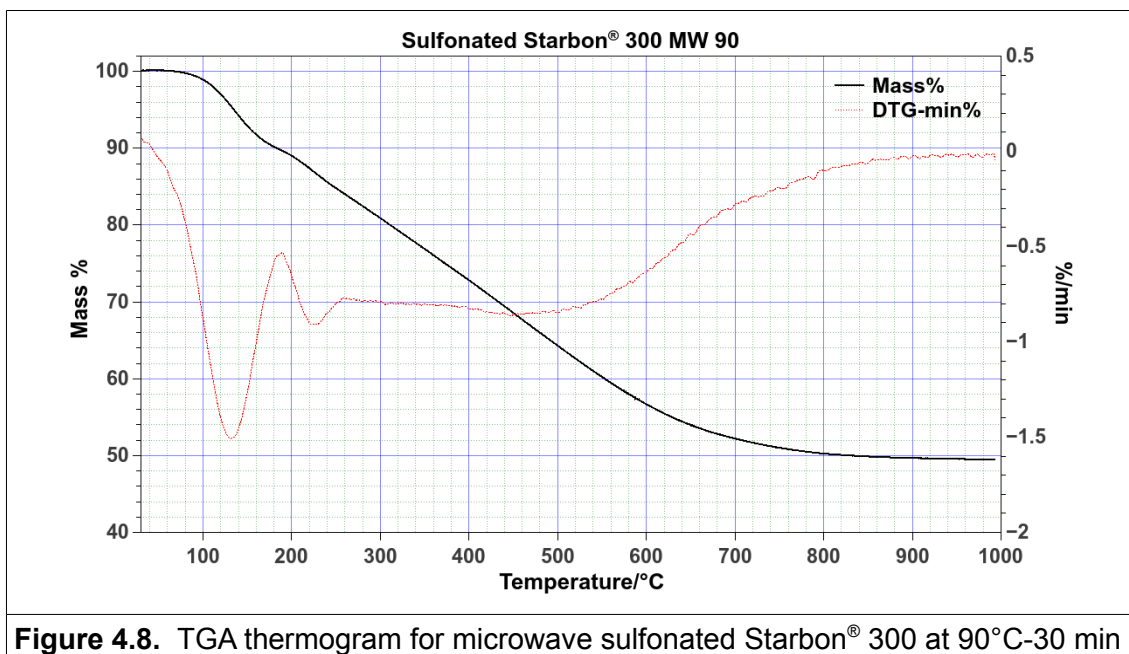
**Figure 4.7.** Comparison in the re-usability of sulfonated Starbons® 300 and 800

Diagrams presented in **Figure 4.6.** also contain the IR spectra of gases evolved at three different temperatures: the beginning and the end of SO<sub>2</sub> evolution and the temperature with the maximum absorbance for SO<sub>2</sub>. At all three temperatures, CO<sub>2</sub> is observed at ca. 2385, 2338 cm<sup>-1</sup>. At 532 °C, a band appeared at 2100 cm<sup>-1</sup> which would suggest the formation of carbon monoxide (CO). In addition, a small band at 3000-3100 cm<sup>-1</sup> appears at this high temperature; which can be related to a C-H bond vibration<sup>83</sup> from methyl groups released.<sup>142</sup> Sin *et al*, suggests the formation of hydrocarbon products (alkanes, alkenes and aromatics) occurred at 450°C during the heating of a composite of polyvinyl alcohol-cassava starch,<sup>145</sup> it is therefore very likely to be related to a hydrocarbon product. The band between 3000 and 3100 cm<sup>-1</sup> was also observed during the degradation of Nafion®, which was ascribed to methyl groups formed during the breaking of bonds.<sup>149</sup>

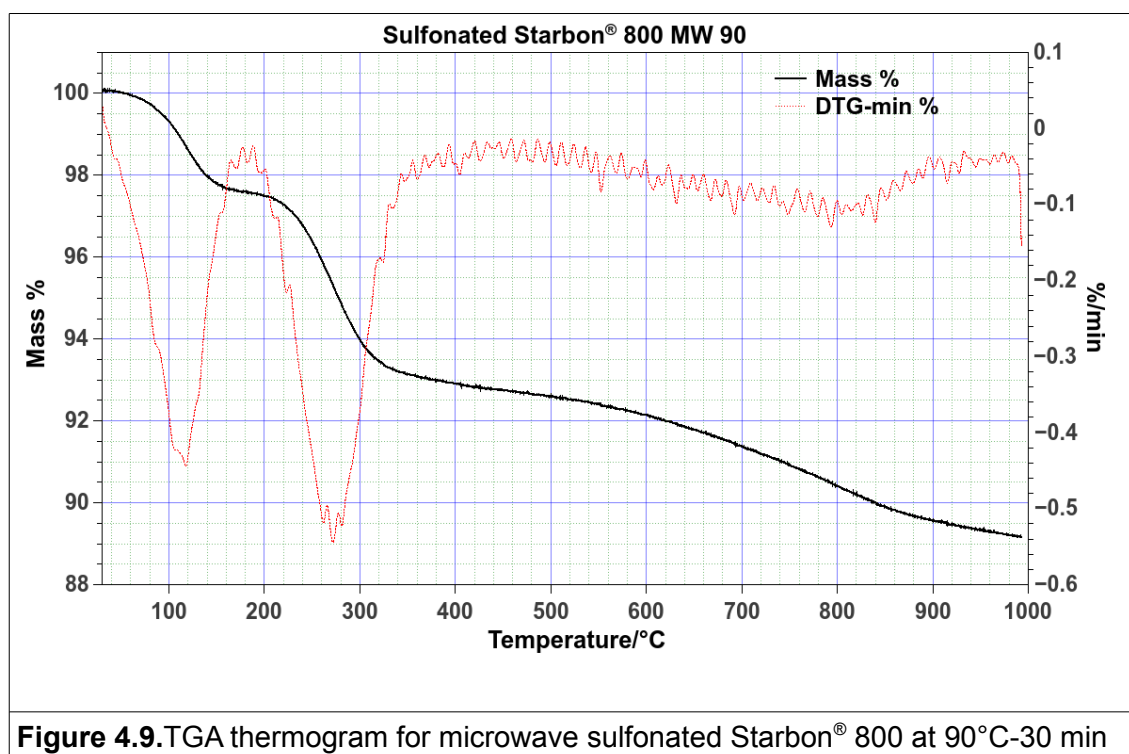
Carbon dioxide (CO<sub>2</sub>) was also identified in the gases evolving from sulfonated Starbon<sup>®</sup> 800 between 200 and 395 °C, the obtained absorbances for this gas seem very similar for the three selected temperatures. As well, IR vibrations related with water are observed coming from the sample. It is worth mentioning that CO is not distinguished for sulfonated Starbon<sup>®</sup> 800 in this narrow range of temperature in which SO<sub>2</sub> is released. This observation can be attributed to the lower observed temperature (395 °C) and also to the lower C:O molar ratio for this sample with respect to sulfonated Starbon<sup>®</sup> 300.

#### 4.4. Thermal stability of microwave sulfonated Starbons<sup>®</sup>

A study on the thermal degradation of sulfonated Starbons<sup>®</sup> prepared using microwave irradiation was also carried out with the aim to observe the main differences to the sulfonated Starbons<sup>®</sup> prepared by conventional heating. TGA thermograms for sulfonated Starbons<sup>®</sup> 300 and 800 prepared at 90 °C using MW are presented in **Figure 4.8.** and **Figure 4.9.** respectively. The TGA thermogram of sulfonated Starbon<sup>®</sup> 300 MW 90 (S300SMW90) presented in **Figure 4.8.** differs from the corresponding one for sulfonated Starbon<sup>®</sup> 300 prepared conventionally, as the microwaved sample presents three stages of decomposition: first stage, assigned as dehydration<sup>142,143</sup> occurs from 80 to 160 °C; the second stage, which would contain the splitting of sulfonic groups<sup>144,147,148</sup> is clearly observed from 200 to 280 °C, whilst this stage was not distinguished clearly in the conventional sulfonated sample, as the decomposition was constant from 200 °C up to 700 °C. The third stage of degradation is observed from 300 °C up to 800 °C at similar rates as for Starbon<sup>®</sup> 300 conventionally sulfonated, because decomposition occurs continuously; at the end of thermal treatment, weight loss reached 50 wt%.



The thermal decomposition of sulfonated Starbon® 800 prepared using microwave irradiation at 90 °C (S800SMW90) presented in **Figure 4.9.** is very similar to the degradation of sulfonated Starbon® 800 prepared by conventional heating. Three stages are observed in both samples: the first one located between 80 to 160 °C assigned to the dehydration of the material; the second stage is identified from 220 to 320 °C, in which has been identified the decomposition of sulfonic groups; the last degradation stage starts at 400 °C up to 1000 °C. The weight loss after thermal treatment is close to 11 %, with a value similar to the one obtained for the sample prepared by conventional heating.



As mentioned previously, SO<sub>2</sub> release was monitored through its absorbance at 1375 cm<sup>-1</sup> as a function of temperature. For S300SMW90, the SO<sub>2</sub> absorbance is observed in a range of 200 to 420 °C and it shows two maxima, the first one is observed at 240 °C and another at 315 °C (**Figure 4.10.a**), it appears that sulfur dioxide is released in two steps, suggesting two kinds of sulfur groups are attached to the materials. In the range of temperature from 200 to 400 °C there is a significant decrease in the weight around 15 %, which is attributed to splitting of attached sulfonic groups as well as decarboxylation and dehydroxylation of material, as shown in the FTIR spectra of the evolving gases analysed, in which traces of CO<sub>2</sub> and H<sub>2</sub>O are observed. It is interesting to note that IR spectrum obtained at 475 °C shows CO absorbance at ca. 2100 cm<sup>-1</sup> and a small peak at 3000 cm<sup>-1</sup> associated with C–H vibrations, mentioned earlier.<sup>149</sup>

Sulfonated Starbon® 800 microwaved at 90°C (S800SMW90) shows a narrow temperature range in which SO<sub>2</sub> is released, which goes from 200 to 380 °C (**Figure 4.10.b**) comparable to the sulfonated Starbon® 800 formed conventionally (S800SW3). The maximum absorbance was observed at ca. 287 °C. FTIR spectra recorded at 201, 287 and 389 °C showed CO<sub>2</sub> and water

released from the sample. It is interesting to note that the absorbance intensity for CO<sub>2</sub> is lower for Starbon<sup>®</sup> 800 sulfonated using microwave than the one prepared conventionally.

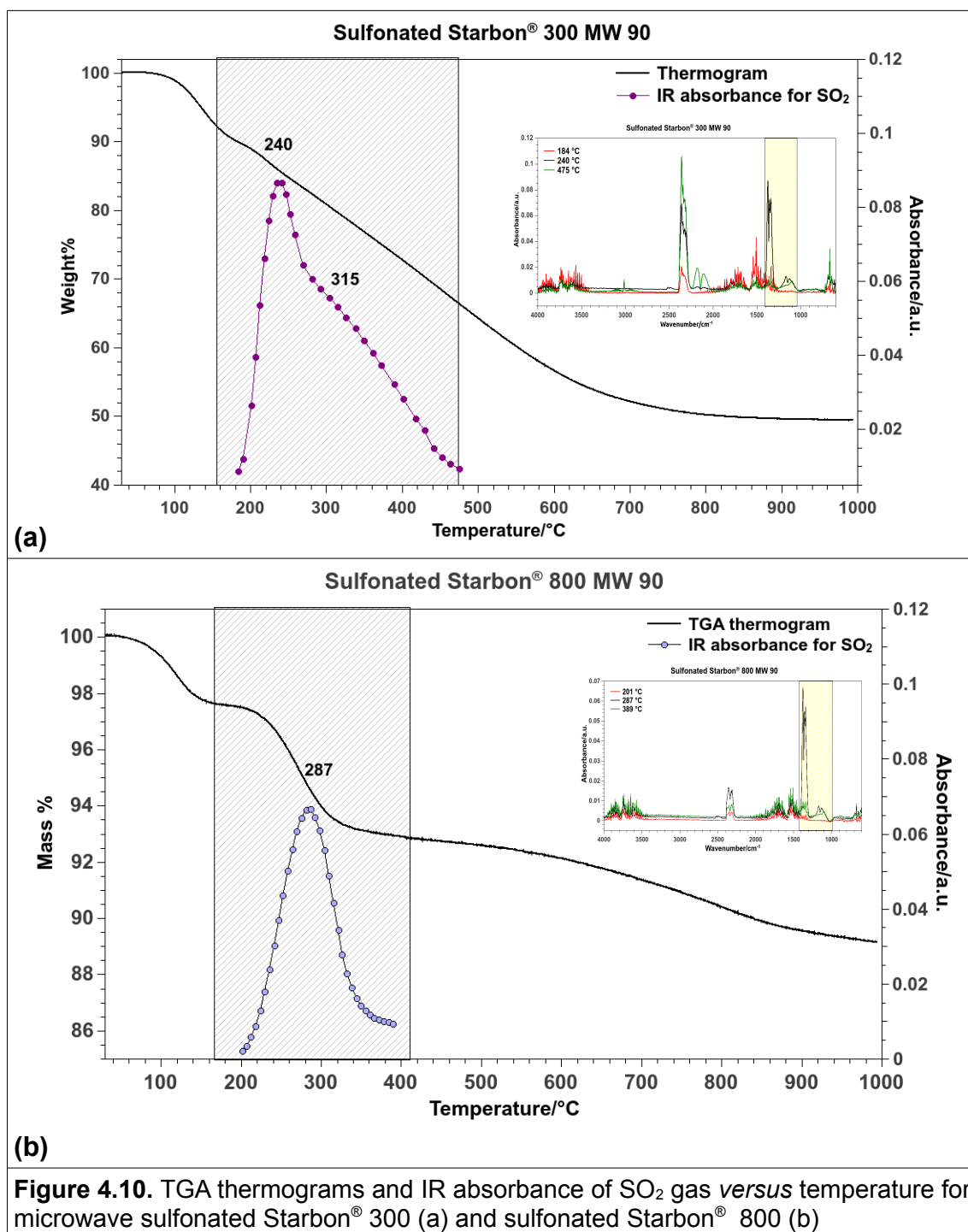


**Figure 4.10.** TGA thermograms and IR absorbance of SO<sub>2</sub> gas *versus* temperature for microwave sulfonated Starbon<sup>®</sup> 300 (a) and sulfonated Starbon<sup>®</sup> 800 (b)

#### 4.5. Sulfur dioxide released during decomposition of Starbon® 300 sulfonated at different temperatures using microwaves

Microwave sulfonation of Starbon® 300 was carried out at three different temperatures: 90, 120 and 150 °C. The weight loss for these samples present similar decomposition pattern, independent of temperature of sulfonation (**Figure 4.11.a**). A high rate of degradation from 200 to 700 °C is assigned to dehydroxylation and decarboxylation of samples as mentioned beforehand, as well as the detachment of sulfonic groups.<sup>142,145,146</sup>

The SO<sub>2</sub> release monitored as a function of temperature for these three sulfonated Starbons® 300 is presented in **Figure 4.11.b**. The profiles exhibit some similarities, a maximum in a low temperature range of 230–240 °C and with a secondary broad release over a range of temperatures, with a maximum around 300 °C. The absorbance for SO<sub>2</sub> released from sulfonated Starbon® 300 MW 150 (S300SMW150) decreases steadily over the temperature range 260 to 450 °C; whilst samples sulfonated at 90 and 120 °C have similar profiles. At this point, it is worth mentioning that sulfur content for microwave sulfonated Starbons® 300 at 90 °C and 120 °C have similar values of 0.95 and 0.98 mmol g<sup>-1</sup>, respectively, whereas the sample sulfonated at 150 °C has a slightly higher content 1.33 mmol g<sup>-1</sup>. This could therefore contribute to the wider temperature range required to break down the sulfonic groups and release sulfur dioxide.

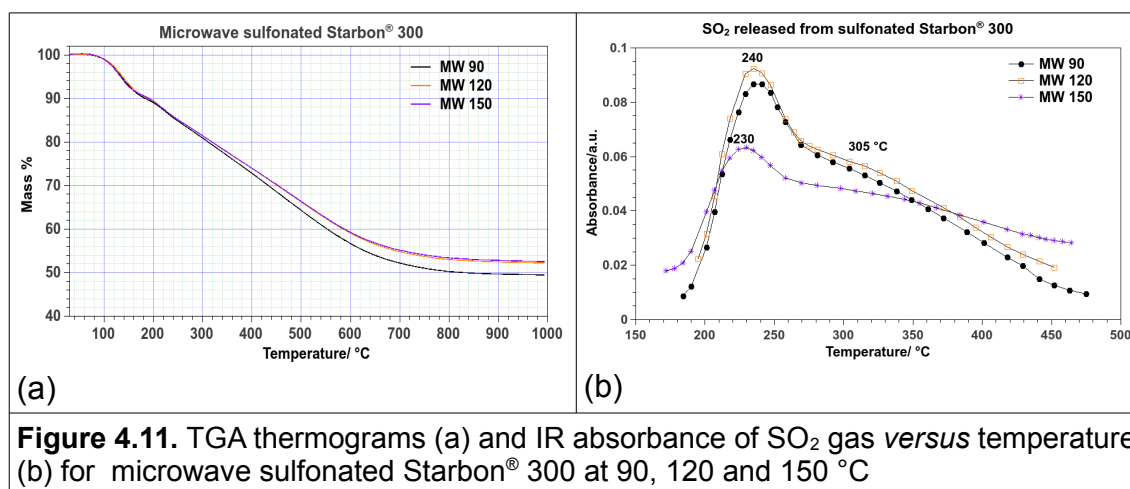


**Figure 4.11.** TGA thermograms (a) and IR absorbance of SO<sub>2</sub> gas versus temperature (b) for microwave sulfonated Starbon® 300 at 90, 120 and 150 °C

#### 4.6. Sulfur dioxide released in the decomposition of sulfonated Starbons® 800

As shown previously, the SO<sub>2</sub> absorbance observed for sulfonated Starbons® 800, present a smaller temperature range than the SO<sub>2</sub> absorbance profile obtained for sulfonated Starbons® 300. Unlike the profile obtained for sulfonated Starbons® 300, the curves correlated with the sulfur dioxide evolved from sulfonated Starbons® 800 are very symmetric and present a maximum close to 290 °C (Figure 4.12.).

The sulfur content for samples sulfonated at 90 °C have comparable values, for instance, 0.52 and 0.48 mmolg<sup>-1</sup> for conventional and microwave procedures, respectively. However, the analysis of the FTIR spectra of released SO<sub>2</sub> as a function of temperature, shows that absorbance for the microwave sample starts at lower temperatures (210 °C) than the samples prepared conventionally, in which the initial temperature of decomposition shifts to 240 °C. This observation indicates that sulfur groups attached to S800SMW90, present slightly weaker bonds. Although the sulfur content for samples sulfonated at 120 °C is a bit higher (0.76 mmolg<sup>-1</sup>), there is not a notable difference in the SO<sub>2</sub> release profile. On the contrary, the absorbance observed for this sample is lower than the one obtained for samples prepared at 90 °C. The curve of SO<sub>2</sub> release from the sample sulfonated at 120°C under microwave conditions, follows the one observed for conventional sulfonated Starbon® 800 (S800SW3), in which SO<sub>2</sub> absorbance appears at temperature over 220 °C.

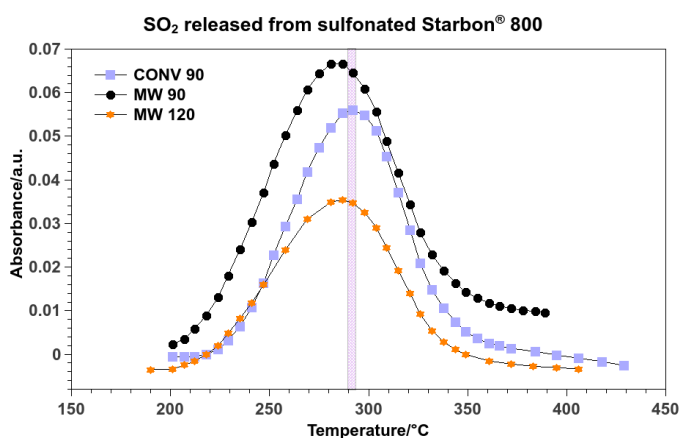


**Figure 4.12.** IR absorbances for evolving SO<sub>2</sub> as function of temperature for sulfonated Starbons® 800

The temperature at which SO<sub>2</sub> loss from sulfonated Starbons® 800 reaches its maxima is very similar to the temperatures observed for sulfonated polycyclic aromatic carbons<sup>24</sup> or for other sulfonated carbonaceous materials like lignosulfonate materials, for which a maxima at 230 °C was observed,<sup>40</sup> or of sulfonated chitosan, in which decomposition of sulfonic groups is observed between 200–250 °C.<sup>150</sup> However, the temperature of the splitting of sulfonic groups in sulfonated Starbons® is found below the range observed for Nafion®-H, which is reported as 310–380 °C<sup>151</sup> and for composites with SiO<sub>2</sub>, the temperature of SO<sub>2</sub> release is even higher, close to 600 °C.<sup>149</sup>

#### 4.7. The effect of methanol washing

As presented previously, the SO<sub>2</sub> evolution from microwave sulfonated Starbons® 300 showed a maximum at a low temperature of ~240 °C. Looking for a possible explanation for this observation, a comparison between sulfonated Starbon® 300 prepared conventionally before and after methanol washing was made. In **Chapter 3** it was mentioned that microwave sulfonated Starbons® were not washed with methanol, as the aim was to prepare stable sulfonated materials that did not require additional purification procedures. It was interesting to discover that sulfonated Starbon® prior to methanol washing has a similar profile to microwave sulfonated Starbons®, showing a maximum in the absorbance of SO<sub>2</sub> at 241 °C (**Figure 4.13**).

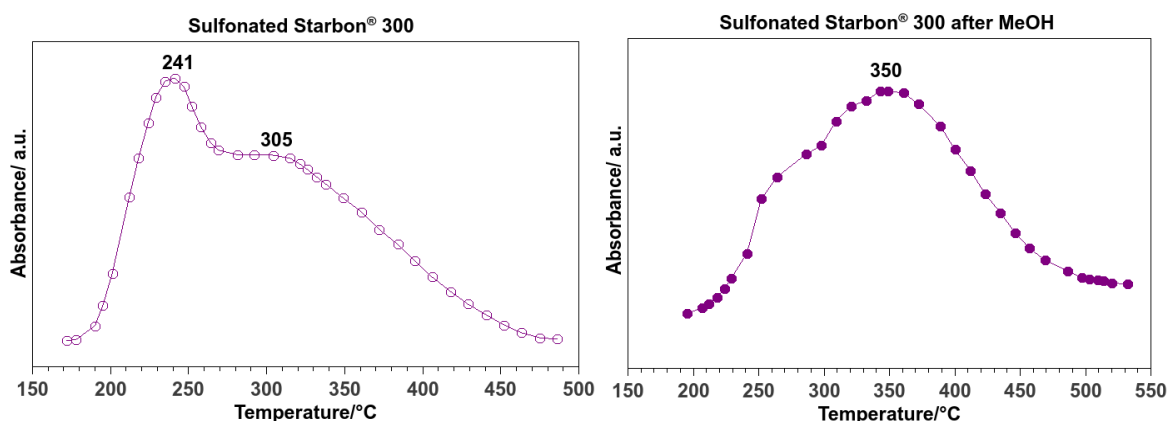


**Figure 4.13.** IR absorbances for evolving SO<sub>2</sub> from sulfonated Starbon® 300 before (left) and after (right) methanol washing

This observation would suggest that there are sulfur groups weakly bounded to the materials, whose decomposition occurs at lower temperature and could be removed with methanol using microwave treatment. These groups could be related to physisorbed sulfates, remaining from sulfuric acid used during sulfonation, the presence sulfate esters or even sulfuric acid on the surface (**Figure 4.14.**). It is also worth mentioning that another source of released  $\text{SO}_2$  could originate from desulfonation of the materials, as some authors have discussed that the detachment of sulfonic groups from sulfonated resins may occur on the very external surface of the particles.<sup>152</sup>

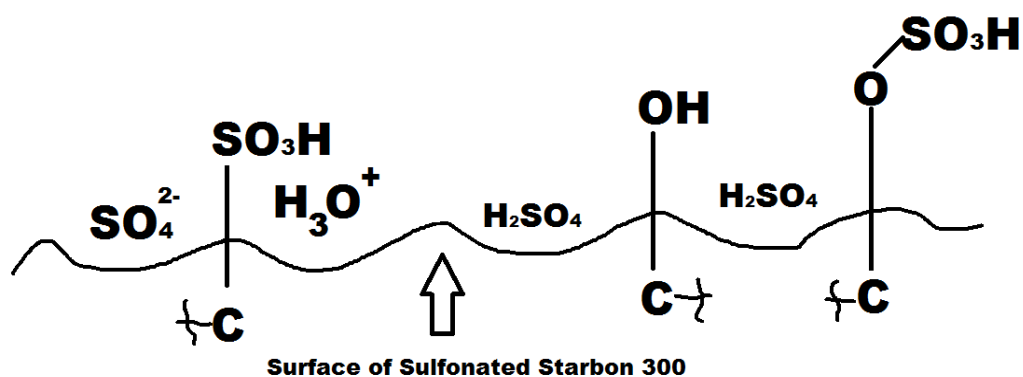


**Figure 4.14.** Schematic representation of likely sulfur groups present on surface of sulfonated Starbon<sup>®</sup> 300

Microwave sulfonated Starbon<sup>®</sup> prepared at 90 °C was also subjected to methanol treatment. The evolved  $\text{SO}_2$  profile showed a significant decrease in the maximum observed at 250 °C (**Figure 4.15**), as also observed for the previous sample treated with methanol.

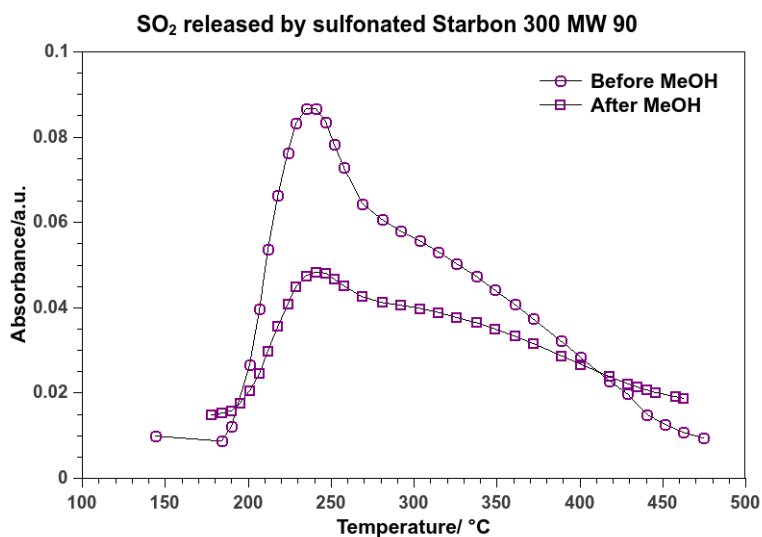


**Figure 4.15.** IR absorbances for evolving SO<sub>2</sub> versus temperature for microwave sulfonated Starbon® 300 before and after methanol washing

Elemental analysis of the materials after washing with methanol shows that the sulfur content decreases (**Table 4.2.**), indicating the removal of sulfur groups. The most significant decrease is observed for the conventional sulfonated Starbon® 300, in which the content dropped by 32%; whilst for sulfonated Starbon® 300 microwaved at 90 °C, the change is close to 8 %.

<b>Table 4.2.</b> Sulfur content (mmolg <sup>-1</sup> ) for sulfonated Starbons® 300				
		<b>Original</b>	<b>After MeOH</b>	<b>After EtOH</b>
Sulfonated Starbon® 300	<b>Conventional 90</b>	1.08	<b>0.73</b>	0.83
	<b>Microwave 90</b>	0.97	<b>0.90</b>	

Studies on the deactivation of sulfonated carbonaceous materials have been carried out by several researchers. A remarkable approach was carried out by *Mo et al.*,<sup>26</sup> whose investigation found sugar catalyst prepared by Hara's group is not as stable as they claimed.<sup>25</sup> The high activity obtained during esterification of fatty acids with methanol were achieved because of the leaching of active sites, identified as polycyclic aromatic carbons containing sulfonic groups ~SO<sub>3</sub>H. Those authors also found significant leaching of sulfonic groups in other

solvents like ethanol, water and hexane.<sup>26</sup> However, our studies using X-ray fluorescence (XRF), showed that the sulfur content leaching from sulfonated Starbons<sup>®</sup> using other alcohols like ethanol or 2-propanol were lower than the sulfur found in methanol (**Chapter 2**). Sulfur content for sulfonated Starbon<sup>®</sup> 300 after washing with ethanol is shown in **Table 4.2.**, its value is a bit higher than the one obtained for sample washed with methanol, it might allude that less sulfur groups are removed from the material.

Other studies on the deactivation of sulfonated carbon-base catalysts suggest that the decrease in catalytic activity during esterification of palmitic acid with methanol is due to the formation of sulfonic esters.<sup>153</sup> Whilst other authors attribute desulfonation of Amberlyst-15 to the hydrolysis of sulfonic acids.<sup>154</sup> At this point, it is worth mentioning that solid-state <sup>13</sup>C NMR spectra obtained for sulfonated Starbon<sup>®</sup> 300 after methanol washing, shows the formation of methoxy groups in the material (**Chapter 2**), therefore splitting of sulfonic groups via hydrolysis or methanolysis could happen.

Another approach to explain the decrease in the activity of sulfonated carbons is related to structural changes in the material, such as through swelling and opening of the structure using methanol in the production of biodiesel.<sup>155</sup> In our study then, methanol may allow to open the structure of sulfonated Starbons<sup>®</sup> allowing the interaction with those “weak” sulfur groups attached on the surface, promoting their removal.

#### **4.8. Physisorbed sulfuric acid?**

To try to discover whether the SO<sub>2</sub> released at lower temperature (~240 °C) was related to an excess of sulfuric acid due to the lack of washing, an analysis of the sulfonated Starbon<sup>®</sup> 300 microwaved at 150 °C only washed once was performed. This sample corresponds to the material washed with water at room temperature, immediately after filtration of the reaction mixture (**Figure 4.16.**).

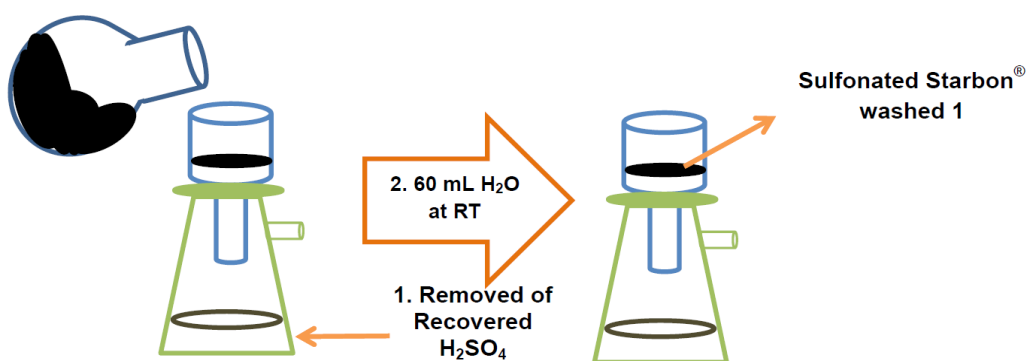


**Figure 4.16.** Schematic representation of sulfonated sample at the first wash

The absorbance of  $\text{SO}_2$  evolved from sulfonated Starbon<sup>®</sup> 300 washed once as a function of temperature, shows a prominent maximum at 212 °C (**Figure 4.17a**). The release of  $\text{SO}_2$  starts at a relatively low temperature, ~150°C, with respect to previous samples. The  $\text{SO}_2$  released from the excess of sulfuric acid appears in a temperature range from 150 to 260 °C. After this point, the evolving  $\text{SO}_2$  decreases gradually up to 450 °C. After 14 washes (**Figure 4.17b**), the released  $\text{SO}_2$  profile changes significantly, as the appearance of  $\text{SO}_2$  determined by FTIR starts at 180 °C and the maximum of the absorbance obtained from sulfonated sample shifts to a higher temperature, at 230 °C. There is a small inflection in the curve at ~260 °C and after this temperature the absorbance of sulfur dioxide decreases gradually up to 450 °C. These observations would insinuate that excess or physisorbed sulfuric acid decomposes at lower temperatures.

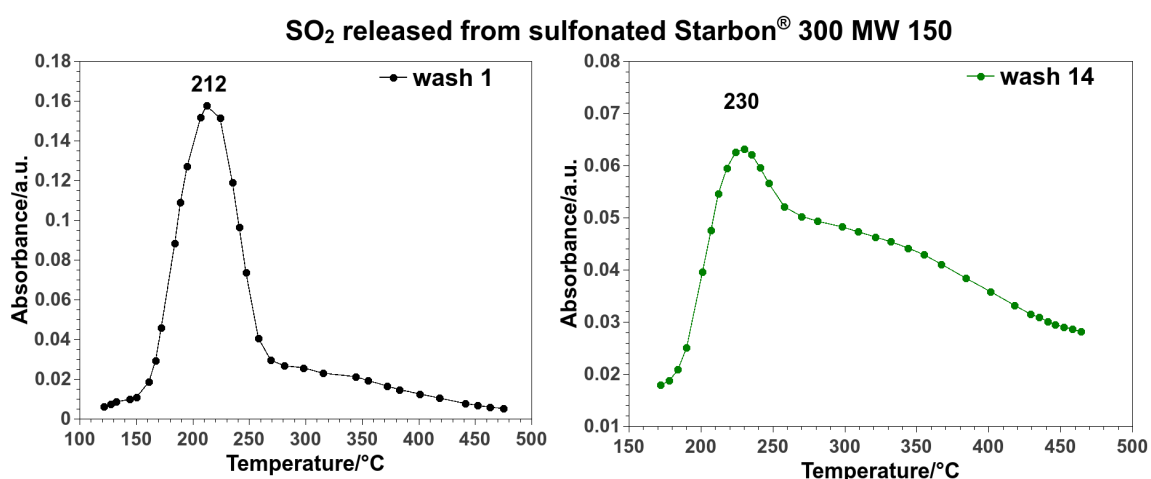


**Figure 4.17.** IR absorbances for evolving  $\text{SO}_2$  versus temperature for sulfonated Starbon<sup>®</sup> 300 microwaved at 150 °C after first wash (a) and after 14 washes (b)

#### 4.9. FTIR spectra of sulfonated Starbons<sup>®</sup>: looking at washing effect

As presented in **Scheme 4.2.**, there are several possible sulfur functionalities on the surface of sulfonated Starbons<sup>®</sup>. Combined with the changes observed in the sulfur dioxide release profiles during thermal decomposition of the materials, it was further proposed to investigate their surfaces, looking at the infrared spectra (FTIR-ATR) of the materials before and after washing treatments. **Figure 4.18.** shows the spectra for sulfonated Starbon<sup>®</sup> 300 microwaved at 150 °C after the first and fourteenth washes. The spectrum shows distinguishable differences, such as the massive decrease in the band centered at 1030 cm<sup>-1</sup> after 14<sup>th</sup> washes. This band has been assigned to S=O stretching vibrations, previously.<sup>83</sup> It is also interesting to notice the disappearance of bands situated at ~1210 cm<sup>-1</sup> which could be attributed to sulfuric acid,<sup>156</sup> along with the band located at ca. 950 cm<sup>-1</sup>. The presence of sulfate ions, SO<sub>4</sub><sup>2-</sup>, has been attributed to vibrations observed at 680–650 cm<sup>-1</sup> according to Socrates' infrared characterisation chart.<sup>83</sup> Whilst bands observed at 870 and 770 cm<sup>-1</sup> could be assigned to asymmetric and symmetric vibrations, of the S–O–C bond in sulfate esters.<sup>83,157,158</sup>

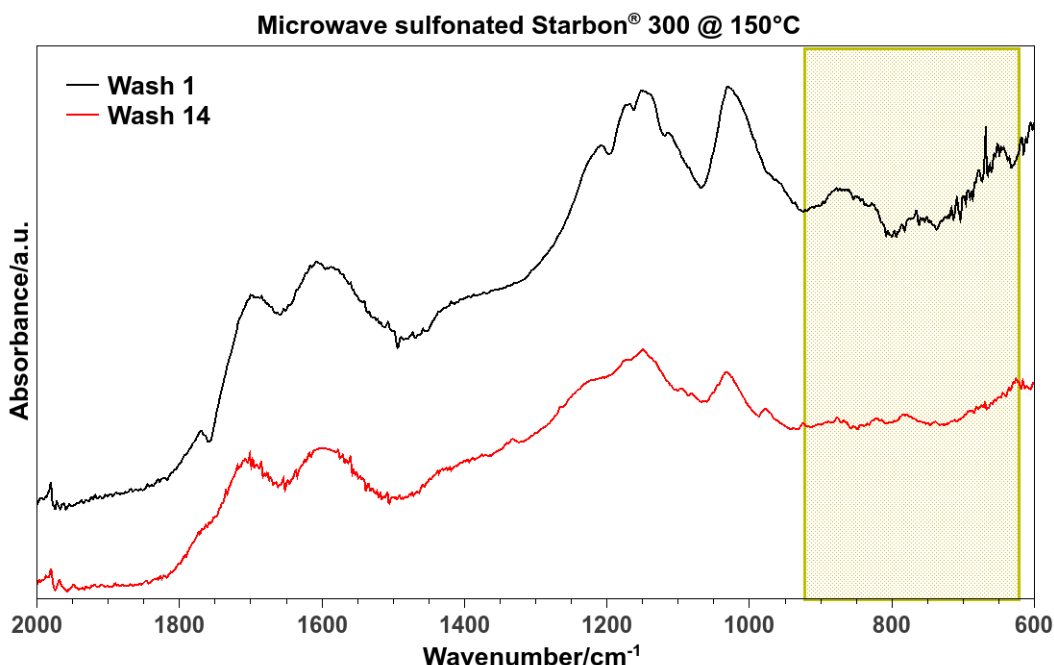


**Figure 4.18.** Infrared spectra of microwave sulfonated Starbon<sup>®</sup> 300 prepared at 150 °C, after the first and fourteenth washes.

The changes in the spectra of sulfonated Starbons after methanol washing (**Figure 4.19**) are less obvious than the changes observed after several washes with hot water presented in the previous spectra. The most visible change is the diminution in intensity and broadness of the band situated at  $1030\text{ cm}^{-1}$ , as well the flattening of bands situated at  $1180$  and  $980\text{ cm}^{-1}$ , which are tentatively attributed to vibrations of sulfates and sulfuric acid, respectively.<sup>83</sup>

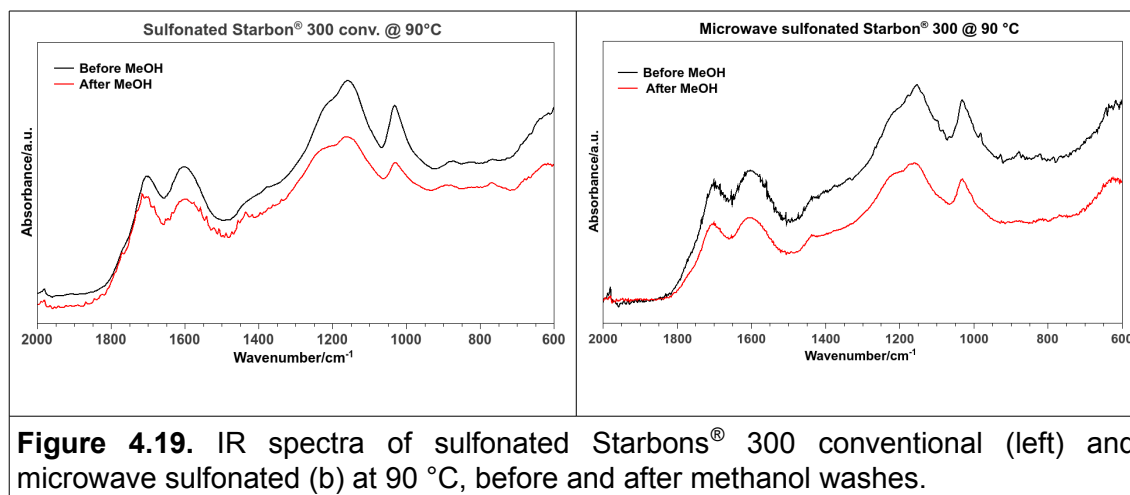


**Figure 4.19.** IR spectra of sulfonated Starbons<sup>®</sup> 300 conventional (left) and microwave sulfonated (b) at  $90\text{ }^{\circ}\text{C}$ , before and after methanol washes.

#### 4.10. Conclusions

Studies on thermal stability of sulfonated Starbons<sup>®</sup> using the coupled technique TG-IR were carried out. The analysis of  $\text{SO}_2$  released during heating of sulfonated Starbons<sup>®</sup> showed that sulfonated Starbons<sup>®</sup> 300 present a broader temperature of release range than sulfonated Starbons<sup>®</sup> 800. This suggests that sulfur is attached to the structure of sulfonated Starbons<sup>®</sup> 300 (via sulfur-carbon or sulfur-oxygen bonds) in a more stable way than in sulfonated Starbon<sup>®</sup> 800. This can also be related to the number of uses of those catalysts during esterification reactions, as sulfonated Starbon<sup>®</sup> 800 loses its activity in fewer cycles than sulfonated Starbon<sup>®</sup> 300.

TG-IR analysis also allowed the analysis of the effect of repeated washings on sulfonated Starbons<sup>®</sup>. It was found that samples with an excess of sulfuric acid released  $\text{SO}_2$  at lower temperatures ( $212^{\circ}\text{C}$ ) than samples after 14 washes ( $230^{\circ}\text{C}$ ). This observation suggests that low temperature  $\text{SO}_2$  release can be

related to physisorbed sulfuric acid. This was further confirmed by the analysis of FTIR spectra.

A change in the SO<sub>2</sub> release profile is observed in sulfonated Starbon® 300 after washing with methanol, as the maximum observed at ~240 °C does not appear in the SO<sub>2</sub> profile of the sample after the sample is washed with methanol (3 times), this suggests that methanol could remove weak bonded sulfur components.

Quantification of sulfur dioxide released during sulfonation of Starbons® using hydrogen peroxide solution could be a useful tool to get more information about sulfonation mechanisms, trying to correlate the sulfur species involved, like the SO<sub>2</sub> released, the sulfur content on sample with the initial content of sulfuric acid. However, this approach needs to be improved.



## **Chapter 5**

### ***Uses of sulfonated Starbons<sup>®</sup> in esterifications***



## 5.1. Introduction

Since the end of last century, the efforts to find alternatives to displace the petroleum-based materials and build a strong bio-based industry have increased significantly. Among the molecules identified as “platform” are found several organic acids, i.e. levulinic acid, succinic acid, etc. The development of this biorefinery industry also includes the transformation of fatty acids through esterifications or transesterifications.<sup>159,160</sup> Then, the exploration of chemical reactions of some of these platform molecules would be of interest using our also biobased catalysts, Starbons®.

Esterification is one of the most fundamental reactions in organic chemistry extensively employed in industrial synthesis of several products that include fragrances, monomers, solvents, plasticizers, etc.<sup>161</sup> Esters are produced when carboxylic acids react with alcohols; although esterification is a self-catalysed reaction due to the presence of the “acid”, it is slow, requiring catalysts to proceed. The catalysts promote the protonation of the carbonyl oxygen on the carboxylic group, activating nucleophilic attack by an alcohol to form a tetrahedral intermediate. Release of a water molecule leads to the formation of the ester.<sup>162</sup> (See **Figure 5.1.**)

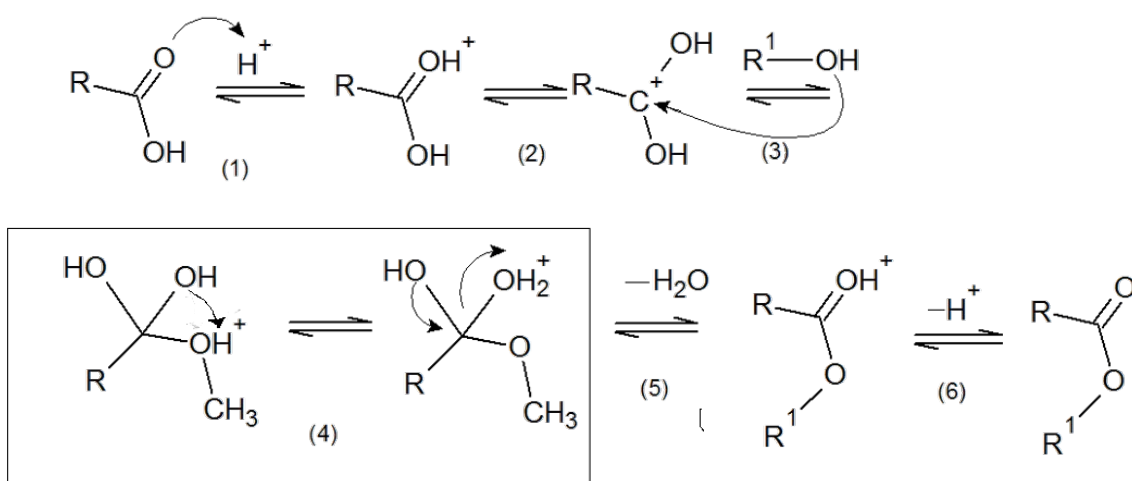


**Figure 5.1.** Mechanistic route of acid catalysed esterification (adapted from Liu *et al*, 2006)

Many industrial esterification processes are carried out using mineral acids such as sulfuric acid, hydrofluoric acid or phosphoric acid; however, these are considered as environmentally unfriendly catalysts due their toxicity, difficulty in handling and disposing, as well, because of the amount of waste formed.<sup>10</sup> Several approaches to get efficient solid-acid catalysts based on silica or aluminosilicates materials and mesoporous zirconia-based have been developed,<sup>10,24,25</sup> in which the key properties wanted include thermal and chemical stability and evenly distributed of the active sites on the materials. In this sense, mesoporous sulfonated Starbon<sup>®</sup> become to an alternative to be used in acid-catalysed reactions. In the early stages of production of sulfonated Starbons<sup>®</sup>, a comparison with other acid catalysts (zeolites, sulfated zirconias and acidic clays) was performed in the esterification of diacids in aqueous media, results showed that Starbons<sup>®</sup> were superior in those conditions.<sup>13</sup> The high activity observed in Starbons<sup>®</sup> is attributed to their mesoporosity as well as to the hydrophobic/hydrophilic ratio of the functional groups present in the material, promoting the effectiveness in the esterification of those chosen diacids. Preliminary synthesized Starbons<sup>®</sup> have been also tested in other acid-catalysed reactions<sup>13,163</sup> as well as glycerol transformations. As mentioned previously, tests in esterification reactions like succinic acid<sup>14,75</sup> have been carried out using Starbons<sup>®</sup>, however the conditions used water in the media, then an examination of Starbons<sup>®</sup> activity in usual conditions (without water) were of interest.

In this chapter is presented the tests carried out in esterification reactions using the new sulfonated Starbons<sup>®</sup> as solid acid catalysts. The aim is to get a general overview of the performance in catalysis of this range of sulfonated Starbons<sup>®</sup>, as described in **Chapter 2**, which were prepared in a wider carbonization temperature range and using a different starting material: *Cleargum* starch. It is worth remembering that these new sulfonated Starbons<sup>®</sup> present other main variations from previous synthesized Starbons<sup>®</sup> as they were manufactured at a larger scale: carbonization (over 10 Kg) and sulfonation (80 g) compared with the small quantities prepared previously. Other modifications in the preparation of sulfonated Starbons<sup>®</sup> were the suppression of “conditioning steps” with toluene after sulfonation, looking for a greener method to achieve an “ideal

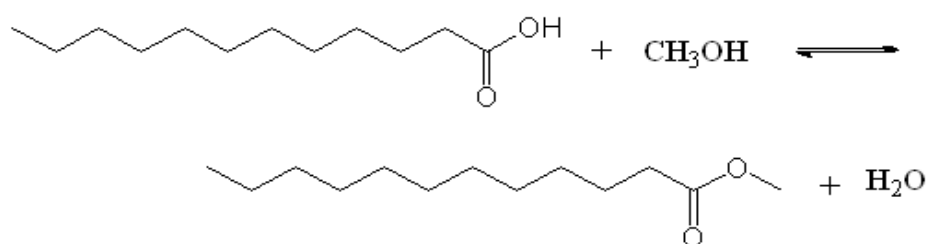
synthesis”<sup>1</sup>, decreasing the number of reagents and steps in preparation and avoiding some toxic components. The 300, 400 and 800 were examined “as received” and the other Starbons<sup>®</sup> were prepared from these by lab-scale carbonization of the 300 to produce 350 and 400 for further temperatures. Sulfonation was carried out at 1 g Starbon:7 mL H<sub>2</sub>SO<sub>4</sub> (95%) ratio, using less pure sulfuric acid than before (99.999%)<sup>13</sup>, and increasing the ratio of Starbon<sup>®</sup> to acid to a more realistic level. Further reduction in acid content led to mixtures which were very hard to stir.

Monitoring of the performance of sulfonated Starbons was done through the conversion of the ester through GC analysis. At this point, it is worth mentioning that the approximation to the conversions was done in a simplified way only considering the peak area ratios of the ester and acid observed in the GC chromatogram. This would not affect the relative trends observed in the performance of the materials in esterifications.

## 5.2. Esterification of lauric acid

### 5.2.1. Microwave irradiation or conventional heating?

Studies on the esterification of lauric acid by methanol (**Scheme 5.1.**) were carried out using sulfonated Starbons<sup>®</sup> (S-Starbons<sup>®</sup>), prepared as mentioned in **Chapter 2.**



**Scheme 5.1.** Esterification of lauric acid by methanol

The reaction was done using conventional heating and microwave irradiation to compare the effectiveness of both procedures. **Figure 5.2.** shows that for the chosen S-Starbons<sup>®</sup> 300 and 800, higher conversions are obtained in 30 minutes of reaction using microwave than 12 hours of reaction in refluxing

methanol. Similar conversions over 80 % are observed for both catalysts using microwave irradiation; however, when the reaction is done by conventional heating, the lower temperature S-Starbon® 300 seems to be more effective in the reaction than S-Starbon® 800, as the difference in conversion is more evident: 77 % of conversion for S-Starbon® 300 and less than 50 % for S-Starbon® 800. Conversions for blank reactions of esterification of lauric acid with methanol are lower than 10% for both procedures (conventional and microwave-assisted reactions). This observation is similar to previous reports that describes decreasing reaction times, combining microwave irradiation and sealed vessel processes.<sup>164</sup> The significant difference between conversion obtained using S-Starbon® 800 and S-Starbon® 300 could be attributed to the availability of acid sites on the material. As it was shown in **section 2.6.**, S-Starbon® 800 contains less sulfur than S-Starbon® 300; and part of this sulfur is found as reduced sulfur according to the oxidation states study done by XPS. Then, microwave-assisted chemistry may allow to reach high conversions because the energy transfer efficiency<sup>120</sup> together with the fact that reaction reached higher temperature (~105 °C) than conventional heating reactions, carried out in refluxing methanol (~70 °C); the difference between temperatures is over 30 °C which could be very significant to achieve high conversions.

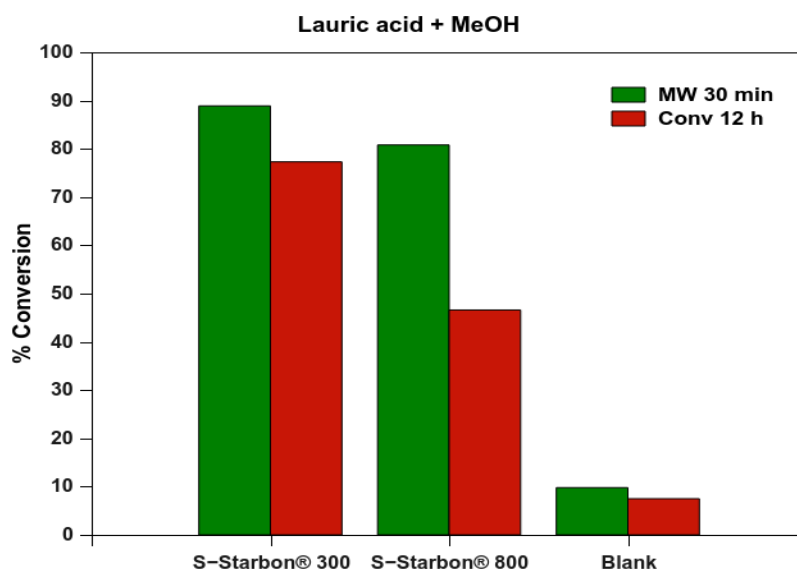


**Figure 5.2.** Comparison of the esterification of lauric acid by methanol using microwave irradiation and conventional heating

### 5.2.2. Microwave irradiation: time effect

Effect of the reaction times for the esterification of lauric acid with methanol using microwave irradiation was investigated. A different reaction was run every time due to set-up of the microwave system, reactions were carried out at closed vessel with automatic cooling, making difficult to take samples at established times. Time of reaction comprehends the total reaction time, including ramping and holding time at determined temperature. **Figure 5.3** shows the performance of the reaction of lauric acid and methanol at fixed power 200 W, using S-Starbons<sup>®</sup> 300 and 350 as catalysts. For S-Starbon<sup>®</sup> 300, high conversion is observed during 5 minutes of reaction, obtaining over 60 %; increasing time to 10 minutes, conversion slightly increases to 70 %; conversion reaches 85 % when time is set to 20 minutes; after 30 minutes of reaction, conversion did not change significantly from previous time, ~85 %; increasing reaction times up to 45 minutes, conversion rises to 95 %. However, the behaviour for S-Starbon<sup>®</sup> 350 differs from the S-Starbon<sup>®</sup> 300, as the former shows a very low conversion for 5 minutes reaction; when time increases to 10 minutes, the increment is very pronounced, since it changes from 13 % to 58 %; whilst the reaction time increases up to 20 minutes, the conversion changes to 77 %; after 30 minutes the conversion observed is 84 %. After 40 and 45 minutes of reaction, both S-Starbons<sup>®</sup> 300 and 350 showed conversions of approximately 95 %.

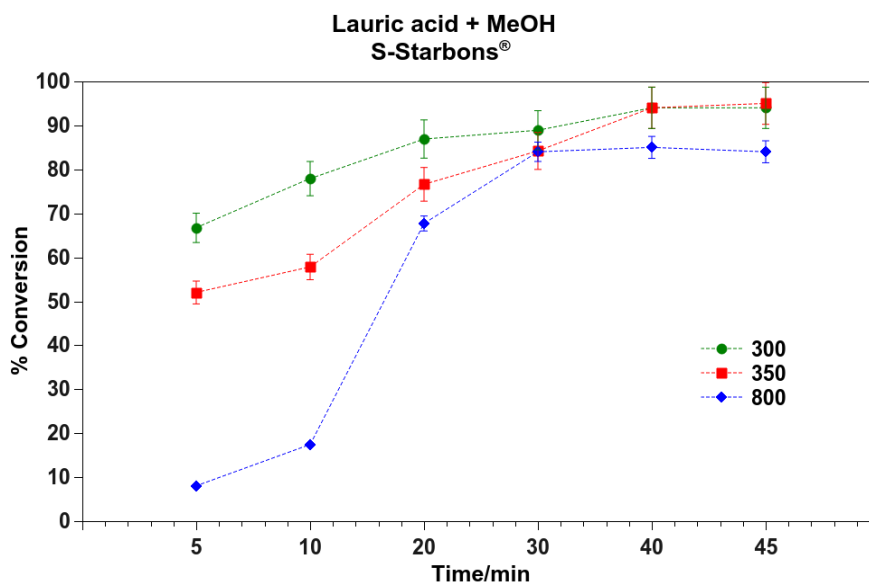


**Figure 5.3.** Esterification of lauric acid by MeOH at different times (MW fixed power 200 W)

### 5.2.3. Evaluation of Sulfonated Starbons®

As mentioned previously, a range of carbonized Starbons® were sulfonated and tested in esterification reactions. Then, reaction time set to 30 minutes and fixed power at 200 W were chosen to evaluate the performance of the range of prepared S-Starbons® in the esterification of lauric acid (5 mmol) by methanol (75 mmol); using 20 mg of catalyst. In **Figure 5.4.**, it can be observed that, when using low temperature S-Starbons®, 300 to 450, higher conversions are obtained; however, there is a decrease in the conversion when pyrolysis temperature of Starbon® increments up to 600, showing a deficiency in the catalytic activity. This is then reversed, with high temperature S-Starbons®, 700 and 800 showing conversions similar to those obtained using low temperature S-Starbons®. It is interesting to note that trend observed in conversion in the esterification of lauric acid with methanol is very similar to the trend in bulk sulfur determined on the materials and presented in **Figure 2.12.** Decreasing in catalytic activity with increased of carbonization temperature of carbon-base materials have been reported previously.<sup>28,30</sup> This has been attributed to difficulty of sulfonation of high-temperature carbonized materials, then lower -SO<sub>3</sub>H groups are attached to the carbonaceous catalyst.<sup>30</sup> However, these

approaches did not perform carbonizations over 700 °C and origins of materials are different from Starbons®.

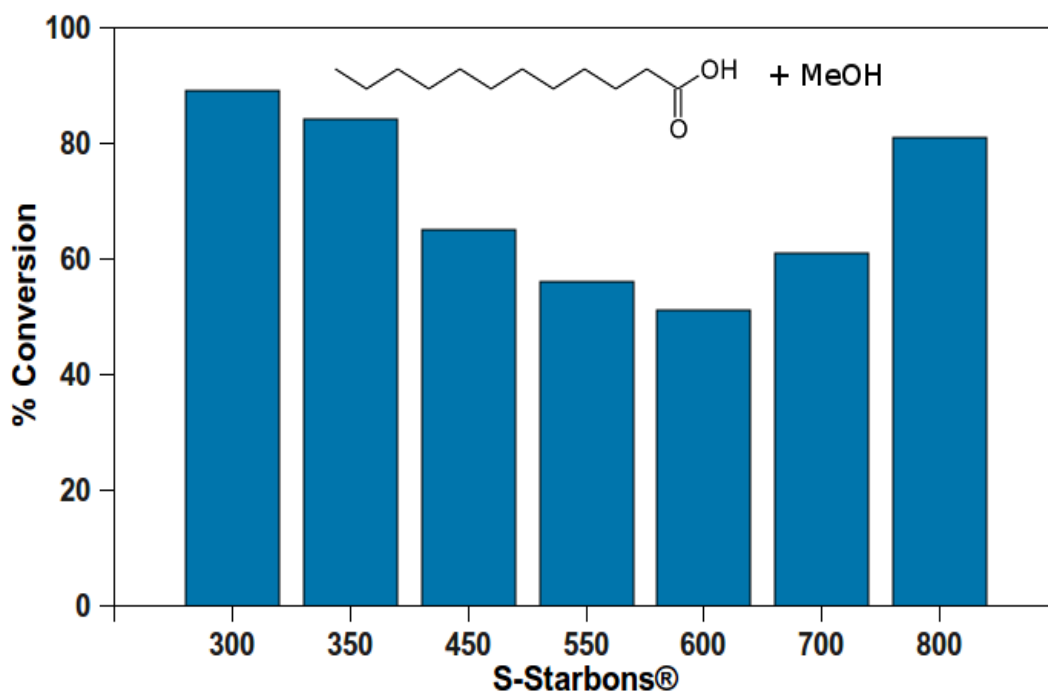


**Figure 5.4.** Conversion in the esterification of lauric acid by MeOH using S-Starbons® (30 min, 200W)

The esterification of lauric acid by ethanol was also examined to compare with the reaction using methanol. In this study, S-Starbons® 300, 450 and 800 were evaluated. As **Figure 5.5.** shows, conversion is lower in all cases for the esterification of lauric acid using ethanol. The decrease is more perceptible for S-Starbons® 300 and 800; although similar results are found for the three chosen catalysts, conversions in all cases falling between 45-55 %. It seems that maintaining the same quantity of catalyst, 20 mg, is not enough to get conversions similar to the ones obtained in the esterification of lauric acid by methanol. The decrease in reactivity could be related to the increasing chain of primary alcohol.<sup>165</sup>

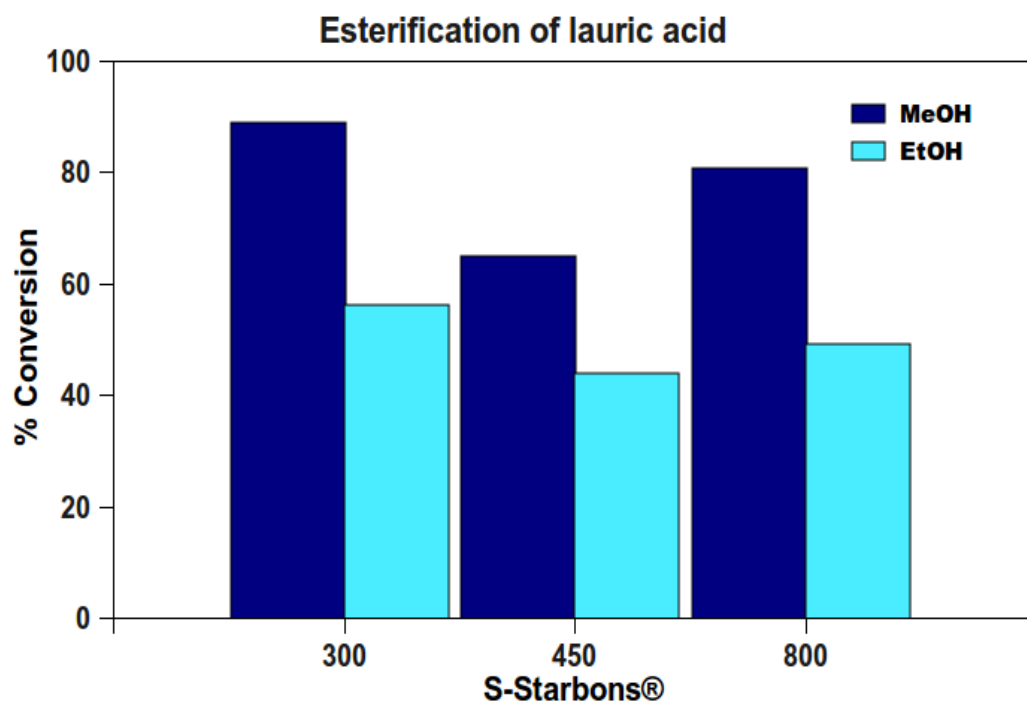


**Figure 5.5.** Comparison of the esterification of lauric acid using MeOH and EtOH (30 min, 200 W)

Esterification of lauric acid by ethanol using 20 mg showed conversions around 50 %, reactions with a higher catalyst loading (40 mg/ 4 wt%) were also carried out. In **Figure 5.6**, it can be seen that low temperature S-Starbons® 300 and 350 achieved conversions over 80 %; however for the high temperature ones, conversions are less than 60 %. It is worth mentioning that increasing the quantity of catalyst for S-Starbon® 800 did not show an obvious improvement, since the conversion for 20 mg was 49 % and using double quantity, 40 mg, conversion raised up to 59 %. In the case, of S-Starbon® 300, the difference in conversion was more noticeable, as it changed from 56 % to 84 %. The behaviour of catalysts are very similar to the one observed using methanol, low-temperature Starbons® (300 and 350) present higher conversions, then there is a drop in the middle of the range, S-Starbon® gives the lowest conversion for both alcohols; then a slight increase is obtained for S-Starbons® 700 and 800. As mentioned, previously, it seems to maintain a relation with the sulfur groups loading on materials, as S-Starbon® 600 presents the lowest bulk quantity. With respect to the fact that both Starbons® 700 and 800 did not get comparable conversions to the ones obtained using methanol, could be referred as a bulky

hindrance interaction between materials and reagents. A screening in the performance of S-Starbons in the esterification of lauric acid by i-PrOH using 20 mg of catalyst was carried out, however conversions were very low, then no more studies were done.

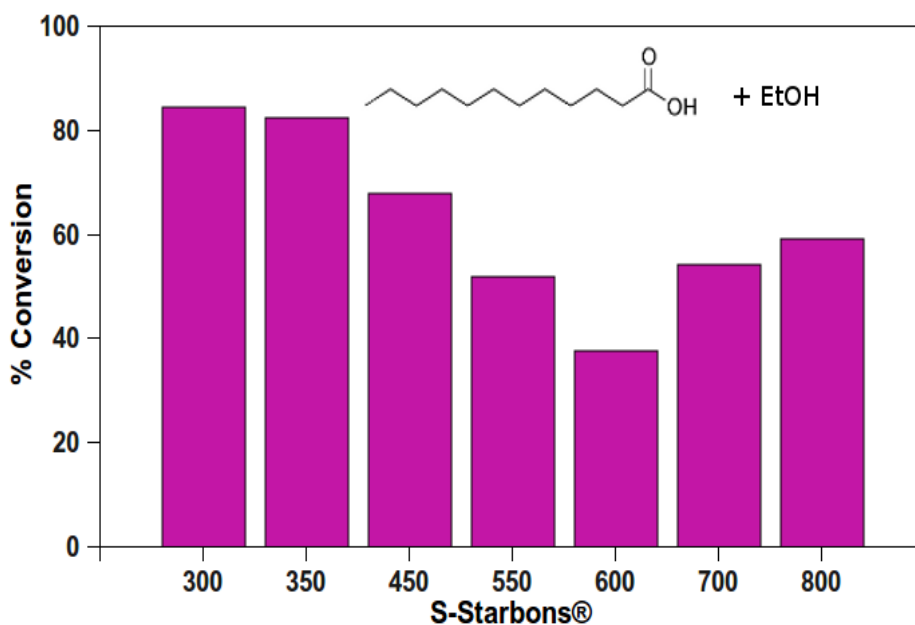


**Figure 5.6.** Esterification of lauric acid by EtOH, using 40 mg S-Starbons® (30 min, 200 W)

#### 5.2.4. Reusability of S-Starbons®

One of the main concerns when working with catalysts is lifetime. A study of the deactivation of S-Starbons® was also done. Chosen catalysts were the two extremes of the range of carbonized S-Starbons®, 300 and 800, the performance of which was evaluated in the esterification of lauric acid by methanol. Reactions were carried out as previous studies: 5 mmol of lauric acid, 3 mL of methanol and 20 mg of catalyst using microwave irradiation 200 W for 30 minutes. A summary of the recovery and reuse treatment is presented in **Figure 5.7**, acetone was used to remove unreacted lauric acid on materials.

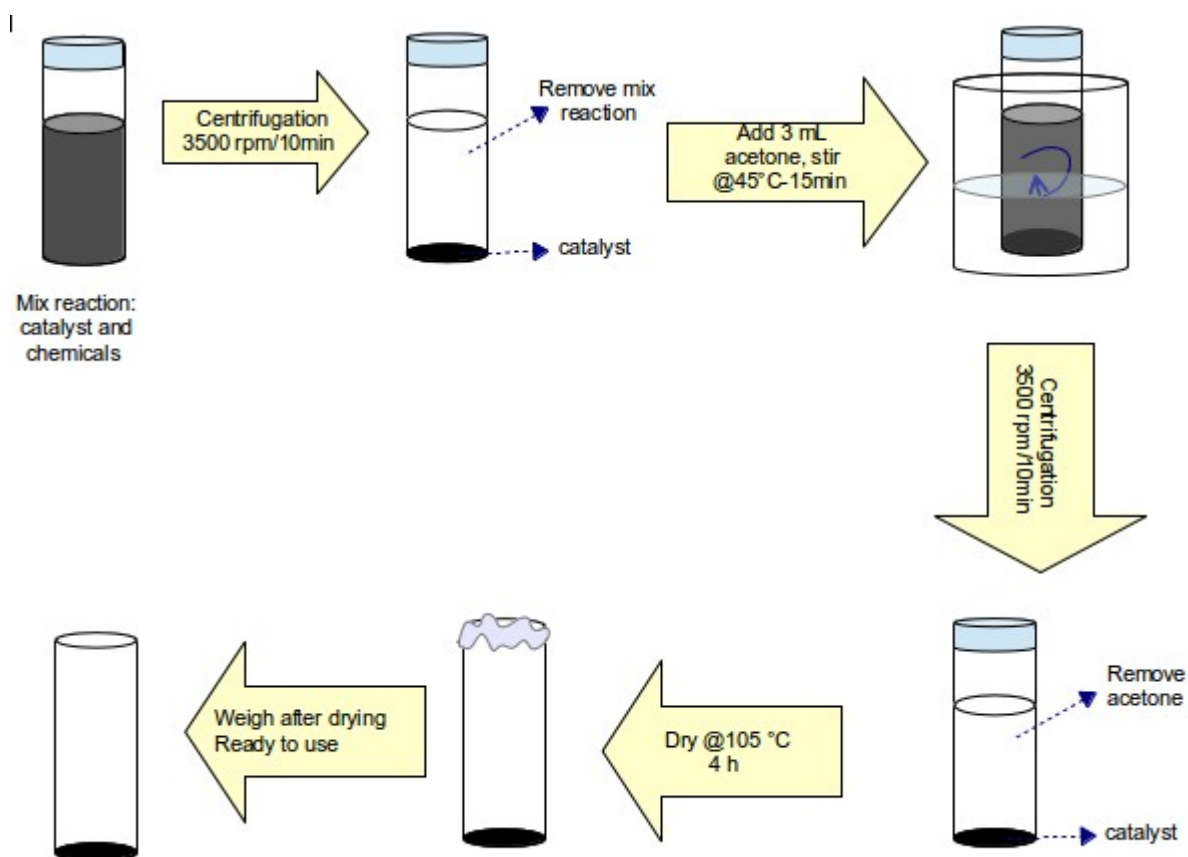


**Figure 5.7.** Diagram of recovery and reuse of catalyst

When S-Starbon<sup>®</sup> 300 is compared with S-Starbon<sup>®</sup> 800, it is found that the latter loses its activity after the third run, dropping to less than 40 %, meanwhile, conversion obtained using S-Starbon<sup>®</sup> 300 remains steady at around 60 % after five runs (**Figure 5.8**). The lack of activity observed in S-Starbon<sup>®</sup> 800 could be attributed to the lower quantity of sulfonic groups attached to the material, compared with S-Starbon<sup>®</sup> 300, shown in **Chapter 2**. This decrease in activity can be also correlated with the findings presented in **Chapter 4** about more stable sulfur groups attached to sulfonate Starbons<sup>®</sup> 300.

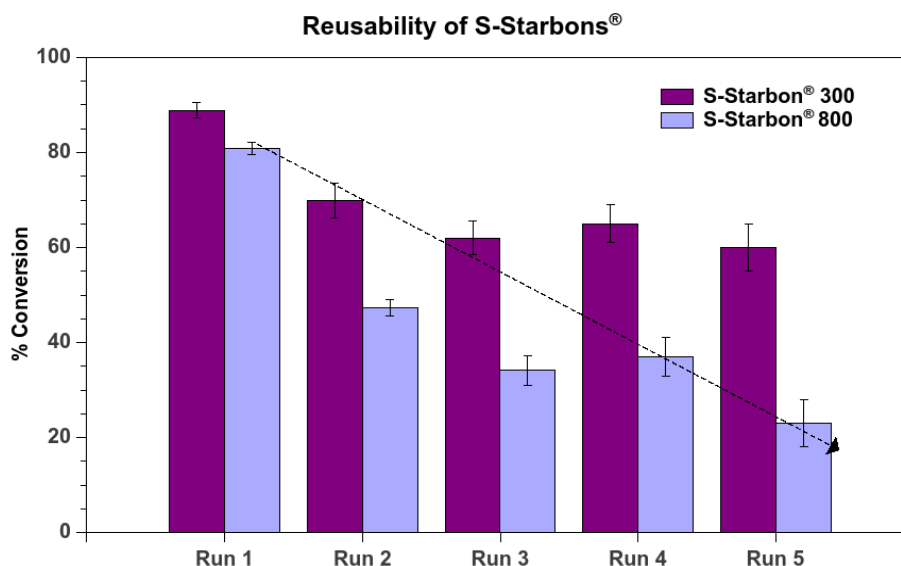


**Figure 5.8.** Reusability of S-Starbons® 300 and 800 in esterification of lauric acid with methanol

### 5.3. Esterification of levulinic acid

Levulinic acid or 4-oxo-pentanoic acid (**Figure 5.9.**) is a product formed by treatment with acid of 6-carbon sugar carbohydrates from starch and lignocellulosics. This material has been identified as one of the top value added chemicals from biomass, as it can serve as a primary biorefinery building block and a platform chemical because it can be transformed to other valuable compounds. The high reactivity of this compound could be attributed to its functional groups: a ketone group and carboxylic group; making this material very attractive for several chemical reactions.

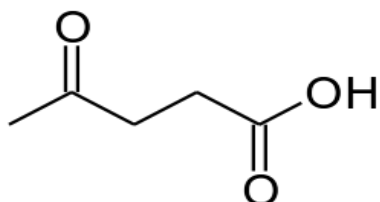


**Figure 5.9.** Molecular structure of 4-oxo-pentanoic acid/levulinic acid

In the present work, esterification of levulinic acid with methanol and ethanol was carried out using sulfonated Starbons<sup>®</sup>. During the monitoring of esterification of levulinic acid by Gas Chromatography (FID) an extra peak was observed in the chromatogram (**Figure 5.10**) aside from the methyl ester and levulinic acid; this peak was attributed to an “intermediate” and its identity will be discussed further. An interesting observation about this component was its appearance and permanence through the course of the reactions.

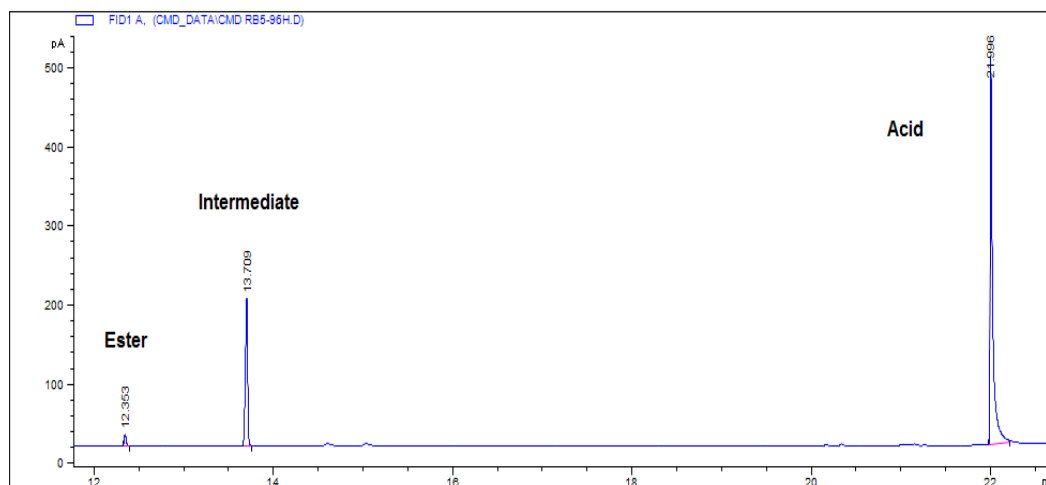


**Figure 5.10.** GC -FID chromatogram of mixture of levulinic acid and methanol (1:15, day 4)

Conversions to ester or intermediate were measured using the GC peak areas obtained in the chromatogram as mentioned initially; as the only components observed are the “products” and the “acid”, the determination of intermediate was done as following:

$$\% i = \frac{Area_i}{\sum_{i=1}^{i=n} Area_i}$$

One of the first approaches to study the activities of sulfonated Starbons<sup>®</sup> 300 and 800 (S-Starbon<sup>®</sup> 300 and S-Starbon<sup>®</sup> 800 respectively) consisted of monitoring the esterification of levulinic acid in refluxing methanol at different run times. A blank reaction (without catalyst) was also carried out under the same conditions. Ester was not found in the blank reaction, during the 12 hours

of running (**Figure 5.11.**). Comparison between the sulfonated Starbons<sup>®</sup> aforementioned, showed that S-Starbon<sup>®</sup> 300 promotes the conversion to ester in 5 % after 30 minutes of reaction, which subsequently increases up to 78 % after 12 hours. For S-Starbon<sup>®</sup> 800, ester formation appears in 10 % after 4 hours of reaction, the maximum obtained is 40 % in 12 hours of reaction (**Figure 5.11 a**). This suggests the S-Starbon<sup>®</sup> 800 has lower activity than S-Starbon<sup>®</sup> 300, which could be attributed to the quantity and type of sulfur groups attached to the materials, already discussed in **Chapter 2**. In Section 2.2 it was found that S-Starbon<sup>®</sup> 300 has higher sulfur content (0.73 mmolg<sup>-1</sup>) than S-Starbon<sup>®</sup> 800 (0.52 mmolg<sup>-1</sup>) combined with the XPS results about reduced sulfur (IV) present in high-temperature Starbons<sup>®</sup>.

The first measurement of the intermediate appearance in the blank reaction was 16 %; as time of reaction increases, slight variations between 16 to 22 % were observed without a clear correlation with time (**Figure 5.11 b**). However, in the case of S-Starbon<sup>®</sup> 300, this intermediate decreases as time of reaction increases, after 6 hours of reaction it is not seen any more. In the case, of S-Starbon<sup>®</sup> 800, this intermediate disappears after 12 hours of reaction. It was noticed this intermediate does not change greatly during the first hours of reaction using S-Starbon<sup>®</sup> 800, however, when ester appears for first time, the intermediate gets lower, suggesting that its permanence is affected by the production of ester; and that it may be converted to ester indirectly or directly.

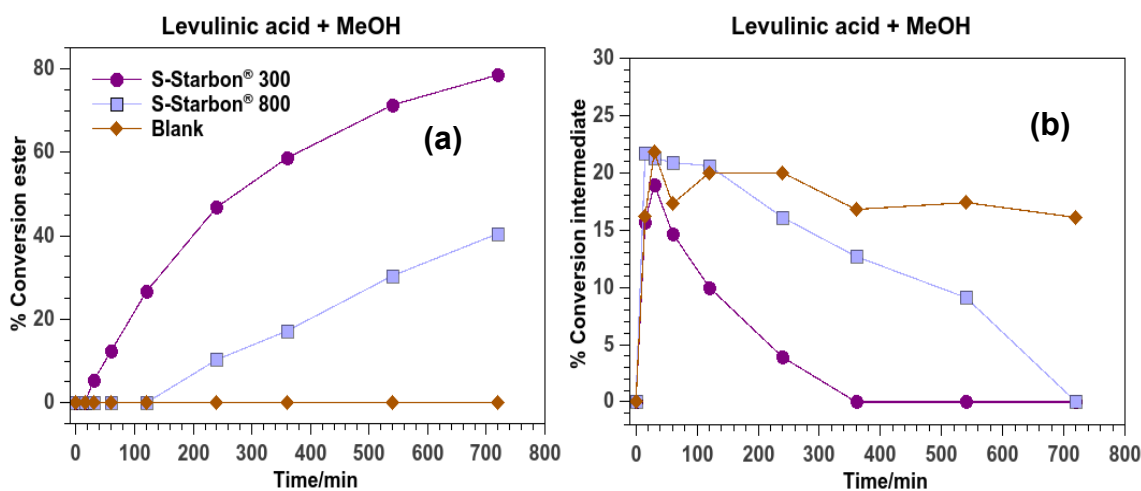


**Figure 5.11.** Reaction of levulinic acid with refluxing methanol (15 mmol acid, 10 mL alcohol, at 75 °C) (a) Conversion to ester (b) Conversion to intermediate

### 5.3.1. The Shu-Lawrence approach

The formation of an “extra peak” during GC analysis was also observed by Shu and Lawrence<sup>166</sup> (1995) during the storage of levulinic acid with several alcohols (ethanol, geraniol and benzyl alcohol) at room temperature. In their observations, the peak that appears at slightly higher retention time than ester, is formed prior to the ester and got to a maximum in 3 weeks. After this time, the intermediate peak starts decreasing, while the corresponding ester peak increases. According to the authors, the intermediate would be assigned to the formation of 4-alkoxy- $\gamma$ -valerolactone (**Figure 5.12**).

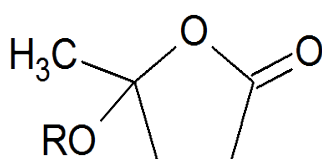


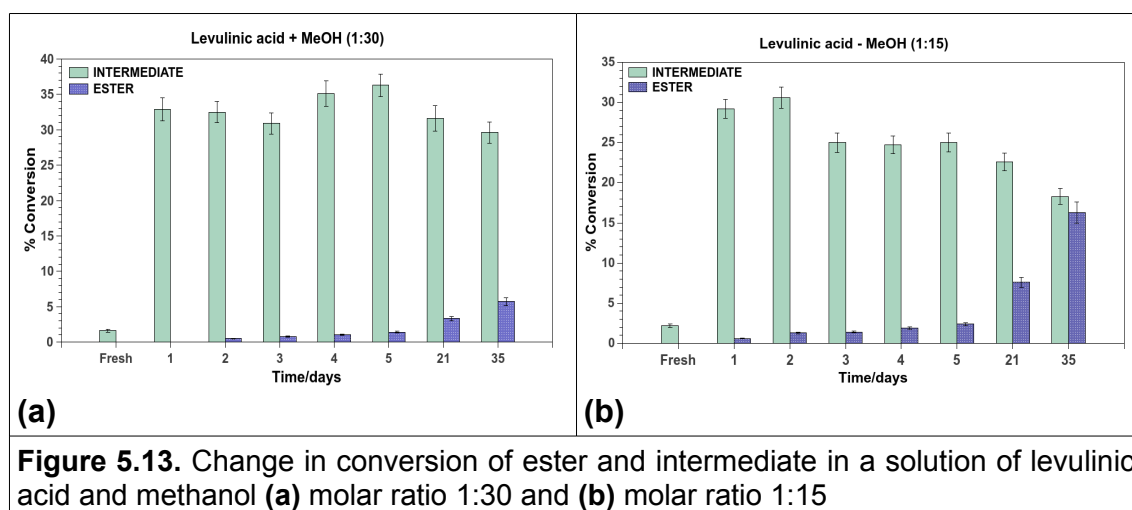
**Figure 5.12.** Molecular structure of 4-alkoxy- $\gamma$ -valerolactone proposed by Shu and Lawrence (1995)

However, in their published work, no reference to methanol was made. Due to these circumstances, a monitoring of the methanol and levulinic acid was carried out as well monitoring of a mixture of levulinic acid and ethanol. The study was done using two different concentrations, one that corresponds to the concentrations prepared according with Shu and Lawrence and the other corresponds to the concentration used in reactions of esterification of levulinic acid; this could be summarized in **Table 5.1**, from this table it is observed that proposed mixtures have double of alcohol than mixtures prepared by Shu and Lawrence.

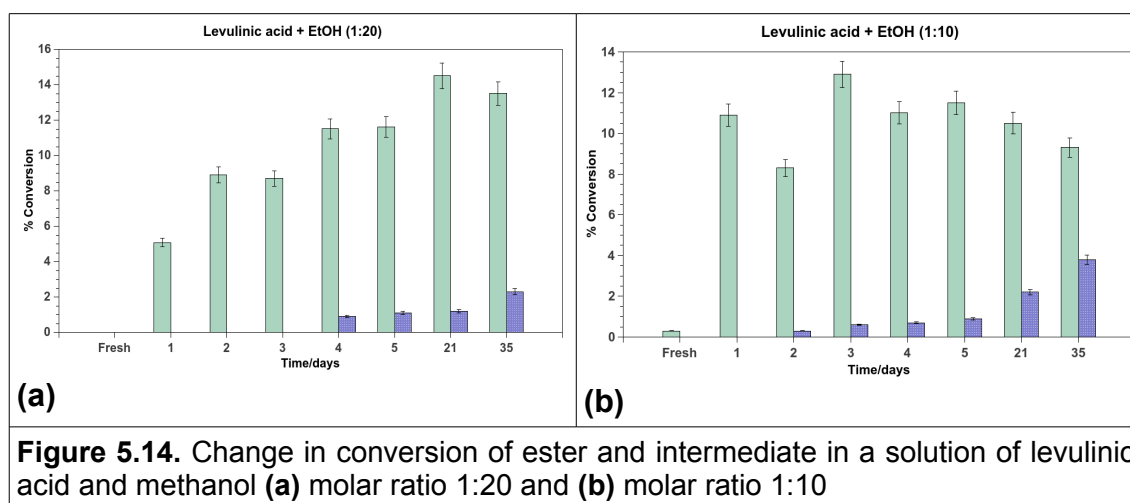
<b>Table 5.1.</b> Molar ratios of the mixtures of levulinic acid in alcohols		
	<b>Molar ratio acid:alcohol</b> Shu-Lawrence conditions	<b>Molar ratio acid:alcohol</b> C.MenaD conditions
MeOH	1:30	1:15
EtOH	1:20	1:10

**Figure 5.13a** shows the conversion obtained by GC analysis of the formation of the ester and intermediate during the storage time. The intermediate appeared from the first day in a concentration over 32 % and remained around 35 % after 5 days. The appearance of ester is in the second day which slightly increases through time, up to 6 % after 5 weeks of storage at room temperature.

For the solution of levulinic acid and methanol prepared in a molar ratio 1:15, a similar trend to the previous sample was observed (**Figure 5.13b**). In the first day of storage, the intermediate was present around 30 %; but in the third day, the intermediate decreases slightly to 25 %. Meanwhile, the conversion to ester increases gradually up to 3 % in the first 5 days. The changes were more noticeable after three and five weeks, when ester increases up to 8% and 16 %, respectively. This conversion to ester is almost three times the one found for the sample prepared with a higher ratio of methanol (6 %); meanwhile, the conversion to intermediate obtained after 5 weeks of storage is significantly lower (18 %) than the one obtained for the sample in excess of methanol (30 %). This would suggest that excess of methanol inhibits the ester formation and allows the permanence of the intermediate; this also could be related to the fact of less concentrated “acid” present in the mixture, which does not promoting the conversion to ester through an acid-catalysed reaction.

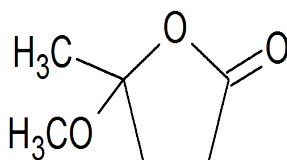


An evaluation of the storage of levulinic acid with ethanol was also carried out (**Figure 5.14.**). Conversion to the formed intermediate was lower than the one obtained in the methanol solution, with a maximum of 14 %. The permanence of the intermediate does not show a clear trend for the solution with excess of ethanol; whereas, for solution prepared in the acid:alcohol ratio 1:10, the intermediate concentration decreases with respect to time. However, in both ethanol mixtures it is observed that formation of ester increases with increased storage time. As in the case of methanol solution, ester seems to be a bit more favoured in lower acid:alcohol ratio.



### 5.3.2. Identification of the 'intermediate'

Based on the proposal made by Shu and Lawrence about the formation of 4-alkoxy- $\gamma$ -valerolactone during storage time in alcohols, further analysis were carried out to confirm the aforementioned structure. Then, in a methanol solution is expected to see a 4-methoxy- $\gamma$ -valerolactone (**Figure 5.15.**)<sup>166</sup>



molecular mass  $C_6H_{10}O_3$ :  $130.12 \text{ gmol}^{-1}$

**Figure 5.15.** Proposed structure formed during methanol storage of levulinic acid

Before taking Shu-Lawrence proposal as the definitive compound formed as an intermediate, a review of possible derivatives formed from levulinic acid<sup>167</sup> was made and presented in **Figure 5.16**. Then through different analytical techniques, compounds were confirmed or discarded.

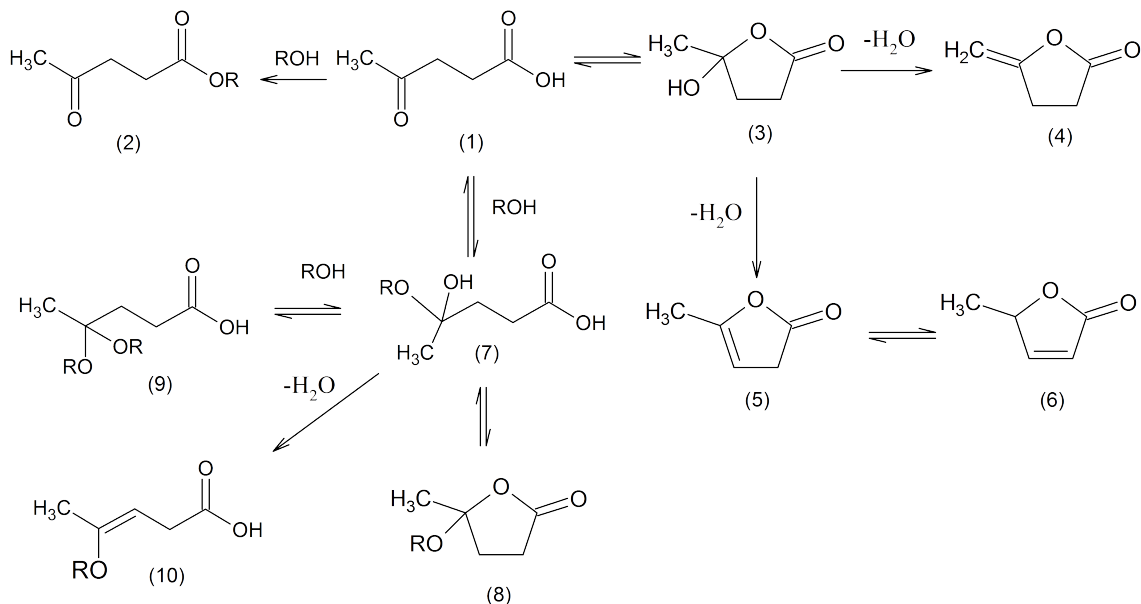


**Figure 5.16.** Levulinic acid and relationship to its derivatives

One of the most common derivatives from levulinic acid are the angelicalactones (structures **5** and **6**) which are formed by dehydration.<sup>160,167</sup> Then an attempt to identify them in the mixture was made. However, the <sup>13</sup>C NMR spectra (**Figure 5.17.**) does not show signals between 115–140 ppm, region where it is expected to find carbon alkenes resonances.<sup>34</sup> Then, with this information, angelicalactones are discarded (**5** and **6**), as well structures **4** and **10** which contain carbon double bonds.

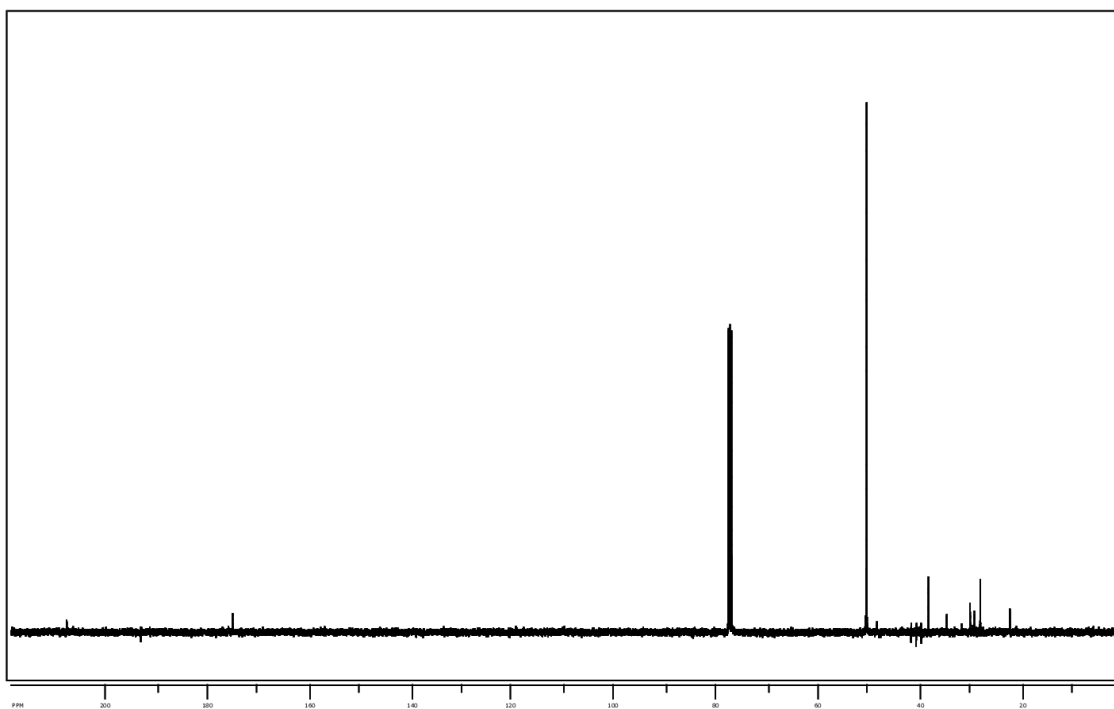


**Figure 5.17.**  $^{13}\text{C}$  NMR spectra for mixture of levulinic acid-MeOH 48 h

Another useful technique used for characterization of intermediate was Gas Chromatography coupled to Mass Spectrometry (GC-MS) analysis by Electron Ionization. This analysis was carried out taking into account molecular masses of possible derivatives from levulinic acid and presented in **Table 5.2**. Some of them have been already discarded, but it is worth having them in mind.

<b>Derivatives</b>	<b>Molecular Mass</b>
Levulinic acid (1)	116
Pseudo-levulinic acid (3)	116
$\alpha$ -angelica lactone / $\beta$ -angelica lactone (5, 6)	98
4-methoxy- $\gamma$ -valerolactone (8)	130

**Figure 5.18.** shows the mass spectra obtained for the intermediate peak in the mixture of levulinic acid–methanol (1:30 ratio) after 48 h. The mass obtained for the formed molecular ion was of 115.17; this mass is lower than the one expected for the 4-methoxy- $\gamma$ -valerolactone, 130.12; differing from Shu-Lawrence proposal.

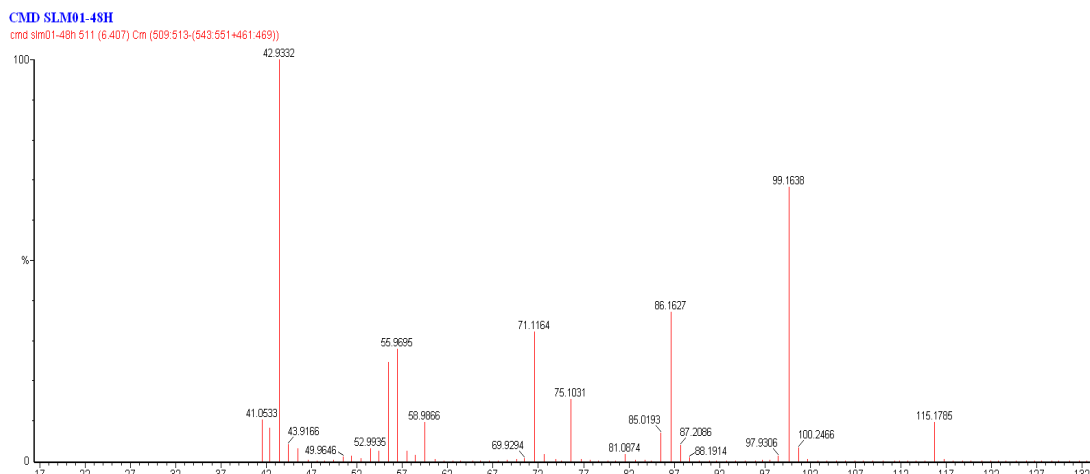


**Figure 5.18.** Mass spectra of intermediate identified in levulinic acid and methanol (1:30) solution

Another test made to determine the mass of the “intermediate” through GC-MS analysis consisted in the preparation of a solution of levulinic acid with deuterated methanol (MeOD-d<sub>4</sub>) in the ratio acid:alcohol, 1:30, as the one prepared by Shu and Lawrence. The mass spectra for the intermediate peak is presented in **Figure 5.19.**, in where it is observed that the mass did not increase greatly (up to 130) discarding again the attachment of a methoxy group in the position 4 of the  $\gamma$ -valerolactone; the molecular ion mass was found between 118–119 amu, which would suggest a proton-deuterium exchange, likely to happen with the methyl group of the ketone, giving up to 3 deuterium atoms in the molecule.

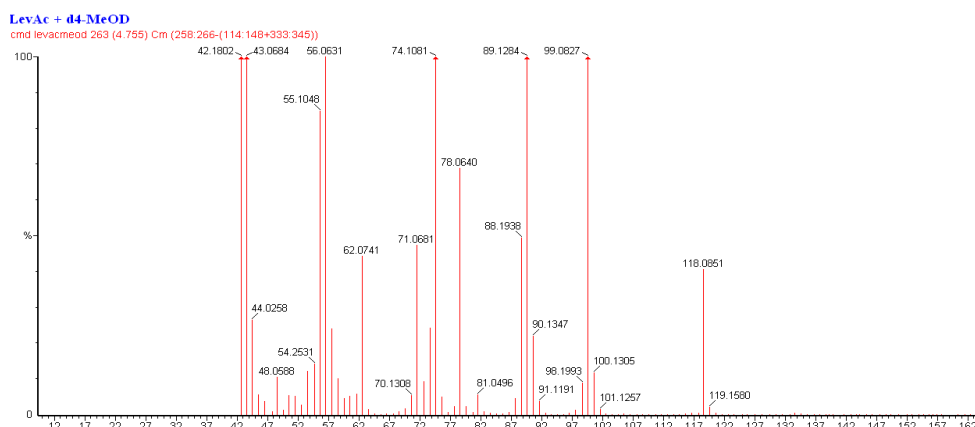


**Figure 5.19.** Mass spectra of intermediate identified in levulinic acid and methanol-d<sub>4</sub> (1:30) solution

The intermediate formed in the solution of ethanol and levulinic acid was also examined. It was interesting to find that ethanol intermediate appears at similar retention time in the chromatogram obtained for methanol by GC-FID (**Figure 5.20**). When analysis of the peak corresponding to intermediate formed from levulinic acid–ethanol mixture is done by GC-MS, the molecular ion mass obtained was 116; these results are comparable with the ones obtained from MSc project on levulinic acid esterifications by EtOH carried out by Ms. Petchey, who also identified the formation of this intermediate. In the assumption of 4-ethoxy- $\gamma$ -valerolactone would be produced during the storage with ethanol, then the mass expected for the molecular ion would be close to 144. These findings differ again from the proposal made by Shu and Lawrence.<sup>166</sup>

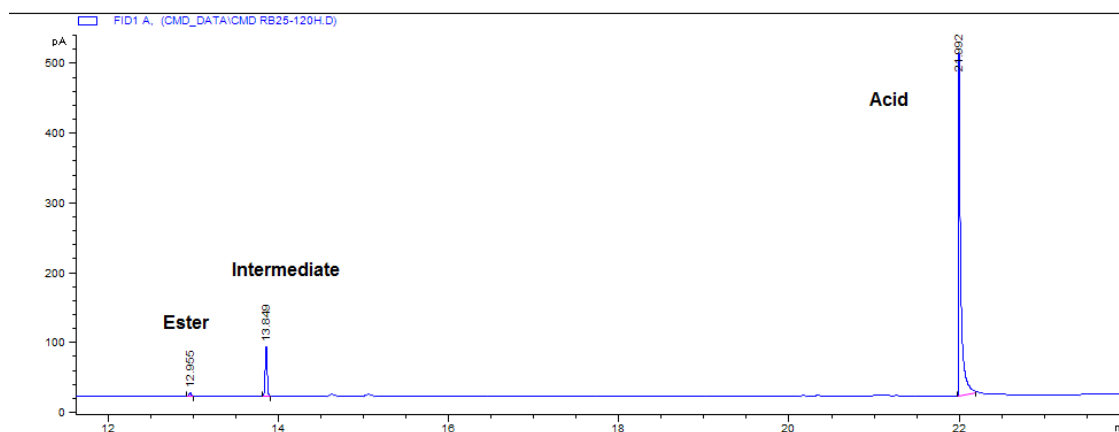


**Figure 5.20.** GC -FID chromatogram of mixture of levulinic acid and ethanol (1:15, day 5)

With these findings, we get back to **Figure 5.16.**, to try to point out the corresponding structure to this intermediate. Then, it seems that derivative formed during the mixing of levulinic acid and methanol/ethanol resembles with 5-hydroxy- $\gamma$ -valerolactone or *pseudo-levulinic acid*,<sup>167</sup> which appears to be better dissolved in methanol than ethanol. The formation of 5-hydroxy- $\gamma$ -valerolactone (**3**) is attributed to the facility in the transfer of the proton from the carboxy group to the carbonyl atom of oxygen.<sup>168</sup>

### 5.3.3. Performance of sulfonated Starbons® in the esterification of levulinic acid

Esterification of levulinic acid by methanol was carried out using conventional and microwave irradiation, using sulfonated Starbons® 300 and 800 (**Figure 5.21.**). As observed for esterification of lauric acid by methanol, conversion obtained using microwave irradiation in 30 minutes is higher than the obtained using conventional heating by 12 hours. This increment in conversion for reactions carried out under microwave irradiation could be associated with the high temperatures reached during reaction<sup>119</sup> (105 °C vs 75 °C). Sulfonated Starbon® 300 seems to be more effective than sulfonated Starbon® 800, as previous observation during esterification of lauric acid by methanol.

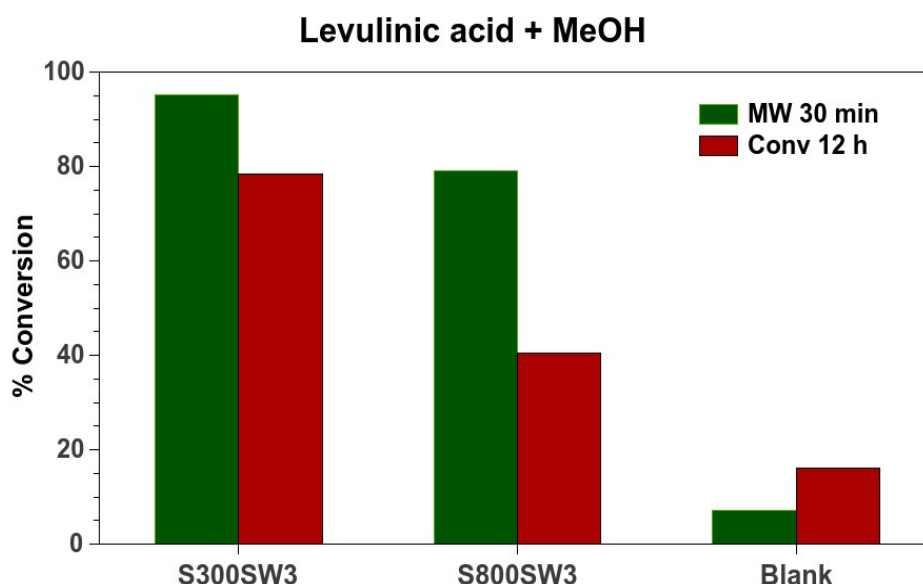


**Figure 5.21.** Comparison of the esterification of lauric acid by methanol using microwave irradiation and conventional heating

A scope of efficiency of sulfonated Starbons® in the esterification of levulinic acid with methanol was also performed employing 20 and 40 mg of catalyst loading (**Figure 5.22.**). As expected, higher catalyst loading gives higher conversions; complete conversions to the ester are observed using sulfonated Starbons® 300, and over 95 % is obtained using sulfonated Starbons® 350, 550 and 800.

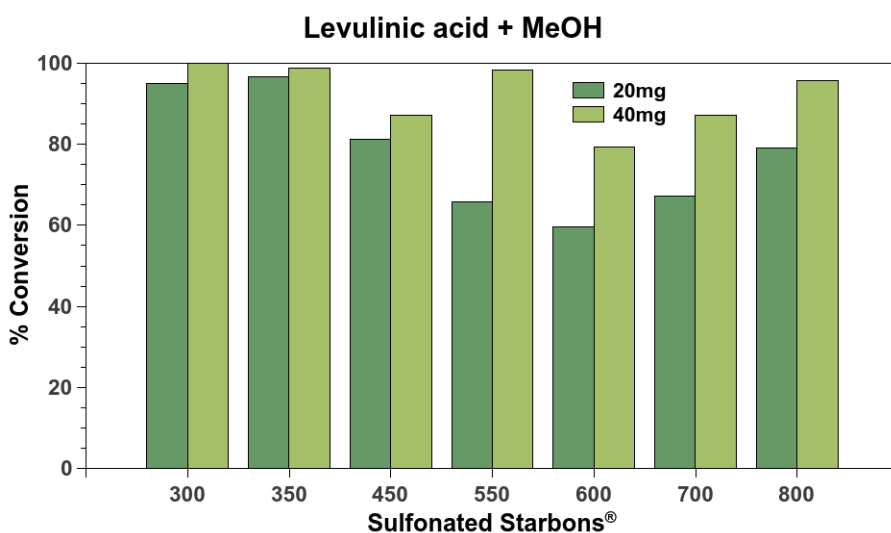


**Figure 5.22.** Esterification of levulinic acid by MeOH, using 20 and 40 mg of sulfonated Starbons® (30 min, 200 W)

A quick test on reusability of sulfonated Starbons® 300, 350, 550 and 800 in esterification of levulinic acid with methanol was carried out, using 40 mg of sample (**Figure 5.23.**). It was interesting to find out that activity of high-temperature Starbons® decreased dramatically just in the second use to approximately 50 %.

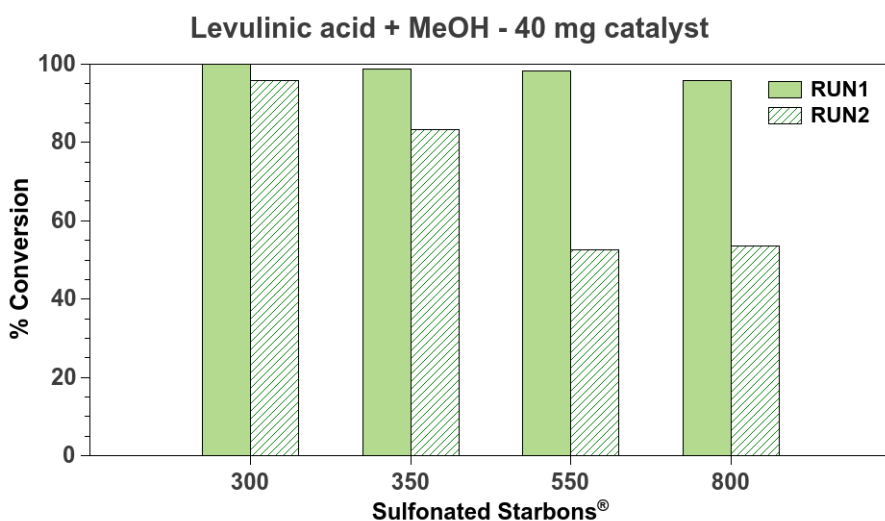


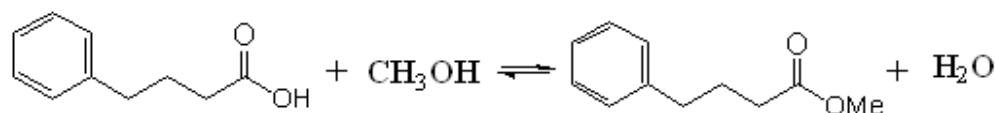
**Figure 5.23.** Reusability of sulfonated Starbons® in esterification of levulinic acid with methanol (catalyst 400 mg; MW 200 W, 30 min)

A summary of some compositional properties of sulfonated Starbons<sup>®</sup> is presented in **Table 5.3.** with the aim to find a correlation between these characteristics and catalytic performance. It is observed that both sulfonated Starbons<sup>®</sup> 550 and 800 have higher C:O ratio, implying that they contain less oxygenated groups. When sulfur content is analysed, the samples have less sulfur loading on bulk or on surface, which could explain the loss in activity. This observation was also made in esterification of lauric acid by methanol, so it seems that high-temperature sulfonated Starbons<sup>®</sup> are less stable than low-temperature ones.

Sulfonated Starbon <sup>®</sup>	C:O atomic ratio	S/mmolg <sup>-1</sup> bulk	S (VI)/mmolg <sup>-1</sup> surface
300	2.45	0.73	1.61
350	2.97	0.94	1.22
550	5.61	0.43	0.98
800	5.94	0.52	0.46

#### 5.4. Test in esterification of 4-phenyl butyric acid and benzoic acid with methanol

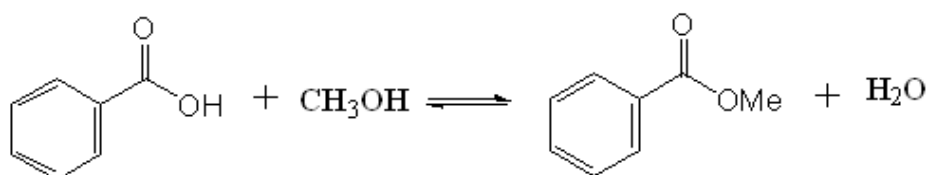
An evaluation of performance of sulfonated Starbons<sup>®</sup> in esterification of 4-phenyl butyric acid and benzoic acid with methanol was also carried out. Two different catalyst loading were tested: 20 and 40 mg to find out main differences (**Figure 5.24.**). Similar trends are observed as with the previous reactions: low-temperature sulfonated Starbons<sup>®</sup> (300 and 350) show better catalytic activity than high-temperature sulfonated Starbons<sup>®</sup>.



**Scheme 5.2.** Esterification of 4-phenyl butyric acid with methanol

**Figure 5.24a** presents a comparison between conversion to methyl ester of 4-phenyl butyric acid and sulfur content in sulfonated Starbons<sup>®</sup>, trying to find a correlation between these findings. In general, content of sulfur (VI) on the surface is higher than the content on the material in bulk. However, the trend of conversion obtained seems to be more related to sulfur content in the material, as conversion decreases in the middle samples just as sulfur content does for these samples. It is worth mentioning that the decrease in sulfonic groups [referred as S(VI)] is also observed for other sulfonated carbonaceous materials.<sup>28,30</sup> It seems that increasing the temperature of carbonization of carbonaceous materials, incrementing their similitude to graphitic-like materials, affects the attachment of sulfonic groups to the structure.

Regarding the esterification of benzoic acid by methanol, using sulfonated Starbons<sup>®</sup> (**Figure 5.24b**), it was found that materials with higher sulfur content promoted higher conversions, although this was achieved using 40 mg of catalyst, reaching a maximum of 60 % of conversion. It is well-known that aromatic carboxylic acids are quite stable and esterification could be very slow.<sup>165</sup>



**Scheme 5.3.** Esterification of benzoic acid with methanol

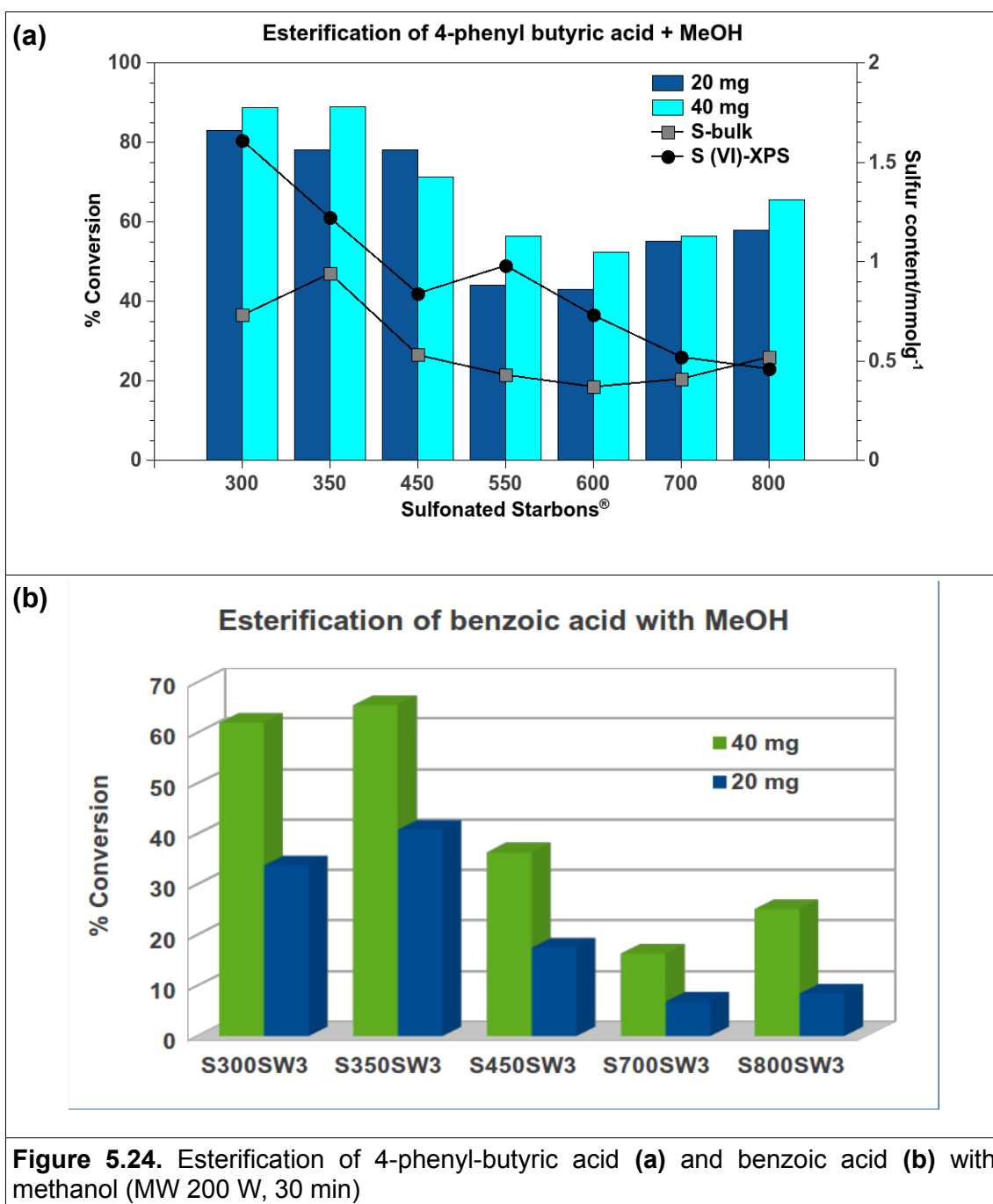


**Figure 5.24.** Esterification of 4-phenyl-butyrac acid **(a)** and benzoic acid **(b)** with methanol (MW 200 W, 30 min)

### 5.5. Short test of microwave sulfonated Starbons®

Preparation and characterization of sulfonated Starbons® using microwave irradiation were presented in **Chapter 3**. As it was mentioned, there were not extra washes with methanol, aiming to decrease steps in preparation of stable sulfonated catalysts.

Test of the efficiency of these microwave sulfonated catalysts was carried out in the esterification of lauric acid by methanol, using the standards measurements: MW 200 W, 30 min and 20 mg of catalysts. As presented in previous chapters, these materials were sulfonated at three different temperatures, due to the facility provided by microwave open vessel equipment. A brief summary, describing the preparation of microwave sulfonated samples is presented in **Table 5.4.**

<b>300</b>	<b>S300SW3</b>	Starbon <sup>®</sup> 300 conventionally sulfonated @ 90°C, washed with MeOH
	<b>S300SMW90</b>	Starbon <sup>®</sup> 300 sulfonated @ 90°C by microwave irradiation
	<b>S300SMW90RH</b>	Starbon <sup>®</sup> 300 sulfonated @ 90°C by microwave irradiation using recycled sulfuric acid
	<b>S300SMW120</b>	Starbon <sup>®</sup> 300 sulfonated @ 120°C by microwave irradiation
	<b>S300SMW150</b>	Starbon <sup>®</sup> 300 sulfonated @ 150°C by microwave irradiation
<b>450</b>	<b>S450SMW90</b>	Starbon <sup>®</sup> 450 sulfonated @ 90°C by microwave irradiation
	<b>S450SMW120</b>	Starbon <sup>®</sup> 450 sulfonated @ 120°C by microwave irradiation
	<b>S450SMW150</b>	Starbon <sup>®</sup> 450 sulfonated @ 150°C by microwave irradiation
<b>800</b>	<b>S800SMW90</b>	Starbon <sup>®</sup> 800 sulfonated @ 90°C by microwave irradiation
	<b>S800SMW120</b>	Starbon <sup>®</sup> 300 sulfonated @ 120°C by microwave irradiation
	<b>S800SMW150</b>	Starbon <sup>®</sup> 300 sulfonated @ 150°C by microwave irradiation

The performance of the catalysts described is presented below. **Figure 5.25.** shows the conversion obtained during esterification of lauric acid by methanol using microwave sulfonated Starbons<sup>®</sup> 300. In the first run all the catalysts of Starbon<sup>®</sup> 300 showed the highest conversion, which decreases to less than 80 % in second use and it drops slightly in the third run, being more noticeable in microwave sulfonated Starbon<sup>®</sup> 90 °C. These observations would suggest that first run is equivalent to the conditioning step using methanol as for the methanol washed Starbon<sup>®</sup> 300 sulfonated by conventional heating, because

the conversion for the second and third run are very similar to the one obtained for S300SW3.

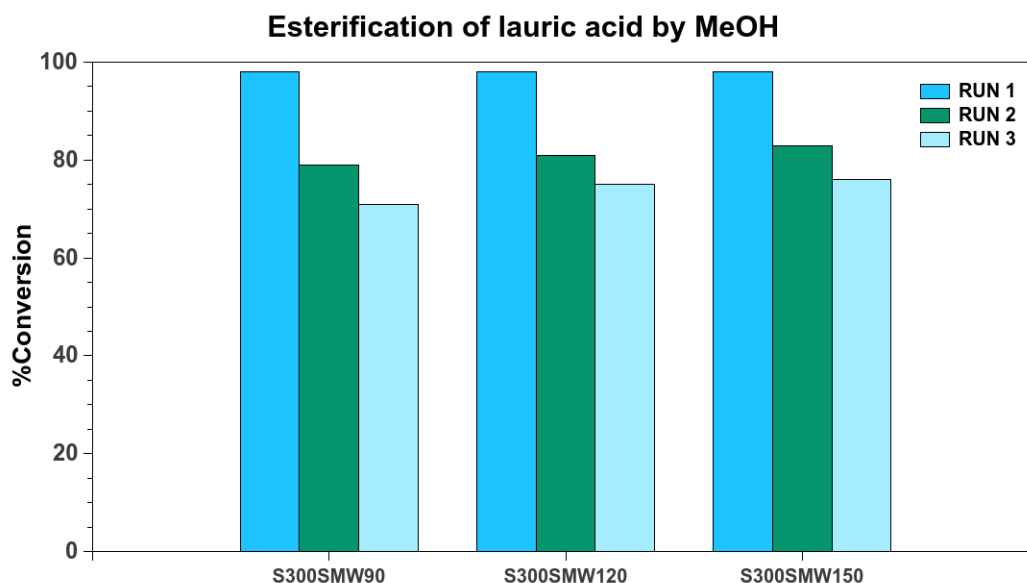


**Figure 5.25.** Esterification of lauric acid by methanol using microwave sulfonated Starbons<sup>®</sup> 300

Effectiveness in the esterification of lauric acid by methanol using microwave sulfonated Starbons<sup>®</sup> 450 and 800 are presented in **Figure 5.26.** and **Figure 5.27.**, respectively. Both sample batches displayed very high conversions in the first use, but a massive drop in conversion to methyl lauric ester in the second use of the catalyst, alluding to the weak stability of sulfonated high-temperature Starbons<sup>®</sup>. Continued use showed that during the third use of sulfonated catalyst, conversion obtained is scarcely over 30 %, for sulfonated Starbons<sup>®</sup> 450 and 800. Temperature of sulfonation seems to have more effect in microwave sulfonated Starbon<sup>®</sup> 450 than for Starbon<sup>®</sup> 800; as samples prepared at 150 °C showed better conversions than lower temperatures. For sulfonated Starbons<sup>®</sup> 800, the trend in deactivation is similar.

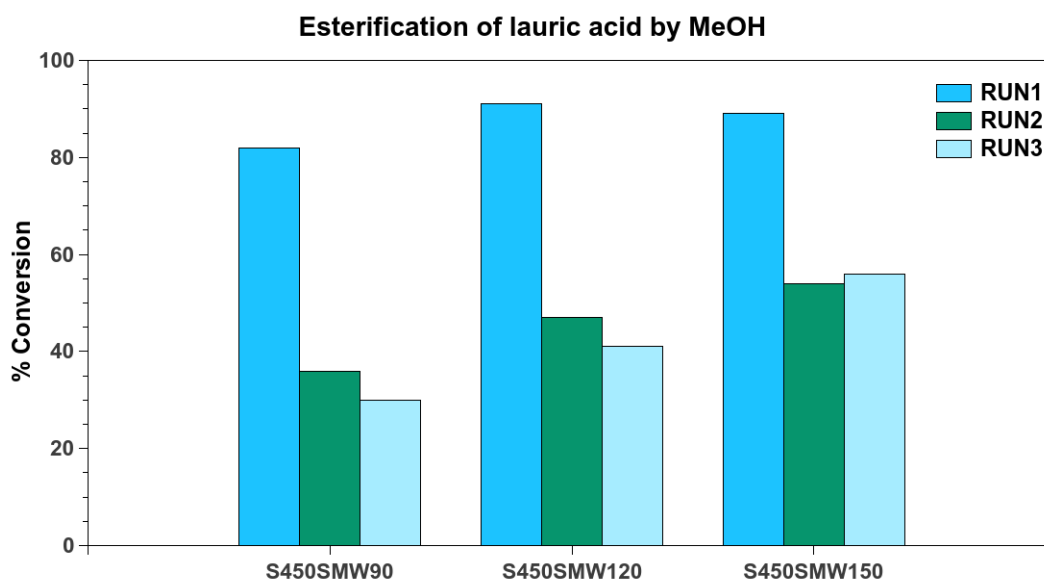


**Figure 5.26.** Esterification of lauric acid by methanol using microwave sulfonated Starbons® 450

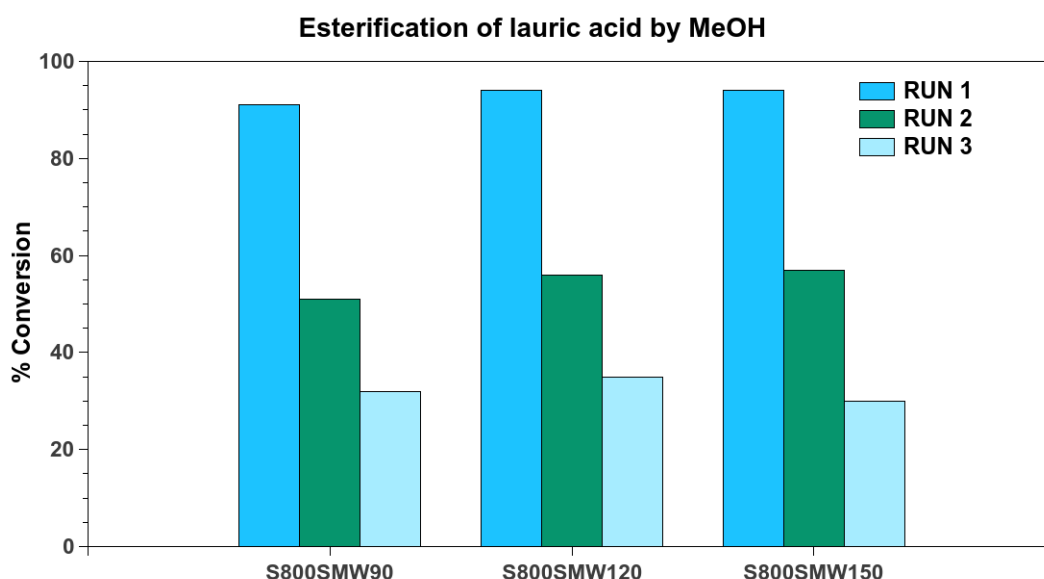


**Figure 5.27.** Esterification of lauric acid by methanol using microwave sulfonated Starbons® 800

Although these last two samples, 450 and 800, deactivated after few uses, sulfonated Starbons® 300 appear to be more stable for further uses. Microwave sulfonated Starbon® 300 at 90 °C seem to be slightly better when it is compared with conventional sulfonated Starbon® 300, because it maintains conversions over 70 % after three uses (**Figure 5.28.**). An additional benefit we discovered was related to the conversion to methyl laurate ester obtained using microwave sulfonated Starbon® 300 prepared using recycled sulfuric acid, which appears to

have similar activity to samples prepared with “new sulfuric acid” 95 %.

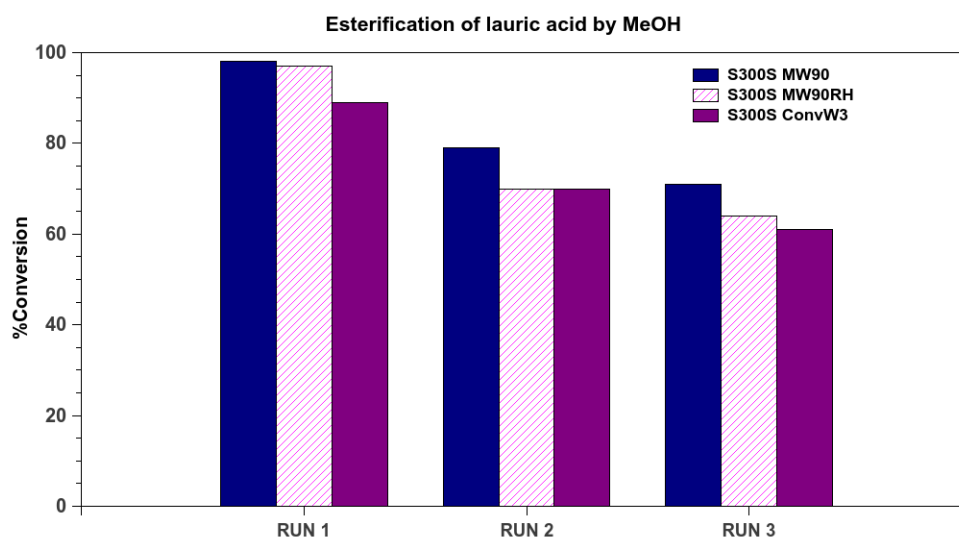


**Figure 5.28.** Esterification of lauric acid by methanol using microwave sulfonated Starbons® 300 prepared at 90°C, conventional and recycled sulfuric acid

A general overview of sulfonated Starbons® 300 used as catalysts in the esterification of lauric acid by methanol is depicted in **Figure 5.29**. It is found that all microwave sulfonated Starbons® 300 gave high conversions in the first use, as mentioned previously, this could be taken as “the conditioning step” with methanol. After that, in the second run, conversions dropped for all samples, even for sample sulfonated by conventional heating. In the third use, conversions dropped even more, although microwave sulfonated Starbons® 120 and 150 showed conversions over 75 % and the sample conventionally sulfonated shows the lowest conversion close to 60 %. It is also noticeable that the sample prepared using recycled sulfuric acid also presented a faster deactivation than other microwave sulfonated samples.

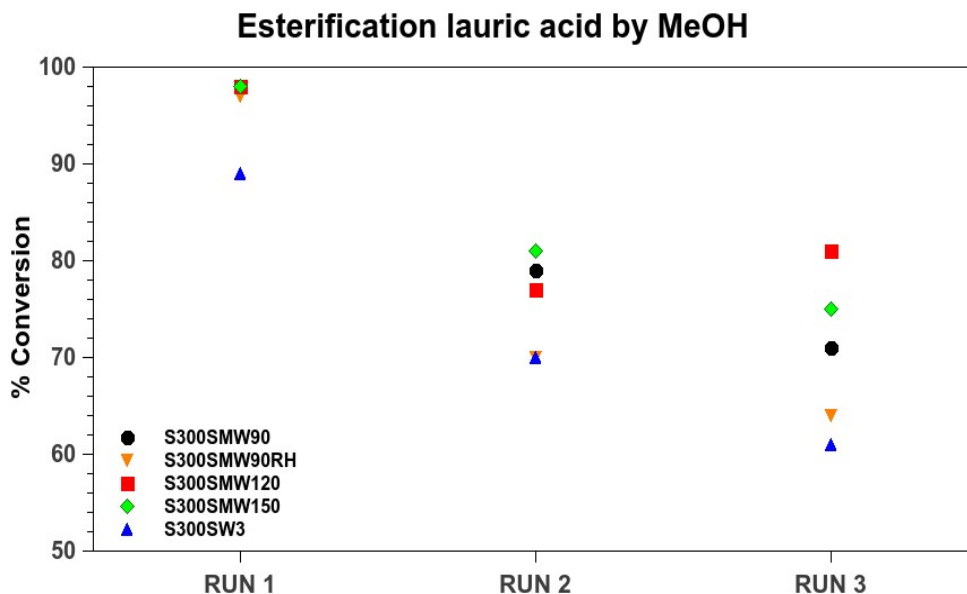


**Figure 5.29.** Reusability of sulfonated Starbons<sup>®</sup> 300 in the esterification of lauric acid by methanol

### 5.6. Deactivation of sulfonated Starbons<sup>®</sup>

In the preparation of solid-acid catalysts it is desirable that they are recyclable to allow reactions to be carried out many times; however, the loss of activity and/or deactivation of material could happen when catalyst is reused. As it has been shown previously, sulfonated Starbons<sup>®</sup> show a decrease in conversion of ester after first use, characteristic which may put Starbons<sup>®</sup> at a disadvantage when compared with other carbon-base catalysts, as some authors have reported very 'stable' sulfonated carbonaceous materials,<sup>24,28</sup> and others claiming to use sugar catalyst carbonized at 400 °C for 50 consecutive cycles.<sup>32</sup> Although some authors have reported recyclability without any treatment, there are some others which gave an extra treatment to recovered catalysts, among post-recovery treatment, using solution of sulfuric acid or concentrated sulfuric acid to "reactivate" the materials<sup>37,38</sup> which activity is retained after several cycles more. The use of sulfuric acid in treatment of reused catalysts seems to be more a kind of adding this mineral acid to the material than a proper regeneration.

In the case of sulfonated Starbons<sup>®</sup>, recovery and regeneration is presented in **Figure 5.7.** in which acetone was used to remove “residues” from reactants, next sample was dried in an oven prior to use again. Although loss of activity could be attributed to loss of materials, in the case of sulfonated Starbons<sup>®</sup>, this was less than ~0.2 mg in ~20 mg of catalyst. Mo *et al*<sup>26</sup> investigated the deactivation of sulfonated carbon materials based on Hara's results.<sup>24</sup> Former authors found that deactivation is a common problem for sulfonated catalysts as fresh and washed methanol showed very similar conversions in esterification reactions monitored; indicating that catalytically active species leached into methanol after washing procedure. These species were identified as sulfonic polycyclic carbons. Elemental analysis of sulfur left in the materials after 3 cycles (**Figure 5.30.**), showed that sulfonated Starbon<sup>®</sup> 800 just retained 55 % of initial sulfur while sulfonated Starbon<sup>®</sup> 300 contained 72 % of original sulfur; this might explain the lower conversion to the methyl ester observed during use of sulfonated Starbon<sup>®</sup> 800. Decreased sulfur content was also observed by Mo *et al*<sup>26</sup> during their deactivation studies, mentioned earlier.

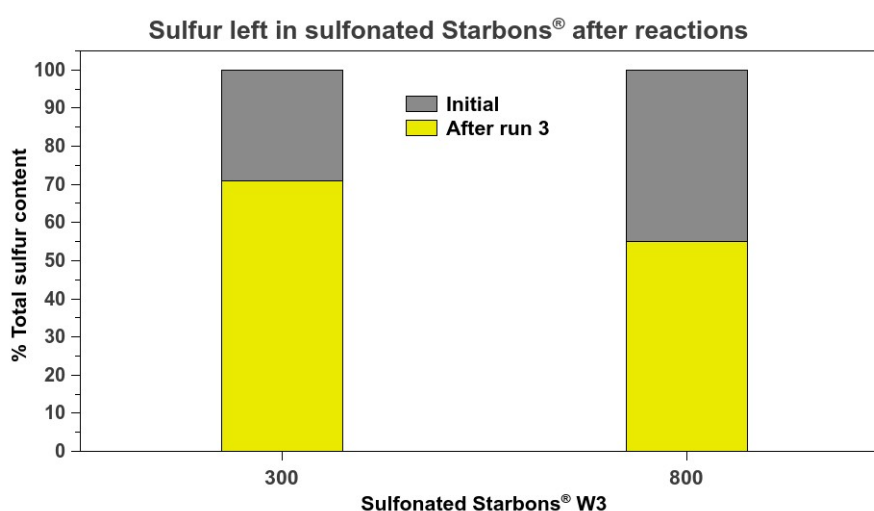


**Figure 5.30.** Comparison in sulfur content left after three runs in sulfonated Starbons 300 and 800

Deactivation has been suggested to depend on reaction media, in the case of sulfonated carbonaceous materials, differences are observed from aqueous media to less polar solvents as alcohols<sup>153</sup> and being more noticeable when methanol is used. This statement agrees with our observations about sulfur

leaching shown in **Chapter 2**, where significant differences in sulfur leached among the studied alcohols were found, being quite higher for methanol than for 2-propanol. It is also worth mentioning that deactivation of sulfonated carbon-base materials can also be related to the formation of methyl ethers on materials;<sup>153</sup> this suggestion coincides with our results presented in **Chapter 2**, in which a methoxy group is identified in sulfonated Starbons<sup>®</sup> after methanol treatment, through <sup>13</sup>C CP/MAS NMR studies.

A scope about leaching and stability of microwave sulfonated Starbons<sup>®</sup> 300 was carried out and depicted in **Figure 5.31**. Reactions were carried out in 5 minutes instead of regular time of 30 minutes. Results shown that during first use all sulfonated Starbons<sup>®</sup> reached high conversions, over 60 %; and values obtained are very alike between leached methanol and fresh methanol with catalyst. There is a significant decrement in the second run, in which the maximum conversion was slightly over 35 %; and for third use, conversion to methyl ester was approximately of 30 %. It is interesting to note that the contribution from leaching decreases as well, during the second and third uses; suggesting that conversions to methyl ester observed during second and third run are more related to heterogeneous capacity of sulfonated Starbons<sup>®</sup>. Although, conventional sulfonated Starbon<sup>®</sup> 300 showed slightly lower conversions, it is important to emphasize that this material has already been washed with methanol, while microwave sulfonated Starbons were not treated with methanol before these reactions.

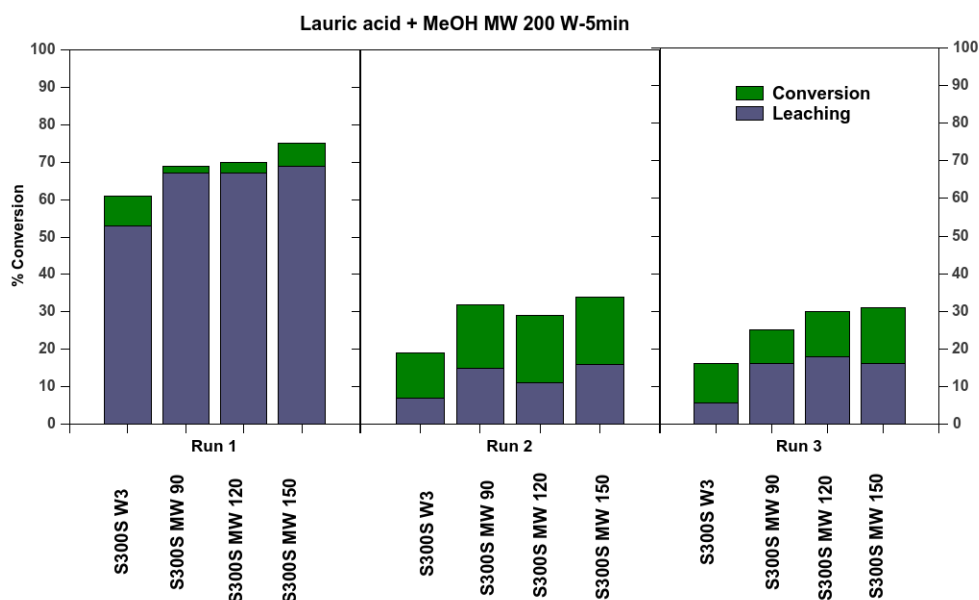


**Figure 5.31.** Studies on leaching of sulfonated Starbons<sup>®</sup> 300

## 5.7. Conclusions

A general overview of the performance of sulfonated Starbons<sup>®</sup> in esterification reactions was carried out. The conversion to ester was evaluated using the GC peak areas of the ester and acid, which gives an approximate value. Reactions were carried out by conventional heating and microwave irradiation; higher conversions were achieved in reactions done using microwaves, which could be attributed to the reaction conditions, as reactions were carried out in closed vessel and temperatures reached over 100 °C.

Assessment of the range of sulfonated Starbons<sup>®</sup> prepared, showed differences in their activity according to their carbonization temperature of materials, obtaining higher conversions to the ester when low-temperature sulfonated Starbons<sup>®</sup> are used. The weak activity of high-temperature Starbons<sup>®</sup> could be attributed to less sulfonic groups attached to the material as presented in **Chapter 2** and **Chapter 3**. This characteristic has been already reported as a difficulty to introduce sulfonic groups to aromatic polycyclic carbons<sup>24</sup>.

Although there are not references of studies on recyclability of previous sulfonated Starbons<sup>®</sup> to compare with directly, our results showed the rapid deactivation of materials in reactions with methanol and among the range of sulfonated Starbons<sup>®</sup> prepared, sulfonated Starbon<sup>®</sup> 300 showed to be the most stable.

Synthesis of sulfonated Starbons<sup>®</sup> using microwave irradiation could be an efficient approach to get solid-acids, however, high-temperature carbonized Starbons<sup>®</sup> (450 and 800) would require higher temperatures of sulfonation (120 or 150) because deactivation occurs easily for samples prepared at 90 °C. In this section, it was also shown that sulfonated Starbon<sup>®</sup> 300 prepared from recycled sulfuric acid (S300SMW90RH) has similar activity to the sulfonated Starbons<sup>®</sup> 300 prepared from new and clean sulfuric acid. This observation opens the opportunity to explore further the preparation and characterisation of sulfonated Starbons<sup>®</sup> using recycled sulfuric acid.

# **Chapter 6**

## ***Experimental***



## 6.1. Chemical reagents

### 6.1.1. Chemicals used for synthesis and characterisation of sulfonated Starbons®

Sulfuric acid ( $\geq 95\%$ ) was purchased from Fischer Scientific. Deionised water obtained from a Purite system at the Department of Chemistry was used for washings. Methanol AR grade (VWR chemicals) was used for the methanol extra wash carried out on sulfonated Starbons®. Sodium chloride (Fischer Scientific) was used to prepare a 2 M solution ( $\text{H}_2\text{O}/\text{MeOH}$ , 1:1 v/v) for acidity determination. Barium chloride dihydrate (99 %) was purchased from Alfa Aesar for the preparation of  $\text{BaCl}_2$  solution 0.1 M (0.1 M HCl). Hydrochloric acid (HCl) 0.1 M used in the preparation of solution  $\text{BaCl}_2$  0.1 M was purchased from Fischer Scientific. Collection of gases released during sulfonation of Starbons® via microwave irradiation was done using a solution of hydrogen peroxide  $\text{H}_2\text{O}_2$  (30 % v/v). Sodium hydroxide, NaOH solution (0.1 M) from Fischer Scientific was used as base to prepare more diluted solutions for titrations.

### 6.1.2. Chemicals used in reactions

Lauric acid ( $\geq 98\%$ ) and benzoic acid (99 %) were purchased from Sigma-Aldrich. 4-phenylbutyric acid (99 %) was purchased from Alfa Aesar; levulinic acid (98%) was purchased from Acros Organics. Methanol, ethanol and acetone used for reactions and reactivation of catalyst were AR grade (VWR Chemicals). The comparable catalysts used during reactions were activated carbon Norit® (Fluka) and sulfated zirconia, 13 %  $\text{Al}_2\text{O}_3$  (Engelhard Exceptional Technologies).

## 6.2. Carbonization treatment

Starbons® used in this research were prepared from *Cleargum* starch. Expansion of the material was done at Contract Chemicals Inc., according with Budarin methodology.<sup>9,48</sup> The carbonization of expanded starch was carried out at three different temperatures at 300, 400 and 800 °C at Nabertherm,

Germany, received in batches of 10 kilograms. They were the starting materials for the range of new carbonized Starbons<sup>®</sup>. Carbonization was carried out in a furnace Thermolyne 6000 under nitrogen flow at 100 mLmin<sup>-1</sup> according to diagram presented in **Figure 6.1**.

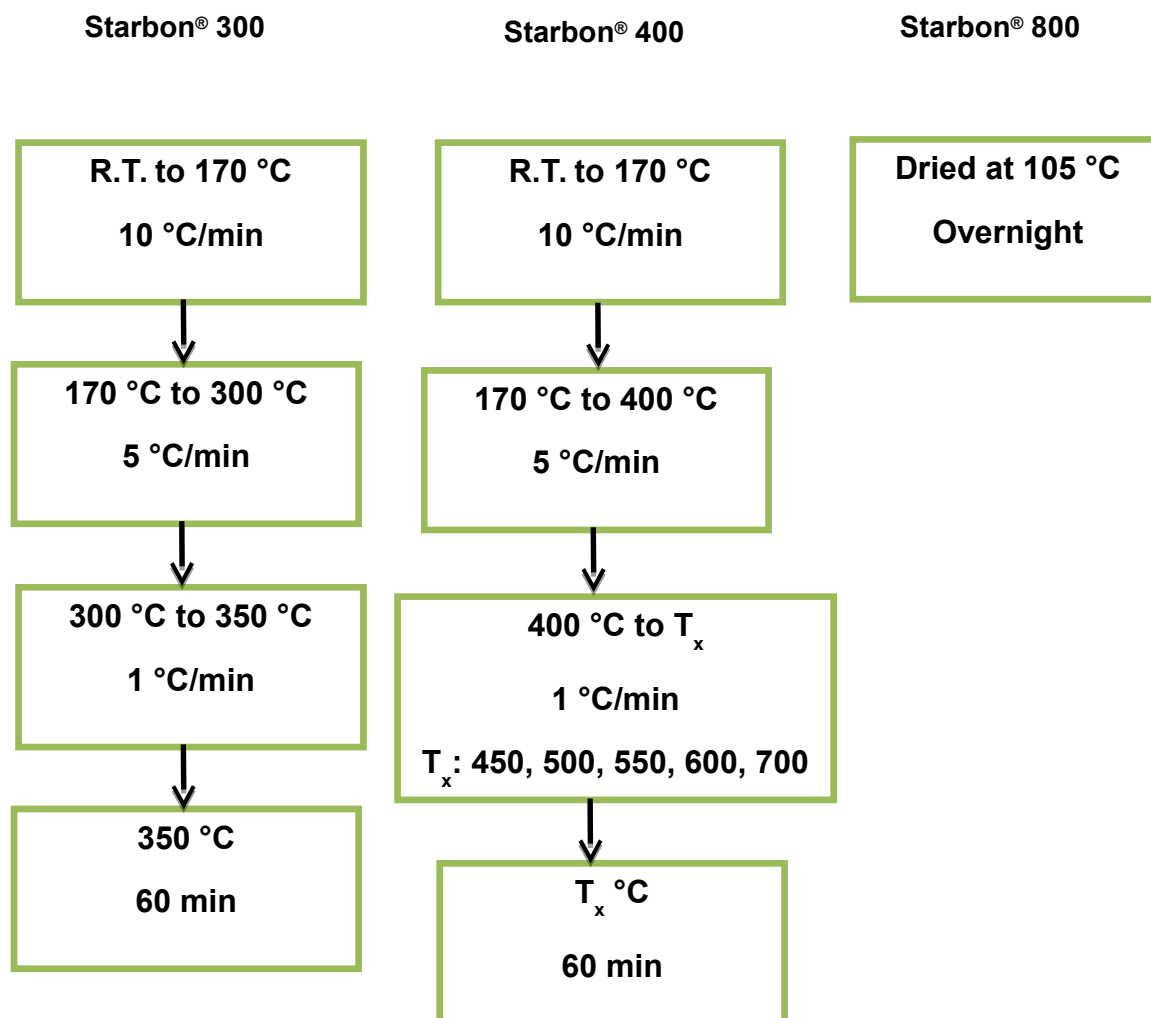


**Figure 6.1.** Carbonization procedure for Starbons<sup>®</sup>

### 6.3. Sulfonation process

Sulfonation of Starbons<sup>®</sup> were carried out through different methodologies: using conventional heating and microwave irradiation.

### 6.3.1. Conventional sulfonation

The sulfonation was carried out in a round-bottom flask with an adapted condenser. This reaction was heated in a sand bath at 90 °C for 6 hours (**Figure 6.2**). The ratio used in this synthesis was 1 g of Starbon® to 7 mL of sulfuric acid 95 % (at scale of 80 g). Solid was filtered off and unreacted sulfuric acid was recovered (~30% of the original volume), afterwards samples were extensively washed with hot water (over 80 °C) until test with solution BaCl<sub>2</sub> 0.1M was negative to the presence of sulfates coming off from washes. The pH of washes was measured using a pH meter and conductivity Jenway 3540. After washing treatment, samples were dried at 105 °C overnight in a CarbolYTE oven.

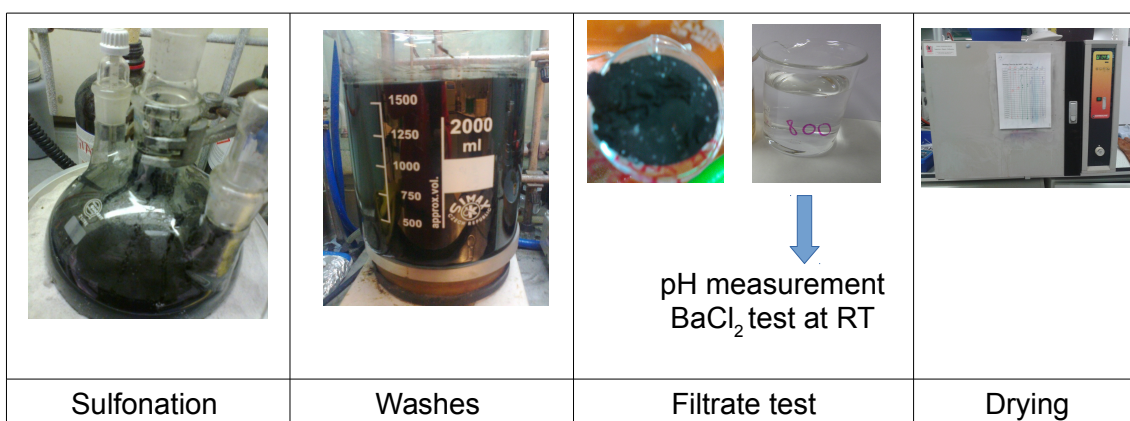


**Figure 6.2.** Schematic representation of the sulfonation of Starbons® by conventional heating

### 6.3.2. Methanol washing

Leaching of sulfuric acid was observed in the first reactions done using these sulfonated samples (**Chapter 2**), it was decided to give an extra treatment wash with methanol, using similar conditions to reactions, then it was done using microwaves. So, sulfonated Starbons® were washed with methanol (reagent grade) in a ratio 1 g solid : 5 mL methanol. Washes were done in a CEM Discover SP microwave reactor at 200 W during 10 minutes with constant stirring. The procedure was repeated three times. Finally samples were dried in an oven at 105 °C overnight, before reaction testing.

### 6.3.3. Microwave sulfonation

Sulfonation of Starbons<sup>®</sup> using microwaves was carried out in a microwave CEM Discover reactor with PC control. “Open vessel” was the mode selected to do the sulfonation and the maximum power was set to 200 W. Samples were prepared in the same ratio as conventional sulfonation 1 g of Starbon<sup>®</sup> to 7 mL of acid, but in a lower scale, using 2 g of solid. The samples were heated at fixed temperatures (90, 120 and 150 °C) during 30 minutes with constant stirring. Gases released during sulfonation were collected in a H<sub>2</sub>O<sub>2</sub> solution (30% v/v) using nitrogen as carrier, according to the system presented in **Figure 6.3**.

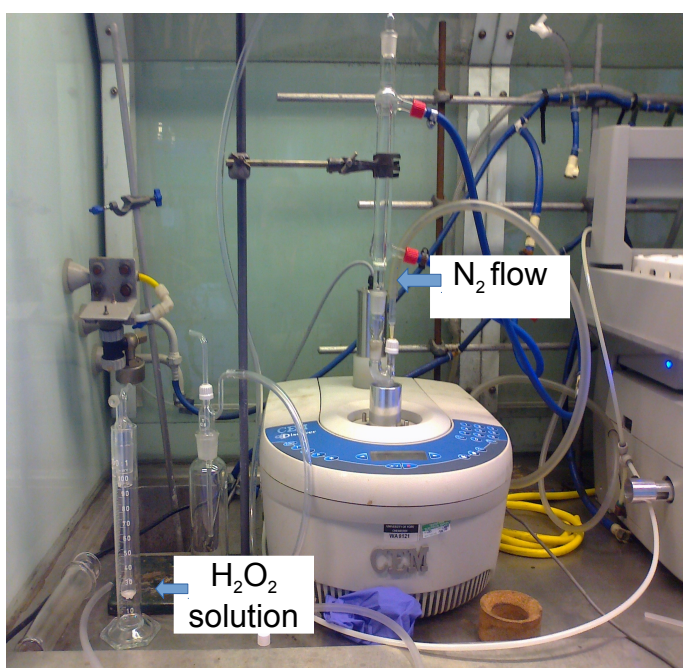


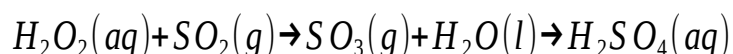
**Figure 6.3.** Experimental set up used during sulfonation of Starbons<sup>®</sup> by microwave irradiation. Collection of gases using H<sub>2</sub>O<sub>2</sub> solution (30% v/v)

After sulfonation, samples were filtered off to remove excess of sulfuric acid. Then, samples were washed using microwaves. The ratio was 1 g of solid to 30 mL of water. The microwave set conditions were an open vessel mode, constant stirring at fixed temperature at 90 °C, during 10 minutes; the maximum power was set to 200 W.

Most of the microwave sulfonated Starbons<sup>®</sup> were not treated with methanol as conventional sulfonated Starbons<sup>®</sup>, with the aim to evaluate the effectiveness of this new method of sulfonation. However, if a comparison with conventional sulfonated Starbons<sup>®</sup> was needed, the methanol wash treatment of microwave sulfonated Starbons<sup>®</sup> was carried out and it consisted of heating samples (1 g of sulfonated Starbon<sup>®</sup> to 15 mL of methanol), using microwaves in open vessel mode, during 30 minutes with constant stirring at 75 °C. After treatment, sample was filtered off and oven dried at 105 °C.

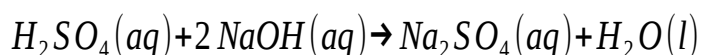
#### 6.3.4. Quantification of sulfur dioxide (SO<sub>2</sub>) released during sulfonation

SO<sub>2</sub> was identified in the released gases during sulfonation and collected in a hydrogen peroxide (H<sub>2</sub>O<sub>2</sub>) solution (30% v/v) at room temperature (**Figure 6.3.**). Thus, it is possible to quantify SO<sub>2</sub> with the aim of correlating the released SO<sub>2</sub> quantity with the sulfur content obtained in sulfonated Starbons<sup>®</sup>, taking into account the mass of sulfuric acid used. It is worth mentioning that this method was based in a proposal used in wine industry.<sup>169</sup> According to this method, the SO<sub>2</sub> dissolved in hydrogen peroxide solution will form sulfuric acid (**Equation 6.1.**).



**Equation 6.1.** Formation of sulfuric acid during reaction of hydrogen peroxide with sulfur dioxide

An aliquot (10 mL) was taken from this sulfuric acid (H<sub>2</sub>SO<sub>4</sub>) solution and titrated potentiometrically with a sodium hydroxide (NaOH) solution, according with a neutralization reaction. **Equation 6.2.** Titration was done by triplicate.



**Equation 6.2.** Neutralization reaction between sulfuric acid and sodium hydroxide, used to determine quantity of SO<sub>2</sub> released.

The determination of SO<sub>2</sub> released per gram of Starbon® is related to the mole number of H<sub>2</sub>SO<sub>4</sub>, considering the dilution factor (5) and taking into account the mass of Starbon® used in sulfonation. This is schematically presented in **Figure 6.4**.

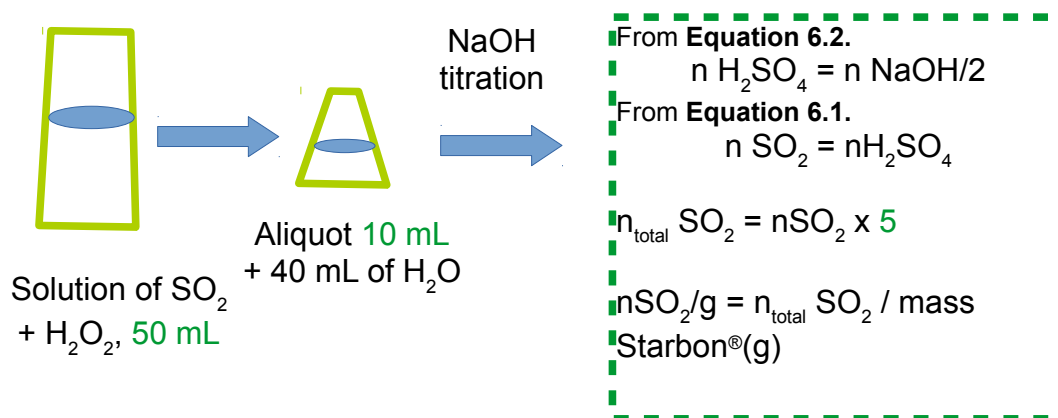


**Figure 6.4.** Schematic representation of the quantification of sulfur dioxide through potentiometric titration

## 6.4. Materials characterisation

### 6.4.1. Elemental analysis

Elemental composition (carbon, hydrogen, oxygen) of samples was determined by CHN analysis through the service provided by the Department of Chemistry, University of York, York, UK. This analysis was done by Dr. Graeme Mcallister using a Sartorius SE2 analytical balance for weighing samples and an Exeter Analytical Inc CHN analyser.

Sulfur content in sulfonated samples was determined externally by Lancrop Laboratories, Manor Place, Wellington Road, The Industrial Estate, Pocklington, York, YO42 1DN. The methodology described by the external analyst consists in putting a weighed sample in a microwable digestion tube, then reverse aqua regia [9 mL of HNO<sub>3</sub> (conc.) and 3 mL of HCl (conc.)] is added. The sample is then digested with the aid of a Mars Xpress microwave digester. Once digestion

has taken place, the sample is made up to 25 mL using deionised water and filtered. It is then analysed on a axial Varian vista ICP. Results are automatically corrected by dilution factor. This information was provided by Darren Clegg, Business manager of Analytical Services and Lancrop Laboratories.

#### **6.4.2. Infrared spectroscopy**

FTIR spectra were recorded using a Bruker Vertex 70 FTIR spectrometer fitted with an ATR golden gate attachment with diamond top plate analysis window; controlled throughout Opus software. The spectrum was recorded in the wavenumber range 4000–600  $\text{cm}^{-1}$ . The number of scans used for background and samples was set at 64 and 32 scans, respectively. The resolution selected was 4  $\text{cm}^{-1}$ .

#### **6.4.3. X-Ray photoelectron spectroscopy (XPS)**

XPS analysis was conducted by Dr Benjamin Johnson, EPSRC XPS service at the University of Leeds, School of Physics and Astronomy, Leeds, LS2 9JT. XPS spectra were recorded on a Kratos Axis Ultra DLD photoelectron spectrometer using a hemispherical photoelectron analyser with a monochromatic  $\text{AlK}\alpha$  X-ray source (75-150 W) and analyser pass energies of 160 eV (for survey scans) and 40 eV (for detailed scans). Samples were mounted using double-sided tape. Binding energies were referenced to the C 1s binding energy 284.5 eV. Prior to analysis samples were dried overnight at 105  $^{\circ}\text{C}$ . The analysis of the spectra was carried out using CasaXPS software.

#### **6.4.4. Solid-state $^{13}\text{C}$ CP/MAS Nuclear Magnetic Resonance**

Solid-state  $^{13}\text{C}$  CP/MAS NMR spectra were obtained at the EPSRC UK National Solid-state NMR Service at Durham, the University of Durham, Department of Chemistry, Durham, DH1 3LE. The analysis was carried out by Dr David Apperley.

$^{13}\text{C}$  CP/MAS NMR spectra were obtained using a Varian VNMRS spectrometer

with a frequency of 100.56 MHz. Spectra were recorded following a “black carbon” acquisition conditions: extended spectra width, rotor synchronised spin-echo, adjusted Hartmann-Hahn match and 14 kHz spin-rate. CP linear on H, contact time 1.00 ms and two-phase two-modulated (TPPM) decoupling at 77.5 kHz. Spectral referencing was with respect to tetramethylsilane.

#### **6.4.5. Surface area and porosity**

Nitrogen-adsorption measurements were carried out at 77 K by using an ASAP 2020 volumetric adsorption analyser from Micromeritics. Prior analysis, weighed samples (80 – 100 mg) were degassed for 5 hours at 160 °C. The equilibration time established for the measurement was of 10 seconds. Surface area was determined by using the BET model (**Equation 1.2.**) and the pore size distribution on the materials was determined using the BJH model.

#### **6.4.6. Scanning Electron Microscopy (SEM) analysis**

Electron microscopy images were acquired with the help of Ms Meg Stark at the Technology Facility in the Department of Biology, University of York, UK. SEM images were recorded using a JEOL JSM-6490LV. Samples were mounted on alumina plates and coated with a 7 nm layer of Au/Pd using a high resolution sputter SC-7640 coating device prior to analysis. Typical magnifications used were x1500, x3000, x4500 and x7000.

#### **6.4.7. Thermo gravimetric analysis coupled to infrared spectroscopy (TG-FTIR)**

TG-FTIR studies were carried out using a Netzch 409 STA thermal analyser coupled to a Bruker Equinox 55 infrared spectrometer via a transfer line. The temperature of the transfer line was set at 200 °C and the IR detector used was a MCT (HgCdTe) cooled with liquid nitrogen. For the measurement, approximately 50 mg of sample was mounted in a 3.5 mL ceramic crucible and heated under a flow of nitrogen (100 mLmin<sup>-1</sup>). Prior to analysis the oven chamber was evacuated and backfilled three times with nitrogen. Samples were

heated at 10 °C min<sup>-1</sup> to 1000 °C.

#### 6.4.8. Acidity determination

Quantity of sulfonic groups (~SO<sub>3</sub>H) attached to sulfonated samples was determined by titration using an aqueous solution of NaOH. The procedure used for sulfonated Starbons<sup>®</sup> is a modification of the method proposed by P. Lin *et al*<sup>46</sup> for sulfonated carbon nanocage materials. In our work, 20 mg of sample was dispersed in 15 g of methanol-aqueous (1:1) solution of NaCl (2 M); sample was stirred overnight at room temperature. Afterwards, the dispersion was filtered to remove the solid sulfonated Starbon<sup>®</sup> and the filtrate was then titrated potentiometrically using NaOH 0.005 M. Considering that number of equivalents (H<sup>+</sup>-OH<sup>-</sup>) are in a 1:1 ratio; the quantity of H<sup>+</sup> neutralized can be found using the volume of NaOH solution in the equivalent point and its concentration, as shown in **Equation 6.3**.

$$\sim\text{SO}_3\text{H}/\text{mmol g}^{-1} = \frac{(\text{vol. NaOH}/\text{mL})(\text{conc. NaOH}/\text{M})}{\text{mass of Sulfonated Starbon } \text{®}/\text{g}} *$$

**Equation 6.3.** Calculation of the quantity of sulfonic groups through potentiometric titration with NaOH \* vol. = volume; conc.= concentration; assuming all H<sup>+</sup> come from SO<sub>3</sub>H groups

#### 6.5. Catalytic testing

##### 6.5.1. Sample preparation

Conventional heating reactions were carried out using a Radleys Discovery multipoint with set temperature at 75 °C and continuous stirring. In this test, reaction mixture contained: 15 mmol of organic acid, 225 mmol of alcohol and 60 mg of catalyst. Reaction progress was monitored by sampling aliquots of reaction mixture taken at specific times, which were subsequently analysed by gas chromatography.

Microwave experiments were carried out in a CEM Discover model with PC control, the experiments were conducted in close vessels (pressure controlled) under continuous stirring. The microwave method was set to be a fixed power output at 200 W during 30 minutes. The reaction mixture kept the same ratio as those carried out on the multipoint reactor: 5 mmol of lauric acid, 75 mmol of methanol and 20 mg of catalyst. Samples were analysed by GC, as mentioned previously.

### **6.5.2. Catalyst recycling**

Regeneration of catalyst for microwave reactions was done as follows: reaction mixture was separated from catalyst by decantation. Then 3 mL of acetone was added to the microwave vial and stirred at 45 °C during 15 minutes, to remove unreacted reagents. Afterwards, samples were centrifuged in Thermo Scientific Megafuge 40R centrifuge at 3500 rpm for 10 minutes and acetone was removed. Recovered catalysts were dried at 105 °C for 4 h before next use (presented in **Figure 5.7.**).

### **6.5.3. Gas Chromatography and Mass Spectra analysis**

Gas chromatography (GC) analysis was done using an Agilent 6890 GC model chromatograph with a flame ionization detector (FID). This was fitted with a carbowax DB-wax capillary column (30 m x 0.25 mm x 0.25  $\mu\text{m}$ ) at constant pressure of 14.3 psi. The carrier gas used was helium with a flow rate of 35.8 mLmin<sup>-1</sup>. The split ratio was set at 25:1. The initial temperature in oven was maintained at 50 °C for 3 min, then temperature incremented at a rate of 8 °Cmin<sup>-1</sup> to 150 °C, it was held at this temperature for 1 minute. Then, temperature rose at 10 °Cmin<sup>-1</sup> to 240°C and was maintained for 1 minute. Both injector and FID detector were heated at 240 °C.

Peaks were identified by comparison with standard compounds. The performance of the sulfonated Starbons<sup>®</sup> in esterification reactions was monitored through the estimated conversion to the ester. This approximation was done using the ratio peak areas between the ester and acid components

according to **Equation 6.4**. This approach employs simple manipulations to obtain a general picture of the reaction behaviour. It is worth mentioning that studies on reproducibility in the microwave esterifications of lauric acid with methanol, the reactions mixtures were analysed by GC following this peak area ratio approach, the results yielded standard deviations of  $\pm 3.6\%$  (**Figure 6.5**). These observations give us enough confidence with the approximations carried out. As well, it is worth mentioning that similar quantities of analyte was taken (~50 mg).

$$\% i = \frac{Area_i}{\sum_{i=1}^{i=n} Area_i}$$

**Equation 6.4.** Determination of conversion to ester (component i) in an esterification reaction

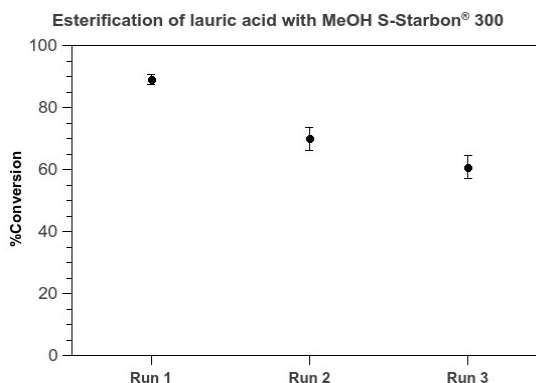


**Figure 6.5.** Reproducibility of results obtained in esterification of lauric acid with methanol (MW, 200W, 30 min) and associated errors

Gas chromatograph mass spectrometry (GC-MS) was performed on a Perkin Elmer Clarus 500 GC coupled with a Clarus 560 S quadrupole mass spectrometer. This equipment was fitted with a DB5HT capillary column (30m x 250  $\mu\text{m}$  x 0.25  $\mu\text{m}$  nominal) at constant pressure of 22.35 psi with a helium carrier gas. The temperature of the injector was maintained at 350  $^{\circ}\text{C}$  and the flow rate was set to 1.00  $\text{mLmin}^{-1}$ . The split ratio used was 10:1. The temperature of the injector and transfer line were maintained at 300  $^{\circ}\text{C}$  and 350  $^{\circ}\text{C}$ , respectively. The initial oven temperature was maintained at 60  $^{\circ}\text{C}$  for 1 minute. The temperature was then ramped at a rate of 8  $^{\circ}\text{Cmin}^{-1}$  to 360  $^{\circ}\text{C}$  and held for 10 minutes. The Clarus 500 quadrupole mass spectra was operated in

the electron ionization mode (EI) at 70 eV, a source temperature of 300 °C with the quadrupole at 300 °C. The scanning mass range was of 30 - 1200 amu. per second. The data was collected with the PerkinElmer enhanced TurboMass (V.5.4.2) chemical software and compounds were identified by comparison of mass fragmentation patterns with spectra contained in the NIST library (v. 2.2) and by direct comparison with standard compounds.

#### **6.5.4. NMR spectroscopy**

Reaction mixtures were dissolved in chloroform-d for <sup>13</sup>C NMR spectra, which were obtained using a JEOL JNM-ECS400 NMR operating at 100.52 MHz, 256 scans. Spectral referencing was with respect to tetramethylsilane.

#### **6.5.5. XRF analysis**

Analysis of elemental sulfur in washing alcohols (MeOH, EtOH and i-PrOH) for leaching tests were measured in a Rigaku NEX-CG X-ray fluorescence spectrometer equipped with a X-ray tube with Pd anode. Control of the instrument and data storage was performed through a Hewlett Packard PC with RPF-SQX software. This software allows to obtain semi-quantitative values (without standards) of the chosen elements to be analysed. Measurements were carried out in a helium atmosphere.

# **Chapter 7**

## ***Thesis conclusion and further work***



## 7.1. Conclusion

### 7.1.1. New synthesis approaches

The general objective of this project was to prepare solid-acid catalysts from Starbons<sup>®</sup>, starch derived materials. These solid acid catalysts were prepared by sulfonation of a range of carbonized Starbons<sup>®</sup> with sulfuric acid. The sulfonation approach consisted of using commercial sulfuric acid (95 %) instead of high purity (99.999 %) which had been used in earlier versions of these materials; low solid (g): acid (mL) ratio of 1:7 compared to 1:10 of previous works done using Starbons<sup>®</sup> or even to 1:50 used in the synthesis of solid acid catalysts based on sugars. Our approach of sulfonation of Starbons<sup>®</sup> avoids the use of “conditioning steps” that include toluene; the removal of excess of sulfuric acid after sulfonation was done using hot washes.

A range of carbonized Starbons<sup>®</sup> from 350 °C to 700 °C was prepared using as starting material Starbons<sup>®</sup> 300 and 400 (°C) prepared for scale up. It is worth mentioning that this work is the first one in using carbonized materials prepared at scale of 10 Kg for further modifications with the availability of large scale manufactured Starbon<sup>®</sup> 800; the temperature of carbonized Starbons<sup>®</sup> extends from 300 to 800 °C. Elemental composition of these materials showed that C:O ratio increases with temperature of carbonization, obtaining high values for Starbon<sup>®</sup> 800, indicating the carbon-like nature of the material.

The sulfonation of Starbons<sup>®</sup> was done following two methodologies: sulfonation by conventional heating and by the use of microwave irradiation. The conventional sulfonation was done for a range of carbonized Starbons<sup>®</sup>, whilst microwave sulfonation explores only three Starbons<sup>®</sup>, the two extremes, 300 and 800 and the middle 450. In the conventional approach the reaction is carried out at 90°C for 6 h; for microwave sulfonations, the temperatures examined were 90, 120 and 150 °C, and the reaction lasted 30 minutes. During preliminary tests of conventional sulfonated Starbons<sup>®</sup> in esterifications, the leaching of sulfuric acid from the materials was found. Then a new approach was proposed to decrease the contribution of homogeneous catalysis. This

consisted in “washing” the original conventional sulfonated Starbons<sup>®</sup>, with methanol using similar reaction conditions. In this way, the new sulfonated Starbons<sup>®</sup> were born: S-Starbons<sup>®</sup> (temperature) W3. However, this extra washing with methanol was not performed for microwave sulfonated Starbons<sup>®</sup>, trying to evaluate the efficiency of these sulfonated materials.

## 7.1.2. Characterisation outcomes

### 7.1.2.1. Sulfonated Starbons<sup>®</sup> by conventional heating

The elemental composition analysis for sulfonated Starbons<sup>®</sup> prepared by conventional heating showed an increase in the oxygen:carbon ratio compared with their respective parent Starbons<sup>®</sup>. This observation was attributed to the introduction of sulfonic acid groups as well as the oxidation of some carbon functionalities present in the original material during sulfonation. This observation was further supported by XPS analysis and <sup>13</sup>C solid-state NMR; which show the increase in carbonyl, carboxyl, esters, lactones groups in sulfonated Starbons<sup>®</sup>; this increase in oxygenated compounds was more noticeable on high-temperature Starbons<sup>®</sup> 700 and 800, which showed a significant decrease in the C:O ratio after sulfonation.

The <sup>13</sup>C solid-state NMR showed a transition from a complex broad spectrum for sulfonated Starbon<sup>®</sup> 300 to a narrow band centred at 130 ppm for sulfonated Starbon<sup>®</sup> 600, interpreted as the change from more oxygenated structures for low-temperature Starbons<sup>®</sup> (300) to more carbon-like for high-temperature carbonized Starbons<sup>®</sup>; in agreement with the C:O ratio obtained by elemental analysis.

The sulfur content seems to change as well with temperature, being noticeably higher for low-temperature Starbons<sup>®</sup> than for high-temperature Starbons<sup>®</sup>. The XPS analysis showed that reduced sulfur, S(II) is observed in carbonized Starbons<sup>®</sup> from 450 °C onwards; while sulfonated Starbons<sup>®</sup> 300 and 350 only present sulfur (VI), associated with sulfonic acid groups. It is worth mentioning that sulfonic groups are also observed in Starbons<sup>®</sup> prepared at higher

temperature, however the ratio of S(VI) is lower than the one obtained for sulfonated Starbons® 300 and 350.

#### *7.1.2.2. Microwave sulfonated Starbons®*

Similar to the conventional sulfonated Starbons®, microwave sulfonated Starbons® showed an increase in oxygenated groups due to the oxidation promoted by sulfuric acid. The main difference between microwave and conventional sulfonation relied on the sulfur components obtained after microwave sulfonation. Thus, an extra sulfur species is identified in microwave sulfonated Starbons® 300, ascribed to S(VI) in the form of organosulfates,  $\text{ROSO}_2\text{OR}$ . The sulfonation temperature used in the microwave approach, seems to have a greater effect on the sulfur content in sulfonated Starbon® 800 than for 300 and 450; because microwave sulfonated Starbon® 800 prepared at 150 °C presents a significant higher sulfur content than samples sulfonated at 90 or 120 °C.

Independent from the sulfonation approach used in their preparation, Sulfonated Starbons® present a characteristic absorption band in the infrared attributed to symmetric stretching of S=O of sulfonic acids at  $\sim 1030\text{ cm}^{-1}$ .

#### **7.1.3. Catalyst performance overview**

The conventional sulfonated Starbons® were tested in esterifications reactions, it was found that reactions carried out using microwave irradiation gave higher conversions than reactions done by conventional heating. The test of conventional sulfonated Starbons® in microwave-assisted esterification, showed that low temperature Starbons® (300, 350) have a better performance than sulfonated Starbons® situated in the middle carbonization range (550, 600), getting slightly better at the end (700, 800). This trend is similar to the trend of sulfur bulk content observed in the materials.

Reusability of conventional sulfonated Starbons® 300 and 800 tested in esterification of lauric acid with methanol, showed that materials promoted

higher conversions in the first run, which drops during second use. In that reaction, conventional sulfonated Starbon® 300 can be used more times than sulfonated Starbon® 800. This observation was correlated to the thermal stability studied by TG-FTIR. This study shows that SO<sub>2</sub>(g) is released in a broader range of temperature in sulfonated Starbon® 300 than sulfonated Starbon® 800; with a maximum temperature at 350 °C and 280 °C, respectively. This outcome would indicate that sulfur species present in Starbon® 300 are thermally more stable than those present in sulfonated Starbon® 800.

The test using microwave sulfonated Starbons® in esterification of lauric acid with methanol, showed that high conversions are achieved in the first use; but the conversion decreases in the second run, being significant lower for microwave sulfonated Starbons® 450 and 800 than for Starbon® 300.

A leaching test performed using sulfonated Starbons® 300 in esterification of lauric acid with methanol in MW reactions for 5 minutes, showed that the first run gives high conversions, but in subsequent runs, conversion decreased. In this test the contribution of leaching to reaction is over 50% in most cases.

The acidity, in terms of density of sulfonic groups present on the materials, was determined using a NaCl solution as interchange media. The values determined for sulfonated Starbons® 300 is lower than the expected according to the S(VI) measured by XPS. This difference would suggest that S(VI) exists in other species rather than solely sulfonic acids.

Finally, as a general conclusion, it can be added that during the realization of this work a broad range of sulfonated Starbons® were prepared following two sulfonation methodologies. These materials were widely characterised using several techniques, although their activities as catalyst would require some improvement, the findings from this work can be used as a reference framework for future studies on sulfonation of other carbonaceous and possibly other biobased materials.

## 7.2. Further work

This work presents a general overview of the application of sulfonated Starbons<sup>®</sup> in esterification reactions using methanol, which could be a strong deactivating solvent. Then it would be worth to try other acid-catalysed reactions, to determine activity of sulfonated Starbons<sup>®</sup> in another media.

Microwave sulfonation offers the option to obtain novel sulfonated Starbons<sup>®</sup>, then it would be interesting to explore new synthesis conditions; like increasing reaction time. This would be explored with a better system for the quantification of SO<sub>2</sub> released to find out a relationship between the sulfur content obtained in sample, the SO<sub>2</sub> released and the quantity of input. sulfuric acid.

Changes observed on the properties i.e. surface area of the microwave sulfonated Starbons<sup>®</sup> can be more explored using different solvents such as water or methanol, to identify whether the increase in surface area is related to the interaction of the solvent and the material under microwave conditions or it is directly related to the sulfonation process. In this sense, it would be interesting as well to explore another analysis methodology such as Density Functional Theory, DFT model.

The use of recycled sulfuric acid in the sulfonation Starbons<sup>®</sup> is as well worth to be studied in-depth, as our results are promising for the preparation of active solid acid catalyst.

With the information obtained throughout the different characterisation techniques and further analysis, it would be interesting to work out the mechanisms of sulfonation of Starbons<sup>®</sup>.

A better understanding of the deactivation of sulfonated Starbons<sup>®</sup> could be done using XPS and TGIR to analyse the sulfonated Starbons<sup>®</sup> after reaction; this would help to determine the chemical states left on materials and their thermal stability.



# **Chapter 8**

## ***Abbreviations***



## 8.1. List of abbreviations

amu	Atomic mass unit
AR	Analytical reagent
ATR	Attenuated total reflectance
BJH	Barrett Joyner and Halenda
BE	Binding energy
BET	Brunauer Emmet and Teller
CP	Cross polarization
eV	Electron volts
FID	Flame ionization detector
FT	Fourier transform
g	grams
GC	Gas chromatography
GHz	Gigahertz
IR	Infrared
IUPAC	International Union of Pure and Applied Chemistry
kg	Kilogram
M	Molar (mol per litre)
MAS	Magic angle spinning
MHz	Megahertz
mL	Mililitres
MW	Microwaves
nm	Nanometer
NMR	Nuclear magnetic resonance
p-TSA	Para-toluenesulfonic acid
ppm	Parts per million
rpm	Revolutions per minute
SEM	Scanning Electron Microscopy
TGA	Thermogravimetric analysis
TGIR	Thermogravimetric infrared analysis
v/v	Volume/volume
XRF	X-ray fluorescence spectroscopy
XPS	X-ray photoelectron spectroscopy



# **Chapter 9**

## ***References***



## 9.1. References

1. Clark, J. Green chemistry: challenges and opportunities. *Green Chemistry* 1–8 (1999).
2. Brundtland, G. Report of the World Commission on environment and development: “our common future.” 300 (1987).
3. P. T. Anastas and J. C. Warner. *Green Chemistry: Theory and Practice*. (Oxford University Press, 1998).
4. Anastas, P. & Eghbali, N. Green chemistry: principles and practice. *Chem. Soc. Rev.* **39**, 301–312 (2010).
5. Sheldon, R. a. Fundamentals of green chemistry: efficiency in reaction design. *Chemical Society reviews* **41**, 1437–51 (2012).
6. Anastas, P. T. & Kirchhoff, M. M. Origins, current status, and future challenges of green chemistry. *Accounts of chemical research* **35**, 686–94 (2002).
7. Beach, E. S., Cui, Z. & Anastas, P. T. Green Chemistry: A design framework for sustainability. *Energy & Environmental Science* **2**, 1038 (2009).
8. Clark, J. H. Green chemistry: today (and tomorrow). *Green Chemistry* **8**, 17 (2006).
9. Budarin, V. *et al.* Starbons: new starch-derived mesoporous carbonaceous materials with tunable properties. *Angewandte Chemie* **45**, 3782–6 (2006).
10. Clark, J. H. Solid acids for green chemistry. *Accounts of chemical research* **35**, 791–7 (2002).
11. Dodson, J. R., Hunt, a. J., Parker, H. L., Yang, Y. & Clark, J. H. Elemental sustainability: Towards the total recovery of scarce metals. *Chemical Engineering and Processing: Process Intensification* **51**, 69–78 (2012).
12. Clara, N., Tortato, C., Ronchin, L. & Bianchi, C. On the acidity of liquid and solid acid catalysts : Part 1 . A thermodynamic point of view. **56**, 159–164 (1998).
13. Budarin, V. L., Clark, J. H., Luque, R. & Macquarrie, D. J. Versatile mesoporous carbonaceous materials for acid catalysis. *Chemical communications (Cambridge, England)* 634–6 (2007).
14. Clark, J. *et al.* Catalytic performance of carbonaceous materials in the esterification of succinic acid. *Catalysis Communications* **9**, 1709–1714 (2008).

15. Anastas, P. T., Kirchoff, M. M. & Williamson, T. C. Catalysis as a foundational pillar of green chemistry. *Applied Catalysis A: General* **221**, 3–13 (2001).
16. Anastas, P. T., Bartlett, L. B., Kirchoff, M. M. & Williamson, T. C. The role of catalysis in the design, development, and implementation of green chemistry. *Catalysis Today* **55**, 11–22 (2000).
17. Rothenberg, G. *Catalysis: Concepts and Green Applications*. (Wiley-VCH Verlag GmbH & Co. KGaA, 2008).
18. Sheldon, R. A., Arends, I. W. C. E. & Hanefeld, U. *Green Chemistry and Catalysis*. (Wiley-VCH Verlag GmbH & Co. KGaA, 2007).
19. Sejidov, F., Mansoori, Y. & Goodarzi, N. Esterification reaction using solid heterogeneous acid catalysts under solvent-less condition. *Journal of Molecular Catalysis A: Chemical* **240**, 186–190 (2005).
20. Semwal, S., Arora, A. K., Badoni, R. P. & Tuli, D. K. Biodiesel production using heterogeneous catalysts. *Bioresource technology* **102**, 2151–61 (2011).
21. Wang, Y. *et al.* Grafting sulfated zirconia on mesoporous silica. *Green Chemistry* **9**, 540 (2007).
22. Kapoor, M. P. *et al.* An alternate approach to the preparation of versatile sulfonic acid functionalized periodic mesoporous silicas with superior catalytic applications. *Journal of Materials Chemistry* **18**, 4683 (2008).
23. Xing, R. *et al.* Active solid acid catalysts prepared by sulfonation of carbonization-controlled mesoporous carbon materials. *Microporous and Mesoporous Materials* **105**, 41–48 (2007).
24. Hara, M. *et al.* A carbon material as a strong protonic acid. *Angewandte Chemie (International ed. in English)* **43**, 2955–8 (2004).
25. Toda, M. *et al.* Green chemistry: biodiesel made with sugar catalyst. *Nature* **438**, 178 (2005).
26. Mo, X. *et al.* Activation and deactivation characteristics of sulfonated carbon catalysts. *Journal of Catalysis* **254**, 332–338 (2008).
27. Takagaki, A. *et al.* Esterification of higher fatty acids by a novel strong solid acid. *Catalysis Today* **116**, 157–161 (2006).
28. Okamura, M. *et al.* Acid-Catalyzed Reactions on Flexible Polycyclic Aromatic Carbon in Amorphous Carbon. *Chemistry of Materials* **18**, 3039–3045 (2006).
29. Suganuma, S. *et al.* Hydrolysis of cellulose by amorphous carbon bearing

- SO<sub>3</sub>H, COOH, and OH groups. *Journal of the American Chemical Society* **130**, 12787–93 (2008).
30. Kitano, M. *et al.* Preparation of a Sulfonated Porous Carbon Catalyst with High Specific Surface Area. *Catalysis Letters* **131**, 242–249 (2009).
  31. Suganuma, S. *et al.* SO<sub>3</sub>H-bearing mesoporous carbon with highly selective catalysis. *Microporous and Mesoporous Materials* **143**, 443–450 (2011).
  32. Zong, M.-H., Duan, Z.-Q., Lou, W.-Y., Smith, T. J. & Wu, H. Preparation of a sugar catalyst and its use for highly efficient production of biodiesel. *Green Chemistry* **9**, 434 (2007).
  33. Zhang, B. *et al.* Novel sulfonated carbonaceous materials from p-toluenesulfonic acid / glucose as a high-performance solid-acid catalyst HO HO OH. *Catalysis Communications* **11**, 629–632 (2010).
  34. R. M. Silverstein, F.X. Webster, D. J. K. *Spectrometric Identification of Organic Compounds*. 502 (John Wiley & Sons, Ltd, 2005).
  35. Tipson, R. Infrared Absorption Spectra of p-Toluenesulfonic Acid and of Some of Its Esters. *Journal of the American Chemical Society* **74**, 1354 (1952).
  36. Pejov, L., Ristova, M. & Soptrajanov, B. Quantum chemical study of p-toluenesulfonic acid, p-toluenesulfonate anion and the water-p-toluenesulfonic acid complex. Comparison with experimental spectroscopic data. *Spectrochimica acta. Part A, Molecular and biomolecular spectroscopy* **79**, 27–34 (2011).
  37. Chen, G. & Fang, B. Preparation of solid acid catalyst from glucose-starch mixture for biodiesel production. *Bioresource technology* **102**, 2635–40 (2011).
  38. Liu, X.-Y. *et al.* Preparation of a carbon-based solid acid catalyst by sulfonating activated carbon in a chemical reduction process. *Molecules (Basel, Switzerland)* **15**, 7188–96 (2010).
  39. Ji, J. *et al.* Sulfonated graphene as water-tolerant solid acid catalyst. *Chemical Science* **2**, 484 (2011).
  40. Lee, D. Preparation of a sulfonated carbonaceous material from lignosulfonate and its usefulness as an esterification catalyst. *Molecules (Basel, Switzerland)* **18**, 8168–80 (2013).
  41. Sing, K. S. W. Reporting physisorption data for gas / solid systems with special reference to the determination of surface area and porosity. *Pure and Applied Chemistry* **54**, 18 (1982).

42. Taguchi, A. & Schüth, F. *Ordered mesoporous materials in catalysis. Microporous and Mesoporous Materials* **77**, 1–45 (2005).
43. White, R. J., Budarin, V., Luque, R., Clark, J. H. & Macquarrie, D. J. Tuneable porous carbonaceous materials from renewable resources. *Chemical Society reviews* **38**, 3401–18 (2009).
44. Ma, T.-Y., Liu, L. & Yuan, Z.-Y. Direct synthesis of ordered mesoporous carbons. *Chemical Society reviews* **42**, 3977–4003 (2013).
45. Ryoo, R. *et al.* Ordered mesoporous carbon molecular sieves by templated synthesis : the structural varieties. (2001)
46. Lin, P. *et al.* Synthesis of Sulfonated Carbon Nanocage and Its Performance as Solid Acid Catalyst. *Catalysis Letters* **141**, 459–466 (2010).
47. Janaun, J. & Ellis, N. Role of silica template in the preparation of sulfonated mesoporous carbon catalysts. *Applied Catalysis A: General* **394**, 25–31 (2011).
48. Budarin, V. & Clark, J. Starbons: cooking up nanostructured mesoporous materials. *Mater. Matters* 20–22 (2009).
49. Shuttleworth, P. & Parker, J. *Cleargum starch*. (2011).
50. Hara, M. Environmentally benign production of biodiesel using heterogeneous catalysts. *ChemSusChem* **2**, 129–35 (2009).
51. Nüchter, M., Ondruschka, B., Bonrath, W., Gum, A. & Jena, D.-. Microwave assisted synthesis – a critical technology overview. *Green Chemistry* **6**, 128–141 (2004).
52. Polshettiwar, V. & Varma, R. S. Microwave-assisted organic synthesis and transformations using benign reaction media. *Accounts of chemical research* **41**, 629–639 (2008).
53. Loupy, A. Solvent-free microwave organic synthesis as an efficient procedure for green chemistry. *Comptes Rendus Chimie* **7**, 103–112 (2004).
54. Hayes, B. L. *Microwave Synthesis Chemistry at the speed of light*. (CEM Publishing, 2002).
55. Lidström, P., Tierney, J., Wathey, B. & Westman, J. Microwave assisted organic synthesis—a review. *Tetrahedron* **57**, (2001).
56. Lew, A., Krutzik, P. O., Hart, M. E. & Chamberlin, A. R. Increasing Rates of Reaction: Microwave-Assisted Organic Synthesis for Combinatorial Chemistry. *Journal of Combinatorial Chemistry* **4**, 95–105 (2002).
57. Stueriga, D., Gonon, K. & Lallemand, M. Microwave selectivity heating as a

- new way to induce between competitive to isomeric ratio control of naphthalene . Application in sulfonation. **49**, 6229–6234 (1993).
58. Loupy, A. *Microwaves in Organic Synthesis: Second, Completely Revised and Enlarged Edition, Volume 2*. 1–482 (Wiley-VCH Verlag GmbH & Co. KGaA, 2006).
59. Polshettiwar, V. & Varma, R. S. *Aqueous Microwave Assisted Chemistry Synthesis and Catalysis*. (Royal Society of Chemistry, 2010).
60. Berlan, J. Microwaves in Chemistry: Another Way of Heating Reaction Mixtures. *Radiat. Phys. Chem.* **45**, 581–589 (1995).
61. Venkatesh, M. S. & Raghavan, G. S. V. An Overview of Microwave Processing and Dielectric Properties of Agri-food Materials. *Biosystems Engineering* **88**, 1–18 (2004).
62. Settle, F. *Handbook of instrumental techniques for analytical chemistry*. (Prentice Hall, 1997).
63. Robinson, J., Frame, E. & Il, G. F. *Undergraduate instrumental analysis*. (Marcel Dekker, Inc., 2004).
64. Leofanti, G., Padovan, M., Tozzola, G. & Venturelli, B. Surface area and pore texture of catalysts. *Catalysis Today* **41**, 207–219 (1998).
65. Kruk, M. & Jaroniec, M. Gas Adsorption Characterization of Ordered Organic - Inorganic Nanocomposite Materials. 3169–3183 (2001).
66. Gregg, S. & Sing, K. *Adsorption, Surface Area, and Porosity*. (1983).
67. Trunschke, A. *Surface area and pore size determination*. Modern Methods in Heterogeneous Catalysis Research. **1**, (2007).
68. Micromeritics. *TriStar 3000 Manual*. **08**, (2007).
69. Vickerman, J. *Surface analysis, The principal techniques*. (Wiley, 1997).
70. Williams, D. H. & Fleming, I. *Spectroscopic Methods in Organic Chemistry*. (McGraw-Hill, 2005).
71. Ahuja, S. & Jespersen, N. *Modern instrumental analysis*. (Elsevier, 2006).
72. Laws, D., Bitter, H. & Jerschow, A. Solid-State NMR Spectroscopic Methods in Chemistry. *Angewandte Chemie ...* (2002).
73. Mullens, J. in *Handbook of Thermal Analysis and Calorimetry Vol. 1: Principles and Practice* (ed. Brown, M. E.) **1**, 509–546 (Elsevier Science B.V., 1998).
74. McNair, H. & Miller, J. *Basic gas chromatography*. (Wiley, 2009).

75. Budarin, V., Luque, R., Macquarrie, D. J. & Clark, J. H. Towards a bio-based industry: benign catalytic esterifications of succinic acid in the presence of water. *Chemistry (Weinheim an der Bergstrasse, Germany)* **13**, 6914–9 (2007).
76. Luque, R., Budarin, V., Clark, J. H. & Macquarrie, D. J. Microwave-assisted preparation of amides using a stable and reusable mesoporous carbonaceous solid acid. *Green Chemistry* **11**, 459 (2009).
77. Suganuma, S., Nakajima, K., Kitano, M. & Yamaguchi, D. Hydrolysis of Cellulose by Amorphous Carbon Bearing SO<sub>3</sub>H, COOH, and OH Groups. 12787–12793 (2008).
78. Loyd, A., Dogson, K., Price, R. G. & Rose, F. A. Infrared studies on sulfate esters. I. Polysaccharides sulfates. *Biochem Biophys Acta* **46**, 108–115 (1961).
79. Guiotoku, M., Rambo, C. R., Hansel, F. a., Magalhães, W. L. E. & Hotza, D. Microwave-assisted hydrothermal carbonization of lignocellulosic materials. *Materials Letters* **63**, 2707–2709 (2009).
80. Sevilla, M. & Fuertes, A. B. Chemical and structural properties of carbonaceous products obtained by hydrothermal carbonization of saccharides. *Chemistry (Weinheim an der Bergstrasse, Germany)* **15**, 4195–203 (2009).
81. Van Krevelen, D. W. Method for the study of structure and reaction processes of coal. *Fuel* **29**, 269–284 (1950).
82. Kizil, R., Irudayaraj, J. & Seetharaman, K. Characterization of irradiated starches by using FT-Raman and FTIR spectroscopy. *Journal of agricultural and food chemistry* **50**, 3912–8 (2002).
83. Socrates, G. *Infrared and Raman Characteristic Groups Frequencies. Tables and Charts*. (Wiley, 2001).
84. Zhou, W., Yoshino, M., Kita, H. & Okamoto, K. Carbon Molecular Sieve Membranes Derived from Phenolic Resin with a Pendant Sulfonic Acid Group. *Industrial & Engineering Chemistry Research* **40**, 4801–4807 (2001).
85. Günter Gauglitz and Tuan Vo-Dinh. *Handbook of Spectroscopy*. (Wiley-VCH Verlag GmbH & Co. KGaA, 2003).
86. Yang, J. C., Jablonsky, M. J. & Mays, J. W. NMR and FT-IR studies of sulfonated styrene-based homopolymers and copolymers. *Polymer* **43**, 5125–5132 (2002).
87. Risberg, E. D. *et al.* Sulfur X-ray absorption and vibrational spectroscopic

- study of sulfur dioxide, sulfite, and sulfonate solutions and of the substituted sulfonate ions  $X_3CSO_3^-$  ( $X = H, Cl, F$ ). *Inorganic chemistry* **46**, 8332–48 (2007).
88. Townsend, T. M., Allanic, A., Noonan, C. & Sodeau, J. R. Characterization of sulfurous acid, sulfite, and bisulfite aerosol systems. *The journal of physical chemistry. A* **116**, 4035–46 (2012).
89. Szmant, H. H. in *Sulfur in organic and inorganic chemistry* (ed. Senning, A.) (Marcel Dekker, Inc., 1971).
90. Yu, H., Jin, Y., Li, Z., Peng, F. & Wang, H. Synthesis and characterization of sulfonated single-walled carbon nanotubes and their performance as solid acid catalyst. *Journal of Solid State Chemistry* **181**, 432–438 (2008).
91. Zhang, X. & Solomon, D. Carbonization reactions in novolac resins, hexamethylenetetramine, and furfuryl alcohol mixtures. *Chemistry of materials* **11**, 384–391 (1999).
92. Kelemen, S., Afeworki, M., Gorbaty, M. & Cohen, A. Characterization of organically bound oxygen forms in lignites, peats, and pyrolyzed peats by X-ray photoelectron spectroscopy (XPS) and solid-state  $^{13}C$  NMR. *Energy & fuels* 1450–1462 (2002).
93. Zawadzki, J. & Wisniewski, M.  $^{13}C$  NMR study of cellulose thermal treatment. *Journal of Analytical and Applied Pyrolysis* **62**, 111–121 (2002).
94. Fonseca, A., Zeuthen, P. & Nagy, J. B. Assignment of an average chemical structure to catalyst carbon deposits on the basis of quantitative  $^{13}C$  n.m.r. spectra. *Fuel* **75**, 1413–1423 (1996).
95. Hu, J. Z., Solum, M. S., Taylor, C. M. V., Pugmire, R. J. & Grant, D. M. Structural Determination in Carbonaceous Solids Using Advanced Solid State NMR Techniques. *Energy & Fuels* **15**, 14–22 (2001).
96. Zhang, X., Golding, J. & Burgar, I. Thermal decomposition chemistry of starch studied by  $^{13}C$  high-resolution solid-state NMR spectroscopy. *q*. **43**, 5791–5796 (2002).
97. Sevilla, M. & Fuertes, a. B. The production of carbon materials by hydrothermal carbonization of cellulose. *Carbon* **47**, 2281–2289 (2009).
98. Titirici, M.-M., Antonietti, M. & Baccile, N. Hydrothermal carbon from biomass: a comparison of the local structure from poly- to monosaccharides and pentoses/hexoses. *Green Chemistry* **10**, 1204 (2008).
99. Zhao, L. *et al.* Sustainable nitrogen-doped carbonaceous materials from biomass derivatives. *Carbon* **48**, 3778–3787 (2010).

100. Demir-cakan, R., Baccile, N., Antonietti, M. & Titirici, M. Carboxylate-Rich Carbonaceous Materials via One-Step Hydrothermal Carbonization of Glucose in the Presence of Acrylic Acid. 484–490 (2009).
101. Hiura, H., Ebbesen, T. & Tanigaki, K. Opening and purification of carbon nanotubes in high yields. *Advanced Materials* 275–276 (1995).
102. Desimoni, E., Casella, G. & Salvi, A. XPS investigation of ultra-high-vacuum storage effects on carbon fibre surfaces. *Carbon* **30**, 527–531 (1992).
103. Biniak, S., Szymański, G., Siedlewski, J. & ŚwiąTkowski, a. The characterization of activated carbons with oxygen and nitrogen surface groups. *Carbon* **35**, 1799–1810 (1997).
104. Vandencastele, N. & Reniers, F. Plasma-modified polymer surfaces: Characterization using XPS. *Journal of Electron Spectroscopy and Related Phenomena* **178-179**, 394–408 (2010).
105. Ruangchuay, L., Schwank, J. & Sirivat, A. Surface degradation of a-naphthalene sulfonate-doped polypyrrole during XPS characterization. *Applied Surface Science* **199**, 128–137 (2002).
106. Briggs, D. & Seah, M. P. *Practical Surface Analysis, Auger and X-ray Photoelectron Spectroscopy*. (Wiley, 1990).
107. Okpalugo, T. I. T., Papakonstantinou, P., Murphy, H., McLaughlin, J. & Brown, N. M. D. High resolution XPS characterization of chemical functionalised MWCNTs and SWCNTs. *Carbon* **43**, 153–161 (2005).
108. Briggs, D., Brewis, D. M., Dahm, R. H. & Fletcher, I. W. Analysis of the surface chemistry of oxidized polyethylene: comparison of XPS and ToF-SIMS. *Surface and Interface Analysis* **35**, 156–167 (2003).
109. Zhang, L. *et al.* Electronic structure and chemical bonding of a graphene oxide-sulfur nanocomposite for use in superior performance lithium-sulfur cells. *Physical chemistry chemical physics : PCCP* **14**, 13670–5 (2012).
110. Zielke, U., Hüttinger, K. & Hoffman, W. Surface-oxidized carbon fibers: I. Surface structure and chemistry. *Carbon* **34**, 983–998 (1996).
111. Desimoni, E., Casella, G. & Salvi, A. XPS/XAES study of carbon fibres during thermal annealing under UHV conditions. *Carbon* **30**, 521–526 (1992).
112. Lindberg, B. J. *et al.* Molecular spectroscopy by means of ESCA. II. *Physica Scripta* **1**, 286–298 (1970).
113. Huntley, D. The mechanism of the desulfurization of benzenethiol by nickel

- (110). *The Journal of Physical Chemistry* **37831**, 4550–4558 (1992).
114. Petit, C., Kante, K. & Bandosz, T. J. The role of sulfur-containing groups in ammonia retention on activated carbons. *Carbon* **48**, 654–667 (2010).
115. Bourg, M.-C., Badia, A. & Lennox, R. B. Gold–Sulfur Bonding in 2D and 3D Self-Assembled Monolayers: XPS Characterization. *The Journal of Physical Chemistry B* **104**, 6562–6567 (2000).
116. Moulder, J., Stickle, W., Sobol, P. & Bomben, K. *Handbook of X-ray photoelectron spectroscopy: a reference book of standard data for use in X-ray photoelectron spectroscopy*. (Physical Electronics Division, Perkin-Elmer Corp., 1979).
117. Budarin, V. *Starbons-scale up carbonization*. (2012).
118. Kuhnert, N. Microwave-assisted reactions in organic synthesis--are there any nonthermal microwave effects? *Angewandte Chemie* **41**, 1863–6 (2002).
119. Wiesbrock, F., Hoogenboom, R. & Schubert, U. S. Microwave-Assisted Polymer Synthesis: State-of-the-Art and Future Perspectives. *Macromolecular Rapid Communications* **25**, 1739–1764 (2004).
120. Roberts, B. a & Strauss, C. R. Toward rapid, “green”, predictable microwave-assisted synthesis. *Accounts of chemical research* **38**, 653–61 (2005).
121. Umrigar, V. M., Chakraborty, M. & Parikh, P. a. Microwave Assisted Sulfonation of 2-Naphthol by Sulfuric Acid: Cleaner Production of Schaeffer’s Acid. *Industrial & Engineering Chemistry Research* **46**, 6217–6220 (2007).
122. Retzko, B. I. & Unger, W. E. S. Analysis of Carbon Materials by X-ray Photoelectron Spectroscopy and X-ray Absorption Spectroscopy *Advanced Engineering Materials* **5**, 519–522 (2003).
123. Peng, F., Zhang, L., Wang, H., Lv, P. & Yu, H. Sulfonated carbon nanotubes as a strong protonic acid catalyst. *Carbon* **43**, 2405–2408 (2005).
124. Nasef, M. M. & Saidi, H. Surface studies of radiation grafted sulfonic acid membranes: XPS and SEM analysis. *Applied Surface Science* **252**, 3073–3084 (2006).
125. Datsyuk, V. *et al.* Chemical oxidation of multiwalled carbon nanotubes. *Carbon* **46**, 833–840 (2008).
126. Lee, W. H., Kim, J. Y., Ko, Y. K., Reucroft, P. J. & Zondlo, J. W. Surface

- analysis of carbon black waste materials from tire residues. *Applied Surface Science* **141**, 107–113 (1999).
127. Paynter, R. W. Angle-resolved XPS study of the effect of x-radiation on the aging of polystyrene exposed to an oxygen/argon plasma. *Surface and Interface Analysis* **33**, 14–22 (2002).
128. Feng, W., Borguet, E. & Vidic, R. D. Sulfurization of a carbon surface for vapor phase mercury removal – II: Sulfur forms and mercury uptake. *Carbon* **44**, 2998–3004 (2006).
129. Shen, S. *et al.* Preparation of a novel carbon-based solid acid from cocarbonized starch and polyvinyl chloride for cellulose hydrolysis. *Applied Catalysis A: General* **473**, 70–74 (2014).
130. Selvarani, G. *et al.* A phenyl-sulfonic acid anchored carbon-supported platinum catalyst for polymer electrolyte fuel cell electrodes. *Electrochimica Acta* **52**, 4871–4877 (2007).
131. Siow, K. S., Britcher, L., Kumar, S. & Griesser, H. J. Sulfonated Surfaces by Sulfur Dioxide Plasma Surface Treatment of Plasma Polymer Films. *Plasma Processes and Polymers* **6**, 583–592 (2009).
132. Gidley, M. J. & Bociek, S. M. <sup>13</sup>C CP / MAS NMR Studies of Amylose Inclusion Complexes, Cyclodextrins, and the Amorphous Phase of Starch Granules: Relationships between Glycosidic Linkage Conformation and Solid-state <sup>13</sup>C Chemical Shifts. *Journal of the American Chemical Society* **110**, 3820–3829 (1988).
133. Fonseca, a., Zeuthen, P. & Nagy, J. B. <sup>13</sup>C n.m.r. analysis of catalyst carbon deposits simulated by model compounds. *Fuel* **74**, 1267–1276 (1995).
134. Pradhan, A., Wu, J., Jong, S., Tsai, T. & Liu, S. An ex situ methodology for characterization of coke by TGA and <sup>13</sup>C CP-MAS NMR spectroscopy. *Applied Catalysis A: General* **165**, 489–497 (1997).
135. Moreno-Castilla, C., López-Ramón, M. . & Carrasco-Marín, F. Changes in surface chemistry of activated carbons by wet oxidation. *Carbon* **38**, 1995–2001 (2000).
136. Milczarek, G. & Nowicki, M. Carbon nanotubes/kraft lignin composite: Characterization and charge storage properties. *Materials Research Bulletin* **48**, 4032–4038 (2013).
137. Krasovskii, A. & Kalnin'sh, K. IR spectra of long-chain alkylsulfonic acids. *Journal of Applied Spectroscopy* **26**, 745–749 (1977).
138. Testa, M. L., La Parola, V. & Venezia, A. M. Transesterification of short

- chain esters using sulfonic acid-functionalized hybrid silicas: Effect of silica morphology. *Catalysis Today* **223**, 115–121 (2014).
139. Hamoudi, S., Royer, S. & Kaliaguine, S. Propyl- and arene-sulfonic acid functionalized periodic mesoporous organosilicas. *Microporous and Mesoporous Materials* **71**, 17–25 (2004).
  140. Kučera, F. & Jančář, J. Homogeneous and heterogeneous sulfonation of polymers: a review. *Polymer Engineering & Science* **3**, 783–792 (1998).
  141. Schmidt M. and Siebert W. *The Chemistry of Sulphur, Selenium, Tellurium and Polonium*. (Pergamon Press, 1973).
  142. Liu, X. *et al.* Thermal-oxidative degradation of high-amylose corn starch. *Journal of Thermal Analysis and Calorimetry* **115**, 659–665 (2013).
  143. Liu, X., Yu, L., Liu, H., Chen, L. & Li, L. In situ thermal decomposition of starch with constant moisture in a sealed system. *Polymer Degradation and Stability* **93**, 260–262 (2008).
  144. Kruczek, B. & Matsuura, T. Development and characterization of homogeneous membranes de from high molecular weight sulfonated polyphenylene oxide. *Journal of Membrane Science* **146**, 263–275 (1998).
  145. Sin, L. T., Rahman, W. a. W. a., Rahmat, a. R. & Mokhtar, M. Determination of thermal stability and activation energy of polyvinyl alcohol–cassava starch blends. *Carbohydrate Polymers* **83**, 303–305 (2011).
  146. Aggarwal, P. & Dollimore, D. A thermal analysis investigation of partially hydrolyzed starch. *Thermochimica Acta* **319**, 17–25 (1998).
  147. Malik, D. J., Trochimczuk, A. W., Jyo, A. & Tylus, W. Synthesis and characterization of nanostructured carbons with controlled porosity prepared from sulfonated divinylbiphenyl copolymers. *Carbon* **46**, 310–319 (2008).
  148. Yoshimune, M. & Haraya, K. Flexible carbon hollow fiber membranes derived from sulfonated poly(phenylene oxide). *Separation and Purification Technology* **75**, 193–197 (2010).
  149. Deng, Q., Wilkie, C. A., Moore, R. B. & Mauritz, K. A. TGA – FTi . r . investigation of the thermal degradation of Nafion and Nafion /[ silicon oxide ] -based nanocomposites. **39**, 5961–5972 (1998).
  150. Tsai, H., Wang, Y., Lin, J. & Lien, W. Preparation and Properties of Sulfopropyl Chitosan Derivatives with Various Sulfonation Degree. *Journal of Applied Polymer Science* **116**, 1686-1693 (2010).

151. Surowiec, J. & Bogoczek, R. Studies on the thermal stability of the perfluorinated cation-exchange membrane Nafion-417. *Journal of Thermal Analysis and Calorimetry* **33**, 1097–1102 (1988).
152. Siril, P. F., Cross, H. E. & Brown, D. R. New polystyrene sulfonic acid resin catalysts with enhanced acidic and catalytic properties. *Journal of Molecular Catalysis A: Chemical* **279**, 63–68 (2008).
153. Fraile, J. M., García-Bordejé, E. & Roldán, L. Deactivation of sulfonated hydrothermal carbons in the presence of alcohols: Evidences for sulfonic esters formation. *Journal of Catalysis* **289**, 73–79 (2012).
154. Aragón, J., Vegas, J. & Jodra, L. Self -Condensation of Cyclohexanone Catalyzed by Amberlyst-15. Study of Diffusional Resistances and Deactivation of the Catalyst. *Industrial and Engineering Chemistry Research* **33**, 592–599 (2000).
155. Shu, Q. *et al.* Synthesis of biodiesel from cottonseed oil and methanol using a carbon-based solid acid catalyst. *Fuel Processing Technology* **90**, 1002–1008 (2009).
156. Senning, A. *Sulfur in organic and inorganic chemistry*. (Marcel Dekker, Inc., 1971).
157. Taddei, P. *et al.* Chemical and physical properties of sulfated silk fabrics. *Biomacromolecules* **8**, 1200–8 (2007).
158. Chihara, G. Medical and biochemical application of infrared spectroscopy. V. Infrared absorption spectra of organic sulfate esters. *Chem. Pharmacol. Bull.(Tokyo)* **8**, (1960).
159. Bozell, J. J. & Petersen, G. R. Technology development for the production of biobased products from biorefinery carbohydrates—the US Department of Energy’s “Top 10” revisited. *Green Chemistry* **12**, 539 (2010).
160. Bozell, J. J. *et al.* Production of levulinic acid and use as a platform chemical for derived products. **28**, 227–239 (2000).
161. Smith, M. B. & March, J. *Advanced Organic Chemistry*. (Wiley, 2001).
162. Liu, Y., Lotero, E. & Goodwin, J. G. Effect of water on sulfuric acid catalyzed esterification. *Journal of Molecular Catalysis A: Chemical* **245**, 132–140 (2006).
163. Luque, R., Budarin, V., Clark, J. H. & Macquarrie, D. J. Glycerol transformations on polysaccharide derived mesoporous materials. *Applied Catalysis B: Environmental* **82**, 157–162 (2008).
164. Kappe, C. O. & Dallinger, D. Controlled microwave heating in modern

- organic synthesis: highlights from the 2004-2008 literature. *Molecular diversity* **13**, 71–193 (2009).
165. Hoydonckx, H. E., De Vos, D. E., Chavan, S. A. & Jacobs, P. A. Esterification and Transesterification of Renewable Chemicals. *Topics in Catalysis* **27**, 83–96 (2004).
166. Shu, C. & Lawrence, B. Formation of 4-Alkoxy- $\gamma$ -valerolactones from Levulinic Acid and Alcohols during Storage at Room Temperature. *Journal of Agricultural and Food Chemistry* **43**, 782–784 (1995).
167. Leonard, R. Levulinic acid as a basic chemical raw material. *Industrial & Engineering Chemistry* **48**, 1331-1341 (1956).
168. Timokhin, B., Baransky, V. & Eliseeva, G. Levulinic acid in organic synthesis. *Russian chemical reviews* **68**, 73–84 (1999).
169. MBH Engineering Systems 2008. Sulfur Dioxide (SO<sub>2</sub>) Measurement Methods for Wine Analysis: An Assay Comparison. at <[http://www.mbhes.com/so2\\_in\\_wine.htm](http://www.mbhes.com/so2_in_wine.htm)> visited on February 8, 2012